

Investigating senescence and senescence-escape in cancer cells

Fanni Tóth

PhD student; ID number: @00541166

Supervisors: Prof. Federica Sotgia and Prof. Michael Lisanti

University of Salford

School of Science, Engineering and Environment

Biomedical Research Centre

PhD Thesis

2022



University of
Salford
MANCHESTER

Contents

DECLARATION OF ORIGINALITY	6
ACKNOWLEDGEMENTS	7
LIST OF ABBREVIATIONS	8
LIST OF FIGURES.....	10
ABSTRACT	12
1. INTRODUCTION	14
1.1 INTRODUCTION TO CANCER AND CANCER THERAPY	14
1.1.1 <i>Conventional and targeted cancer therapies – limitations and advances</i>	14
1.1.2 <i>Therapy resistance and metastasis</i>	16
1.2 CELLULAR SENESCENCE AND THE CHARACTERISTICS OF SENESCENT CELLS.....	18
1.2.1 <i>Characteristics and markers of cellular senescence</i>	18
1.3 SENESCENCE IN CANCER.....	22
1.3.1 <i>Oncogene induced senescence (OIS)</i>	22
1.3.2 <i>Therapy induced senescence (TIS)</i>	23
1.3.3 <i>Role of senescence in tumorigenesis</i>	25
1.4 THE ROLE OF THE SENESCENCE-ASSOCIATED SECRETORY PHENOTYPE (SASP) IN CANCER	27
1.4.1 <i>Effect of SASP factors in anti-tumour immune responses</i>	27
1.4.2 <i>SASP in cancer therapy</i>	28
1.4.3 <i>Role of SASP factors in metastasis</i>	28
1.5 THE ROLE OF AUTOPHAGY IN SENESCENCE	31
1.6 SENESCENCE-ESCAPE.....	32
1.6.1 <i>Mechanisms of senescence escape</i>	33
1.6.2 <i>Models for senescence escape</i>	35
1.7 TARGETING SENESCENCE IN CANCER THERAPY.....	37
1.7.1 <i>Anti-SASP and SASP modulating therapies</i>	37
1.7.2 <i>Senolytics in cancer therapy</i>	39
1.7. DIPEPTIDYL PEPTIDASE IV (DPP4/CD26).....	42
1.7.1. <i>Physiological functions of DPP4/CD26</i>	42
1.7.2. <i>Role of DPP4/CD26 in cancer</i>	43
1.8. CHALLENGES AND LIMITATIONS IN THE INVESTIGATION OF THERAPY-INDUCED SENESCENCE IN CANCER – SUMMARY ...	48
2. AIMS.....	49
3. MATERIALS AND METHODS	51
3.1 CELL LINES AND CELL CULTURING	51

3.2	SENESCENCE-INDUCTION AND TREATMENTS	51
3.3	FLUOROGENIC SA-B-GALACTOSIDASE STAINING.....	52
3.4	CHROMOGENIC SA-B-GALACTOSIDASE STAINING	53
3.5	IMMUNOSTAINING FOR IMAGING	54
3.6	IMMUNOSTAINING FOR FLOW CYTOMETRY	55
3.7	CELL CYCLE ANALYSIS.....	56
3.8	DPP4/CD26 STAINING FOR FLOW CYTOMETRY	56
3.9	SULPHORHODAMINE B (SRB) ASSAY	57
3.10	CRYSTAL VIOLET STAINING.....	57
3.11	SILENCING OF DPP4/CD26.....	58
3.12	LYSOTracker STAINING	59
3.13	WESTERN BLOT ANALYSIS.....	59
3.14	CELLTRACE CFSE (CARBOXYFLUORESCHEIN SUCCINIMIDYL ESTER) STAINING	60
3.15	FLUORESCENCE-ACTIVATED CELL SORTING (FACS)	60
3.16	MIGRATION ASSAY	61
3.17	MAMMOSPHERE FORMATION ASSAY	61
3.18	COLONY FORMATION ASSAY	62
3.19	ENZYME-LINKED IMMUNOSORBENT ASSAY (ELISA).....	62
3.20	STATISTICAL ANALYSIS	63
4.	RESULTS.....	64
4.1	SENESCENCE INDUCTION IN MCF-7 CELLS.....	64
4.1.1	<i>Establishing and analysing TIS models using bromodeoxyuridine (BrdU), gemcitabine (GEM) and Palbociclib (PALBO) in MCF-7 cells</i>	<i>64</i>
4.1.2	<i>Analysing the cell cycle of senescent MCF-7 cells by the double staining of Ki-67 expression and DNA-content (PI)</i>	<i>69</i>
4.2	EVALUATION OF SENESCENCE-ESCAPE.....	72
4.2.1	<i>Establishing a method to quantify senescence-escape using Ki-67 and crystal-violet staining</i>	<i>72</i>
4.2.2	<i>Comparing senescence-escape in BrdU-, GEM- and PALBO-induced senescent MCF-7 cells</i>	<i>75</i>
4.3	DEVELOPING A TWO-HIT TREATMENT STRATEGY USING AZITHROMYCIN AS A SENOLYTIC DRUG	77
4.3.1	<i>Validating the senolytic effect of azithromycin on senescent MCF-7 cells.....</i>	<i>77</i>
4.3.2	<i>Investigating the effect of azithromycin on autophagy in MCF-7 cells</i>	<i>78</i>
4.3.3	<i>Investigating senescence-escape after AZI treatment of senescent MCF-7 cells</i>	<i>81</i>
4.4	INVESTIGATING THE EXPRESSION AND FUNCTION OF DIPEPTIDYL PEPTIDASE-4 (DPP4/CD26) IN SENESCENT MCF-7 CELLS .	84
4.4.1	<i>Analysing the expression of DPP4/CD26 in senescent MCF-7 cells</i>	<i>84</i>
4.4.2	<i>Silencing the expression of DPP4 in MCF-7 cells.....</i>	<i>85</i>
4.4.3	<i>Investigating the role of DPP4/CD26 in senescence-escape in MCF-7 cells.....</i>	<i>87</i>
4.4.4	<i>Investigating the effect of DPP4 inhibition in senescence-escape using sitagliptin in MCF-7 cells</i>	<i>89</i>

4.4.5 Investigating the effect of the combination treatment with azithromycin and sitagliptin in MCF-7 cells.....	91
4.5 SENESCENCE INDUCTION IN MDA-MB-231 CELLS	93
4.5.1 Establishing and analysing TIS models using bromodeoxyuridine (BrdU), gemcitabine (GEM) and Palbociclib (PALBO) in MDA-MB-231 cells	93
4.5.2 Analysing the cell cycle of senescent MDA-MB-231 cells by the double staining of Ki-67 expression and DNA-content (PI)	98
4.5.3 Comparing senescence-escape in BrdU-, GEM- and PALBO-induced senescent MD-MB-231 cells....	99
4.5.4 Validating the senolytic effect of azithromycin in senescent MDA-MB-231 cells compared with the effect of chloroquine	100
4.6 INVESTIGATING THE EXPRESSION AND FUNCTION OF DIPEPTIDYL PEPTIDASE-4 (DPP4/CD26) IN SENESCENT MDA-MB-231 CELLS	102
4.6.1 Silencing the expression of DPP4 in MDA-MB-231 cells.....	102
4.6.2 Investigating the effect of DPP4/CD26 in senescence-escape (MDA-MB-231)	103
4.7 ISOLATING AND ANALYSING SENESCENCE-ESCAPED CELLS.....	105
4.7.1 Establishing a method to isolate senescence-escaped MCF-7 and MDA-MB-231 cells.....	105
4.7.2 Investigating the effect of senescence-escape in cancer progression.....	109
4.7.2.1 Analysis stem cell activity in senescence-escaped cells by mammosphere formation assay.....	109
4.7.2.2 Analysis of migration capacity in senescence-escaped cells	110
4.7.2.3 Analysis of proliferative capacity in senescence-escaped cells by colony formation assay	111
4.8 SUMMARY OF RESULTS	113
5. DISCUSSION	115
6. CONCLUSION	131
7. SUPPLEMENTARY FIGURES	133
Supplementary Figure 1. γ -H2AX immunostaining, p16 expression of MCF-7 cells, DAPI staining of nucleus (increased image size).....	133
Supplementary Figure 2. Western blot images of DPP4 expression in MCF-7 and MDA-MB-231 cells	134
Supplementary Figure 3. Senescence-escape in BrdU-induced senescent MCF-7 cells	134
Supplementary Figure 4. Analysis of LC3B and p62/SQSTM1 expression without signal area correction	135
Supplementary Figure 5. Effect of 3 days and 5 days of azithromycin treatment in MDA-MB-231 cells..	135
Supplementary Figure 6. Cell cycle analysis of MCF-7 and MDA-MB-231 cells - sub-G1 and polyploid cell populations	136
Supplementary Figure 7. Evaluation of senescence-escape in ctrl siRNA and DPP4 siRNA MCF-7 and MDA-MB-231 cells (representative figures)	137
Supplementary Figure 8. Effect of sitagliptin treatment on senescence-escape in MCF-7 cells – Ki-67 expression and cell numbers	138

<i>Supplementary Figure 9. Effect of AZI+SITA on senescence-escape in MCF-7 cells – Ki-67 expression and cell numbers</i>	139
<i>Supplementary Figure 10. Effect of SITA on control MCF-7 cells, and senescence-escape of MDA-MB-231 cells – crystal violet staining</i>	140
<i>Supplementary Figure 11. Gating strategies for the isolation of senescence-escaped cells by FACS</i>	141
<i>Supplementary Figure 12. SA-β-gal and CD26 expression in BrdU-treated CAMA-1, MDA-MB-468 and T47D cells</i>	142
<i>Supplementary Figure 13. MACS sorting of MCF-7 cells</i>	143
<i>Supplementary Figure 14. SA-β-gal and Ki-67 expression of MACS sorted MCF-7 cells</i>	144
8. SUPPLEMENTARY METHODS	145
8.1. CELL LINES AND CELL CULTURING	145
8.2. MAGNETIC-ACTIVATED CELL SORTING (MACS)	145
9. LIST OF PUBLICATIONS	146
10. APPENDIX	147
11. REFERENCES	148

Declaration of originality



**DOCTORAL
SCHOOL**

DECLARATION 1 FORM

Declaration of Originality by Postgraduate Candidate (for softbound thesis)

1

Candidates for postgraduate degrees must present this completed form to askUS, Student Administration, ground floor, University House, when submitting their **two** soft-bound theses. In addition, an electronic version of the thesis (pdf format) should be sent to the candidate's Research Support Officer.

Name of candidate (in BLOCK CAPITAL LETTERS as it appears on the thesis)

.....FANNI TOTH.....

Student number:@00541166.....

School:School of Science, Engineering and Environment.....

Degree (PhD, DMA, Professional Doctorate, MSc, MPhil, MRes – Please specify):PhD.....

This is to certify that the copy of my thesis, which I have presented for consideration for my postgraduate degree: -

1. embodies the results of my own course of study and research
2. has been composed by myself
3. has been seen by my supervisor before presentation
4. has been granted the appropriate level of ethics approval

If you have a Student support or reasonable adjustment plan, please indicate if you would like this to be shared with your examiners

Signature of candidate:*Fanni Toth*..... Date:12/07/2022.....

Address (to which information concerning examiners' decision and final binding can be sent):

Apt 9.3A Melia House, 19 Lord street, Manchester M4 4AX UK

The candidate's supervisor is asked to declare here that s/he has approved the submission of the thesis. If the supervisor decides to withhold approval, the candidate shall have the right of appeal to the Associate Dean of Research and Innovation. A candidate may be permitted to submit a thesis despite the Supervisor withholding approval, providing the Associate Dean of Research and Innovation approves submission.

HeCoS codes (please add up to 3 HeCoS codes which best fit with the student's research area)

.....100345.....

Signature of Supervisor:*Federica Stipia*..... Date:13/07/2022...

[For your information the dates of the Postgraduate Research Awards Board are published here
[https://testlivesalfordac.sharepoint.com/sites/DoctoralSchoolHub/SitePages/Postgraduate-Research-Awards-Board-\(PRAB\)-Dates.aspx](https://testlivesalfordac.sharepoint.com/sites/DoctoralSchoolHub/SitePages/Postgraduate-Research-Awards-Board-(PRAB)-Dates.aspx)]

Please note that the completed declaration form must accompany the softbound thesis when presented to Student Administration

Acknowledgements

I would like to thank my supervisors, Prof. Federica Sotgia and Prof. Michael Lisanti for the guidance, encouragement and support they have provided throughout my PhD studies. I am grateful for their kindness and patience towards me, and that they trusted me and my knowledge even when I had a lack of self-confidence sometimes.

I would like to thank everyone in our research group, Bela, Camillo, Chiara, Filippo, Gloria, Marco, Marta and Zahra for making these challenging years much easier for me. I am thankful for their suggestions and ideas, that helped me to develop my research skills and knowledge, and most importantly I am thankful for their friendship and all the good memories that we have shared during these years.

I would like to say thank you to Sonia and Rumana for their friendship and support during these years, and for listening to my complaining on the bad days.

I am grateful for the friends that I found at the University, who made the long days in the lab/office filled with laughter: Bela, Chiara, Filippo, Grace, Sonia, Toby and Zahra.

I would like to thank my boyfriend, Patrik for his patience and love, and all the help and support he gave me during the difficult times of my studies.

Finally, I would like to thank my family for their unconditional support throughout these years.

List of abbreviations

ABC – ATP-binding cassette
ADA – adenosine deaminase
AP2M1 – AP-2 complex subunit mu
ATM serine-protein kinase –
AT-rich – DNA-region associated with condensed chromatin
AZI – azithromycin
BCL-2 – B-cell lymphoma 2
Bcl-xL – B-cell lymphoma-extra large
BrdU – bromodeoxyuridine
CAF – cancer-associated fibroblast
CART – chimeric antigen receptor T-cells
CD45RO – RO isoform of protein tyrosine phosphatase, receptor type C
CD47 – cluster of differentiation 47, integrin associated protein
Cdc2/7 – cell division cycle 2/7-related protein kinase
Cdk1/4/6 – cyclin-dependent kinase 1/4/6
CDKN1A/p21^{CIP} – cyclin-dependent kinase inhibitor 1A
CDKN2A/p16^{INK4a} – cyclin-dependent kinase inhibitor 2A
CFSE – Carboxyfluorescein succinimidyl ester
CHK2 – Checkpoint kinase 2
CIS – chemotherapy-induced senescence
CQ – chloroquine
CRISPR – clustered regularly interspaced short palindromic repeats
CRL₄Cdt2 – substrate recognition factor Cdt2
CSC – cancer stem cell
CXCL12 – C-X-C motif chemokine ligand-12
CXCR1/2/4/7 – C-X-C motif chemokine receptor 1/2/4/7
DAPI – 4',6-diamidino-2-phenylindole
DDR – DNA-damage response
DPP4 – dipeptidyl-peptidase 4
EMT – epithelial-mesenchymal transition
ER – oestrogen receptor
EZH2 – enhancer of zeste homolog 2
FACS – fluorescence-activated cell sorting
FDA – Food and Drug Administration
GEM – gemcitabine
GLP-1 – glucagon-like peptide-1
HER2 – human epidermal growth factor receptor 2
HRAS – GTPase HRas, “Harvey Rat sarcoma virus”
hTERT – human telomerase reverse transcriptase

IgG1 – immunoglobulin G1
IL-1 α – interleukin-1 α
IL-6 – interleukin-6
IL-8 – interleukin-8
JAK2/STAT3 – Janus kinase 2/signal transducer and activator of transcription 3
JNK/c-Jun – c-Jun N-terminal kinases/transcription factor Jun
Ki-67 – marker of proliferation Ki-67
LC3B – microtubule-associated proteins 1A/1B light chain 3B
MAPK – mitogen-activated protein kinase
Mcl-1 – induced myeloid leukaemia cell differentiation protein
MEK/ERK – mitogen-activated protein kinase kinase/extracellular signal-regulated kinase
MMTV-Wnt1 – mouse mammary tumour virus-*proto-oncogene* Wnt-1
mTOR – mammalian target of rapamycin
mTORC1 – mammalian target of rapamycin complex 1
NF- κ B – nuclear factor κ B
OIS – oncogene induced senescence
p44/MAPK3 – mitogen-activated protein kinase 3
p53 – tumour suppressor p53
p62/SQSTM1 – ubiquitin-binding protein p62/sequestosome-1
PALBO – Palbociclib
PARP – poly (ADP-ribose) polymerase
PI3K – phosphoinositide 3-kinases
PTEN – phosphatase and tensin homolog
Raf – rapidly accelerated fibrosarcoma kinase
Ras – GTPase Ras, “Harvey Rat sarcoma virus”
Rb – retinoblastoma protein
ROS – reactive oxygen species
RT-PCR – real time reverse transcription polymerase chain reaction
SAHF – senescence-associated heterochromatin foci
SASP – senescence-associated secretory phenotype
SA- β -gal – senescence-associated β -galactosidase
SCF^{Skp2} – Skp, Cullin, F-box containing complex ubiquitin ligase
SCM – senescence-conditioned medium
TCR – T cell receptor based therapy
TIS – therapy induced senescence
TNF- α – tumour necrosis factor alpha
TSP1 – Thrombosporin-1
 γ H2AX – phosphorylated form of H2A histone family member X

List of figures

Figure 1. Characteristics of cellular senescence.....	21
Figure 2. Beneficial and detrimental consequences of therapy induced senescence (TIS) in cancer.....	25
Figure 3. Different functions of senescence-associated secretory phenotype (SASP) in cancer.....	30
Figure 4. Different functions of DPP4/CD26 activity.	47
Figure 5. Evaluation of chromogenic (X-gal) SA- β -galactosidase staining by ImageJ.....	54
Figure 6. Senescence induction in MCF-7 cells.....	65
Figure 7. Analysis of senescence-markers in MCF-7 cells.....	69
Figure 8. Cell cycle analysis of senescent MCF-7 cells.	71
Figure 9. Analysis of BrdU incorporation and Ki-67 expression in MCF-7 cells.	73
Figure 10. Evaluation of senescence-escape in MCF-7 cells.	74
Figure 11. Senescence-escape in BrdU-, GEM- and PALBO-induced senescent MCF-7 cells.. ..	76
Figure 12. Two-hit treatment strategy using the senolytic effect of azithromycin.....	78
Figure 13. Effect of azithromycin and chloroquine treatment.....	81
Figure 14. Analysis of senescence-escape after azithromycin treatment.	83
Figure 15. Analysis of DPP4/CD26 expression in senescent MCF-7 cells.....	85
Figure 16. Effect of DPP4 silencing on the senescence-induction in MCF-7 cells.....	86
Figure 17. Effect of DPP4 silencing on the senescence-escape of MCF-7 cells.....	88
Figure 18. Effect of DPP4-inhibition in senescence-escape.....	91
Figure 19. Analysis of senescence-escape after the combination of azithromycin and sitagliptin treatment.....	92
Figure 20. Senescence induction in MDA-MB-231 cells.....	95
Figure 21. Analysis of senescence-markers in MDA-MB-231 cells.....	98
Figure 22. Cell cycle analysis of senescent MDA-MB-231 cells.	99
Figure 23. Senescence-escape in BrdU-, GEM- and PALBO-induced senescent MDA-MB-231 cells.	100
Figure 24. Effect of azithromycin and chloroquine in MDA-MB-231 cells.....	101

Figure 25. Effect of DPP4-silencing on the senescence-induction in MDA-MB-231 cells...	103
Figure 26. Effect of DPP4 silencing and DPP4 inhibition on the senescence-escape of MDA-MB-231 cells.	105
Figure 27. Analysis of IL-6, IL-8 and CXCL12 secretion of control and senescent MCF-7 and MDA-MB-231 cells.....	Error! Bookmark not defined.
Figure 28. Schematic figure of the isolation of senescence-escaped MCF-7 and MDA-MB-231 cells and the experimental strategy..	109
Figure 29. Analysis of stem cell activity in senescence-escaped MCF-7 and MDA-MB-231 cells by mammosphere formation assay.....	110
Figure 30. Analysis of metastatic-capacity in senescence-escaped MCF-7 and MDA-MB-231 cells by migration-assay.....	111
Figure 31. Analysis of proliferative capacity in senescence-escaped MCF-7 and MDA-MB-231 cells by colony formation assay.....	112

Abstract

Despite the general concept that therapy-induced senescence (TIS) has a tumour-suppressive role, the presence of senescent tumour cells and the ability of cancer cells to escape from senescence could potentially lead to therapy resistance and tumour recurrence. While a wide range of chemotherapeutic drugs are known to induce senescence in cancer, the effect of TIS in tumour progression is still not completely understood.

The project was focused on the development of *in vitro* senescence and senescence-escape models, along with the investigation of a cell surface protein dipeptidyl-peptidase 4 (DPP4/CD26) as a potential marker of senescence in cancer, and the establishment of a treatment strategy exploiting TIS and the senolytic effect of azithromycin. Three different drugs (bromodeoxyuridine, gemcitabine and Palbociclib) were used to induce senescence in MCF-7 and MDA-MB-231 human breast cancer cell lines, and the expression of various senescence markers, such as cell morphology, growth arrest, SA- β -galactosidase activity and cytokine secretion, were investigated. To identify and isolate senescence-escaped cells and to evaluate the senescence-escaping ability of the cells, new methods were established by using the proliferation marker Ki-67, crystal-violet staining and CellTrace CFSE staining.

Our results revealed a variability in the expression of different senescent markers and in the senescence-escaping ability of the cells, depending on the drug used for senescence-induction and the cell type as well. Importantly, the expression of DPP4/CD26 was significantly increased in both senescent MCF-7 and MDA-MB-231 cells. To investigate the function of DPP4/CD26 in senescent cancer cells the expression of DPP4 was silenced in both cancer cell lines, and the cells were subsequently treated with senescence-inducing drugs. Our results indicated that DPP4 expression is not essential for senescence-induction, however, based on the evaluation of senescence-escaping ability of the cells, DPP4/CD26 exhibited a potential role to promote senescence-escape in MCF-7 cells, but not in MDA-MB-231 cell. After senescence-induction MCF-7 and MDA-MB-231 cells were treated with a recently discovered senolytic drug (azithromycin), and its effect was investigated by SRB and immunofluorescent assay in order to test its effect and potential mechanism of action in on our senescent cancer cell models. The results confirmed the senolytic effect of azithromycin in senescent cancer cells via the inhibition of autophagic processes. Furthermore, targeting

senescent cancer cells with azithromycin and a DPP4 inhibitor (sitagliptin) demonstrated a synergistic effect in MCF-7 cells, by decreasing the viability of senescent cells (azithromycin) and reducing the number of senescence-escaped cells (sitagliptin).

Altogether, the research project highlighted the importance of detailed characterisation of senescent cancer cells for the investigation of therapy induced senescence. Our results indicated that senolytic treatments, such as azithromycin treatment, could improve the outcome of senescence-inducing cancer therapies, and that DPP4/CD26 could be a promising marker and a novel target to be exploited in cancer diagnosis and treatment. Moreover, the established methods for the evaluation of senescence-escape could contribute to the comprehensive investigation of the mechanisms of senescence-escape, and to the identification of potential therapeutic targets for decreasing senescence-escape.

1. Introduction

1.1 Introduction to cancer and cancer therapy

Cancer is the second leading cause of mortality worldwide, that poses a substantial clinical, economic and social burden (Mattiuzzi and Lippi, 2019). It is an extremely complex and heterogeneous pathological condition, which includes more than 100 distinct types of cancers originating from different cell types and organs (Bertram, 2000, Krzyszczyk et al., 2018). Hanahan et al. defined the hallmarks of cancer, including unlimited proliferation potential, evasion of growth suppressors, resistance of apoptosis, sustained angiogenesis, and invasion and metastasis to distant parts of the body, accompanied by the two emerging hallmarks including the reprogramming of metabolism and the evasion of immune destruction (Hanahan and Weinberg, 2000, Bertram, 2000, Hanahan and Weinberg, 2011). The genome instability of cancer cells caused by the accumulation of several genetic mutations, together with the impact of tumour microenvironment, contributes to the acquisition of these cancer-specific hallmarks (Hanahan and Weinberg, 2011).

1.1.1 Conventional and targeted cancer therapies – limitations and advances

Conventional treatments, including surgery, radiotherapy and chemotherapy, are widely used therapeutic strategies against cancer. Surgery can be used when the solid tumours are located in an accessible area of the body, however, it is commonly combined with neo-adjuvant or adjuvant radio- or chemotherapy (Bernier et al., 2004). Radiotherapy represents an important and frequently used modality for cancer treatment, with ongoing efforts to improve its effectiveness and minimize therapy related toxicities (Baskar et al., 2012). Traditional chemotherapeutic agents usually target DNA, RNA and protein synthesis in rapidly dividing cells, leading to the induction of apoptotic cell death in cancer cells. Although chemotherapy is highly effective, it is generally associated with therapy resistance and serious side effects due to its toxic effect on non-malignant cells (Amjad et al., 2022).

To overcome the resistance to conventional cancer therapies and improve their effect, several anti-cancer drugs have been developed to target cancer-specific proteins and

signalling pathways, defined as targeted therapies. Targeted therapeutic drugs include macromolecules, for example monoclonal antibodies, polypeptides, nucleic acids, and small molecules, for example inhibitors targeting kinases, epigenetic regulatory proteins and DNA damage repair enzymes (Yan et al., 2011, Zhong et al., 2021). In the last 20 years, there has been a substantial increase in the number of FDA-approved small-molecule targeted drugs for cancer treatment, including receptor tyrosine kinase inhibitors, serine/threonine kinase inhibitors, epigenetic inhibitors, BCL-2 and PARP inhibitors. Because these targeted therapies are effective only in a limited number of patients, the combination of targeted therapies with conventional therapies, or the simultaneous inhibition of different cellular pathways by using different combination therapies represents a promising therapeutic strategy in cancer treatment (Yang et al., 2020, Zhong et al., 2021).

Another rapidly developing field in targeted cancer treatment is the immunotherapy. The aim of immunotherapy is to exploit the natural immune defence against cancer cells by increasing the activation of antitumour immune response (Kruger et al., 2019, Zhang and Zhang, 2020). It includes tumour-specific monoclonal antibodies, immune checkpoint inhibitors, oncolytic virus therapies, cancer vaccines, cytokine therapies, adoptive cell transfer therapies, such as chimeric antigen receptor T cell (CAR T) therapy and T-cell receptor-based (TCR) therapy (Zhang and Chen, 2018, Krzyszczyk et al., 2018). Although several immunotherapeutic agents are approved for cancer treatment, the most frequently used immunotherapeutic strategies are monoclonal antibodies including the immune checkpoint inhibitors, usually used in combination with chemotherapy or other targeted therapies. Despite the advances in immunotherapies, such as the detailed characterisation of tumour-infiltrating immune cells by single-cell RNA sequencing and the development of pre-clinical models, tumour heterogeneity, intra-patient variability and potential side effects can limit the clinical applicability of immunotherapies (Zhang and Chen, 2018, Zhang and Zhang, 2020, Hegde and Chen, 2020).

The intrinsic genetic heterogeneity of tumour cells and the variability of the therapy response of cancer patients led to the emergence of precision and personalised medicine. The aim of personalized therapies is to identify the most suitable treatment strategies for each patient, by characterizing the patients' genetic traits and disease state based on genetic, transcriptomic, proteomic or metabolomic data (Krzyszczyk et al., 2018). Furthermore, the

progression of liquid biopsy-based detection of circulating tumour DNA, tumour cells and microRNAs from blood samples holds a great promise to monitor cancer progression and predict therapy response in cancer patients (Domínguez-Vigil et al., 2018).

To overcome the limitations and reduce the side-effects of conventional and targeted cancer therapies, different techniques have been developed to widen the therapeutic window of anti-cancer drugs by improving their specificity and delivery. For example, antibody-drug conjugates are composed of a cytotoxic drug linked to a monoclonal antibody, that binds to the specific antigen expressed on the surface of the targeted cancer cells (Drago et al., 2021). To improve the delivery of drugs inside the cells and to maintain a relatively stable drug concentration within the circulation system, nanotechnology-based drug delivery systems (nanocarriers) have been developed, that are based on different types of nanoparticles, such as liposomal, polymeric and micellar nanoparticles (Hinge et al., 2020). Moreover, some of the antibody-drug conjugates and nanocarriers, such as brentuximab vedotin, ado-trastuzumab emtansine, Doxil (liposomal doxorubicin) and Abraxane (albumin-particle bound paclitaxel) have already been approved for cancer treatment (Drago et al., 2021, Hinge et al., 2020, Anselmo and Mitragotri, 2019).

1.1.2 Therapy resistance and metastasis

Therapy resistance and the development of metastasis represent the biggest challenge in cancer therapy, and they are responsible for most of the cancer-related mortalities (Chaffer and Weinberg, 2011). There are different cellular mechanisms that can lead to therapy resistance, such as the inactivation of anti-cancer drugs by the alteration of their molecular characteristics, the increased efflux of drugs through ATP-binding cassette (ABC) transporters, inhibition of cell death by suppressing apoptotic pathways, enhanced DNA-damage repair via O6-methylguanine DNA methyltransferase (MGMT), nucleotide excision repair or homologous recombination (Housman et al., 2014, Li et al., 2021). The main underlying reason for these mechanisms is drug-resistance gene mutations (p53, PTEN), gene amplification, altered gene expression (upregulation of Bcl2, AKT, downregulation of Bax, Bclxl), and epigenetic alteration such as DNA methylation, and histone alterations (hypermethylation of the MDR1 or hMLH1 promoter). These genetic alterations could be induced by the therapeutic drugs or they could already exist in a population of cancer cells (Zhong et al., 2021, Housman et al., 2014, Mansoori et al., 2017). However, there are growing

evidence demonstrating the role of tumour microenvironment in the development of drug resistance, including non-malignant cells in tumour stroma, components of the extracellular matrix and several soluble factors as well (Mansoori et al., 2017).

Tumour recurrence and metastasis are generally associated with tumour heterogeneity and the phenotypic plasticity of cancer cells, that contributes to the development of drug resistance during cancer treatment (Fanelli et al., 2020). A subpopulation of cancer cells known as cancer stem cells (CSC) has been described as the main driver of therapy resistance and malignant progression in cancer (Chaffer and Weinberg, 2011). Cancer stem cells exhibit specific traits such as self-renewal, increased motility and invasiveness, increased resistance to apoptosis, and the ability to retreat reversibly to a non-cycling quiescent state, leading to a highly increased resistance to conventional therapies (Li et al., 2021, Moore and Lyle, 2011). Moreover, several studies have demonstrated a link between epithelial-mesenchymal transition (EMT) and the acquirement of stemness properties, that can provide an explanation to the long clinical latency of metastatic recurrence (Chaffer and Weinberg, 2011, Weidenfeld and Barkan, 2018, Mani et al., 2008, May et al., 2011, Malanchi et al., 2011). Although the process of metastasis is still not completely understood, it has been suggested that the epithelial-mesenchymal transition promotes the dissemination of cancer cells from primary tumours, and the acquired stemness properties promote the survival of the cancer cells and the colonization of distant tissues (Chaffer and Weinberg, 2011).

In the most recently published paper by *Hanahan (2022)* cellular senescence has been described as an additional hallmark of cancer, that is involved in the activation of cancer specific cellular programs necessary for tumour growth and progression (Hanahan, 2022). Moreover, a wide range of the previously described conventional and targeted therapeutic drugs has already been demonstrated to induce senescence in different types of cancers, and based on the growing evidence about the effect of therapy induced senescence, senescence plays an important role in therapy resistance and tumour recurrence (Mongiardi et al., 2021, Chakrabarty et al., 2021, Dou and Berger, 2018, Triana-Martinez et al., 2020). These detrimental effects of therapy induced senescence could ultimately contribute to poor clinical outcome of cancer therapy; therefore, cellular senescence represents a potential therapeutic target in cancer treatment.

1.2 Cellular senescence and the characteristics of senescent cells

Cellular senescence has been described as the irreversible arrest of cell proliferation in response to a wide range of cellular stress. Telomere shortening during replication, sustained genomic damage, oxidative stress, oncogene activation or tumour suppressor activation and other forms of stress that activate the DNA damage response pathway can induce cellular senescence (Campisi, 2013, Ovadya and Krizhanovsky, 2018) (Faget et al., 2019). Although most of these cells have permanently lost their proliferative capacity, senescent cells have an intense paracrine activity with distinct biological effects on the surrounding cells depending on the physiological context (Coppe et al., 2010).

1.2.1 Characteristics and markers of cellular senescence

Senescent cells are usually identified by a group of characteristics, however, these senescent markers are not restricted to the senescent state and they are not exhibited in all senescent cells (Campisi, 2013). The most accepted markers to identify senescent cells are persistent proliferation arrest, enlarged and flattened morphology, increased activity of senescence-associated β -galactosidase (SA- β -gal), increased lysosomal content and nuclear alterations such as the formation of senescence-associated heterochromatin foci (SAHF) (**Figure 1**) (Hernandez-Segura et al., 2018, Faget et al., 2019).

When cellular senescence is induced by DNA damage, the expression of phosphorylated H2AX histone protein (γ H2AX) or the phosphorylated p53 are frequently used as markers of senescence, along with the downstream effectors of the DNA damage pathways, such as the CDKN2A/p16^{INK4a} and CDKN1A/p21^{CIP} cyclin-dependent kinase inhibitors (Hernandez-Segura et al., 2018). Other regularly used markers are the loss of Lamin-B1 and the senescence-associated heterochromatin foci (SAHF), that refers to nuclear foci with strong DAPI (4',6-diamidino-2-phenylindole) staining and increased repressive epigenetic marks (Sadaie et al., 2013).

The most frequently used and widely accepted senescence marker is senescence-associated β -galactosidase (SA- β -gal) staining. The enhanced SA- β -gal activity can be attributed to the increased lysosomal content, and it can be measured at a suboptimal pH of 6.0 in senescent cells (Lee et al., 2006, Morgunova et al., 2015). The increased lysosomal content can be connected to increased biogenesis of lysosomes but also to the impaired removal of old

lysosomes, which results in the accumulation of lipofuscin. Lipofuscins are granules containing oxidized proteins and lipids, and their accumulation has been suggested as a marker of senescence (Georgakopoulou et al., 2013).

Along with the different morphology of senescent cells, alterations in the composition of the plasma membrane can also be observed. For example, the expression of caveolin-1, the main component of the caveolae (small invaginations of the plasma membrane) was found to be increased in senescent cells. According to a recent study, caveolin-1 mediated signalling has an essential role in the development and regulation of cellular senescence (Volonte and Galbiati, 2020). Using a high-throughput mass spectrometry analysis, Kim et al. (2017) identified the cell surface protein DPP4/CD26 (dipeptidyl peptidase 4) as a new marker of cellular senescence, which was highly expressed on the surface of senescent human fibroblasts. Moreover, the overexpression or silencing of DPP4/CD26 consequently increased or decreased the expression of senescence markers in fibroblast cells (Kim et al., 2017a).

Other characteristics of senescence, such as production of senescence-associated secretory phenotype (SASP), the increased number of mitochondria and increased ROS (reactive oxygen species) production, or the enhanced expression of anti-apoptotic proteins from the Bcl-2 family were proposed to be used as a marker of senescence (Korolchuk et al., 2017, Park et al., 2018). However, due to the lack of specificity and heterogeneity of the metabolic alterations and SASP composition of senescent cells, it is currently difficult to use them as an unequivocal marker for senescence (Hernandez-Segura et al., 2017).

Bojko *et al.* (2019) demonstrated the diversity of senescence markers expressed in cancer cells by inducing senescence in various cancer cell lines using different treatments for senescence-induction and analysed the expression of several senescence markers, such as cell morphology and granularity (generally caused by increased lysosome content), SA- β -gal activity, DNA damage markers and secretory phenotype. Their results revealed a large variability in the expression of senescence markers in response to the different treatments and different susceptibility of cancer cells to senescence-induction. Moreover, unequivocal correlation between the expression of different senescence markers has not been detected (Bojko et al., 2019).

In summary, none of the markers described above can be used to conclusively identify senescent cells due to the various distinct senescence programs. Therefore, to achieve a better accuracy, the combination of several senescence markers should be used for the detection of senescent cells (Matjusaitis et al., 2016, Hernandez-Segura et al., 2018).

Despite the significant progression in the *in vitro* identification and investigation of senescent cancer cells, clinically applicable diagnostic tests to detect senescent cells in cytological or histological samples with high levels of confidence are still lacking. In fact, some of the hallmarks of senescence observed in cell cultures, such as morphological changes or cell cycle associated proteins are difficult to detect in patient samples, due to the structure of tumours and the non-specific expression of senescence-associated proteins (Wyld et al., 2020, González-Gualda et al., 2021). Moreover, the heterogeneity of senescent phenotypes together with the intrinsic complexity of tumours further restricts the assessment of senescence *in vivo*. Although SA- β -galactosidase staining is the most widely used marker of senescence in tissue samples, it can only be detected in fresh or cryopreserved samples due to its incompatibility with paraffin fixation, which is limiting its applicability (Hernandez-Segura et al., 2018, González-Gualda et al., 2021). Therefore, identifying new markers and developing the *in vivo* detection of senescent cancer cells are crucial to improve the diagnostic and therapeutic strategies used in clinical settings.

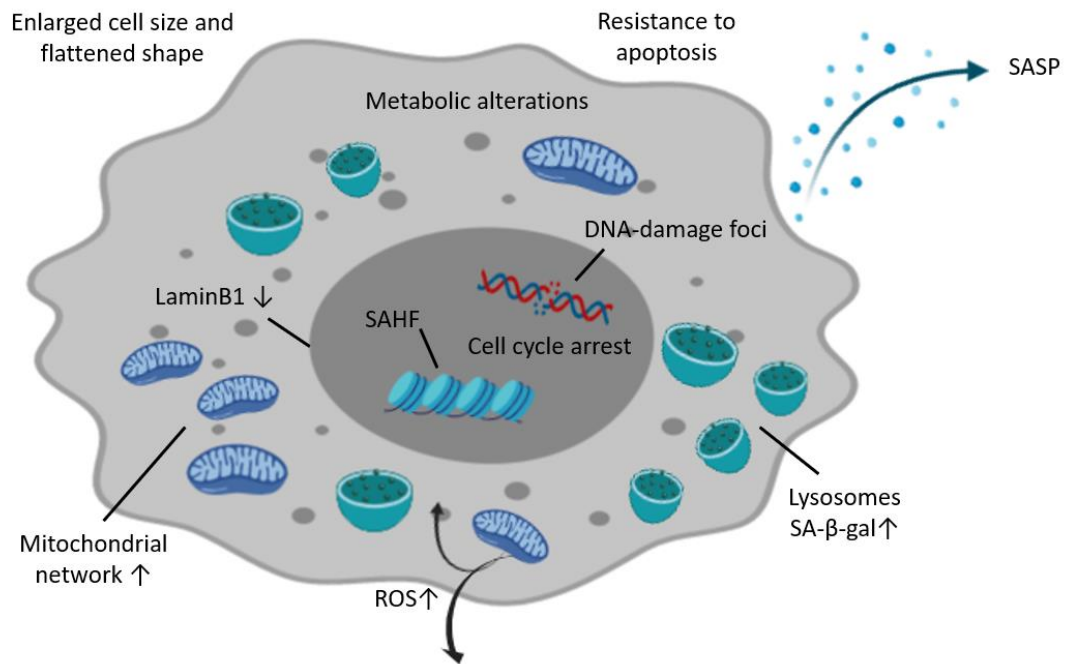


Figure 1. Characteristics of cellular senescence. The figure presents the most common markers of cellular senescence, that can be used to identify senescent cells in vitro. SAHF: senescence-associated heterochromatin foci; SASP: senescence-associated secretory phenotype; SA-β-gal: senescence-associated β-galactosidase expression. The figure was created with BioRender, modified from Yun M. H. *et al.* (2018) (Yun, 2018).

1.3 Senescence in cancer

The induction of senescence has been thought to serve as a protection against tumour development, but according to recent studies this hypothesis was found to be only partly true (Schosserer et al., 2017). In early experiments cellular senescence was considered to function as a tumour suppressor, halting the proliferation of potentially malignant cells. However, the SASP factors secreted by the senescent cells, along with the ability of cancer cells to escape from the senescence program can promote the proliferation of non-senescent tumour cells and induce the acquisition of stem cell properties (Milanovic et al., 2018, Faget et al., 2019, Triana-Martinez et al., 2020). According to recent studies the detrimental effects of senescence in cancer outweigh the beneficial effects, although, the impact of senescent cells in various types of tumours and the features of different senescent cell types are still not completely understood (Sieben et al., 2018).

1.3.1 Oncogene induced senescence (OIS)

It is known that oncogene activation promotes cell proliferation and tumorigenesis, however, it may induce senescence due to genetic stress caused by unbalanced mitotic signals (Courtois-Cox et al., 2008). Oncogene induced senescence (OIS) is considered to be a response mechanism against oncogenic stress, limiting tumour proliferation and progression, however its roles in cancer cells have not been fully elucidated. The most-studied examples are the senescence responses induced by the overexpression of Ras/Raf/MAPK pathway components or the inactivation of tumour suppressor genes, such as PTEN (Collado and Serrano, 2006, Mooi and Peeper, 2006). For example, Sarkisian et al. (2007) demonstrated that high increase in the expression of HRAS oncogene (encoding Raf) leads to tumour progression, however, only to a pre-malignant stage due to senescence, whereas lower increase in the expression of HRAS leads to malignant tumour formation (Sarkisian et al., 2007). Similarly, the occurrence of oncogene induced senescence has been described *in vivo* in murine and human pre-malignant tumours as well, but not in malignant tumours, suggesting that OIS functions as a barrier against malignant tumour progression (Collado and Serrano, 2010). Moreover, acute PTEN inactivation induced cellular senescence *in vitro* and *in vivo* via p53 pathway in prostate cancer and restricted further tumour progression, and it was detected in early-stage prostate cancer tissues (Chen et al., 2005). Oncogene induced senescence is associated with DNA

damage checkpoint response and its two major cellular regulators are the tumour suppressor p53 and Rb (retinoblastoma protein) (Campisi, 2013, Takebayashi et al., 2015, Liu et al., 2018). It has been described that the constitutive hyperproliferative signals result in high degree of DNA replication stress, leading to DNA double-strand breaks. The subsequent activation of the DNA damage response causes cell cycle arrest and the induction of cellular senescence (Patel et al., 2016).

1.3.2 Therapy induced senescence (TIS)

The induction of senescence has been detected in tumour tissues of patients with different types of cancer after receiving chemotherapy, indicating that it is a clinically relevant response to cancer therapy (Roberson et al., 2005, te Poele et al., 2002, Wagner and Gil, 2020). The activation of the senescence programme is a natural intrinsic response to cancer treatment in addition to the desired apoptotic response of tumour cells. In conventional cancer therapy, the onset of cellular senescence seems to improve the therapeutic outcome by keeping tumour proliferation in control (Ewald et al., 2010). For example, Schmitt et al. demonstrated in a lymphoma mouse model that mice harbouring tumours with a defect in apoptotic pathways but not in senescence pathway had a significantly better prognosis compared to mice with harbouring tumours with deficiency in both senescence and apoptotic pathways. Based on these results they described senescence induction as a desirable outcome of cancer treatment (Schmitt et al., 2002).

On the other hand, despite its potential initial benefit, chemotherapy or radiotherapy induced senescence can have a detrimental impact on cancer treatment due to the secretion of SASP or the ability of cancer cells to eventually escape from senescence and regain their proliferative capacity (**Figure 2**) (Ewald et al., 2010, Schosserer et al., 2017). It has been demonstrated that the increased expression of senescence markers in breast cancer patients is associated with tumour recurrence and poor overall survival of patients (Pare et al., 2016). Furthermore, Demaria et al. showed that therapy induced senescence promotes the adverse effect of chemotherapy, reflected in high risk of chemotherapy-induced fatigue in humans and mice, and the elimination of TIS cells several side-effects of chemotherapy, such as bone marrow suppression and cardiac dysfunction and improved the physical activity and strength of mice (Demaria et al., 2017). In a study investigating the effect of p53 mutation in breast cancer, it was found that p53-mediated senescence was associated with impaired apoptotic

response to chemotherapy and poor clinical outcome. Jackson et al. (2012) demonstrated that in response to chemotherapy, wild-type p53 activity induces proliferation arrest and cellular senescence instead of apoptosis, resulting in decreased tumour regression and early relapse in the MMTV-Wnt1 murine model (transgenic mice for studying breast cancer). However, chemotherapy treated tumours with mutant p53 bypassed the senescence induction, and due to abnormal mitosis, they eventually initiated p53-independent cell death leading to an improved therapy response (Jackson et al., 2012).

Senescent cells, particularly those that are developed in response to DNA-damaging therapy, are able to secrete chemo-protective SASP factors protecting neighbouring tumour cells from the same chemotherapeutic agents (Gilbert and Hemann, 2010, Campisi, 2013). Moreover, DNA damage-induced senescent tumour cells can escape from senescence, and potentially lead to a poor outcome of cancer treatment (Calcinotto et al., 2019). The senescence-specific microenvironment created by the secretome of senescent cancer cells can promote the emergence of more aggressive, stem-like cancer cells. These cancer cells with stemness properties together with the cells that escaped from therapy-induced senescence are likely to contribute to tumour relapse after chemotherapy (Milanovic et al., 2018, Triana-Martinez et al., 2020). In addition, senescence-inducing therapies can induce senescence in stromal cells of the tumour microenvironment as well. The senescent stromal cells can promote the proliferation of cancer cells and can spread the senescent state to other cells as well, via the secretion of SASP (Burd et al., 2013, Short et al., 2019). The effect of SASP and senescence-escape in cancer treatment will be described in more details.

Although there is growing evidence about the detrimental effect of therapy-induced, further research should be conducted to increase the amount of experimental data, which would contribute to better understand the impact of TIS in the clinical treatment of cancer (Ewald et al., 2010, Wyld et al., 2020).

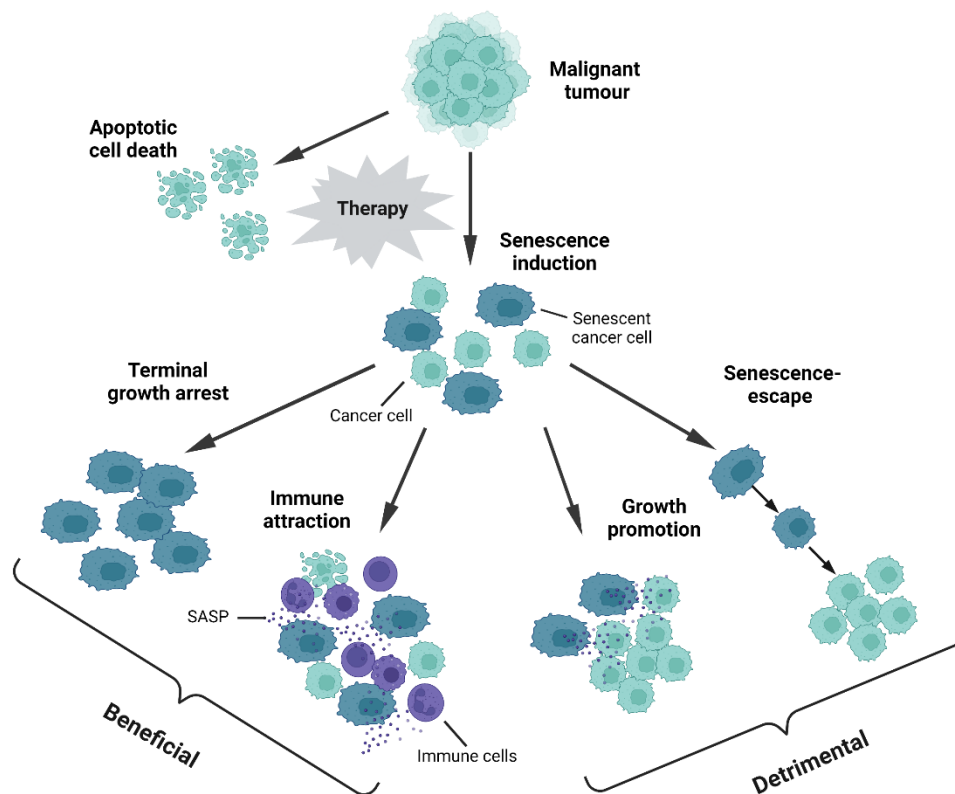


Figure 4. Beneficial and detrimental consequences of therapy induced senescence (TIS) in cancer. The beneficial effects of TIS include the irreversible cell cycle arrest of the cells (terminal growth arrest), and the activation of anti-tumour immune response via the cytokine secretion of senescent cancer cells (SASP). The detrimental effects of TIS include the growth promotion of non-senescent cancer cells via the secretion of cytokines and growth factors (SASP), and the ability of senescent cancer cells to escape from senescence and resume cell proliferation. SASP: senescence-associated secretory phenotype. Figure was created with BioRender, modified from *Kahlem et al. (2004)* (Kahlem et al., 2004).

1.3.3 Role of senescence in tumorigenesis

It has been demonstrated that human primary fibroblast cells undergo a limited number of cell divisions, and they eventually enter to an irreversible senescent state (Krtolica et al., 2001). However, *Romanov et al. (2001)* demonstrated that in contrast with fibroblasts, human mammary epithelial cells are able to restart proliferating after entering in a senescence state. Epithelial cells that appeared after senescence exhibited deficiencies in their telomeric sequences and chromosomal abnormalities similarly to early lesions of breast cancer, indicating that senescence-escape might be a key event in the early steps of the carcinogenesis of breast cancer (Romanov et al., 2001). Similarly to these observations, oncogene induced senescent mammary epithelial cells has been demonstrated to enter in a

reversible senescent state, that favours the appearance of malignant traits (Sherman et al., 2011).

There are different *in vitro* studies demonstrating the direct tumour-promoting role of senescent fibroblasts through paracrine SASP factors (Bavik et al., 2006, Lawrenson et al., 2010, Castro-Vega et al., 2015). It has been observed that pre-neoplastic or neoplastic cells co-cultured with senescent fibroblasts or treated with senescence-conditioned medium had an increased proliferation rate and were able to form tumours in mice (Krtolica et al., 2001). Moreover, the conditioned medium from senescent cells can not only promote tumorigenesis but also promotes the emergence of cancer cells with stem-like phenotype and increased chemotherapy resistance (Cahu et al., 2012, Canino et al., 2012). These results strongly suggest that the senescent microenvironment promotes the transition of premalignant cells towards a malignant state.

Cellular senescence imposes an upper limit on the proliferation of normal cells, therefore it can be considered as a barrier to tumour formation that cancer cells must bypass (Lee and Schmitt, 2019). In a comprehensive analysis of DNA methylation in senescent cells, the methylation pattern (for example global hypomethylation, CpG island hypermethylation and upregulation of DNA Methyltransferase 3 β) was found to be qualitatively similar to those in cancer. This study also suggested that senescence escaping/bypassing cells already harbour an epigenetic landscape that is likely to promote tumour formation (Cruickshanks et al., 2013). In addition, escaping from senescence has been postulated as a crucial step in tumour formation of many cancer types, supporting the concept that cellular senescence is a double-edged sword in tumour development (Schosserer et al., 2017). For example, p53 inactivation in cells without p16^{INK4a} expression (which normally ensures the growth arrest) results in resumed cell proliferation, posing a risk for malignant transformation (Campisi, 2013). Investigating oncogene induced senescent cancer cells, *Patel et al. (2016)* demonstrated that senescence-associated chromatin alterations can eventually lead to the derepression of hTERT (human telomerase reverse transcriptase), that allows the cells to escape from the senescent state. They found that in early neoplastic skin and breast tissue, high levels of hTERT expression were detected only in cells that expressed senescence features, suggesting that cancer cells emerged from senescent cells via the derepression of hTERT (Patel et al., 2016).

1.4 The role of the senescence-associated secretory phenotype (SASP) in cancer

The SASP secretome consists of different chemokines, cytokines, growth factors and proteases, with both tumour-promoting and antitumorigenic effects depending on the secreted molecules and the physiological conditions (Coppe et al., 2010, Calcinotto et al., 2019, Campisi, 2013). Different types of cells and different inducers of senescence generate a variation in the types of expressed SASP factors and in the magnitude of their expression (Wiley et al., 2017). The secretion of SASP factors is regulated by several pathways, including the ATM serine-protein kinase, CHK2 protein kinase, p44/MAPK3, p53 and nuclear factor κ B (NF- κ B) (Faget et al., 2019). However, the SASP factors are not distinctive to senescence. For example, in cancer-associated fibroblasts (CAFs) similar signalling pathways are activated, which generate a similar secretion profile (Peng et al., 2013).

1.4.1 Effect of SASP factors in anti-tumour immune responses

The early investigations of the effect of SASP on immune cells suggested that SASP factors promote an anti-tumour response and lead to the elimination of senescent cells. However, the impact of SASP in immune responses can vary, depending on the secreted chemokines, which depends on the types of senescent cells and the stage of tumorigenesis (Saleh et al., 2018, Faget et al., 2019). In most cases the prominent feature of the SASP is the ability to cause local chronic inflammation, promoting the recruitment and activity of immune cells to eliminate both senescent and cancer cells by CD4(+) T-cell-mediated adaptive immune response (Kang et al., 2011). The two major inflammatory cytokines, the IL-6 and IL-8 are expressed in response to different senescence inducers, and they can directly regulate the immune response along with the other inflammatory factors. SASP factors derived from senescent tumour cells and the associated stroma can promote an immune response against senescent cancer cells *in vivo* (Faget et al., 2019). Moreover, inducing senescence in cancer by ionizing radiation resulted in the expression of immunostimulatory cytokines, that activated the antitumor response in mice. According to Meng et al. (2012), this beneficial effect of the SASP can be exploited to increase the cytotoxic antitumor activity of immune cells (Meng et al., 2012).

On the other hand, some of the secreted proteins can create an immunosuppressive microenvironment that helps senescent cells to evade immune recognition and promotes chemotherapy resistance (Gilbert and Hemann, 2010). This immunosuppressive function of senescent cells was also demonstrated in hepatocellular carcinoma, promoting tumour growth, however, this effect was only found when senescence was induced in the later stages of malignancy (Eggert et al., 2016). In the case of the tumour protecting effects of the SASP, the onset of senescence in cancer or in the tumour stroma can maintain tumour dormancy and its potential recurrence. The cancer-associated inflammation caused mainly by the secretion of IL-6 and IL-8 by senescent cancer cells, can contribute to the spread of cancer cells to distant sites via lymphovascular systems and ultimately lead to metastasis (Saleh et al., 2018).

These observations support the view that SASP factors and the inflammation generated by them can have both beneficial and deleterious effect, depending on the secreted molecules and the physiological conditions (Campisi, 2013, Calcinotto et al., 2019).

1.4.2 SASP in cancer therapy

SASP factors have been reported to be expressed in tumour cells of patients receiving chemotherapy along with increased senescence markers, indicating that the secretion of SASP factors is a clinically relevant response to cancer therapy. SASP resulting from chemotherapy-induced senescent cells shares common secreted factors with other phenotypes of senescence, mostly the IL-6 and IL-8 cytokines (Sidi et al., 2011). In a meta-analysis of data collected from patients with different types of cancer, the elevated SASP cytokine levels were correlated with poor prognosis. In breast, prostate, ovarian, lung and colorectal cancer, increased IL-6 and IL-8 secretion have been found to correlate with greater probability of metastasis development and predicted a low overall survival (Saleh et al., 2018). In spite of the beneficial immunosupporting effect, SASP can contribute to therapy resistance and tumour growth, and it can promote the emergence of stemness features (**Figure 3**) (Cahu et al., 2012, Faget et al., 2019).

1.4.3 Role of SASP factors in metastasis

The influence of SASP factors in migration and invasion of tumour cells has been reported in different *in vitro* studies, where SASP promoted epithelial-to-mesenchymal transition (EMT)

and led to the emergence of metastatic features (Canino et al., 2012, Tato-Costa et al., 2016). The two major secreted cytokines, IL-6 and IL-8 can promote the proliferation and anchorage-independent growth of cancer cells, which are crucial for metastasis development (Fernando et al., 2011, Saleh et al., 2018). Another study, using MCF-7 breast cancer cells treated with IL-6 and IL-8, demonstrated that IL-6 and IL-8 induced the appearance of cells with altered cell morphology increased migration capacity, and the expression of EMT and stemness markers such as CD44, vimentin, ZEB-1, SNAIL-1 and Slug. Treatment with senescence-conditioned medium (SCM) collected from senescent fibroblasts, resulted in a similar outcome, and employing neutralizing antibodies against IL-6 and IL-8 abrogated the effects of SCM on MCF-7 cells. It is important to note that under normal conditions MCF-7 cells express low levels of IL-6 and IL-8 and they have a low metastatic capacity. Based on the results described above, SASP factors can induce the appearance of a more aggressive and invasive type of MCF-7 cells (Ortiz-Montero et al., 2017).

The *in vivo* effect of SASP on metastasis was also demonstrated by different experiments. For example, oncogene induced senescent breast cancer cells enhanced the metastatic potential of neighbouring tumour cells in a paracrine manner (Angelini et al., 2013). Moreover, SASP factors derived from senescent fibroblasts promoted pathological angiogenesis and increased vascularization in retinopathy via the secretion of vascular endothelial growth factor (VEGF) (Oubaha et al., 2016). Investigating the invasion of papillary thyroid carcinoma, senescent tumour cells were often detected in the invasive borderlines, lymphatic vessels and metastatic foci of lymph nodes, indicating a role of senescent cells in collective invasion of tumour cells. Cancer tissues where senescent cells were detected, exhibited an increased expression of IL-6, IL-8, and several matrix metalloproteinases. It was shown that oncogene induced senescent primary thyrocytes led to the collective invasion of non-senescent tumour cells *in vitro* and *in vivo*, via the secretion of a chemogradient regulated by CXCL12/CXCR4 signalling. CXCL12/CXCR4 signalling was also involved in anoikis (a form of programmed cell death that occurs in anchorage-dependent cells) resistance, a crucial mechanism required for metastasis, suggesting that senescent cells migrated alongside the non-senescent tumour cells (Kim et al., 2017b).

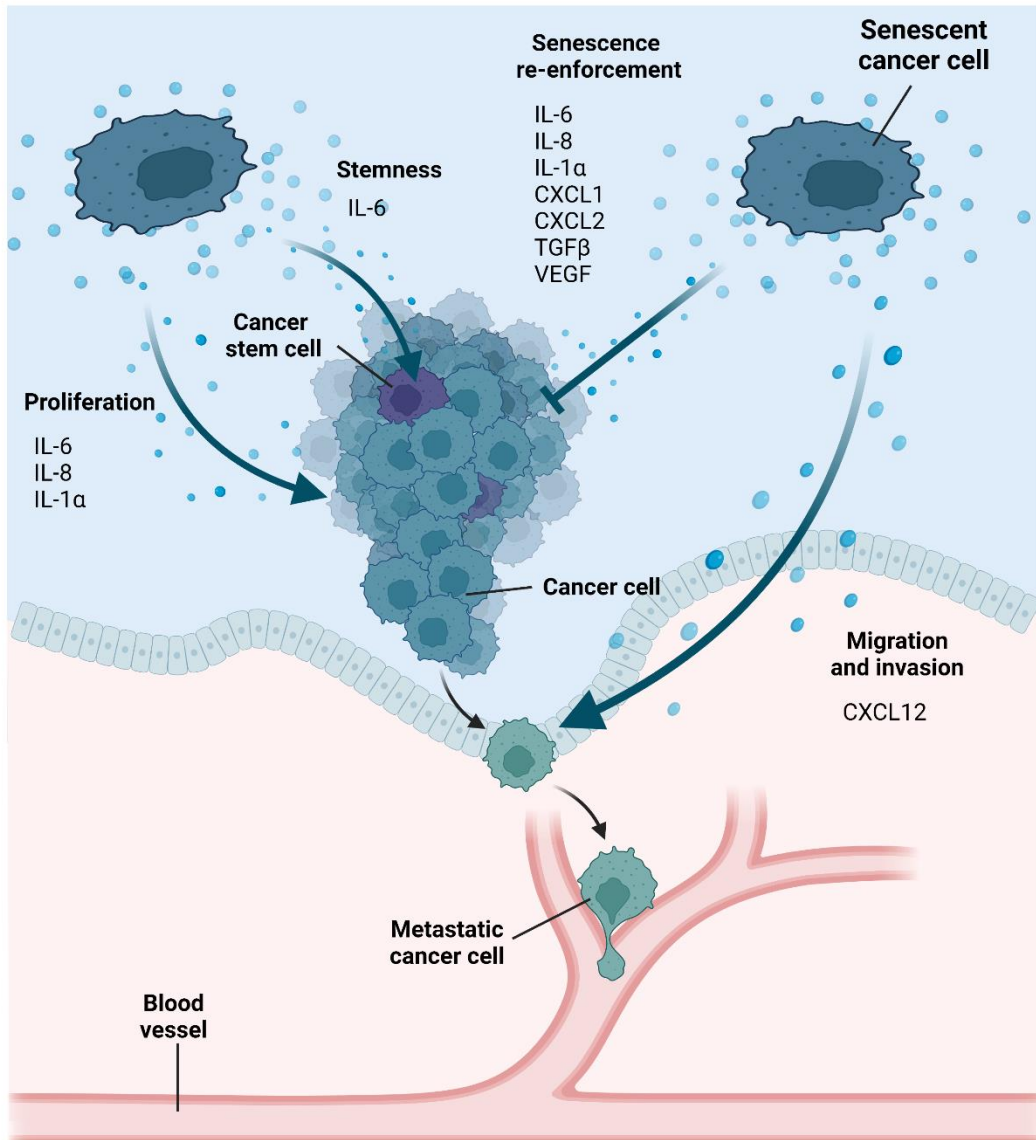


Figure 7. Different functions of senescence-associated secretory phenotype (SASP) in cancer. The figure presents the effect of SASP secreted by senescent cancer cells, such as the promotion of the cell proliferation of non-senescent cancer cells, the promotion of stem-cell development, the re-enforcement of senescent phenotype and the promotion of cancer cell migration and invasion, which leads to the development of metastasis. IL-6/8/1α: interleukin-6/8/1α; CXCL1/2/12: C–X–C motif chemokine ligand 1/2/12; TGFβ: transforming growth factor β; VEGF: vascular endothelial growth factor. Figure was created with BioRender, modified from *Faget et al. (2019)* (Faget et al., 2019).

1.5 The role of autophagy in senescence

In general, autophagy mediates the turnover of damaged organelles and proteins, contributing to the maintenance of cellular homeostasis, and it also functions as a survival pathway in response to cellular stress, such as cancer therapies (Baisantry et al., 2016, Hanahan and Weinberg, 2011). It has been described that the degradation and recycling of molecules via autophagy has a vital role in the development of the senescent phenotype by providing an additional energy source during a prolonged dormant-like state, which makes senescent cells more sensitive to autophagy inhibition (Goehe et al., 2012, Vera-Ramirez et al., 2018). In addition, Dörr et al. (2013) demonstrated in transgenic mouse lymphoma models, that senescent lymphomas rely on intact lysosomal protein degradation due to their elevated protein production (SASP secretion), and they were sensitive to autophagy inhibition. The addition of an autophagy inhibitor (bafilomycin A1) following chemotherapy improved the treatment outcome in lymphoma-bearing mice, indicating that autophagy inhibition is a promising target to eliminate senescent cancer cells (Dörr et al., 2013, Wagner and Gil, 2020).

Interestingly, a recent study revealed a previously unknown phagocytotic activity of chemotherapy-induced senescent cancer cells, allowing them to survive and adapt to the energy-consuming processes of SASP secretion. It was observed that senescent cancer cells engulfed neighbouring cells and processed them to their lysosomes for degradation. This newly discovered process has been proposed to provide an alternative source of energy and building blocks for therapy-induced cancer cells to enhance the survival of senescent cells during chemotherapy, allowing them to potentially escape from senescence (Tonnessen-Murray et al., 2019).

1.6 Senescence-escape

Cellular senescence has been described as the essentially irreversible arrest of cell proliferation (Campisi and d'Adda di Fagagna, 2007). However, cancer cells can challenge this definition of senescence. Now, it is known that the halted proliferation of cancer cells is not always terminal, and some senescent cells can restore their proliferation capacity, implying a dynamic nature of senescence in cancer (Sage et al., 2003). Therefore, senescence should not always be considered as an end point in the life cycle of a cancer cells, but rather as a resilient physiological state (Schosserer et al., 2017). Several studies, which are detailed below, described tumour cells that reverted to active proliferation after a non-proliferative senescent state through a process that has been termed senescence-escape.

By establishing a genetically switchable model, Milanovic et al. (2018) demonstrated that chemotherapy induced senescence cells can spontaneously escape from senescence and re-enter the cell cycle with an enhanced proliferation capacity and tumour-initiating potential compared to cancer cells that had never been senescent. This result was further supported by the enriched populations of senescent-escaped cells with stem-like features found in relapse tumours, driving a much more aggressive tumour growth (Milanovic et al., 2018). In a different study, drug induced senescent cancer cells, after an intermediate non-cycling stage, were able to escape senescence and generate chemo-resistant stem-like cells (Achuthan et al., 2011). A small subpopulation of colorectal cancer cells was also able to start proliferation after chemotherapy induced senescence. This subpopulation consisted of more transformed cells that were able to grow in an anchorage-independent manner and exhibited a more invasive phenotype. Analysing the gene-activation of these senescence escaped cells compared to the senescent population, revealed a significant overlap in the gene-expression of membrane-associated and extracellular proteins connected to increased invasiveness (Jonchere et al., 2015, Yang et al., 2017a). According to several independent studies senescence escaped cells appeared to be resistant to DNA-damaging agents and ionizing radiation, possibly due to the downregulation of apoptotic pathways (Elmore et al., 2005, Karimi-Busheri et al., 2010). However, contrary to these observations, other studies showed that senescence escaped cells did not present increased chemotherapy-resistance in comparison with non-senescent cells (Roberson et al., 2005, Yang et al., 2017a).

Different studies postulate a link between senescence-associated reprogramming and self-renewal capacity cancer cells; however, the real nature of this potential link is not completely understood. For instance, senescence and stemness seem to be co-regulated by overlapping signalling pathways, and senescent cells usually exhibit a stem cell phenotype with an increased plasticity (Lee and Schmitt, 2019). According to a new hypothesis about the origin of cancer stem cells (CSCs), CSCs may arise from senescent cancer cells resulting a hybrid phenotype including both stem cell features and senescent markers (Sotgia et al., 2019).

Altogether, after the termination of cancer treatment, the surviving senescent tumour cells could eventually restart their proliferation, that can possibly lead to cancer recurrence and poor outcome of cancer treatment (Chaffer and Weinberg, 2011, Yang et al., 2017a, Triana-Martinez et al., 2020).

1.6.1 Mechanisms of senescence escape

There are several studies about senescence escape, describing different proteins and pathways that can drive the conversion of senescent cells to proliferative cells. In an early study on p53-null human lung cancer cells, the expression of cell-cycle regulating cyclin-dependent kinase Cdk1/Cdc2 was found to be increased in senescence-escaped cells. Moreover, the inhibition of Cdk1/Cdc2 disrupted the escape from chemotherapy-induced senescence, possibly through mediating apoptotic pathways. These findings suggested that the selective overexpression of Cdk1/Cdc2 might represent a mechanism that promotes senescence-escape (Roberson et al., 2005). In subsequent experiments with p53-null cellular models, a subpopulation of cells emerged after a non-cycling senescent state with increased expression of the cyclin-dependent kinase inhibitor p21^{WAF1/Cip1}, exhibiting genomic instability and increased resistance to DNA-damage. However, p21^{WAF1/Cip1} is a well-known mediator of senescence, in case of p53 inactivation it can adopt a different function, creating cells with genomic instability, promoting senescence-escape and maintaining the viability of senescent cells. In fact, the continuous expression of p21^{WAF1/Cip1} leads to the saturation of two important cell-cycle regulating ubiquitin ligases (CRL₄Cdt2 and SCF^{Skp2}), therefore leading to the unabated activation of their other targets and consequently promoting cell-cycle progression (Galanos et al., 2016, Yosef et al., 2017, Georgakilas et al., 2017). Interestingly, in senescent breast cancer cells the accumulation of autophagy markers and a low rate of autophagic degradation activity (autophagic flux) has been detected, while in senescence-

escaped cells the formation of new autophagosomes and autophagic flux has been substantially increased, indicating a potential role of improved autophagic flux in the senescence-escape (Bojko et al., 2020).

Studying the escaping mechanism of chemotherapy-induced senescent colorectal and breast cancer cells postulated a role of anti-apoptotic pathways and transcriptional regulation in senescence-escape. Two anti-apoptotic proteins, Mcl-1 (induced myeloid leukaemia cell differentiation protein) and Bcl-xL (B-cell lymphoma-extra large) were found to be involved in maintaining the survival and promoting the anchorage-independent growth of senescence-escaped cells. The inactivation of these proteins increased the efficiency of chemotherapy treatment and decreased the emergence and survival of senescence-escaped cells *in vitro* (Jonchere et al., 2015). In a following study the authors further characterised the mechanism of senescence-escape, proposing a role for cdk4-EZH2-AP2M1 (cyclin-dependent kinase 4 - enhancer of zeste homolog 2 - AP-2 complex subunit mu) pathway in chemotherapy resistance and senescence-escape. Their results showed that during the early phase of chemotherapy-induced senescence (CIS) cdk4 and EZH2 are downregulated and then reexpressed in the emerging proliferating cell population. AP2M1 is a target of EZH2 and it was described to be involved in the transmission of SASP and in the regulation of CIS-escape (Le Duff et al., 2018). According to an additional study, senescence-escape can also be regulated through paracrine signalling. Thrombosporin-1 (TSP1) was found to be produced by senescent cells and it was able to prevent the escape of senescent cells. In addition, senescence-escaped cells expressed low levels of CD47, the receptor of TSP1, explaining the regulating function of TSP1. Interestingly, low expression of TSP1 detected in breast cancer patients was associated with tumour relapse after chemotherapy (Guillon et al., 2019).

In other studies, the escape of senescence was associated with the downregulation of mTOR (mammalian target of rapamycin), increased expression of pluripotency markers, enhanced Wnt signalling, along with decreased expression of DNA-damage and DDR (DNA-damage response) markers, such as γ H2AX, Rad51 and pDNA-PKcs^{Ser2056} (Chitikova et al., 2014, Milanovic et al., 2018). The role of hTERT expression and the reactivation of telomerase has also been associated with senescence-escape during therapy- and oncogene-induced senescence (Elmore et al., 2005, Patel et al., 2016). Interestingly, the mechanism of senescence-escape can also be connected to polyploidy (a condition in which cells have

multiple chromosomes). The emergence of polyploid senescent cancer cells during therapy induced senescence was observed in different independent studies, representing a transition stage towards senescence-escape. Moreover, increased polyploidization promotes senescence-escape and self-renewal, suggesting a link between senescence, polyploidy and stemness in order to overcome genotoxic stress (Wang et al., 2013, Erenpreisa and Cragg, 2013, Mosieniak et al., 2015).

1.6.2 Models for senescence escape

In most of the *in vitro* experiments the cellular model of senescence-escape is relatively similar. An early study by Elmore et al. (2005) demonstrated that a 2-hour treatment with a clinically relevant dose of doxorubicin induced early senescence arrest in MCF-7 breast cancer cells. After 2 to 3 weeks following the drug exposure, a clonal population arising from the surviving cells was isolated. To distinguish these cells from the more classic doxorubicin-resistant cells, they analysed the mRNA levels of MDR-1 (multi-drug resistance protein 1), which was highly expressed in doxorubicin-resistant cells but undetectable in the clonal population (Elmore et al., 2005). In a more comprehensive study, a variety of chemotherapeutic agents were analysed based on their ability to induce reversible senescence in H1299 lung cancer cells. The cell line was chosen for its favourable expression profile (-p16INK4A/+pRb/deleted-p53), contributing to the reversibility of cellular senescence. They found that after 4 days of treatment with camptothecin, nearly 90% of the lung cancer cells showed enlarged, flattened morphology, expressed SA- β -galactosidase, and stopped proliferating. After 18 to 24 days the senescent cells sporadically re-entered the cell cycle, forming colonies of cells with a highly similar expression profile compared to the senescent cells (Roberson et al., 2005). Yang et al. (2017) used A549 lung cancer cells treated with low dose doxorubicin for 7 days and confirmed senescence by cell-cycle arrest and positive staining for SA- β -gal. The senescent cells were cultured in drug-free medium for further 20-30 days, which resulted in the emergence of proliferating cell colonies. To determine whether this drug treatment was a selection to cancer stem cells or drug-resistant cells, RT-PCR analysis was performed using a focused cancer stem cell gene panel and senescence-associated gene panel. The cells derived from the colonies had a significantly overlapped expression profile with the senescent cells but not with cancer stem cells,

postulating that they originated from senescent cells. Furthermore, the senescence-escaped cells showed no increase in resistance to different drugs (Yang et al., 2017a).

Using switchable models is also an applicable approach to establish a model for senescence-escape. For example, Galanos et al. (2016) used a Tet-On/Off system to generate p21^{WAF1/Cip1}-inducible p53-null cell models. The Tet-On/Off technique is based on a bacterial regulatory system allowing the activation/silencing of gene expression by using tetracycline-derivatives, for example doxycycline (Das et al., 2016). Sustained expression of p21^{WAF1/Cip1} reduced cell proliferation and induced senescence in p53-null cells, however, 10 days later the senescent phenotype started to diminish and a fraction of non-senescent p21^{WAF1/Cip1} positive cells appeared (Galanos et al., 2016). In a different study, Milanovic et al. (2018) established a switchable system in Eμ-myc transgenic mice (mice overexpressing c-myc oncogene in the B-cell lineage resembling human lymphomas) using 4-hydroxytamoxifen (4-OHT)-inducible senescence mediators Suv39h1 (histone-lysine N-methyltransferase) or p53. The generated lymphoma cells could enter senescence only when exposed to both 4-OHT and doxorubicin. After incubation with drug-free medium, Suv39h1 or p53 was switched off again and the cells started to regain their proliferative capacity and to lose the expression of senescence-markers indicating senescence-escape (Schmitt et al., 2002, Milanovic et al., 2018).

Models for senescence-escape in cancer are generally based on studies in heterogeneous cell culture, where the origin of the escaped cell population cannot be precisely identified. To overcome this limitation of senescence-escape studies, Saleh et al. (2019) isolated the senescent cell population based on their increased cell size and SA-β-gal expression using fluorescence-activated cell sorting (FACS) and demonstrated that this senescence-sorted population was able to escape from senescence and generate tumours *in vivo* (Saleh et al., 2019a, Saleh et al., 2019b). This sorting strategy has been used by Alotaibi et al. (2016) as well to isolate the population of radiation induced senescent cell from non-senescent cells (Alotaibi et al., 2016). Furthermore, Was et al. (2017) used a time-lapse technique to monitor senescence-escape and demonstrated that the proliferating cell progenies emerging after senescence-induction originated from senescent cells (Was et al., 2017).

1.7 Targeting senescence in cancer therapy

The emergence of senescent tumour cells following neoadjuvant chemotherapy were described in patients with different types of cancer. Patients with therapy induced senescent tumours showed a significant decrease in survival and the symptoms of accelerated physiological aging (Sidi et al., 2011, Sanoff et al., 2014, Wood et al., 2016). Moreover, increased numbers of senescent tumour cells correlated with adverse clinical outcome and resistance to first- and second-line treatments (Wang et al., 2016b, Myriantopoulos et al., 2019).

Chemotherapies can induce cellular senescence in the surrounding stroma and in normal tissues as well, which can be responsible for debilitating side effects and the development of local and systemic inflammation. Furthermore, in a murine model, chemotherapy induced senescent non-tumour cells promoted the spread of cancer cells and led to cancer relapse, in response to a variety of DNA-damaging agents administered at a biologically effective dose. The elimination of therapy-induced senescent cells reduced the adverse side-effects of chemotherapy, suggesting that development of drugs to remove senescent cells might be a promising strategy to improve the outcome of current chemotherapies and to alleviate the post-therapeutic morbidities connected to physiological aging (Demaria et al., 2017, Myriantopoulos et al., 2019).

1.7.1 Anti-SASP and SASP modulating therapies

SASP factors are considered to be the most important mediator of the adverse effects of cellular senescence, therefore several approaches aim to suppress or modulate the SASP to improve the outcome of tumour therapies (Short et al., 2019). For example, treatment with the mTOR inhibitor rapamycin successfully abrogated the tumour-promoting effects of senescent fibroblasts, via the inhibition of IL-1 α secretion and consequently the IL-6 secretion by senescent cells (Herranz et al., 2015). The SASP reducing effect of mTOR inhibition by rapamycin has also been reported in other *in vitro* and *in vivo* models (Faget et al., 2019). Another promising drug with anti-SASP effect is metformin, that is a common medication for type 2 diabetes (Nasri and Rafieian-Kopaei, 2014). Metformin has been demonstrated to reduce the secretion of pro-inflammatory SASP factors possibly through the inhibition of NF- κ B signalling (via the inhibition of the nuclear translocation and activation of NF- κ B

complexes), which is the main pathway for regulating pro-inflammatory gene expression. Furthermore, the tumour-promoting effect of senescent-conditioned medium on prostate cancer cells was reduced by using the medium collected from metformin treated senescent cells (Moiseeva et al., 2013). In another study, simvastatin, an antihyperlipidemic drug, was found to be effective to decrease IL-6 secretion by senescent cells and reduced the tumour-promoting effect of senescent-conditioned medium on breast cancer cells (Liu et al., 2015). The analysis of a wide range of anti-inflammatory substances, such as corticosterone, cortisol and other glucocorticoids, showed that they were effective in reducing the secretion of certain SASP factors, including several proinflammatory cytokines independently from the process of senescence induction (Laberge et al., 2012).

Other promising molecules and signalling pathways have been identified, that can be targeted to reduce the secretion of SASP factors. For example, the inhibition of p38MAPK or the JAK2/STAT3 axis has been associated with the inhibition of SASP secretion or the reduction of the immunosuppressing SASP response (Toso et al., 2014, Alimbetov et al., 2016). Targeting the metabolism, autophagy or proteostasis pathways of secretion active senescent cells, has also been proposed as a novel approach to suppress the adverse effects of SASP during cancer therapy (Dörr et al., 2013). Moreover, several clinically approved interleukin inhibitors can be utilised in combination with chemotherapy, however, these strategies have not been investigated in preclinical models of cancer. For example, the IL-1 receptor inhibitor anakinra, the IL-6 receptor inhibitor siltuximab or tocilizumab, and the TNF- α inhibitor infliximab could be promising candidates for drug repurposing as regulators of the effects of SASP (Sieben et al., 2018, Saleh et al., 2018, Faget et al., 2019).

Besides several strategies to inhibit SASP, the beneficial effects of SASP, such as the stimulation of anti-tumour response, can be exploited for therapeutic purposes. Screening a wide range of chemotherapeutic agents for senescence induction in neuroblastomas demonstrated distinct effects of the SASP response associated with different senescence inducing agents. For example, low-dose treatment with topotecan, a topoisomerase inhibitor, induced a tumour-suppressing cytokine profile promoting an anti-tumour response (Taschner-Mandl et al., 2016). In another study, senescent tumour cells induced by ionizing radiation and veliparib (ABT-888) treatment promoted anti-tumour immune response by secreting cytokines, that activated cytotoxic T lymphocytes. Injecting these senescent cells into tumour-

bearing mice enhanced the effects of radiotherapy, resulting in the elimination of tumour cells (Meng et al., 2012).

Several promising approaches has been described to target SASP and based on the available data and results, a synergistic effect with chemo- and radiotherapy may be feasible in clinical settings. However, to potentiate the effect of anti-SASP and SASP modulating therapies, further testing of these strategies in combination with conventional tumour therapies is essential (Sieben et al., 2018, Saleh et al., 2018, Short et al., 2019).

1.7.2 Senolytics in cancer therapy

Senolytics are compounds that have been developed to selectively eliminate senescent cells without compromising the viability of non-senescent cells (Kirkland and Tchkonja, 2020). Using senolytics as adjuvant cancer therapy can be beneficial to improve therapeutic outcome and reduce the risk of tumour recurrence. The mechanism of senolytics is primarily based on apoptosis induction in senescent cells, which are otherwise able to resist cell death (Saleh et al., 2018). For example, inhibitors of Bcl2, such as ABT-263 and ABT-737, have been demonstrated to effectively induce apoptosis in senescent cells (Yosef et al., 2016). ABT-737 and ABT-263 (navitoclax) administered with either ionizing radiation or different chemotherapeutic agents, effectively sensitised tumour cells to radio- or chemotherapy and selectively induced apoptosis in senescent cells *in vitro* and *in vivo* (Lieber et al., 2010, Oakes et al., 2012, Faget et al., 2019). Furthermore, navitoclax demonstrated a synergistic effect in PARP inhibitor-induced senescent breast cancer cells, but only when administered after prolonged PARP-inhibitor treatment, suggesting that navitoclax specifically targeted senescent cells (Fleury et al., 2019). While these preliminary results appear to be promising, the upregulation of Bcl2 in senescent cells is not ubiquitous, therefore some senescent cells might be resistant to Bcl2 inhibitors (Short et al., 2019).

Apart from Bcl2 inhibition, other strategies have been developed to selectively induce apoptosis in senescent cells. According to several studies, two tyrosine kinase inhibitors, quercetin and dasatininb eliminated senescent cells *in vitro* and *in vivo*, possibly via the inhibition of PI3K signalling and the inhibition of other tyrosine kinases of anti-apoptotic pathways (Fan et al., 2022, Novais et al., 2021, Saccon et al., 2021). According to the preliminary results of a clinical study, the combination of dasatinib and quercetin significantly

decreased the effect of senescent cells in patients with diabetic kidney disease (Hickson et al., 2019). Interestingly, dasatinib has been used as targeted drug therapy in some types of leukaemia, and several anti-cancer properties of quercetin have also been described (Brito et al., 2015, Keating, 2017). The connection between the anti-cancer and senolytic activity of dasatinib and quercetin could be exploited for therapeutic purposes (Myriantopoulos et al., 2019). Another promising senolytic is the FOXO4 D-retro-inverse peptide (FOXO4-DRI), which induced apoptosis in senescent cells *in vitro* and *in vivo* by disrupting the interaction of FOXO4 with p53, and it decreased several aging-associated phenotypes as well. However, the senolytic effect of FOXO4-DRI has yet to be investigated in cancer models (Faget et al., 2019). Furthermore, two well-known antibiotics, azithromycin and roxithromycin were also described as novel senolytic drugs targeting senescent fibroblast cells *in vitro*, indicating a promising approach to selectively eliminate senescent cells (Ozsvari et al., 2018). However, further experiments are required to determine the mechanism of its senolytic effect and to confirm its senolytic activity *in vivo*. One suggestion for its senolytic activity is that it can disrupt the degradation of autophagosomes in the targeted cells and the senescent cells could be more sensitive to the disruption of autophagic activity (Ozsvari et al., 2018, Renna et al., 2011). The metabolic reprogramming of senescent cancer cells could also be exploited selectively by treatment strategies. For example, blocking glucose utilization or autophagy pathways led to the elimination of therapy induced senescent lymphomas and promoted *in vivo* tumour regression (Dörr et al., 2013).

Senescence-targeted therapies represents a novel strategy to increase the senolytic effects and decrease the potential side-effects of senolytic drugs by selectively targeting the senescent cells based on the expression of a senescence marker. For example, the newly identified senescence marker, the cell surface protein DPP4/CD26, can be a promising senescence-specific target for anti-DPP antibody-directed immunotherapy and for enhancing the selectivity of the previously described senolytics. In fact, it has already been described that DPP4 selectively sensitized senescent fibroblasts to cytotoxicity by natural killer cells (Kim et al., 2017a). The senescence-associated β -galactosidase (SA- β -gal) can also be used to selectively target senescent cells. Recently, Cai et al. (2020) designed a prodrug that is specifically modified by lysosomal β -gal to generate cytotoxic gemcitabine in senescent cells. This prodrug selectively induced apoptosis in senescent cells, decreased senescence-

associated gene expression and inflammation, and improved physical function in aged mice (Cai et al., 2020).

The concept of intentional senescence-induction and the subsequent elimination of senescent cancer cells as a two-hit lethal strategy has been described as a promising novel anticancer therapy (Lee and Schmitt, 2019, Dörr et al., 2013). For example, Wang et al. (2017) used a CRISPR-mediated genetic screen and compound screens to identify targets for senescence induction, sensitising cancer cells to senolytic drugs, and afterwards they demonstrated the efficacy of this two-hit strategy in mouse xenograft models as well. According to these studies, the combination of a CDC7 inhibitor and an antidepressant agent, sertraline, effectively induced apoptotic cell death in hepatocellular carcinoma cells and resulted in a significant reduction of tumour growth *in vivo*. In this combination therapy the CDC7 inhibitor has been used as the inducer of senescence and sertraline exhibited a senolytic effect via the inhibition of mTOR signalling (Wang et al., 2017, Wang et al., 2019, Wang and Bernards, 2018).

Together, these studies support the concept that involving senolytics in tumour therapies can be of benefit, however additional studies are required to determine safety and efficacy of this strategy. These combination therapies would be the most effective, when the cells have reached a mature senescent phenotype but not yet have escaped from senescence, therefore the timing of the senolytic intervention would be crucial (Sieben et al., 2018, Faget et al., 2019).

1.7. Dipeptidyl peptidase IV (DPP4/CD26)

Dipeptidyl peptidase IV (DPP4/CD26) is a transmembrane glycoprotein with serine exopeptidase activity capable of cleaving polypeptides, by removing the N-terminal dipeptides from several peptides preferably after proline or alanine. Due to this enzymatic activity DPP4 can regulate the activity of different bioactive peptides including neuropeptides, growth factors, incretin hormones and chemokines as well (Mentlein, 1999). The truncation of these peptides by DPP4 either results in the alteration of receptor sensitivity or the inactivation of receptor response, leading to decreased biological activity (Klemann et al., 2016) (**Figure 4**). It is active as a homodimer, however, it also has an enzymatically active soluble monomer form, that can be found in body fluids. It is widely expressed on epithelial and endothelial cells with higher expression in the liver, small intestine, and kidney and on the surface of immune cells (Boonacker and Van Noorden, 2003). Besides its enzymatic function, DPP4 can function as an adhesion molecule for proteins such as eADA (ecto-adenosine deaminase), which is involved in purine metabolism, and to extracellular matrix proteins such as collagen and fibronectin (Boonacker and Van Noorden, 2003, Havre et al., 2008).

1.7.1. Physiological functions of DPP4/CD26

CD26/DPP4 was originally identified as a T cell differentiation antigen, that is mainly expressed on the surface of CD4⁺ CD45RO⁺ memory T cells, however, its expression is significantly increased following T cell activation (Ohnuma et al., 2008). Besides being a marker of T cell activation, CD26/DPP4 stimulates T cell proliferation, and it is associated with T cell signal transduction by functioning as a costimulatory molecule. Costimulatory molecules are defined as cell surface molecules that are able to modulate TCR-associated (T cell receptor complex) signalling, for example, the binding of CD26 and ADA can form a complex with AB2 receptors on antigen-presenting cells, which results in the modulation of T cell functions (Hatano et al., 2013). In addition, CD26 has also been demonstrated to be related to the transendothelial migration of T-cells (Ohnuma et al., 2008). Besides being a biomarker of T cell activation, increased CD26 expression has been associated with B cell activation and NK cell proliferation as well (Hatano et al., 2013, Klemann et al., 2016). As described before, DPP4/CD26 plays a role in the regulation of cytokine activity due to its proteolytic activity.

The post-translational modification of chemokines by DPP4/CD26 is an established regulatory mechanism of the biological activity of chemokines (Mortier et al., 2016, Metzemaekers et al., 2016). A wide range of chemokines has been reported to be truncated by DPP4, however, an analysis of catalytic parameters demonstrated a significantly increased selectivity for the truncation of CXCL12/SDF1 (C-X-C motif chemokine 12/stromal cell-derived factor 1) and CCL22 (C-C motif chemokine 22) (Lambeir et al., 2001). It has also been demonstrated that the inhibition of DPP4 activity increased the secretion of pro-inflammatory cytokines, including IL-6 (interleukin-6) and IL-8 (interleukin-8), indicating a role of DPP4 activity in the regulation of inflammation (Wronkowitz et al., 2014).

Although initially CD26/DPP4 has been recognised for its potential immunologic function, DPP4 became a well-known target for the treatment of type 2 diabetes mellitus (Herman et al., 2007). An early proof of the therapeutic potential of DPP4 inhibition was revealed by Marguet et al. (2000) by using a DPP4-deficient mouse model, that exhibited increased glucose tolerance, improved balance of glucose homeostasis and elevated levels of active GLP-1 (Glucagon-like peptide-1) (Marguet et al., 2000). GLP-1 belongs to the group of insulinotropic incretin hormones, that is produced and secreted by intestinal endocrine cells in response to food intake. Incretins are able to enhance insulin secretion, thus increase glucose clearance which leads to decreased blood sugar levels, however, due to their rapid inactivation through enzymatic cleavage by DPP4, they have a half-life of only a few minutes (Mortier et al., 2016). Therefore, the inhibition of DPP4 has been established as a therapeutic target to prolong the half-life of incretins, improving glucose tolerance in diabetic patients. Sitagliptin (Januvia) is the first inhibitor that has been approved by the Food and Drug Administration (FDA) in 2006, and currently there are nine commercially available DPP4 inhibitors known as gliptins that are approved for the treatment of type 2 diabetes mellitus (Scheen, 2012). Although DPP4 inhibitors are well tolerated by diabetic patients, the previously described immunologic function of DPP4/CD26 should be considered in long-term therapies (Amori et al., 2007, Scheen, 2012).

1.7.2. Role of DPP4/CD26 in cancer

The expression of DPP4/CD26 has been investigated in various types of cancer, however, it shows a high diversity of expression and function in different cancer cell type. Due to its complex biological functions, DPP4/CD26 has been described as a tumour promoter and

tumour suppressor as well, depending on tumour localisation, cell type and tumour microenvironment (Enz et al., 2019) (**Figure 4**). The role of DPP4/CD26 in tumour progression can be attributed either to its enzymatic activity, or its connection to extracellular matrix proteins and cell adhesion proteins, as well as its immunologic function (Havre et al., 2008).

Early studies in melanoma cells described a potential tumour suppressive function of DPP4/CD26. They demonstrated that in melanoma, DPP4/CD26 expression is inversely related to tumour development, reflected in high expression of DPP4/CD26 in normal melanocytes and a decreased expression in malignant melanoma cells (Morrison et al., 1993, Van den Oord, 1998). Similar results were described in neuroblastoma cells, where normal neuronal cells showed a significantly higher expression of DPP4/CD26 compared to neuroblastoma cells, and the decreased expression of DPP4/CD26 was connected to increased cell proliferation in glioma cell lines and in high-grade glioma derived primary cell cultures (Havre et al., 2008). Moreover, in both melanoma and neuroblastoma, the restoration of DPP4/CD26 expression could revert the malignant phenotype (Morrison et al., 1993, Van den Oord, 1998, Havre et al., 2008). In prostate cancer, the loss of DPP4/CD26 has been associated with increased metastatic potential and the inhibition of DPP4/CD26 activity resulted in enhanced invasion and metastasis of prostate cancer cells *in vitro* and *in vivo*. This study also suggested that DPP4 suppressed the malignant phenotype of prostate cancer cells by inhibiting bFGF (basic fibroblast growth factor) and CXCL12-mediated signalling pathways due to its enzymatic activity (Sun et al., 2008).

On the other hand, tissue samples from patients with malignant mesothelioma has been demonstrated to express high levels of DPP4/CD26, however, it was not detected in benign mesothelial tissue samples, suggesting that DPP4/CD26 might have a role in the progression of mesothelioma (Inamoto et al., 2007). Analysing the potential function of DPP4 in mesothelioma cells revealed that DPP4 acts as an extracellular matrix binding protein, that binds to fibronectin and collagen I (Enz et al., 2019). In addition, DPP4/CD26 has also been described as a CSC marker and as a promising target for the treatment of malignant mesothelioma (Ghani et al., 2011, Angevin et al., 2017). The cell surface expression of DPP4/CD26 has been described as a negative prognostic marker in hematologic malignancies. For example, in B-cell chronic lymphocytic leukaemia, high levels of CD26/DPP4 expression is associated with increased tumour mass and clinical disease stage, moreover, it was identified

as a stem cell marker and as a potential therapeutic target in chronic myeloid leukaemia (Cro et al., 2009, Herrmann et al., 2014, Matuszak et al., 2016). In T cell malignancies, such as in T-cell lymphoblastic lymphoma and T-cell acute lymphoblastic leukaemia, the cell surface expression of CD26/DPP4 has been described as a marker for aggressiveness and it was associated with poor prognosis and survival (Chitadze et al., 2021).

The expression of DPP4/CD26 has been intensely studied in colorectal tumours, where it was identified as a marker of stemness (Pang et al., 2010). In colorectal tumours the expression of CD133 is a predictive indicator of poor prognosis and it is used as a marker of cancer stem cells (CSC) (Park et al., 2019). It has been demonstrated that DPP4/CD26 is co-expressed with the CSC marker CD133 and the increased expression of DPP4/CD26 was associated with migration, chemoresistance and survival in colorectal cancer cells. Moreover, isolated CD26+ cells developed distant metastasis when injected into mouse and CD26+ cells have been found in metastatic colorectal tumours in the liver (Pang et al., 2010, Cheung et al., 2017). In colorectal cancer patients CD26+ cells were present in both primary and metastatic tumours, however, DPP4/CD26 expression levels were significantly elevated in patients with distant metastasis (Davies et al., 2015). Furthermore, increased expression of DPP4/CD26 in primary tumours was predictive of the development of metastasis and was associated with advanced tumour staging and significantly worse overall survival of colorectal cancer patients (Lam et al., 2014). These results were supported by a database study evaluating the effect of DPP4 inhibitors in diabetic patients diagnosed with colorectal cancer, which demonstrated that DPP4 inhibition is associated with improved overall survival (Bishnoi et al., 2019).

In breast cancer DPP4/CD26 exhibits a heterogeneous expression pattern, depending on the cell type and individual characteristics, moreover, high levels of DPP4/CD26 expression can be detected in patient samples derived from both oestrogen receptor positive and negative tumours as well (Leccia et al., 2012). Choi et al. (2015) demonstrated that the epithelial-mesenchymal transition was enhanced by DPP4 activity via EGF (epidermal growth factor) induced MEK/ERK and JNK/c-Jun signalling pathways in MCF-7 cells. Furthermore, in mouse metastatic breast cancer model, tumour development was suppressed by DPP4-inhibition, whereas the overexpression of DPP4 resulted in increased tumour formation (Choi et al., 2015). Consistent with these observations, the upregulation of CD26/DPP4 was detected in metastatic breast cancer cells in vitro and in ex vivo metastatic breast cancer tumour explants

as well (Donnenberg et al., 2018). It has been suggested that the role of DPP4/CD26 in the metastasis of breast cancer is connected to its extracellular matrix binding ability, which can increase the adhesion of breast cancer cells, leading to the formation of metastasis (Enz et al., 2019).

As described before that DPP4/CD26 can function as a tumour suppressor or tumour promoter in different tumour types, however, in certain types of cancer both functions has been reported. For example, it has been reported that non-small lung cancer cells present lower expression of DPP4/CD26 compared to normal lung epithelial cells, however, Jang et al. (2019) found a significantly higher expression of DPP4/CD26 in lung adenocarcinoma samples compared to normal tissues (Jang et al., 2019, Zhang et al., 2021). Moreover, the DPP4-inhibitor vildagliptin has been demonstrated to reduce lung cancer growth possibly via the regulation of macrophage and NK cell activity, and DPP4-inhibition was associated with improved overall survival of lung cancer patients (Jang et al., 2019, Bishnoi et al., 2019). Similarly to the these observations, DPP4/CD26 is expressed in normal endometrial cells and down-regulated in endometrial adenocarcinoma cells, although, DPP4 activity has also been associated with increased proliferation and tumorigenesis of endometrial carcinoma cells (Khin et al., 2003, Yang et al., 2017b, Yang et al., 2021).

Although DPP4/CD26 has been described as a prognostic marker in different types of cancer and a marker of cancer stem cells in colorectal cancer, DPP4/CD26 is rarely used as a therapeutic target in cancer treatment. However, a humanized anti-CD26 IgG1 monoclonal antibody (YS110) has been developed for the treatment of mesothelioma and it demonstrated preclinical anti-tumour and it was well tolerated by mesothelioma patients (Angevin et al., 2017). Furthermore, in renal cell cancer (RCC) DPP4 inhibitor treatment decreased tyrosine kinase inhibitor (TKI) resistance *in vitro* and *in vivo*, and DPP4 inhibitors increased the efficacy of TKI treatment in type 2 diabetes patients suffering from RCC (Kamada et al., 2021). Results from clinical database studies demonstrated that DPP4 inhibition is associated with improved overall survival of diabetic patients diagnosed with colorectal and lung cancer (Bishnoi et al., 2019). Although, regarding the risk of developing metastasis opposing effect of DPP4-inhibitors has been described. In certain cases DPP4 inhibitor therapy was not associated with a higher risk of metastasis (Rathmann and Kostev,

2017, Noh et al., 2019), however, in other cases DPP4 inhibitors increased the risk of metastasis in diabetic patients (Wang et al., 2016a).

Altogether, DPP4/CD26 expression has been identified as a promising therapeutic target and as a diagnostic biomarker in different types of cancer. However, further experimental and clinical studies would be essential to better understand the functional role of DPP4/CD26 in different tumour types and to repurpose DPP4 inhibitors for cancer treatment (Havre et al., 2008, Enz et al., 2019).

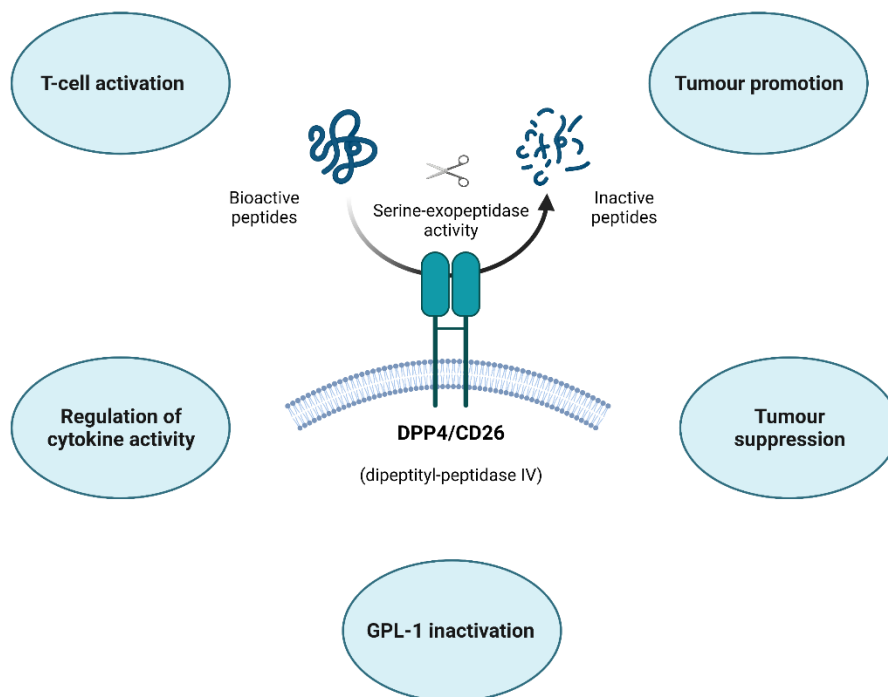


Figure 10. Different functions of DPP4/CD26 activity. The figure presents various functions of DPP4, such as T-cell activation, regulation of cytokine activity, GPL-1 (glucagon-like peptide-1), tumour suppression and tumour promotion, based on its role in the regulation of bioactive peptides. Figure was created with BioRender.

1.8. Challenges and limitations in the investigation of therapy-induced senescence in cancer – Summary

Although cellular senescence has been described as a one of the main hallmarks of cancer, and there is growing evidence about its detrimental effect on the outcome of cancer therapies, the impact of therapy induced senescence (TIS) is rarely considered in the clinical treatment of cancer. The detection of senescence in patient samples represents one of the main challenges in the investigation of TIS. Despite the significant progression in the *in vitro* identification and investigation of senescent cancer cells, clinically applicable diagnostic tests to detect senescent cells in cytological or histological samples with high levels of confidence are still lacking. The *in vivo* assessment of senescence is limited by the heterogeneity of senescent phenotypes, the intrinsic complexity of tumours and the non-specific expression of senescence-associated proteins in cancer cells. Therefore, identifying new markers and developing the *in vivo* detection of senescent cancer cells are crucial to improve the diagnostic and therapeutic strategies used in clinical settings. The heterogeneity of senescent phenotypes results in high variability of experimental results, originating from studies based on different tumour types and different mechanisms of senescence-induction, which represents a major obstacle to better understand the impact of TIS in cancer treatment, and to therapeutically target senescent cancer cells. Although cellular senescence has been originally defined as an irreversible form of cell cycle arrest, in TIS models the emergence of proliferative senescence-escaped cells was reported by several research groups, challenging the definition of senescence. This contradiction with senescence definition limits the number of studies, that are focused on the mechanisms and consequences of senescence-escape. The investigation of the characteristics of senescent cancer cells and the underlying mechanism of senescence-escape is essential to better understand the impact of TIS in cancer therapy, and to identify potential targets to eliminate senescent cancer cells.

2. Aims

Despite the general concept that senescence plays a tumour-suppressive role in various settings, the presence of senescent cells in cancer could be potentially detrimental, leading to therapy resistance and tumour relapse. Investigating the characteristics of senescent cancer cells in response to different senescence-inducing drugs could help to better understand the role of therapy-induced senescence in cancer treatments, and to identify potential targets to eliminate senescent cancer cells. Although there are numerous reports about the effect of therapy-induced senescence (TIS) in cancer, its impact on cancer therapy is still rarely considered in clinical settings; and some aspects of the topic, such as senescence-escape, are still not completely understood.

The aim of this research project is to investigate the characteristics of senescent cancer cells using *in vitro* TIS and senescence-escape models, and to investigate potential markers and treatment strategies, that could be exploited to improve the outcome of cancer therapies.

The objectives of the project are:

- I. Optimising, analysing and comparing different *in vitro* models for therapy-induced senescence using breast cancer cells
 1. Inducing senescence in MCF-7 and MDA-MB-231 human breast cancer cells using bromodeoxyuridine (BrdU), gemcitabine (GEM) and Palbociclib (PALBO)
 2. Analyse and compare the expression of different senescence markers, such as cell morphology, SA- β -galactosidase expression, cell cycle/proliferation arrest and cytokine (SASP) secretion
- II. Developing a two-hit treatment strategy using azithromycin as a senolytic drug
 1. Treat BrdU-, GEM- and PALBO-induced senescent cells with azithromycin and analyse its senolytic effect by SRB assay
 2. Investigate the effect of azithromycin in autophagic degradation by immunostaining assay
- III. Investigating the cell surface protein DPP4 (Dipeptidyl peptidase-4; CD26) as a marker of cellular senescence in cancer and identifying its potential function

1. Measure the expression of DPP4/CD26 on the surface of BrdU-, GEM- and PALBO-induced senescent cells
 2. Silencing the expression of DPP4 in MCF-7 and MDA-MB-231 cells and investigate its effect on senescence-induction and the expression of senescence markers (cell morphology, proliferation arrest, SA- β -gal expression)
- IV. Establishing a method to quantify and isolate senescence-escaped cells for further investigations
1. Establishing a method for the quantification of senescence-escape
 2. Investigate the effect of DPP4 silencing in senescence-escape by using the previously established method
 3. Isolate senescence-escaped cells for functional assays, such as mammosphere formation assay, migration assay and colony formation assay

These research objectives are expected to:

- contribute to the better understanding of *in vitro* senescence and senescence-escape models, potentially explaining the variability of results in the research field,
- validate the effect of azithromycin in senescent cancer cells, that could be included in a treatment strategy to improve the effect of cancer therapies.
- validate a new marker of senescence, that could be included in cancer diagnostics for identifying senescent cancer cells,
- and contribute to the comprehensive investigation of senescence-escape in cancer.

3. Materials and Methods

3.1 Cell lines and cell culturing

MCF-7, MDA-MB-231, MCF-10A and MRC-5 human cell lines were obtained commercially from the ATCC. MCF-7 and MDA-MB-231 breast cancer cells were maintained in Dulbecco's Modified Eagle Medium, High glucose (DMEM, Sigma) supplemented with 10% Heat Inactivated (HI) FBS (Gibco), 1% Glutamax (100X, Gibco), and 1% Penicillin-Streptomycin (Gibco). MCF-10A breast epithelial cells were maintained in Mammary Epithelial Cell Growth Medium (MEGM, Lonza) supplemented with 0.4% bovine pituitary extract (BPE), 0.1% insulin, 0.1% hEGF, 0.1% hydrocortisone, 0.1% GA-1000, and 100 ng/ml of cholera toxin. MRC-5 fibroblast cells were maintained in Minimum Essential Medium (MEM, Sigma) supplemented with 10% HI FBS (Gibco), 1% Glutamax (100X, Gibco), and 1% Penicillin-Streptomycin (Gibco). All the cell lines were maintained in a humidified incubator at 37°C and 5% CO₂. To seed the cells for experiments, culture medium was removed, cells were washed with sterile phosphate buffered saline (1X PBS, Gibco) and detached with Trypsin-EDTA solution (Sigma). Cells were collected by centrifugation (1200 RPM, 5 minutes) and resuspended in culture medium. Cell numbers were counted by BioRad TC20 Automated Cell Counter using 0.4%(v/v) Trypan Blue staining (Gibco) to exclude dead cells from cell counting.

3.2 Senescence-induction and treatments

Cells were seeded at an empirically determined density that allowed logarithmic growth during the senescence-inducing period, without limitation of cell growth due to reaching confluency. For senescence induction in MCF-7 and MDA-MB-231 cells, cells were treated with bromodeoxyuridine (BrdU), gemcitabine (GEM) or Palbociclib (PALBO). The concentrations and incubation times were determined empirically for both cell lines by monitoring the alteration of cell morphology, growth arrest and cell death (apoptotic cell morphology, detachment of the cells) using microscopic examination. The aim was to induce a relatively homogeneous senescence phenotype in both cell lines, avoiding the induction of substantial amount of cell death. The final senescence-inducing treatment strategies are described below. Two days after seeding, MCF-7 cells were treated with 5 µM BrdU for 7 days

or 500 nM PALBO for 14 days, applying the treatment with every medium change (every 2-3 days); or MCF-7 cells were treated with 100 nM GEM for 24 hours and incubated in fresh medium without GEM for 7 days for senescence induction. One day after seeding, MDA-MB-231 cells were treated with 50 μ M BrdU for 7 days, 200 nM GEM for 7 days or 1 μ M PALBO for 14 days, applying the treatment with every medium change (every 2-3 days). Senescent MCF-7/MDA-MB-231 cells were treated with azithromycin (AZI) and chloroquine (CQ) for 72 hours; or sitagliptin (SITA) for 10 days, applying the treatment with every medium change (every 2-3 days), using the concentrations indicated in each experiment. Bromodeoxyuridine, Palbociclib and azithromycin were dissolved in sterile dimethyl sulfoxide (DMSO); gemcitabine, chloroquine and sitagliptin were dissolved in sterile distilled water. All compounds were purchased from Sigma-Aldrich.

3.3 Fluorogenic SA- β -galactosidase staining

1-2x10⁵ cells/well were seeded in 6-well plates and treated with selected compounds to induce senescence or cultured without treatment (control cells). The expression of SA- β -galactosidase was detected with CellEvent™ Senescence Green Flow Cytometry Assay Kit (Thermo Fisher, Invitrogen). After senescence induction, cells were trypsinised, collected and resuspended in PBS at a concentration of 2-5 x 10⁵ cells per sample. The collected samples were centrifuged (5 minutes at 1200 RPM) and resuspended in 100-200 μ l of 4%(v/v) paraformaldehyde (PFA, diluted in PBS) and incubated for 10 minutes at room temperature in dark. To prepare the working solution, the Senescence Green Probe (C₁₂FDG) was diluted x1000 in the pH6 Senescence Buffer provided in the kit. After fixing the samples, the cells were washed with 3 ml of 1%(w/v) bovine serum albumin (BSA, Sigma) dissolved in PBS, resuspended in 100-200 μ l of pre-warmed (37°C) working solution and incubated for 1.5 hours at 37°C without CO₂ in dark. After incubation, working solution was removed and the cells were washed twice with 3 ml of ice-cold PBS to stop the staining reaction. 2x10⁴ single cells were recorded and analysed by Attune NxT Flow Cytometer. The results were evaluated by FlowJo software.

3.4 Chromogenic SA- β -galactosidase staining

The expression of SA- β -galactosidase was detected with Senescence β -galactosidase Staining Kit (Cell Signaling). Senescent and control (untreated) cells were seeded in 96-well optical-bottom plates (Thermo Scientific) at a density of 1×10^4 cells/well. After 48 hours the medium was removed, the cells were washed twice with PBS and fixed with Fixative Solution (provided in the kit) diluted 10x in distilled water, incubated for 15 minutes at room temperature in dark. The working solution was prepared prior to use by mixing 1x Staining Solution, Solution A, Solution B and X-gal solution (20 mg of X-gal dissolved in 1 ml DMSO) according to manufacturer instructions. The pH of the solution was adjusted to pH 6 using NaOH and HCl solutions. After fixation, cells were washed twice with PBS and incubated with the working solution for 6 hours at 37°C without CO₂. After incubation, the working solution was removed, cells were washed twice with PBS and stained with 1 μ M Hoechst solution (Thermo Fisher) diluted in PBS for 15 minutes at room temperature in dark. After the removal of Hoechst staining, cells were washed with PBS and imaged with EVOS FL Auto Imaging System (Thermo Fisher).

Images were analysed with ImageJ software. The percentage of SA- β -galactosidase expressing cells were calculated as the number of SA- β -gal positive cells divided by the total cell number, based on X-gal and Hoechst staining, respectively. The cell numbers were counted by ImageJ software by applying a counting mask adjusted to the appropriate thresholds based on unstained samples (**Figure 5**).

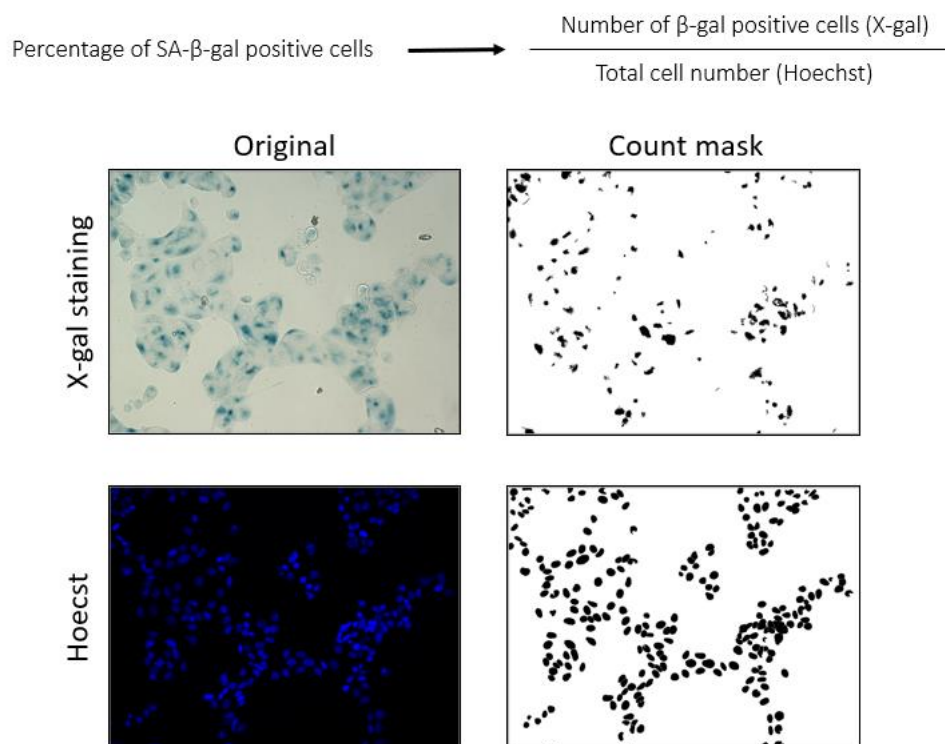


Figure 13. Evaluation of chromogenic (X-gal) SA- β -galactosidase staining by ImageJ. Images on the left represent the original image of X-gal staining (brightfield) and Hoechst staining (DAPI channel) imaged by EVOS Auto Imaging System using magnification of 20X. Images on the right represent the count masks generated by setting up a colour/intensity threshold for positive staining by ImageJ software. The count masks were used to automatically count the positively stained cells by ImageJ software. SA- β -galactosidase staining was evaluated by using the formula presented above the images.

3.5 Immunostaining for imaging

MCF-7/MDA-MB231 cells with or without treatment were seeded in 96-well optical-bottom plates (Thermo Scientific) at a density of 1×10^4 cells/well. Cells were incubated for 48 hours to allow them to attach well onto the plate. For staining, medium was removed, and cells were washed twice with PBS before fixing them with 4% paraformaldehyde (Thermo Fisher, PFA diluted in PBS) for 15 minutes at room temperature in the dark. After, cells were washed twice with PBS and incubated with 0.3%(v/v%) Triton-X100 (Sigma) diluted in 1%(w/v%) BSA (Sigma) for 15 minutes at room temperature to permeabilise the cells. After permeabilization, cells were incubated with 1% BSA for 30 minutes at room temperature to block the samples. For BrdU staining, an additional DNA denaturing step was added after the cells had been fixed. DNA was denatured by 20 minutes incubation with 1M HCl, at 40°C, and samples were washed twice with 0.1M borate buffer pH 8.0 (1.9 g sodium tetraborate and 5 g boric acid

dissolved in water) for 10 minutes to remove the HCl and neutralise the pH. Cells were labelled with primary antibodies against Ki67 (1:250, SP6, 300 µg/ml, Thermo Fisher Invitrogen), BrdU (1:50, IIB5, 200 µg/ml, Santa Cruz) or γH2AX phospho-S139 (1:500, 9F3, 1mg/ml, Abcam) diluted in 1% BSA for 1 hour at room temperature on a microplate shaker (180 RPM). After, samples were washed three times with PBS and incubated with secondary antibodies conjugated with fluorescent compounds (1:1000, Alexa Fluor Plus 488 – anti-mouse, Alexa Fluor 594 – anti-rabbit, Alexa Fluor 594 – anti-mouse, 2 mg/ml, Thermo Fisher Invitrogen) diluted in 1% BSA for 30 minutes at room temperature in dark, on a microplate shaker (180 RPM). After incubation, the cells were washed three times with PBS and incubated with 1 µM Hoechst solution (Thermo Fisher) diluted in PBS for 15 minutes at room temperature in dark. After the removal of Hoechst staining, cells were washed twice with PBS and imaged with EVOS FL Auto Imaging System using magnification of 10X or 20X. Images were analysed with ImageJ software. Background was removed uniformly by ImageJ software.

For imaging the cells with higher magnification (40X), the cells were seeded on round coverslips (15 mm diameter) in a 24-well plate at a density of 4×10^4 cells/wells. Cells were incubated for 48 hours to allow them to attach well onto the coverslips. After staining with secondary antibodies, the coverslips were removed from the 24-well plate and mounted on glass slides using 10 µl mounting medium with DAPI staining (Vector labs). Samples were imaged the following day with EVOS FL Auto Imaging System (Thermo Fisher) using magnification of 40X, and the images were analysed with ImageJ software.

3.6 Immunostaining for flow cytometry

Cells were trypsinized, collected and centrifuged (5 minutes, 1200 RPM) in 5 ml test tubes. Cell pellets were fixed by adding ice-cold 70% (v/v%) ethanol and the samples were kept in -20°C at least overnight. Before the staining samples were thawed, centrifuged (5 minutes, 1200 RPM) and washed with 1 ml of 1% BSA (w/v%, dissolved in PBS) to remove the remaining ethanol. Cells were incubated with primary antibodies (100 µl/ $2-5 \times 10^5$ cells) against γH2AX (1:500, phospho S139, 9F3, 1mg/ml, Abcam) or Ki-67 (1:250, SP6, 300 µg/ml, Thermo Fisher Invitrogen) diluted in 1% BSA for 30 minutes at room temperature. After the incubation, samples were vortexed and centrifuged with an additional 2 ml of 1% BSA to remove the

primary antibody. After the removal of primary antibodies, cells were incubated with secondary antibodies conjugated with fluorescent compounds (1:1000, Alexa Fluor Plus 488 – anti-mouse, Alexa Fluor 660 – anti-rabbit, 2 mg/ml, Thermo Fisher Invitrogen) diluted in 1% BSA for 30 minutes at room temperature in dark. After the incubation, samples were vortexed and centrifuged with an additional 2 ml of 1% BSA to remove the secondary antibody. Cells were resuspended in 1% BSA with a concentration of 5×10^5 cells/500 μ l, and 2×10^4 single cells were recorded and analysed by Attune NxT Flow Cytometer. The results were evaluated by FlowJo software. The gates for positively stained cells were adjusted by using samples incubated only with secondary antibodies (without primary antibodies), representing the gating threshold for the positively stained cells.

3.7 Cell cycle analysis

Cell-cycle analysis was performed by flow cytometry using the double-staining of Ki-67 expression and propidium iodide (PI) nuclear DNA stain. After the immunostaining with Ki-67 antibody (described above), cells were stained with of Muse™ Cell Cycle Assay buffer (200 μ l/ 5×10^5 cells) containing PI stain (Luminex) for 20 minutes at room temperature, protected from light. After incubation, 300 μ l/ 5×10^5 cells of PBS were added to each sample. 2×10^4 single cells were recorded and analysed by Attune NxT Flow Cytometer applying automatic compensation. Samples were manually categorized into cell-cycle stages and evaluated by FlowJo software. The detailed gating strategy is described and presented in the results (**Figure 8**).

3.8 DPP4/CD26 staining for flow cytometry

$1-2 \times 10^5$ cells/well were seeded in 6 well plates and treated with selected compounds to induce senescence or cultured without senescence-inducing treatment (control cells). For the staining, cells were trypsinised, collected and resuspended in 1% BSA dissolved in PBS with a concentration of $3-5 \times 10^5$ cells/sample. After, cells were centrifuged (5 minutes, 1200 RPM) and resuspended in 100 μ l staining solution with antibodies against DPP4/CD26 conjugated with phycoerythrin CD26-PE (1:100, 2A6, 0.1 mg/ml, Invitrogen) diluted in 1% BSA and incubated for 30 minutes on ice protected from light. After incubation, samples were centrifuged (5 minutes, 1200 RPM) with 1 ml additional PBS and washed twice with PBS to

remove the unbound antibodies. Cells were resuspended in 1% BSA with a concentration of 5×10^5 cells/500 μ l, and 2×10^4 single cells were recorded and analysed by Attune NxT Flow Cytometer. Results were evaluated by FlowJo software. The background fluorescence intensity was determined by unstained samples and was subtracted from the fluorescence intensity of stained samples.

3.9 Sulphorhodamine B (SRB) assay

For cell viability and cell growth assays 1×10^4 cells/100 μ l were seeded in 96-well plates. For growth assays, cells were incubated without changing the medium, and fixed after 24-, 48-, 72- and 96-hours. For cell viability assays, 24 hours after seeding the medium was replaced with fresh medium and the cells were treated with selected compounds, using the concentrations and incubation times indicated in each experiment. At the end of the treatment the medium was removed, and cells were washed once with PBS. After, cells were fixed with 10%(v/v%) trichloroacetic acid (TCA) for 1 hour at 4°C, stained with 0.4%(w/v%) Sulphorodamine B (SRB, Sigma) dissolved in 1%(v/v%) acetic acid for 15 minutes, and washed three times with 1% acetic acid and dried for at least 2 hours. The incorporated dye was dissolved in 10 mM Tris-HCl pH 8.8 buffer (Trizma Base, Sigma) solution and the absorbance were read using a plate reader (Thermo Fisher, Varioskan™ LUX microplate reader) at 565 nm. Data was analysed in Excel and GraphPad Prism.

3.10 Crystal violet staining

Crystal violet staining assay was performed to assess senescence-escape. $1-2 \times 10^5$ cells/well were seeded in 6 well plates and treated with selected compounds to induce senescence. After senescence induction, cells were incubated without treatment for 10 days, allowing them to restart proliferation and form colonies of senescence-escaped cells. After, the medium was removed, and cells were fixed in 70% ethanol for 10 minutes at room temperature. After fixation, cells were stained with 0.2% (v/v%) crystal violet solution (Sigma) diluted in 70% ethanol for 30 minutes at room temperature. The staining solution was removed, and the plates were washed with water and dried overnight. The cells were imaged with EVOS FL Auto Imaging System (Thermo Fisher), and the number of colony-forming senescence-escaped cells were quantified with ImageJ software.

3.11 Silencing of DPP4/CD26

1.5×10^6 293Ta packaging cells (human embryonic kidney cells) were seeded in four T75 flasks 48 hours before they were transfected with lentiviral vectors encoding three different clones for DPP4 siRNA (small interfering RNA) (HSH004434-LVRV6GP-a, HSH004434-LVRV6GP-b, HSH004434-LVRV6GP-c) and a scrambled vector (HSH004434-LVRV6GP), using Lenti-Pac™ HIV Expression Packaging Kit (Genecopoeia). For transfection 2.5 µg of each lentiviral siRNA expression plasmid and 5.0 µl of Lenti-Pac HIV mix (Genecopoeia) were diluted in 200 µl of Opti-MEM (Gibco). After, 15 µl of EndoFectin Lenti reagent (Genecopoeia) diluted in 200 µl of Opti-MEM was added dropwise to the DNA solution and gently mixed. The mixture was incubated for 20 minutes at room temperature to form the DNA-EndoFectin complex, then directly added to each flask. Cells were incubated overnight (8-14 hours), and the medium was replaced with 10 ml of fresh medium supplemented with 20 µl of TiterBoost reagent (Genecopoeia). 48 h after transfection, lentivirus-containing culture medium was collected and centrifuged (10 minutes, 500 g), and the supernatant was filtered through a 0.45 µm syringe filter (Merck) and stored at -80°C or used immediately for the transduction. 5×10^5 MCF-7 or MDA-MB-231 cells were seeded in T25 flasks and cultured until they reached 70-80% confluence. For transduction, 3 ml of lentivirus-containing medium diluted with 3 ml of culture medium was added to the target MCF-7 or MDA-MB-231 cells in the presence of 5 µg/ml polybrene (Santa Cruz). Mock control cells were treated only with 5 µg/ml polybrene diluted in 6 ml culture medium. Cells were incubated overnight and incubated in fresh medium until they reached 80-90% confluence. Each of the plasmids used for the experiment encoded a puromycin-resistance gene, therefore the transduced cells were resistant to puromycin, but the mock control cells remained sensitive to it. The transduced cells were selected with a concentration of 1 µg/ml (empirically determined concentration) of puromycin (Sigma) until mock control cells were eliminated. Cells transduced with HSH004434-LVRV6GP-a clone were selected to be used in subsequent experiments by measuring the efficacy of silencing by flow cytometer, labelled as DPP4 siRNA. Cells transduced with scrambled vector were used as experimental controls, labelled as ctrl siRNA.

3.12 LysoTracker staining

1-2x10⁵ cells/well were seeded in 6 well plates and treated with selected compounds to induce senescence or cultured without the senescence-inducing treatment (control cells). For the staining, cells were trypsinised, collected and resuspended in culture medium with a concentration of 3-5x 10⁵ cells/sample. After, cells were centrifuged (5 minutes, 1200 RPM) and resuspended in 1 ml staining solution with LysoTracker Deep Red (Invitrogen) diluted to 50 nM in culture medium and incubated for 20 minutes at 37°C. After incubation, samples were centrifuged (5 minutes, 1200 RPM) and washed twice with PBS. Cells were resuspended in 1% BSA with a concentration of 5x10⁵ cells/500 µl, and 2x10⁴ single cells were recorded and analysed by Attune NxT Flow Cytometer. Results were evaluated by FlowJo software. The background fluorescence intensity was determined by unstained samples and was subtracted from the fluorescence intensity of stained samples.

3.13 Western blot analysis

1-2x10⁵ cells/well were seeded in 6 well plates and treated with selected compounds to induce senescence or cultured without senescence-inducing treatment (control cells). After the removal of cell culture medium, cells were washed twice with cold PBS. Proteins from cells were extracted by RIPA lysis buffer (Sigma) complemented with cComplete™ ULTRA Tablets Protease Inhibitor Cocktail (Sigma) and PhosSTOP™ Phosphatase Inhibitors (Sigma) and cell debris and proteins were collected by using a cell scraper, and incubated for 30 minutes at 4°C, with agitation. Cell debris was removed by centrifugation (10 minutes, 12000 RPM, 4°C) and the supernatant (protein extraction) was collected and stored at -20°C. Protein concentration was evaluated by Pierce™ BCA Protein Assay Kit (Thermo Fisher). 5 µl of protein samples and protein standards (known concentrations of proteins provided in the kit) were added to 200 µl of working solution/well (50:1 mixture solution A and solution B provided in the kit) in a 96 well plate, and incubated for 30 minutes at 37°C. Absorbance was measured at 562 nm, using a plate reader (Thermo Fisher, Varioskan™ LUX microplate reader), and protein concentration was evaluated in Excel, based on the standard curve generated by measuring the standard proteins with known concentrations.

20 µg of protein samples were mixed with 8 µl of NuPAGE™ LDS Sample Buffer (4X, Invitrogen) and additional distilled water to equalize sample volumes, and incubated for 10 minutes at 98°C. After, protein samples were cooled down and subjected to electroporation (100 V, ~1 hour) through 4–20% Mini-PROTEAN® TGX™ Precast Protein Gels (50 µl wells, Bio-Rad), and electroblotted onto a nitrocellulose blotting membrane (0.2 µm) using Trans-Blot Turbo Transfer System (Bio-Rad). Premixed 10x Tris/glycine/SDS running buffer (Bio-Rad) diluted to 1x in distilled water was used as running buffer, and PageRuler™ Plus Prestained Protein Ladder (Thermo Fisher) was used as size standards. Transfer efficiency was examined by Ponceau S Staining Solution (Thermo Fisher). Membranes were washed three times with PBST (1x PBS, 0.1% (v/v%) Tween-20 detergent solution (Thermo Fisher)) and blocked with 5% (w/v%) BSA dissolved in PBS for 1 hour at room temperature. Membranes were incubated overnight at 4°C with primary antibodies against DPP4/CD26 (1:300, D6D8K, Cell Signaling), p16^{INK4a} (1:500, 1D7D2, Invitrogen) and β-actin (1:3000; Sigma). After incubation, membranes were washed three times with PBST. Membranes were incubated with HRP-linked secondary antibodies (anti-rabbit and anti-mouse IgG, 1:3000, Cell Signaling) for 1 hour at room temperature, and washed three times with PBST. Proteins were revealed by using SuperSignal West Pico chemiluminescent substrate (Thermo Fisher) and Syngene G:BOX imaging system.

3.14 CellTrace CFSE (carboxyfluorescein succinimidyl ester) staining

0.8-1.6x10⁶ cells were seeded in T75 flasks or 1-2x10⁵ cells were seeded in 6 well plates, depending on the experiment, and treated with selected compounds to induce senescence or cultured without senescence-inducing treatment (control cells). After, medium was removed and cells were washed with DPBS (Dubecco's phosphate-buffered saline with calcium and magnesium, Gibco) and incubated with 5 µM CellTrace CFSE dye (5 mM, dissolved in DMSO, Thermo Fisher) diluted in DPBS for 20 minutes in the cell culture incubator. After the incubation, the staining solution was removed, and cells were washed with culture medium and incubated in fresh medium for 10 (senescent cells) or 4 (control cells) days.

3.15 Fluorescence-activated cell sorting (FACS)

After CellTrace CFSE staining, cells were collected, centrifuged, resuspended in pre-sort buffer (BD Biosciences) at a concentration of 1x10⁶ cells/ml. Cells were filtered through a 40 µm cell

strainer (Fisherbrand) before sorting them with Sony SH800S Cell Sorter (Sony Biotechnology). The gates were adjusted to separate senescent and senescence-escaped cells by using senescent cells stained with CellTrace CFSE. The detailed sorting strategy is described and presented in the results and supplementary figures (Figure 27-28, Supplementary Figure 11). For migration and mammosphere assays cells were sorted in tubes containing medium without FBS or mammosphere medium, collected by centrifugation (1200 RPM, 5 minutes) and resuspended in the appropriate culture medium (detailed below). For colony formation assay cells were sorted directly in the 6-well plates filled with complete medium (DMEM).

3.16 Migration assay

After sorting, MCF-7 cells were seeded in Falcon™ Cell Culture Inserts (PET membrane with 8 µm pores, for 24 well plates) at a concentration of 5×10^4 cells/500 µl medium without FBS and placed in the wells of 24-well plate filled with 500 µl medium without FBS. Cells were serum-starved for 4 hours, and then the medium in the bottom of the 24-well plates was replaced with medium containing 10% FBS as chemoattractant. The inserts were incubated for 24 hours in the incubator, allowing the cells to migrate to the other side of the membrane. MDA-MB-231 cells were seeded in Falcon™ Cell Culture Inserts at a concentration of 1×10^4 cells/500 µl medium without FBS and placed in the wells of 24-well plate filled with 500 µl medium with 10% FBS. The inserts were incubated overnight in the incubator, allowing the cells to migrate to the other side of the membrane. Before staining, medium and cells were removed from the internal side of the insert using a cotton swab. The insert was placed in 70%(v/v%) ethanol for 10 minutes to fix the migrated cell on the external side of the insert. Migrated cells were stained with 0.2%(v/v%) crystal violet solution (Sigma) diluted in 70% ethanol for 30 minutes at room temperature. The staining solution was removed, and the inserts were washed with water and dried overnight. Membranes were imaged with EVOS FL Auto Imaging System (Thermo Fisher), and images were evaluated with ImageJ software.

3.17 Mammosphere formation assay

To prepare 6-well plates for the mammosphere formation assay, 12 g of poly-HEMA was dissolved in 1 l of 95% ethanol and 2 ml of dissolved poly-HEMA was added to each well of the plates. The plates were incubated for 3 days at 50°C to create a coating on the bottom of

the wells. After sorting, cells were centrifuged (5 min, 1200 RPM), resuspended in mammosphere medium (DMEM-F12 medium without phenol red (Gibco) complemented with 2%(v/v%) B-27 supplement (Gibco), 20 ng/ml EGF (Invitrogen) and 1% Penicillin-Streptomycin (Gibco)) plated at a density of 5000 cells/well in 6-well plates coated with 2-hydroxyethylmethacrylate (poly-HEMA, Sigma) with mammosphere medium. Cells seeded in the coated plates were grown for 5 days in the incubator, and mammospheres bigger than 50 μm were counted using an eye piece graticule of the microscope.

3.18 Colony formation assay

For colony formation assay, cells were seeded in 6-well plates filled with 2 ml culture medium with a density of 1000 cells/well (MCF-7) or 500 cells/well (MDA-MB-231) and incubated in the incubator for 14 days. After incubation cells were stained with crystal violet, following the fixation and staining method described before (crystal violet staining). The number of colonies were quantified with ImageJ software.

3.19 Enzyme-linked immunosorbent assay (ELISA)

The secretion of IL-6, IL-8 and CXCL12A (SDF-1 α) were measured from cell culture medium using ELISA kits (Invitrogen). $1-2 \times 10^5$ cells were seeded in 6 well plates, and treated with selected compounds to induce senescence or cultured without senescence-inducing treatments (control cells). After senescence induction, cells were incubated with fresh medium for 4 days. For collecting control samples, the medium was changed 24 hours after seeding and the cells were incubated for 4 days. After 4 days, the culture medium was collected, centrifuged (1000 g, 10 minutes, 6°C) to remove any cells/cell debris, and the supernatant was collected and used immediately or stored at -80°C in small aliquots. The cells remaining in the plates were trypsinized and cell numbers were counted by BioRad TC20 Automated Cell Counter using 0.4% Trypan Blue staining (Gibco). The levels of IL-6, IL-8 and CXCL12A (SDF-1 α) were detected by ELISA kits (Invitrogen) according to manufacturer instructions. Briefly, standard solutions were prepared with known concentrations of each protein and experimental samples were diluted in sample dilution buffer (Invitrogen) as necessary. Standards and samples were added to the antibody-coated wells and incubated alone or together with the biotin conjugate (Invitrogen). The plate was incubated at room

temperature using the incubation times indicated in each protocol (for each cytokine) and washed three times with wash buffer (Invitrogen). After, freshly diluted streptavidin-HRP solution (Invitrogen) was added to the wells and incubated at room temperature using the incubation times indicated in each protocol (for each cytokine). After incubation, wells were washed three times with wash buffer and incubated with stabilized chromogen solution (Invitrogen) for 30 minutes at room temperature in dark. After, stop solution (Invitrogen) was added to the wells to stop the reaction and the absorbance was read by a plate reader (Thermo Fisher, Varioskan™ LUX microplate reader) at 450 nm. Background signals were measured from fresh culture medium and subtracted from each value. The results were quantified by using a standard logarithmic curve and normalised by the cell numbers.

3.20 Statistical analysis

All the experiments were repeated at least 3 times with 2-3 technical replicates, or as indicated in figure legends. All data are represented as the mean + standard error of the mean (SEM) represented as error bars in the graphs, except for the analysis of the immunostaining of LC3B and p62 expression, where the mean + standard deviation is represented in the graphs. Data normality was assessed by Shapiro-Wilks test. For statistical analysis of pairwise comparisons (two groups) two-tailed unpaired T-test was used with statistical significance set at $P < 0.05$. For multiple group comparisons (3< groups) one-way ANOVA test corrected with Dunnett's multiple comparison test was used, with statistical significance set at $P < 0.05$. All statistical analysis were performed by using GraphPad Prism software.

4. Results

4.1 Senescence induction in MCF-7 cells

4.1.1 Establishing and analysing TIS models using bromodeoxyuridine (BrdU), gemcitabine (GEM) and Palbociclib (PALBO) in MCF-7 cells

The first objective of the project was to develop and analyse different cellular models of therapy-induced senescence (TIS) in cancer cells. Therefore, MCF-7 breast cancer cells were treated with three different drugs, namely bromodeoxyuridine (BrdU), gemcitabine (GEM) and Palbociclib (PALBO), that have been described as potential senescence-inducers (Masterson and O'Dea, 2007, Modrak et al., 2009, Leontieva and Blagosklonny, 2013). Initially, the effect of BrdU, GEM and PALBO was tested on the cell viability of MCF-7 cells to determine the drug concentration to use for senescence-induction (**Figure 6.A**). The aim was to arrest the proliferation of the cells without inducing significant amount of cell death. The cell viability was measured by SRB assay. The IC_{50} of BrdU was 1 mM, the IC_{50} of GEM was more than the highest tested concentration (100 μ M) and the IC_{50} of PALBO was 10 μ M, however, apoptosis and proliferation arrest are not distinguishable with cell viability test (**Figure 6.A**). Based on these results and the relevant literature, the optimal drug concentrations and incubation times were empirically determined and described in detail in the Methods section. Briefly, to induce senescence in MCF-7 cells, the cells were treated for 7 days with 5 μ M BrdU and 100 nM GEM, and 14 days with 500 nM PALBO. To confirm the induction of senescence, different markers of cellular senescence were examined. First, the morphology of the cells was examined under the microscope (**Figure 6.B**) and using the measurements of forward scatter (FSC) and side scatter (SSC) by flow cytometry (**Figure 6.B**). Compared to the control cells, the BrdU- and GEM- and PALBO-induced senescent cells had a flattened shape and larger size, however, the shape of the PALBO-induced senescent cells was more similar to the control (**Figure 6.B**). Increased value of FSC/SSC measured by flow cytometry is a label-free method, that has been used to identify senescent cells based on their increased cell size (FSC) and granularity (SSC) (Jonchere et al., 2015, Bertolo et al., 2019). Compared to control cells FSC/SSC values were both significantly increased in all of the senescent models; however, the SSC values were increased more than the FSC (**Figure 6.C**). To investigate whether these three drugs induce DNA-damage as a senescence-inducing

mechanism, the expression of γ H2AX (phosphorylated form of H2A histone family member X), a highly specific marker to detect double-stranded DNA damage, was analysed by flow cytometry (Mah et al., 2010). After senescence induction with BrdU ~15% of the cells expressed γ H2AX, while the ~80% of GEM-induced senescent cells expressed γ H2AX (**Figure 6.D**), this increased expression was detectable even after 2 days of BrdU/GEM treatment (**Supplementary Figure 1.A**). PALBO-induced senescent cells did not have a significant increase of γ H2AX-expression compared to the control cells (**Figure 6.D**).

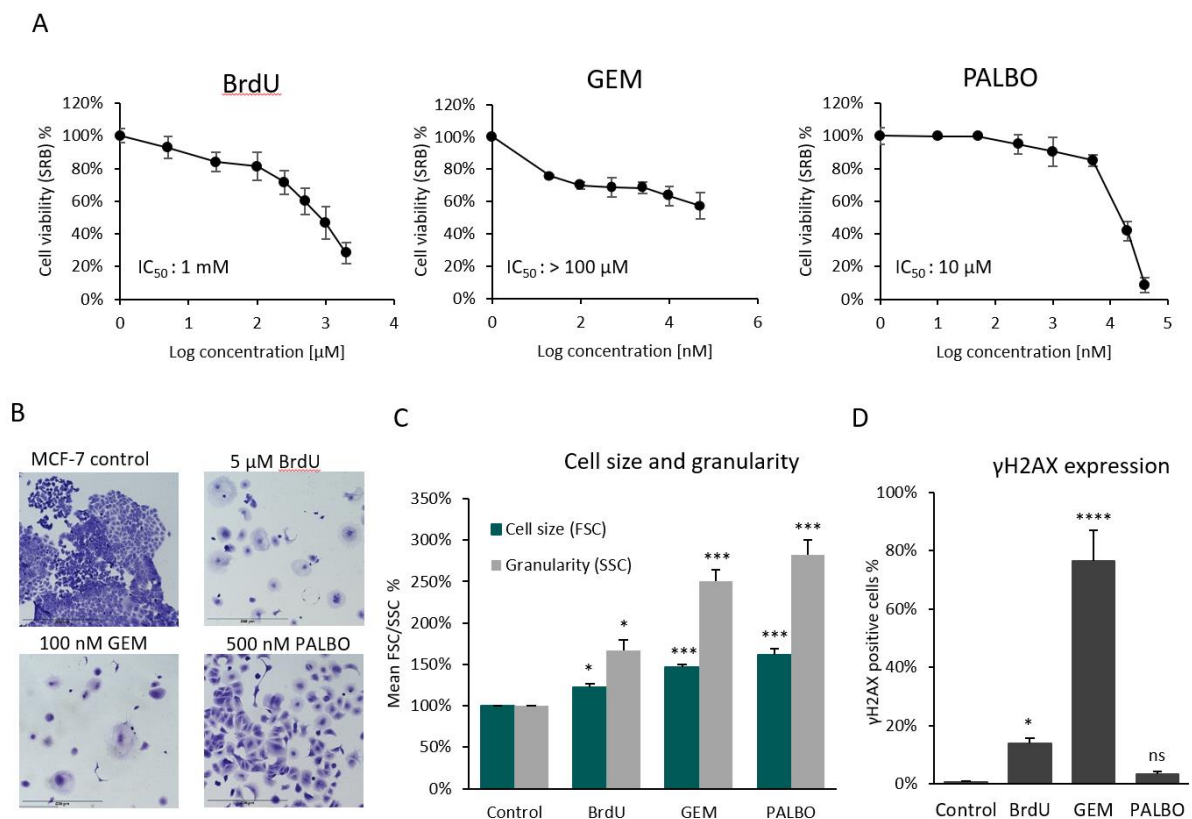


Figure 16. Senescence induction in MCF-7 cells. (A) The cell viability of MCF-7 cells was measured by SRB assay after 72 hours treatment of BrdU, GEM and PALBO using different drug concentrations. Experiments were repeated three times with six technical replicates, values were normalised to vehicle-treated controls, error bars represent \pm SEM. **(B)** Representative images of control and BrdU-, GEM- and PALBO-induced senescent MCF-7 cells. Cells were fixed and stained with crystal violet, imaged by EVOS with 10x magnification, scale bars indicate 500 μ m. **(C)** The cell size and granularity of MCF-7 cells were measured by the mean signal intensity of FSC and SSC by flow cytometry, values were normalised to non-senescent MCF-7 cells. **(D)** The expression of γ H2AX is represented as the percentage of positively stained cells compared to the total population. The gates for γ H2AX-positive cells were adjusted by using unstained cells. Bar graphs represent the mean of three independent experiments \pm SEM. Statistical significance (in relation to control): ns $p > 0.05$; * $p \leq 0.05$; ** $p \leq 0.01$; *** $p \leq 0.001$; **** $p \leq 0.0001$.

The increased expression of senescence-associated β -galactosidase (SA- β -Gal) is the most frequently used marker to detect senescent cells, and it can be measured by using chromogenic (X-Gal) and fluorescent (C₁₂FDG) substrates as well (Matjusaitis et al., 2016). Measured by both methods, SA- β -Gal expression was significantly increased in the senescent cells compared to the control cells, with the highest expression detected in the PALBO-induced senescent cells (**Figure 7.A, Figure 7.B, Figure 7.C**). The lack of proliferation is an essential characteristic of senescent cells, and it can be detected by proliferation markers, such as Ki-67 (González-Gualda et al., 2021). Measured by flow-cytometry, the number of Ki-67 expressing cells was significantly decreased after senescence induction, however, ~20% of BrdU-treated, ~5% of GEM-treated and ~10% of PALBO-treated cells still expressed Ki-67 (**Figure 7.D**). Despite these small populations of cells that remained positive for Ki-67 staining after senescence-inducing treatment, according to a cell proliferation assay (measured by SRB) after BrdU-, GEM and PALBO-treatment MCF-7 cells stopped proliferating (**Figure 7.E**).

Although there are numerous studies about the effects of SASP (senescence-associated secretory phenotype) in cancer, the senescent cancer cell-derived secretory factors has been rarely investigated (Faget et al., 2019). Therefore, to better characterise the senescence-phenotype induced in MCF-7 cells, we assessed and compared the secretion of three SASP factors (IL-6, IL-8 and CXCL12) in BrdU-, GEM- and PALBO-induced senescent MCF-7 cells (**Figure 7.F**). As described before, these three cytokines are well-known SASP factors with a potential a role in cancer progression (Lambeir et al., 2001, Wronkowitz et al., 2014, Faget et al., 2019). Figure 7.F shows that the secretion of IL-6, IL-8 and CXCL12 was significantly increased in BrdU- and GEM-induced senescent MCF-7 cells, but interestingly, there was no significant difference in PALBO-induced senescent MCF-7 cells compared to non-senescent (control) cells (**Figure 7.F**). In more details, IL-6 and CXCL12 had a higher expression in GEM-induced senescent MCF-7 cells, while the expression of IL-8 was increased more after BrdU treatment (**Figure 7.F**). It is important to note that MCF-7 cells had a very low (less than 1 pg/ml/100000 cells) basal expression of IL-6, IL-8 and CXCL12 (**Figure 7.F**).

Based on the assessment of senescence-markers, such as the altered cell morphology (increased cell size, flattened shape, increased granularity), the increased SA- β -Gal expression, decreased Ki-67 expression and SASP secretion (IL-6, IL-8, CXCL12) we confirmed the establishment of senescence models in MCF-7 cells. The results of γ H2AX-expression

indicates that in MCF-7 cells GEM induced senescence via DNA-damage induction, whereas BrdU and PALBO induced senescence through different mechanisms, independently from DNA-damage induction. Furthermore, our results suggested that the SASP secretion of senescent MCF-7 cells were dependent on the mechanism of senescence-induction, and PALBO-induced senescent cells did not show SASP secretion.

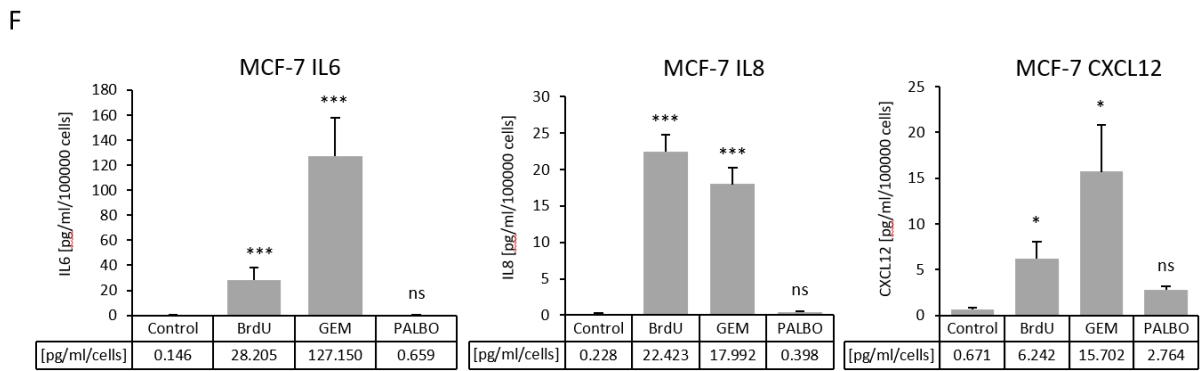
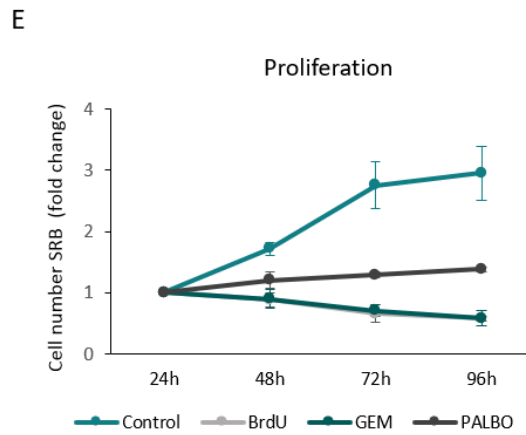
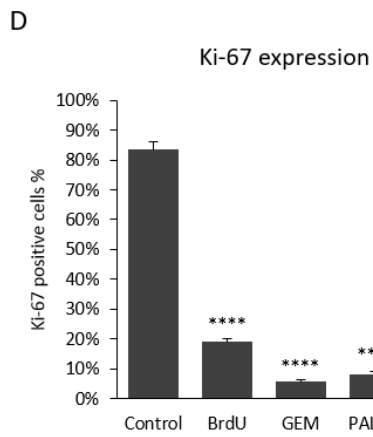
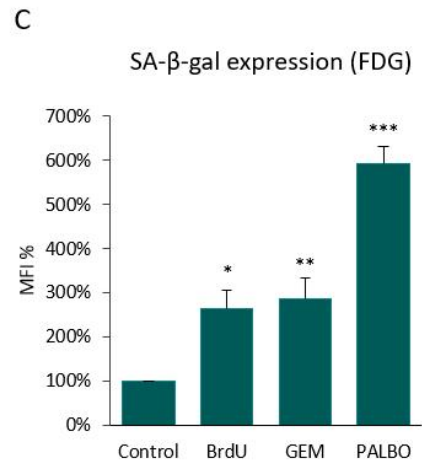
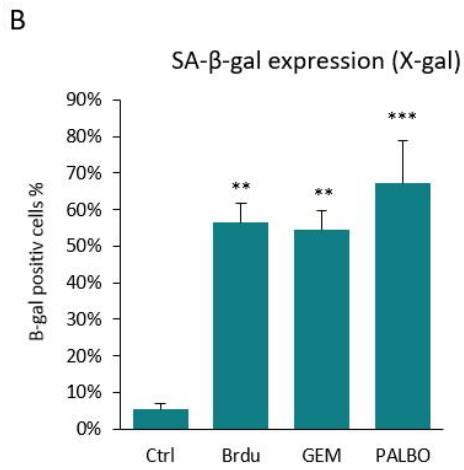
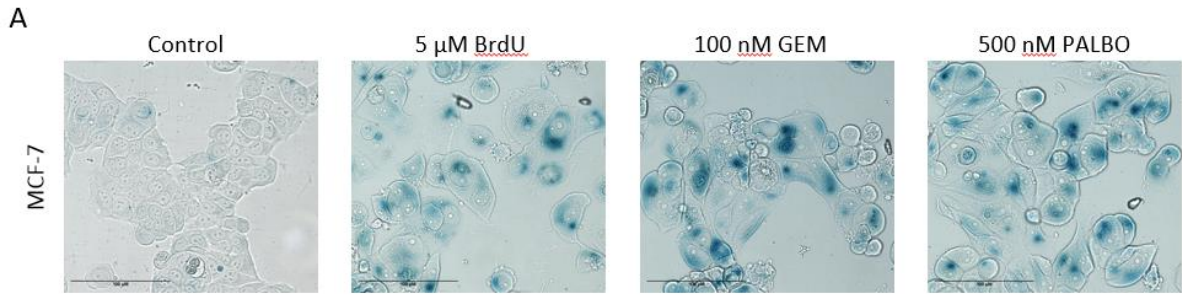


Figure 19. Analysis of senescence-markers in MCF-7 cells. (A) Representative images of control and BrdU-, GEM- and PALBO-induced senescent MCF-7 cells. Cells were fixed and stained with X-gal, imaged by EVOS with 20x magnification, scale bars indicate 100 μ m. The blue colour indicates SA- β -galactosidase activity. **(B)** Quantification of Figure 7.A. The expression of SA- β -galactosidase is represented as the percentage of positively stained cells compared to the total population. For the quantification of total cell number cells were co-stained with Hoechst nuclear stain. The number of positively stained cells and total cell numbers were quantified by ImageJ software, counting masks were adjusted manually based on unstained cells. **(C)** The SA- β -galactosidase expression of MCF-7 cells is represented as mean fluorescence intensity (MFI) of FDG staining measured by flow cytometry, values were normalised to the MFI of non-senescent MCF-7 cells. **(D)** The expression of Ki-67 is represented as the percentage of positively stained cells compared to the total population. The gates for Ki-67-positive cells were adjusted by using unstained cells. Bar graphs represent the mean of three independent experiments \pm SEM. **(E)** Cell proliferation of control and senescent MCF-7 cells was measured by SRB assay at different time-points, values were normalised to the baseline values measured 24 hours after cell seeding and represented as fold change. Graph represents the mean of two independent experiments \pm SEM. **(F)** The secretion of IL-6, IL-8 and CXCL12 was measured by ELISA assay. The cells were seeded in 6 well plates and cultured for 4 days before collecting the culture medium containing the secreted cytokines. The graphs represent the amount of IL-6, IL-8 and CXCL12 as pg/ml/cells, quantified by known-concentrations of standards and normalised by cell numbers. Experiments were repeated with two technical replicates, bar graphs represent the mean of three independent experiments \pm SEM. Statistical significance (in relation to control): ns $p > 0.05$; * $p \leq 0.05$; ** $p \leq 0.01$; *** $p \leq 0.001$; **** $p \leq 0.0001$.

4.1.2 Analysing the cell cycle of senescent MCF-7 cells by the double staining of Ki-67 expression and DNA-content (PI)

To further characterise the proliferation arrest in the senescent cells, cells were co-stained with Ki-67 and propidium-iodide (PI) (**Figure 8.A**). Ki-67 is expressed in the nucleus during all active phases of the cell cycle (G1, S, G2, and mitosis), but is absent from resting/quiescent (G0) and growth-arrested/senescent cells; while DNA-staining (PI) can differentiate between the G0/G1, S and G2/M phases of the cell cycle (Scholzen and Gerdes, 2000, Kim and Sederstrom, 2015). Cells without Ki-67 expression, but with $>2N$ DNA content has been described to represent the population of cells, that was arrested during the transition from S-G2-M phase (G2-arrest) (Miller et al., 2018). The double staining of Ki-67 expression and PI provides a method for more detailed cell cycle analysis by generating the following cell cycle categories: G0/G1 arrest (2N, Ki-67 negative), G1 phase (2N, Ki-67 positive), S phase ($>2N$, Ki-67 positive), G2/M phase (4N, Ki-67 positive) and G2 arrest ($>2N$, Ki-67 negative) (**Figure 8.A**). This cell cycle analysis does not differentiate between quiescent (G0) and senescent (G1-

arrest) population, however, it has been demonstrated before that based on the expression of different senescence markers, the BrdU-, GEM- and PALBO- treated cells are in a senescent state (**Figure 6, Figure 7**).

According to the results of cell cycle analysis, the number of cells in G1-arrest and G2-arrest was significantly increased after senescence-induction using BrdU, GEM and PALBO treatment, while the number of cells associated with active proliferation (G1-S-G2-M) was significantly decreased (**Figure 8.B-C**). The cell cycle analysis indicated that ~70% of the senescent cells has been arrested in G1 phase, and ~15% of BrdU- and PALBO-treated, and ~30% of GEM-treated cells has been arrested in G2 phase (**Figure 8.C**). This proliferation arrest can be visualised by nuclei-staining as well, due to the characteristic distribution of DNA-staining in senescent cells (senescence-associated heterochromatin foci, SAHF) (Swanson et al., 2015, Aird and Zhang, 2013). Staining the nuclei with DAPI, the senescent cells had a larger nucleus with the characteristic pattern of SAHF (senescence-associated heterochromatin foci), and stain-free areas, indicating the visible nucleolus during interphase, while the non-senescent control cells showed a more uniform distribution of DAPI-staining (**Figure 8.D, Supplementary Figure 1.C**). The cell cycle analysis can also provide indicative information about apoptosis and polyploidy. Reduced (sub-G1 phase) or increased (>4N) DNA content can indicate apoptotic and polyploid cells, which can be detected by flow cytometry (Plesca et al., 2008, Coward and Harding, 2014). Regarding the senescent models, GEM-treatment increased the sub-G1 population of MCF-7 cells, but compared to the control, there was no significant difference in the number of polyploid cells after senescence-inducing treatments (**Supplementary Figure 6.A-C**). Consistent with the increased γ -H2AX expression induced by GEM-treatment (**Figure 6.D**), the increased sub-G1 population after can indicate apoptotic cells in GEM-induced senescent cells.

Based on these results, the double staining of Ki-67 expression and DNA content (PI) could be useful to analyse the cell cycle of senescent cells by distinguishing the cell-cycle arrested cells from the proliferating cells. The detection of cell cycle arrest and the characteristics of senescent nuclear morphology (increased size of the nucleus, SAHF) further confirms the senescence phenotype of BrdU-, GEM- and PALBO-treated MCF-7 cells.

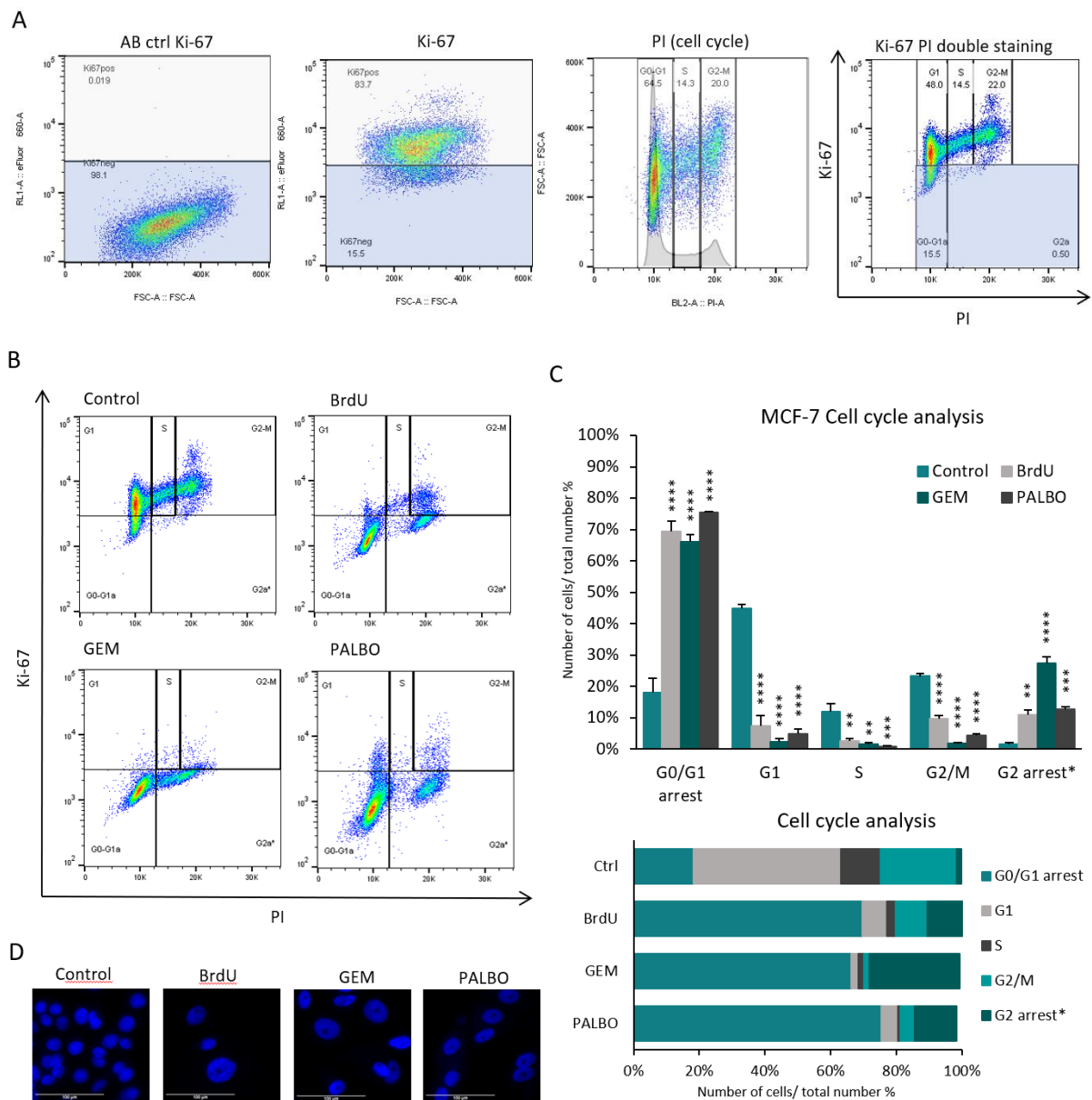


Figure 22. Cell cycle analysis of senescent MCF-7 cells. Representative figures of control MCF-7 cells showing the gating strategy used for analysing of cell cycle. Cells were manually categorised to cell-cycle stages based on their DNA content detected by PI staining, and the gates for Ki-67-positive cells were adjusted by using AB ctrl cells (stained only with secondary antibodies). **(B)** Representative figure of the cell cycle analysis of control, BrdU-, GEM- and PALBO-induced senescent MCF-7 cells using Ki-67 and PI staining. **(C)** The upper graph represents the percentage of cells in each category of cell cycle compared to the total cell population. * The category of G2 arrested cells were based on the research of Miller et al. (2018). Bar graphs represent the mean of three independent experiments \pm SEM. Statistical significance (in relation to control): ns $p > 0.05$; * $p \leq 0.05$; ** $p \leq 0.01$; *** $p \leq 0.001$; **** $p \leq 0.0001$. The bottom graph represents the distribution of cell cycle categories in control, BrdU-, GEM- and PALBO-induced senescent MCF-7 cells. **(D)** Representative images of nuclei staining of control and senescent MCF-7 cells. Cells were fixed and stained with DAPI nuclei stain, imaged by EVOS using 20x magnification, scale bars indicate 100 μ m.

4.2 Evaluation of senescence-escape

4.2.1 Establishing a method to quantify senescence-escape using Ki-67 and crystal-violet staining

Another objective of the project was to establish a method to quantify senescence-escape, that can be used for further investigations. As described before, Ki-67 is not expressed in senescent cells, but it is expressed in actively growing cells. Therefore, it could be a potential marker to detect cells that re-entered the cell cycle after senescence-induction and escaped from senescence. Firstly, to confirm the correlation of senescence induction and the decreased expression of Ki-67, the incorporation of BrdU was compared with the expression of Ki-67 using co-immunostaining of MCF-7 cells with BrdU and Ki-67 antibodies (**Figure 9.A**). For this experiment we hypothesised that the rate of BrdU-incorporation is proportional to the rate of senescence-induction in the cells. The percentage of BrdU-incorporated cells time-dependently increased, and after 7 days treatment, nearly 100% of the cells were positively stained for BrdU. The percentage of Ki-67 expressing cells were inversely proportional, reaching its minimal expression after 7 days of BrdU treatment (**Figure 9.B**). Based on this result, the decreasing expression of Ki-67 is a suitable marker to detect the development of senescence phenotype, and due to connection of Ki-67 expression with active cell proliferation, it could be a potential marker to detect senescence-escape.

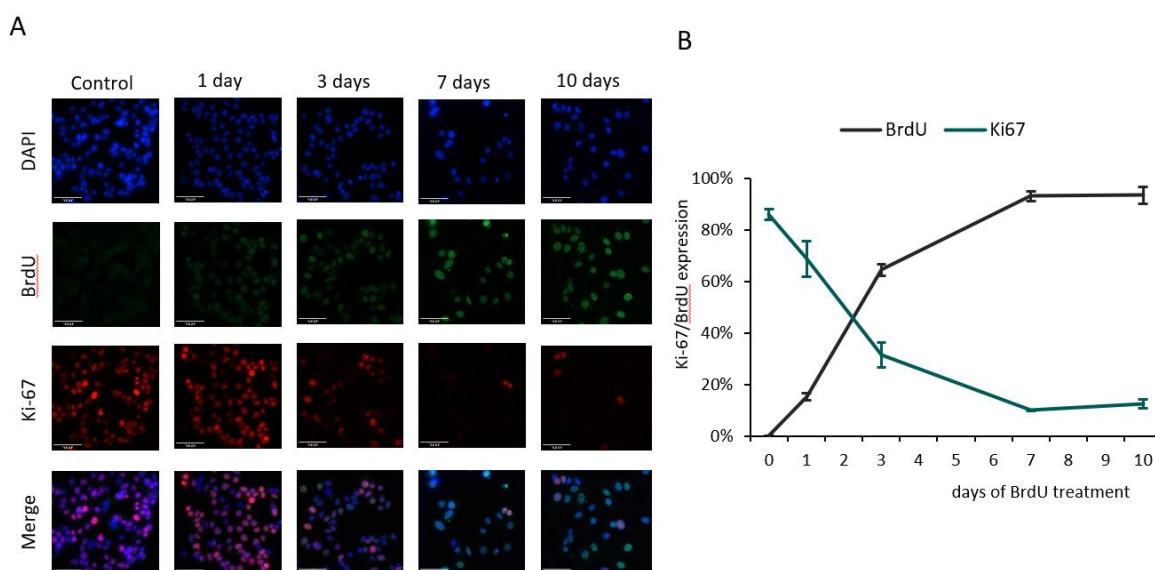


Figure 25. Analysis of BrdU incorporation and Ki-67 expression in MCF-7 cells. (A) Representative images of nuclei staining with DAPI, BrdU-incorporation and Ki-67 expression. Cells were fixed at different time points during senescence induction by BrdU-treatment, stained by immunostaining and imaged by EVOS using 20x magnification. Control represents day 0 of BrdU-treatment, scale bars indicate 100 μ m. **(B)** The graph represents the percentage of cells stained positively for BrdU or Ki-67 compared to the total cell number (DAPI staining). The number of positively stained cells (BrdU, Ki-67) and total cell numbers (DAPI) were quantified by ImageJ software, counting masks were adjusted manually based on unstained cells. The graph represents the mean of three independent experiments \pm SEM.

To create senescence-escaped cells, after senescence-induction MCF-7 cells were incubated without the senescence-inducing drug, allowing cells to escape from senescence. For most of the experiments, cells were incubated in drug-free medium for 10 days to generate sufficient number of senescence-escaped cells for accurate detection (**Figure 10.A, Supplementary Figure 3**). Compared to senescent cells, senescence-escaped cells had an increased expression of Ki-67, indicating that they regained their proliferative capacity (**Figure 10.B**). During senescence-escape, MCF-7 cells form small colonies of Ki-67 expressing cells, that could be easily visualised by crystal-violet staining and quantified by counting the number of crystal-violet stained senescence-escaped colonies (**Figure 10.C-D**). The increase in cell proliferation during senescence-escape can also be detected and quantified by flow cytometry, by using the number of cells positively stained for Ki-67 compared to the total cell number, expressed as percentage of Ki-67 expressing cells (**Figure 10.E**). These methods for the detection and evaluation of senescence-escaped cells provides a basis for a quantitative approach to investigate senescence-escape. In subsequent experiments, the number of colonies consisting of senescence-escaped cells and the percentage of Ki-67 expressing cells are used to quantify the senescence-escaping ability of the cells.

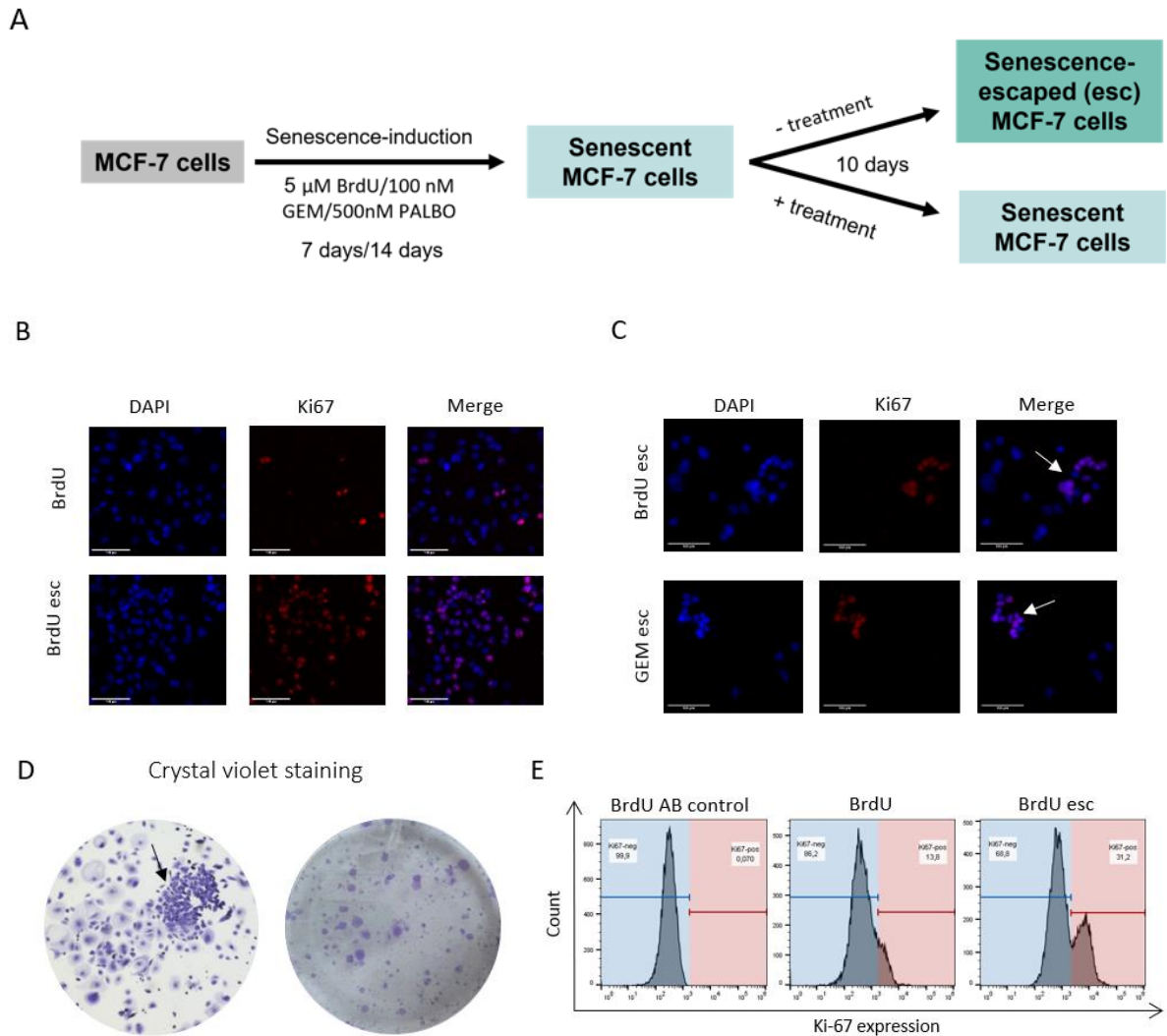


Figure 28. Evaluation of senescence-escape in MCF-7 cells. (A) Schematic figure representing the workflow of senescence induction in MCF-7 cells. **(B)** Representative images demonstrating the increase of Ki-67 expression in BrdU-induced senescence-escaped MCF-7 cells compared to the senescent cells. **(C)** Representative images demonstrating the colony-forming Ki-67-positive senescence-escaped cells. Arrows indicate the senescence-escaped cells. Cells were stained by immunostaining, imaged by EVOS using 20x magnification, scale bars indicate 100 μ m. **(D)** Representative images of senescence-escaped colonies of MCF-7 cells stained with crystal violet. Image on the left was taken by EVOS using 10x magnification, arrow indicates the senescence-escaped colony. Image on the right shows a representative well of a 6-well plate, in which the number of senescence-escaped colonies could be quantified. **(E)** Representative figure of evaluating senescence-escape in BrdU-induced senescent MCF-7 cells, based on Ki-67 expression measured by flow cytometry. The figures demonstrate the adjustment of gates based on AB control cells (antibody control, stained only with the secondary antibody), that represent the background staining. The cells were categorised to Ki-67 negative (blue) and Ki-67 positive (red) populations.

4.2.2 Comparing senescence-escape in BrdU-, GEM- and PALBO-induced senescent MCF-7 cells

To compare the senescence-escaping ability of BrdU-, GEM- and PALBO-induced senescent cells, the escaping MCF-7 cells were monitored for 10-12 days. Our results showed that senescence-escaped cells started to appear ~7 days after the removal of BrdU/GEM, interestingly, the PALBO-induced senescent cells started to escape from senescence shortly (~3 days) after the removal of PALBO, indicated by the increased number of cells with non-senescent (normal) morphology (**Figure 11.A**). Analysing the percentage of Ki-67 expressing cells confirmed that the number of senescence-escaped cells started to increase ~5-7 days after senescence-induction with BrdU and GEM, however, the initial expression of Ki-67, as presented before, was different depending on the drug used to induce senescence (**Figure 11.B**). The analysis also confirmed that PALBO-induced senescent cells regained their proliferative capacity even after 3 days of incubation with drug-free medium, indicating that PALBO-treatment induced a less stable growth-arrest compared to the BrdU- and GEM-treatment (**Figure 11.B**). After senescence-escape, the morphology of the cells changed gradually, becoming smaller and less flattened, looking identical to control (non-senescent) MCF-7 cells, and the size of the colonies formed by senescence-escaped cells was gradually increased (**Figure 11.C**). Based on these results, BrdU- and GEM-treatment induced a more stable but reversible cell cycle arrest in MCF-7 cells compared to PALBO-treatment, that induced only a transient growth-arrest. Due to this transient growth-arrest induced by PALBO-treatment, PALBO-induced senescent cells might not be a suitable model to study senescence-escape, therefore in subsequent experiments senescence-escape was assessed only in BrdU- and GEM-induced senescent cells.

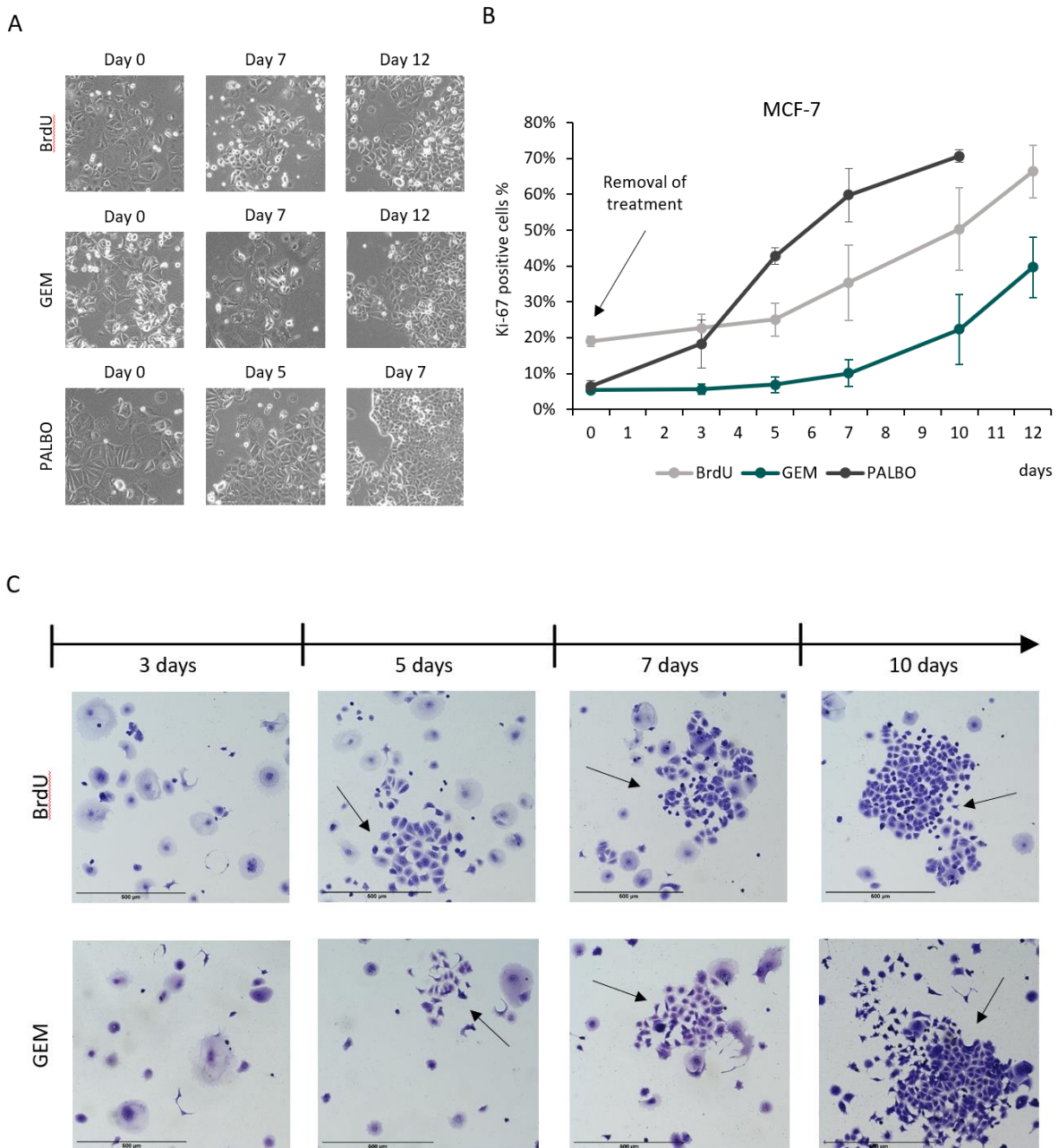


Figure 31. Senescence-escape in BrdU-, GEM- and PALBO-induced senescent MCF-7 cells. (A) Representative images of the senescence-escape of BrdU-, GEM- and PALBO-induced senescent MCF-7 cells, imaged at different time points after the removal of senescence-inducing drug. Images were taken by EVOS using 10x magnification and phase-contrast, (B) Analysis of senescence-escape based on the percentage of Ki-67-expressing cells compared to the total cell number measured by flow cytometry at different time points. Arrow indicates the removal of treatment representing day 0. The graph represents the mean of three independent experiments \pm SEM. (C) Representative images of senescence-escape demonstrating the appearance of senescence-escaped colonies at different time points after treatment removal. Arrows indicate the senescence-escaped cells. Cells were stained with crystal violet, imaged by EVOS using 10x magnification, scale bars indicate 500 μ m.

4.3 Developing a two-hit treatment strategy using azithromycin as a senolytic drug

4.3.1 Validating the senolytic effect of azithromycin on senescent MCF-7 cells

The second objective of the project was to develop a two-hit treatment strategy using azithromycin as a senolytic drug. The two-hit treatment strategy consist of a senescence-inducing drug (first hit) and a senolytic drug (second hit) that eliminates the senescent cancer cells (**Figure 12.A**). Azithromycin was described as a novel senolytic drug, selectively targeting senescent fibroblast cells, however its effect has not been tested in senescent cancer cells (Ozsvari et al., 2018). To test its senolytic effect in senescent cancer cells as well, senescent MCF-7 cells were treated with azithromycin for 72 hours using the concentration of 50 μM , 75 μM and 100 μM , based on the concentrations that had been used to target senescent fibroblasts. Based on the cell viability assays, azithromycin concentration-dependently decreased the viability of senescent MCF-7 cells, however, at lower concentration (50 μM) it had a significant effect only on GEM-induced senescent cells, but not on BrdU- and PALBO-induced senescent cells (**Figure 12.B**). Comparing the three senescent models, the PALBO-induced senescent cells were less affected by the azithromycin treatment, which had a significant effect only at 100 μM concentration. Although using 100 μM azithromycin decreased the viability of control MCF-7 cells to $\sim 80\%$, the viability of BrdU- and PALBO-induced senescent cells were reduced to $\sim 50\%$, and the viability of GEM-induced senescent cells was $\sim 30\%$, indicating that the senescent cells were more sensitive to the treatment (**Figure 12.B**). As mentioned before, apoptosis and proliferation arrest are not distinguishable with cell viability test, however, based on the previous results demonstrating that senescent cells stopped proliferating (**Figure 7.D, 8.C, Supplementary Figure 2.A**), the decrease of cell viability of senescent cells indicates cell death. Although further experiments should be conducted to investigate the induction of apoptosis in senescent cancer cells after azithromycin treatment. The toxicity of azithromycin was tested on MCF-10A non-malignant breast epithelial cells, showing that azithromycin treatment is not toxic to normal epithelial cells, and a reduction of cell viability was only detected at higher ($\geq 750 \mu\text{M}$) concentrations (**Figure 12.C**). Based on these results, the senolytic effect of azithromycin could be exploited in cancer treatment to reduce the number of senescent cancer cells generated by cancer therapy.

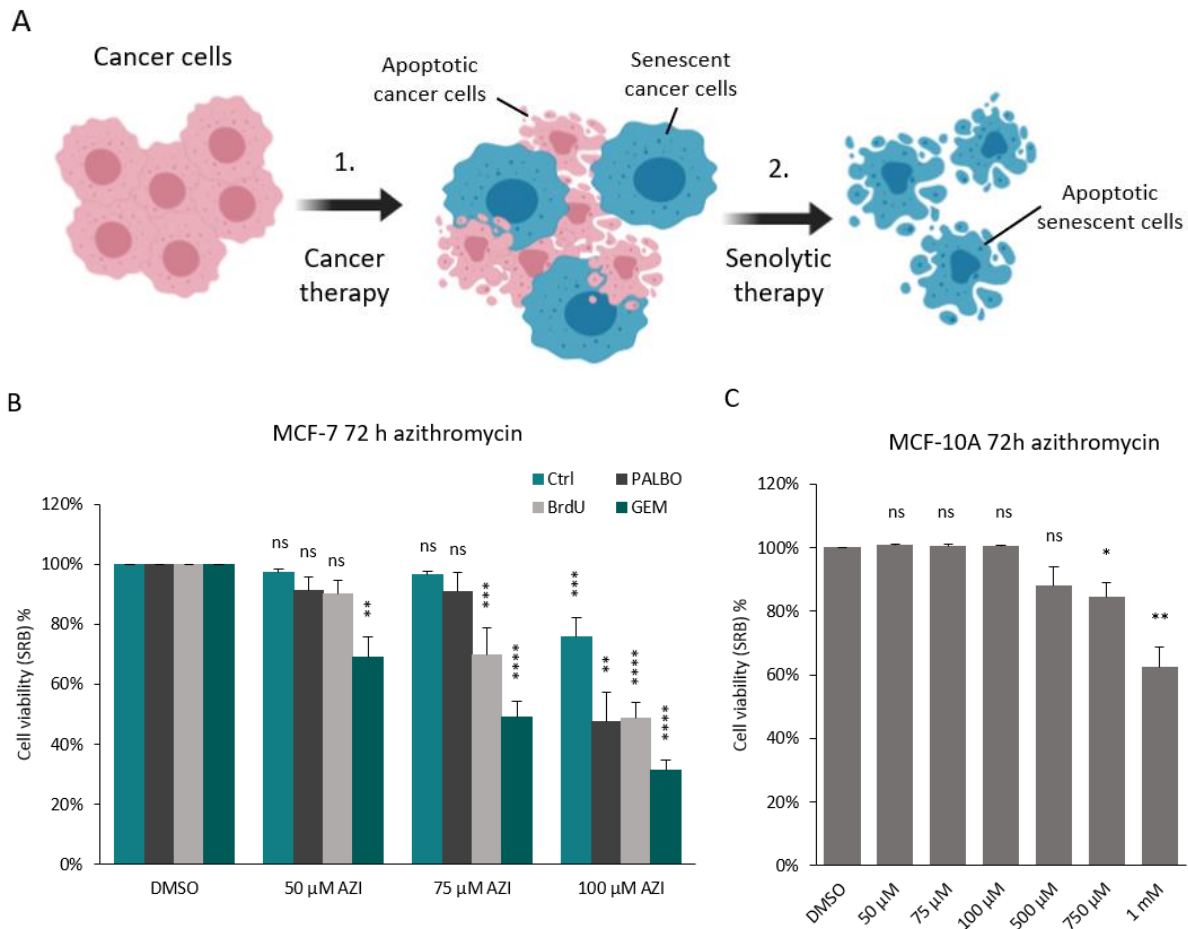


Figure 34. Two-hit treatment strategy using the senolytic effect of azithromycin. (A) Representative figure of the two-hit strategy, first hit: cancer therapy, resulting in apoptosis and senescence-induction, second hit: senolytic therapy, resulting in the elimination of senescent cancer cells. **(B-C)** The cell viability of control, BrdU-, GEM- and PALBO-induced senescent MCF-7 cells **(B)** and MCF-10A cells **(C)** was measured by SRB assay after 72 hours treatment of azithromycin. Experiments were repeated three times with six technical replicates, values were normalised to vehicle-treated controls (DMSO), error bars represent \pm SEM. Statistical significance (in relation to control): ns $p > 0.05$; * $p \leq 0.05$; ** $p \leq 0.01$; *** $p \leq 0.001$; **** $p \leq 0.0001$.

4.3.2 Investigating the effect of azithromycin on autophagy in MCF-7 cells

Besides its antibiotic effect, azithromycin has been described to have an impact on autophagic processes as well, which could be a potential mechanism explaining its senolytic effect (Renna et al., 2011, Ozsvari et al., 2018). Measuring the expression of LC3B (LC3-II, microtubule-associated protein 1 light chain 3) and p62/SQSTM1 (sequestosome-1) is a widely used method to study autophagic flux in mammalian cells. LC3B/LC3-II is localised to autophagic membranes, and its expression correlates with the number of autophagosomes (Runwal et al., 2019). p62/SQSTM1 is an adaptor protein of selective autophagy, and is itself degraded

by autophagy, therefore, the reduced expression of p62 indicates induced autophagy, and the accumulation of p62 together with LC3B is an indicator of autophagy inhibition (Jiang and Mizushima, 2015). According to our results, azithromycin (AZI) treatment increased the expression of both LC3B and p62/SQSTM1, indicating that it inhibited autophagy in both control and senescent MCF-7 cells (**Figure 13.A**). The effect of azithromycin was compared with chloroquine (CQ), which has a well-known effect to inhibit autophagy by interrupting the fusion of autophagosomes with lysosomes and it has been described to act as a senolytic in several studies (Mauthe et al., 2018). As expected, CQ treatment of control and senescent MCF-7 cells increased the expression of both LC3B and p62, however, the expression of LC3B was higher and the expression of p62/SQSTM1 was lower compared to the effect of AZI (**Figure 13.B**). The analysis of immunostaining revealed that LC3B and p62/SQSTM1 was expressed heterogeneously in the AZI/CQ treated cell populations, especially in the senescent cells (**Figure 13.C, Supplementary Figure 4.A**). The analysis also confirmed that the expression of LC3B was increased more after CQ treatment, while the expression of p62/SQSTM1 showed a higher increase after AZI treatment (**Figure 13.C, Supplementary Figure 4.A**). Based on these results, AZI and CQ demonstrated a similar effect on autophagic processes in control and senescent MCF-7 cells. Based on the evaluation of LC3B and p62 expression, both AZI and CQ treatment inhibited autophagy, however, the different levels of increase in LC3B and p62 expression suggests a different mechanism of action of AZI and CQ. The heterogeneous expression of both markers in response to AZI treatment indicates a heterogeneous response of senescent MCF-7 cells to AZI treatment, which could be responsible for the ~50% of surviving senescent cell populations measured by cell viability assay after 72 hours AZI treatment (**Figure 12.B**).

The effect of chloroquine (CQ) was tested on the viability of control and senescent MCF-7 cells as well to assess its senolytic activity. According to the cell viability assay (SRB), CQ treatment did not have a selective effect on BrdU-induced senescent cells, and it showed lower selectivity (the ratio of the affinity of a compound towards an off-target cell type/molecule relative to the targeted cell type/molecule) towards GEM- and PALBO-induced senescent cells compared to azithromycin (**Figure 12.B, Figure 13.D**). The toxicity of CQ was tested on MRC-5 human fibroblast cells, and compared to azithromycin treatment, MRC-5

cells were more sensitive to chloroquine treatment (**Figure 13.E**). These results indicate that AZI could be more suitable to use as a senolytic drug in cancer treatment compared to CQ.

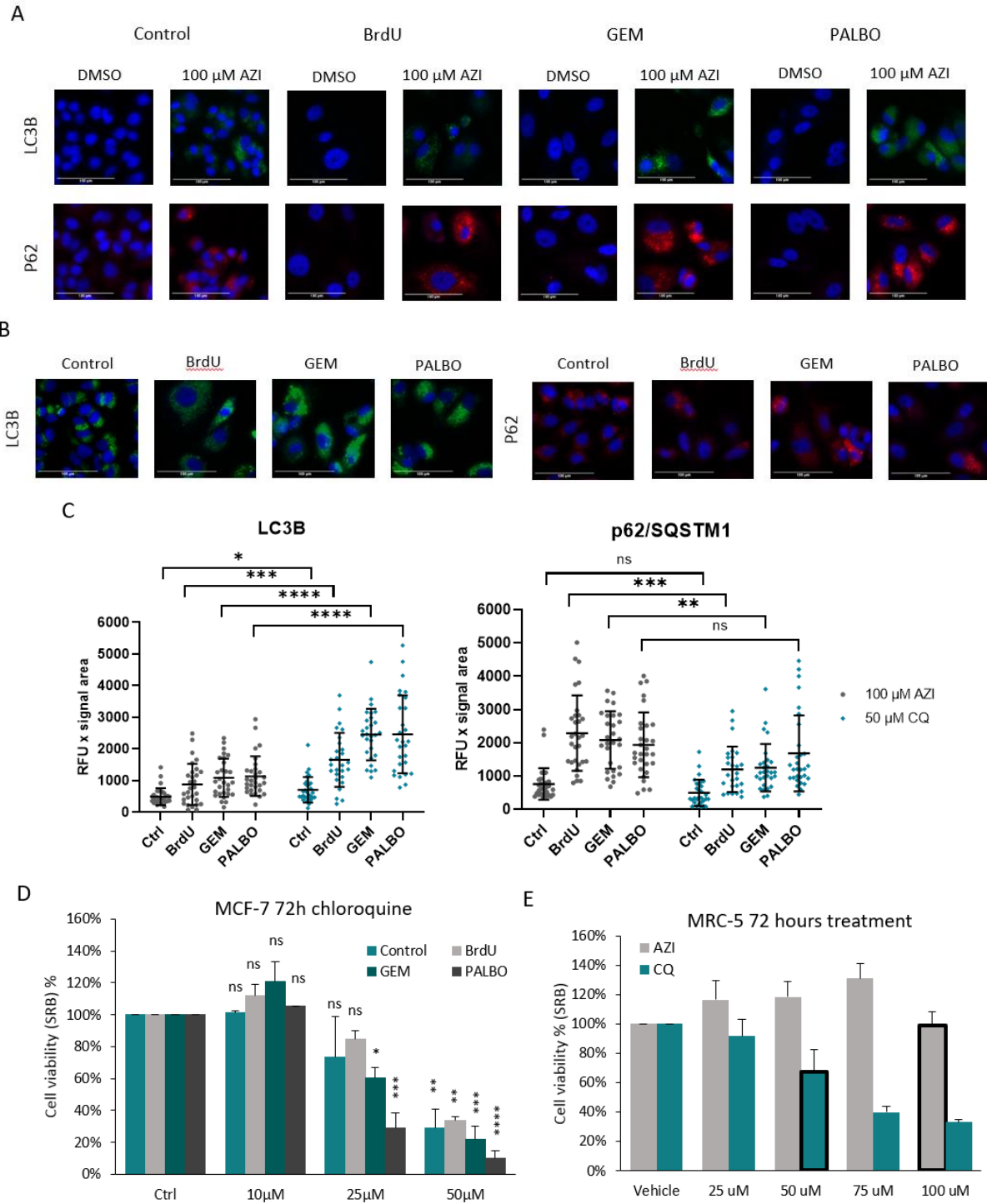


Figure 37. Effect of azithromycin and chloroquine treatment. (A-B) Representative images of LC3B and p62/SQSTM1 immunostaining of control, BrdU-, GEM- and PALBO-induced senescent cells after 48 hours of 100 μ M azithromycin **(A)** and 50 μ M chloroquine **(B)** treatment. By using the same imaging settings for each condition, in untreated MCF-7 cells (DMSO) the signal intensity was below the detection threshold. Cells were imaged by EVOS using 20x magnification, scale bars indicate 100 μ m. **(C)** Analysis of LC3B and p62/SQSTM1 expression in control, BrdU-, GEM- and PALBO-induced senescent cells after azithromycin or chloroquine treatment. Experiments were repeated three times with two technical replicates. The graphs represent the relative fluorescent unit (RFU) multiplied by the signal area based on the analysis of fluorescent signal intensity of 30 cells for each condition (10 cells from each experimental replicates) measured by ImageJ software. Error bars represent mean \pm SD. Graphs representing the RFU without the signal area are included in supplementary (Supplementary Figure 3.A). **(D)** The cell viability of control, BrdU-, GEM- and PALBO-induced senescent MCF-7 cells was measured by SRB assay after 72 hours treatment of chloroquine. Experiments were repeated three times with six technical replicates, values were normalised to vehicle-treated controls, error bars represent \pm SEM. Statistical significance (in relation to control): ns $p > 0.05$; * $p \leq 0.05$; ** $p \leq 0.01$; *** $p \leq 0.001$; **** $p \leq 0.0001$. **(E)** The cell viability of MRC-5 cells was measured by SRB assay after 72 hours of treatment with azithromycin (AZI) or chloroquine (CQ). The bars highlighted indicate the highest concentrations that has been used for the treatment of senescent MCF-7 cells. Experiments were repeated two times with six technical replicates, values were normalised to vehicle-treated controls, error bars represent \pm SEM.

4.3.3 Investigating senescence-escape after AZI treatment of senescent MCF-7 cells

Although azithromycin treatment decreased the viability of senescent cells, ~50% of BrdU- and PALBO-induced senescent cells, and ~30% of GEM-induced senescent cells remained viable after the treatment with 100 μ M AZI **(Figure 12.B)**. Moreover, 5 days treatment with 100 μ M AZI did not decrease the viability of senescent cells more than the 3-days treatment, indicating that a population of senescent MCF-7 cells could be resistant to AZI treatment **(Figure 14.A)**. To test whether these remaining cells are able to escape from senescence, the Ki-67 expression of the cells along with the cell numbers (cell concentration) were measured 10 days after the removal of AZI treatment **(Figure 14.B)**. According to the results, BrdU- and GEM-induced senescent cells were able to escape after AZI treatment, however, the Ki-67 expression was significantly decreased in the BrdU-induced senescent cells compared to the non-treated (without AZI) senescent cells, but not in GEM-induced senescent cells **(Figure 14.B)**. Regarding the non-senescent MCF-7 cells, azithromycin treatment did not affect the Ki-67 expression of control cells, indicating that after the removal of AZI the cell proliferation rate of MCF-7 cells remained unchanged **(Figure 14.B)**. The evaluation of cell concentration of BrdU- and GEM-induced senescent cells with or without AZI treatment showed that after

10 days drug-free incubation the number of AZI-treated senescence-escaped cells were significantly reduced compared to the number of senescence-escaped without AZI treatment (**Figure 14.C**). The decreased number of senescence-escaped cells would normally indicate decreased senescence-escaping ability, however, AZI treatment can influence the number of senescence-escaped cells by decreasing the number of senescent cells (as demonstrated before) (**Figure 12.B**). Due to this effect of AZI treatment, the decreased number of senescence-escaped cells is more likely to be a result of decreased cell viability rather than decreased senescence-escaping ability (**Figure 14.C**). PALBO-induced senescent cells, as demonstrated before (**Figure 11.A-B**), can continue their growth shortly after the removal of PALBO, and although the AZI treatment decreased the viability of PALBO-induced senescent cells, it did not decrease the senescence-escaping ability of the remaining cell population (**Supplementary Figure 9.C**). These results indicate that although AZI reduced the viability of senescent MCF-7 cells, the surviving cells can escape from senescence and regain their proliferative capacity.

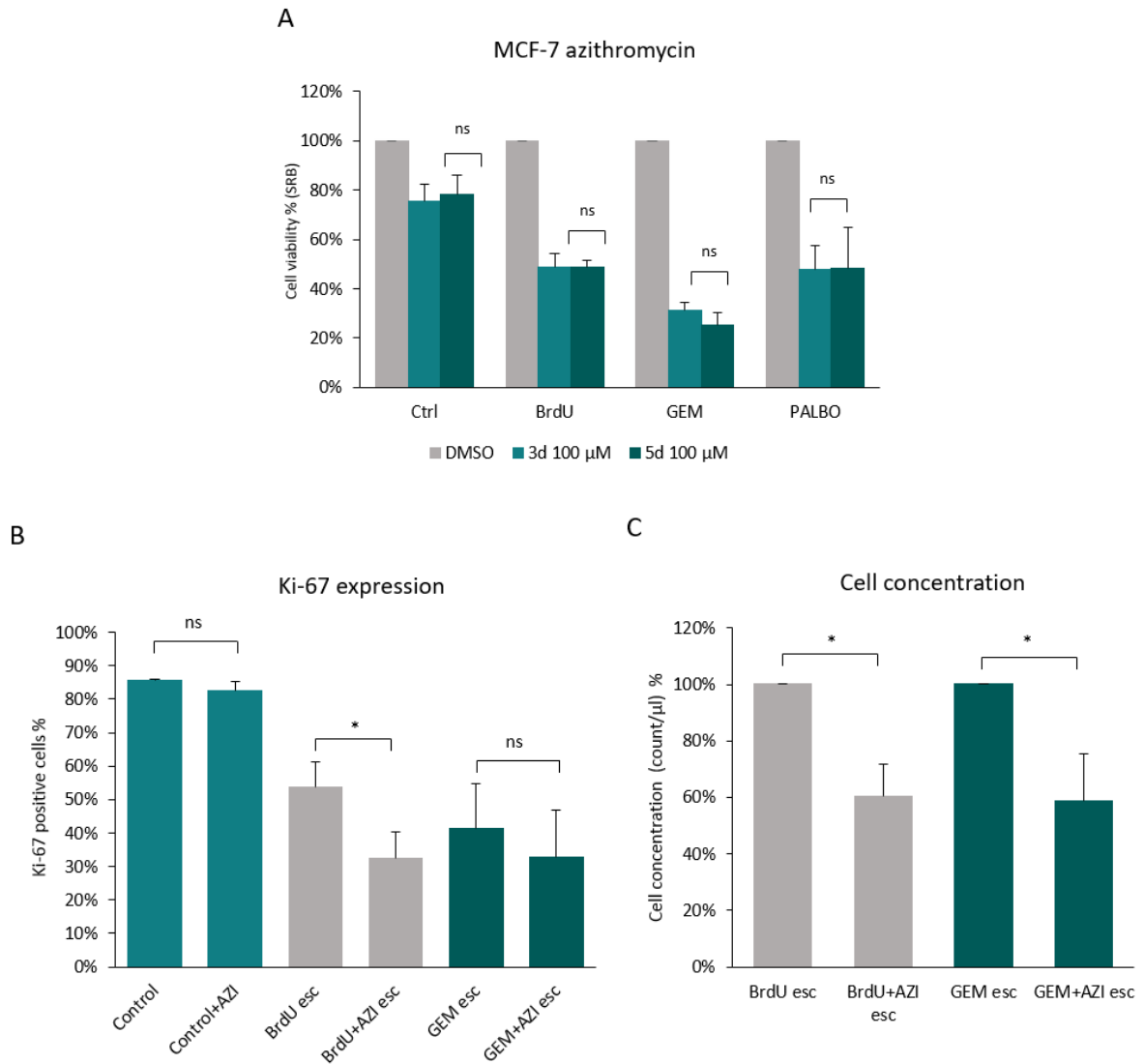


Figure 40. Analysis of senescence-escape after azithromycin treatment. (A) The cell viability of control, BrdU-, GEM- and PALBO-induced senescent MCF-7 cells was measured by SRB assay after 3 days and 5 days of treatment with azithromycin. Experiments were repeated three times with six technical replicates, values were normalised respectively to vehicle-treated (DMSO) control BrdU-, GEM- and PALBO-induced senescent cells **(B)** Control and senescent MCF-7 cells were treated with DMSO or 100 μM AZI for 72 hours. After, control cells were incubated 3 days without AZI, and senescent cells were incubated 10 days without AZI. The senescence-escaping ability of the cells was assessed by Ki-67 staining. The expression of Ki-67 is represented as the percentage of positively stained cells compared to the total population. The gates for Ki-67-positive cells were adjusted by using unstained cells. **(C)** The cell concentrations were measured by flow cytometry using the samples from the measurement of Ki-67 expression represented as count/μl (cell number/μl). The samples were collected with the same volume; therefore the cell concentration is proportional to the cell numbers of each sample. Values were respectively normalised to the untreated BrdU- and GEM-escaped cells. Bar graphs represent the mean of three independent experiments ± SEM. Statistical significance: ns $p > 0.05$; * $p \leq 0.05$; ** $p \leq 0.01$; *** $p \leq 0.001$; **** $p \leq 0.0001$.

4.4 Investigating the expression and function of dipeptidyl peptidase-4 (DPP4/CD26) in senescent MCF-7 cells

4.4.1 Analysing the expression of DPP4/CD26 in senescent MCF-7 cells

The third objective of the project was to investigate the cell surface protein DPP4/CD26 as a marker of senescence in cancer and to identify its function in senescence. Although DPP4/CD26 was identified as a marker of senescence in fibroblast cells, its expression and potential function has not been investigated in senescent cancer cells (Kim et al., 2017a). Firstly, the expression of DPP4/CD26 was measured in control MCF-7 cells and in BrdU-, GEM- and PALBO-induced senescent cells by flow cytometry (**Figure 15.A**). Based on the results, senescent cells had a significantly increased expression of DPP4/CD26, demonstrated in a ~4-5-fold increase in PALBO- and GEM-induced senescent cells, and a ~10-fold increase in BrdU-induced senescent cells (**Figure 15.A**). Similar increase of DPP4/CD26 expression in senescent MCF-7 cells was detected by western blot as well (**Supplementary Figure 2.A**). To further confirm the connection between the increased expression of DPP4/CD26 and senescence, the expression of DPP4/CD26 was monitored for 14 days, compared to the expression of SA- β -Gal (**Figure 15.B**). Both markers showed a time-dependent increase of expression; however, the levels of their increase were different in each senescent model, showing a maximal expression of DPP4/CD26 after 14 days of BrdU treatment (**Figure 15.B**). Based on these results, the expression of DPP4/CD26 is significantly increased in senescent cells, however, the levels of increase were dependent on the drugs used for senescence-induction. The expression of DPP4/CD26 was time-dependently increased during senescence-induction, indicating a strong connection between DPP4/CD26 expression and the development of senescence-phenotype.

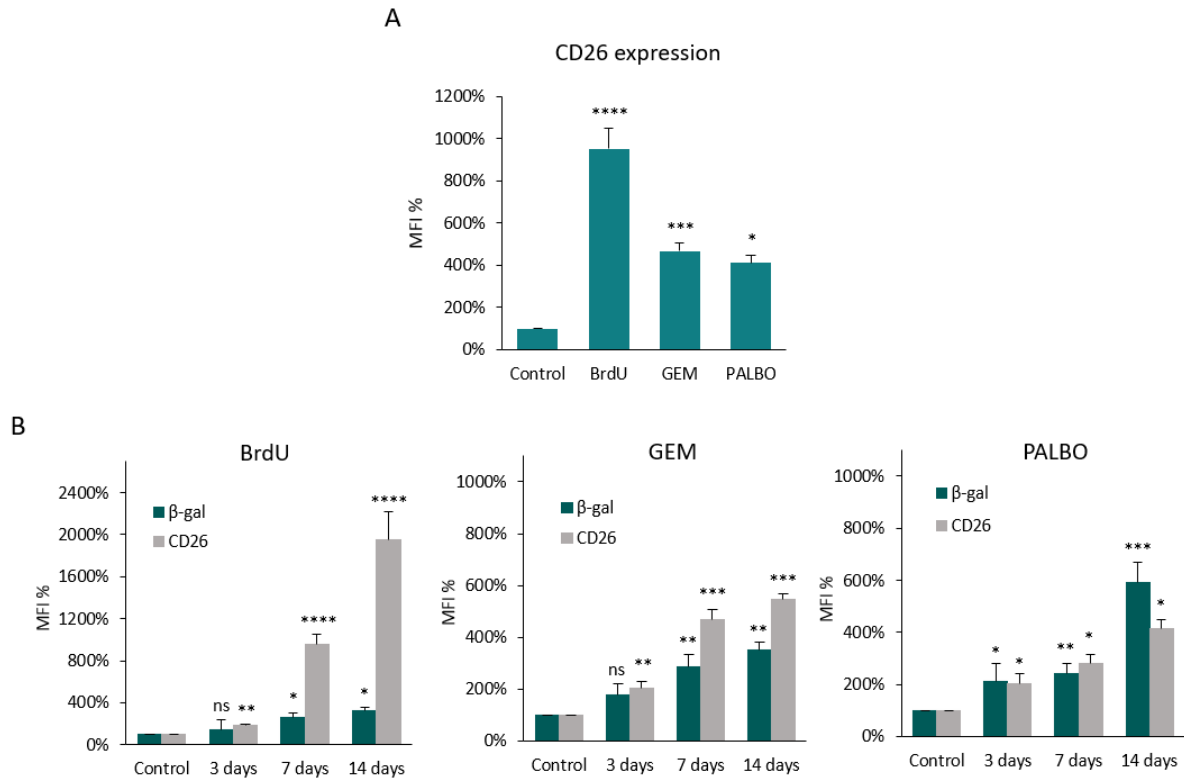


Figure 43. Analysis of DPP4/CD26 expression in senescent MCF-7 cells. (A) The expression of CD26 was measured by flow cytometry, represented as mean fluorescence intensity (MFI) of CD26-PE staining. Values were normalised to the MFI of non-senescent (control) MCF-7 cells. **(B)** The expression of SA-β-galactosidase and CD26 in control, BrdU-, GEM- and PALBO-induced senescent MCF-7 cells was measured at different time-points by flow cytometry. The SA-β-galactosidase and CD26 expression is represented as mean fluorescence intensity (MFI) of FDG, and CD26-PE staining measured separately by flow cytometry, values were normalised to the MFI of non-senescent MCF-7 cells. Bar graphs represent the mean of three independent experiments \pm SEM. Statistical significance (in relation to control): ns $p > 0.05$; * $p \leq 0.05$; ** $p \leq 0.01$; *** $p \leq 0.001$; **** $p \leq 0.0001$.

4.4.2 Silencing the expression of DPP4 in MCF-7 cells

To investigate the potential function of DPP4/CD26 in senescence, senescent MCF-7 cells with silenced expression of DPP4 (DPP4 siRNA) were generated by lentiviral vector-mediated gene silencing. The silencing was confirmed by both western blot and flow cytometry (**Figure 16.A-B**). However, the silencing of DPP4 expression had no effect on cell proliferation, and it did not affect the expression of SA-β-Gal and lysosomal mass in senescent cells (**Figure 16. C-E**). Due to the GFP-expression of the transduced cells, the fluorogenic SA-β-Gal staining (FDG) could not be detected, therefore the assessment of lysosomal mass was used as an additional marker, that could be quantified easier than chromogenic SA-β-Gal staining (X-gal) (**Figure**

16.E). These results indicate that although the expression of DPP4/CD26 is increased in senescent cells, its expression is not essential for senescence-induction in MCF-7 cells.

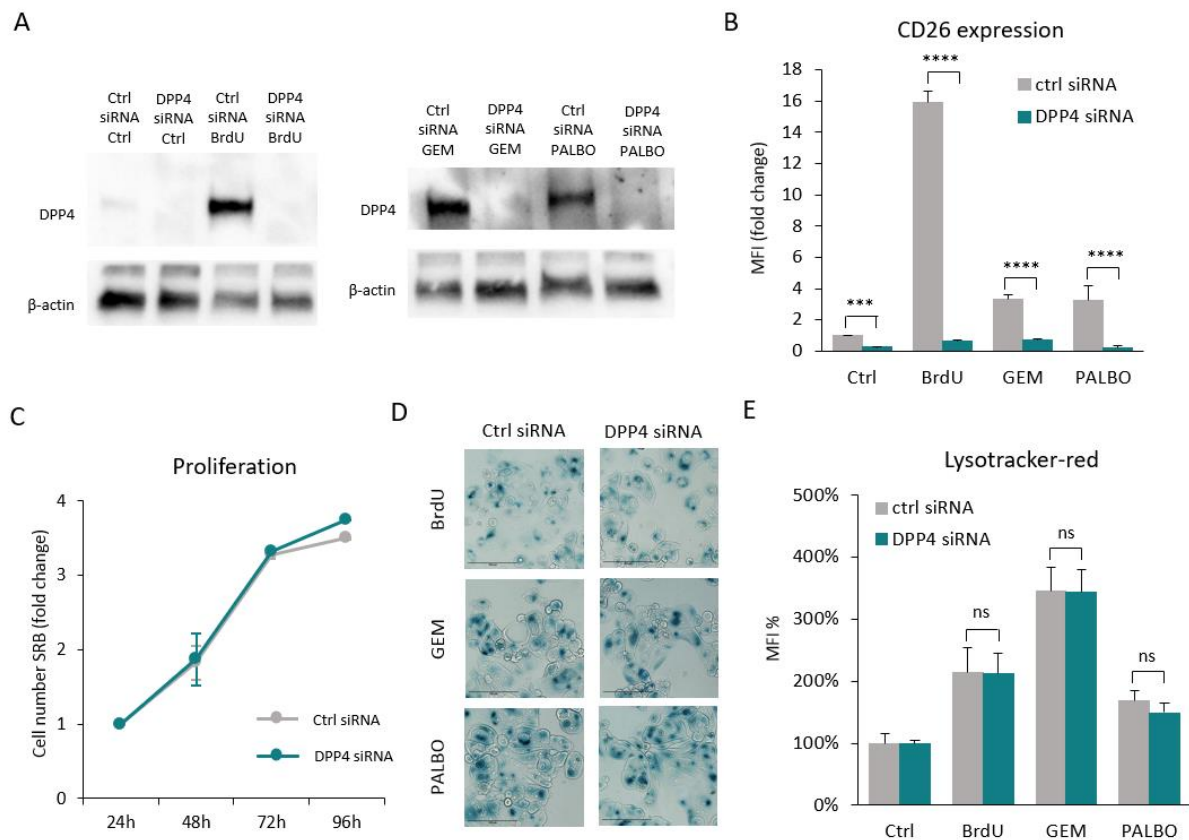


Figure 46. Effect of DPP4 silencing on the senescence-induction in MCF-7 cells. The expression of DPP4 was silenced in MCF-7 cells by lentiviral vector-mediated gene silencing, cells were labelled as DPP4 siRNA. Cells transduced with scrambled vector were used as experimental controls, labelled as ctrl siRNA. **(A)** Representative images of western blot analysis of control and senescent MCF-7 cells, demonstrating the silencing of DPP4 expression. **(B)** CD26 expression is represented as mean fluorescence intensity (MFI) of CD26-PE staining measured by flow cytometry, values were normalised to the MFI of non-senescent ctrl siRNA cells and represented as fold change. **(C)** Cell proliferation was measured by SRB assay at different time-points, values were normalised to the baseline values measured 24 hours after cell seeding and represented as fold change. Graph represents the mean of three independent experiments \pm SEM. **(D)** Representative images of BrdU-, GEM- and PALBO-induced senescent ctrl siRNA and DPP4 siRNA cells. Cells were fixed and stained with X-gal, imaged by EVOS with 20x magnification, scale bars indicate 100 μ m. The blue colour indicates SA- β -galactosidase activity. **(E)** Lysosomal content is represented as mean fluorescence intensity (MFI) of LysoTracker deep red staining measured by flow cytometry, values were normalised to the MFI of non-senescent ctrl siRNA cells. Bar graphs represent the mean of three independent experiments \pm SEM. Statistical significance: ns $p > 0.05$; * $p \leq 0.05$; ** $p \leq 0.01$; *** $p \leq 0.001$; **** $p \leq 0.0001$.

4.4.3 Investigating the role of DPP4/CD26 in senescence-escape in MCF-7 cells

To investigate whether the expression of DPP4/CD26 has a role in senescence-escape, the senescence-escaping ability of DPP4-silenced (DPP4 siRNA) senescent cells was analysed by Ki-67 and crystal violet staining and compared with control senescent cells (ctrl siRNA). As described before, due to the transient growth-arrest/senescence induced by PALBO-treatment (**Figure 11.A-B**), PALBO-induced senescent cells might not be a suitable model to study senescence-escape, therefore senescence-escape was assessed only in BrdU- and GEM-induced senescent cells. The adjustment of gates for the measurement of Ki-67 expression by flow cytometry is presented in Supplementary Figure 7.A. Consistent with the previous observation that DPP4 is not required for senescence-induction in MCF-7 cells (**Figure 16**), DPP4 silencing did not change the Ki-67 expression in control and senescent (BrdU/GEM) cells (**Figure 17.A, Supplementary Figure 7.A**). However, the proportion of Ki-67 expressing cells was significantly decreased in the senescence-escaped DPP4 siRNA cells compared to ctrl siRNA senescence-escaped cells (**Figure 17.A, Supplementary Figure 7.A**). According to our previous results, the silencing of DPP4 did not affect cell proliferation (**Figure 16.C**), therefore the decreased Ki-67 expression could indicate the decreased ability of senescent cells to regain their proliferative capacity. It is important to note, that although the percentage of Ki-67 expressing cells indicates the proportion of senescence-escaped (actively proliferating) cells, it does not give an information about the actual number of escaping-cells. To better demonstrate the difference in the senescence-escaping ability of DPP4 siRNA and ctrl siRNA senescence-escaped cells, the analysis of Ki-67 expression was combined with the measurement of cell numbers after senescence-escape (**Figure 17.B-C**). Based on this combined assessment, the number of senescence-escaped cells were significantly decreased to ~70% in BrdU-induced and to ~30% in GEM-induced senescent DPP4 siRNA cells compared to ctrl siRNA cells (**Figure 17.C**). These results were similar to the results of crystal violet staining, that showed that the silencing of DPP4 expression significantly reduced (~40%) the formation of senescence-escaped colonies in both BrdU- and GEM-induced senescent cells, while the colony formation ability of control cells were not affected by DPP4 silencing (**Figure 12.D-E**). Based on these results we concluded that DPP4 silencing decreased the senescence-escaping ability of BrdU- and GEM-induced senescent MCF-7 cells. However, further

experiments are needed to identify the molecular pathways that could mediate the effect of DPP4 expression in senescence-escape.

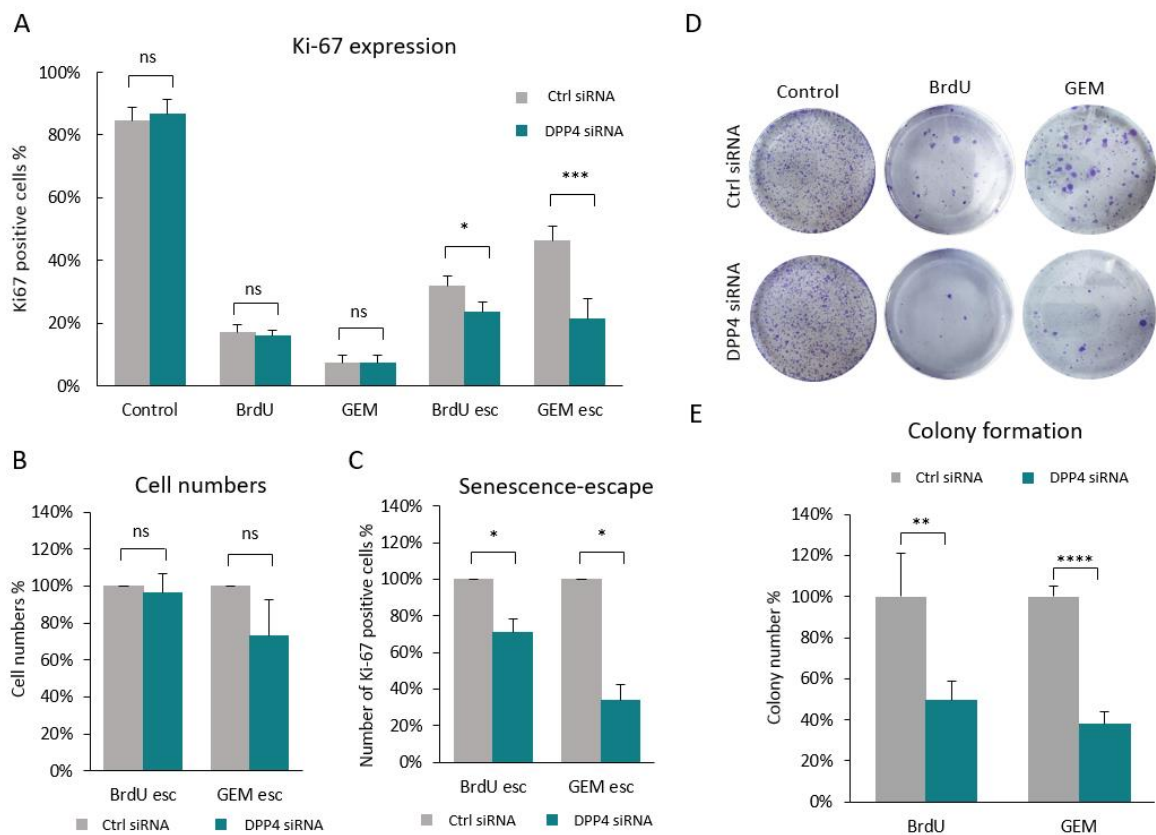


Figure 49. Effect of DPP4 silencing on the senescence-escape of MCF-7 cells. (A) The expression of Ki-67 is represented as the percentage of positively stained cells compared to the total population. The gates for Ki-67-positive cells were adjusted by using unstained cells, represented in Supplementary Figure 7.A. **(B)** The cell concentrations were measured by flow cytometry using the samples from the measurement of Ki-67 expression represented as count/ μl (cell number/ μl). The samples were collected with the same volume; therefore, the cell concentration is proportional to the cell numbers of each sample. Values were respectively normalised to the BrdU- and GEM-escaped ctrl siRNA cells. **(C)** The senescence-escaping ability of the cells are assessed by the combination of Ki-67 expression and cell concentration represented as the number of Ki-67 positive cells. Values were respectively normalised to the BrdU- and GEM-escaped ctrl siRNA cells. **(D)** Representative images of the colony formation of control and senescence-escaped ctrl siRNA and DPP4 siRNA cells. Control cells were seeded with 1×10^4 cells/well, senescent cells were seeded with 3×10^5 cells/well, incubated for 10 days and stained with crystal violet. **(E)** The senescence-escaping ability of the cells were assessed by colony formation assay, represented as the number of colonies normalised respectively to the BrdU- and GEM-escaped ctrl siRNA cells. Experiments were repeated with three technical replicates. Bar graphs represent the mean of three independent experiments \pm SEM. Statistical significance: ns $p > 0.05$; * $p \leq 0.05$; ** $p \leq 0.01$; *** $p \leq 0.001$; **** $p \leq 0.0001$.

4.4.4 Investigating the effect of DPP4 inhibition in senescence-escape using sitagliptin in MCF-7 cells

Based on the results of DPP4 silencing (**Figure 17**), we tested whether the inhibition of the enzymatic activity of DPP4 could decrease the senescence escape of MCF-7 cells. Firstly, the effect of a widely used DPP4-inhibitor, sitagliptin, on cell viability was tested in MCF7 and MCF-10A cells (**Figure 18.A**). The experiment demonstrated that sitagliptin treatment decreased the viability of MCF-7 cells at a concentration of 500 μ M or higher, and it showed no toxicity in normal epithelial MCF-10A cells (**Figure 18.A**). In addition, sitagliptin treatment did not decrease the viability of senescent cells up to a concentration of 1 mM (**Figure 18.B**). These results indicate that sitagliptin treatment does not affect the viability of control and senescent MCF-7 cells. Sitagliptin has been found to inhibit the enzymatic activity of DPP4 in MCF-7 cells at a concentration of \sim 300 μ M or higher (Choi et al., 2015), therefore, in subsequent experiments it is used at a concentration of 250 μ M and 500 μ M. Next, the effect of sitagliptin on senescence-escape was assessed by measuring the Ki-67 expression of senescence-escaped cells combined with the number of cells (**Figure 18.C, Supplementary Figure 7**). According to the results, sitagliptin treatment concentration-dependently decreased the number of Ki-67 expressing cells in BrdU- and GEM-induced senescent cells, however, in PALBO-induced senescent cells sitagliptin treatment only had an effect at the concentration of 500 μ M (**Figure 18.C, Supplementary Figure 7**). The results were confirmed by crystal violet staining as well, that demonstrated decreased number of senescence-escaped colonies after sitagliptin treatment in BrdU- and GEM-induced senescent cells (**Figure 18.D-E**). Although 72 hours sitagliptin treatment showed no significant effect on the viability of non-senescent (control) MCF-7 cells at 250 μ M concentration (**Figure 18. A**), prolonged treatment (10 days) with 250 μ M sitagliptin decreased the colony formation of control MCF-7 cells (**Supplementary Figure 10.A**). These results indicate that the effect of DPP4 in the senescence-escape of MCF-7 cells is based on the enzymatic activity of DPP4, and the senescence-escaping ability of MCF-7 cells could be decreased by DPP4-inhibition.

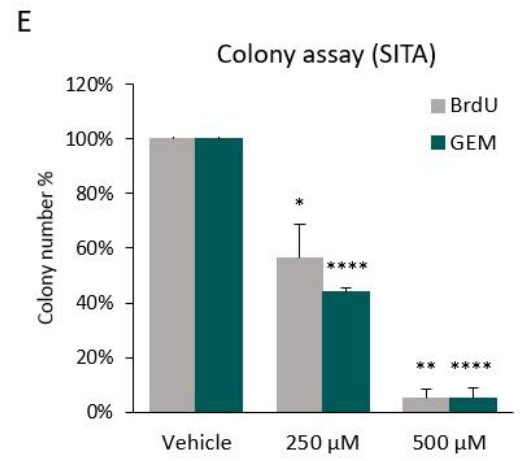
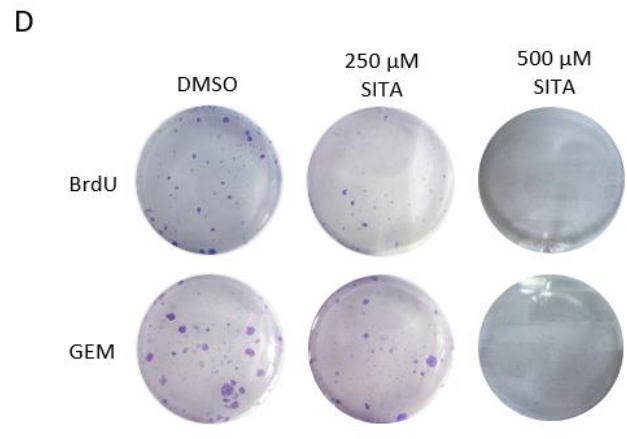
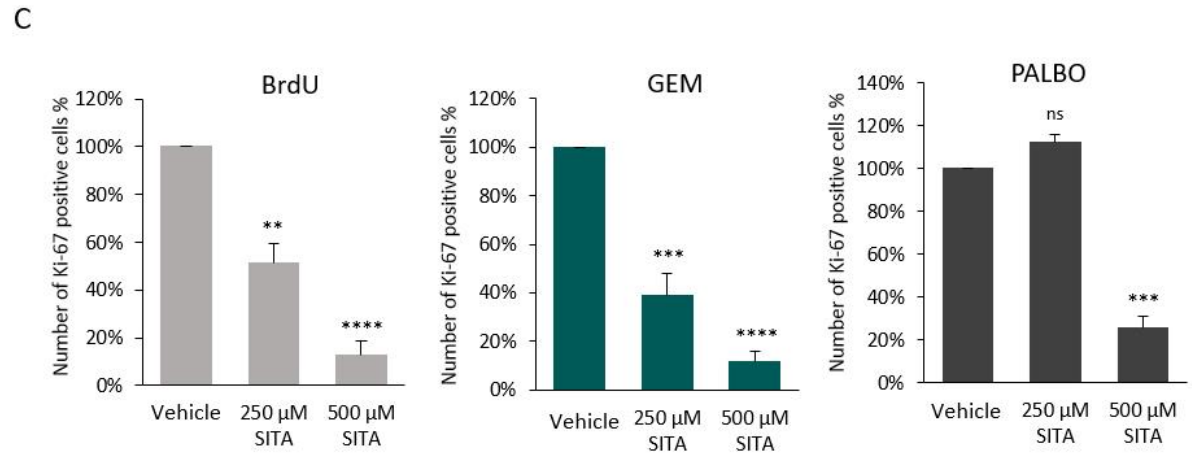
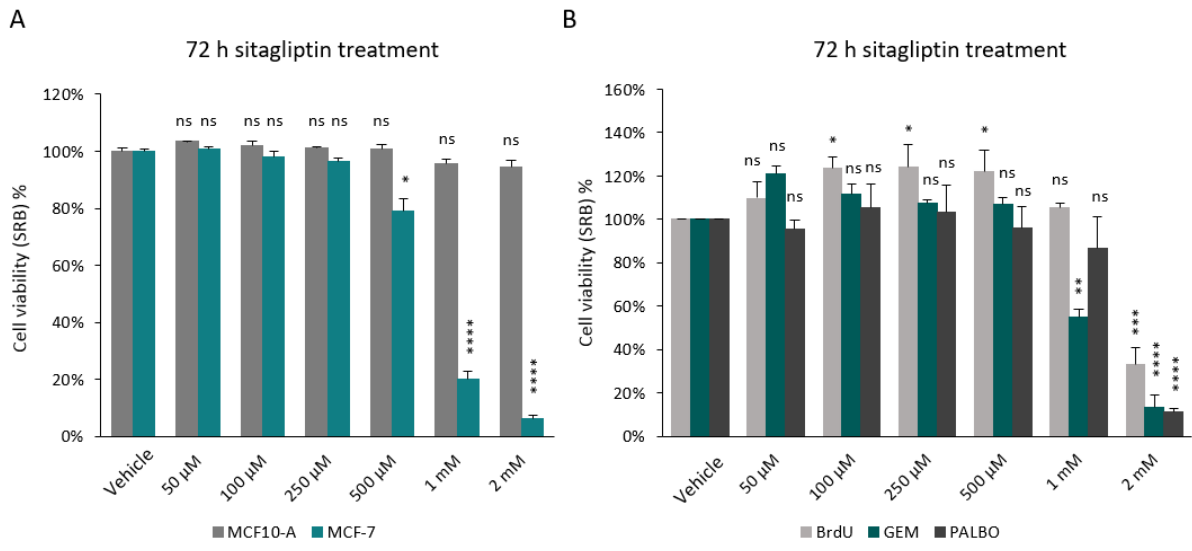
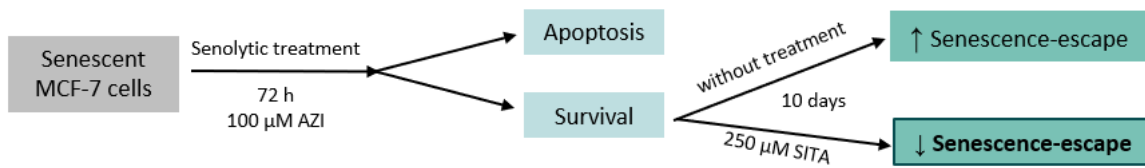


Figure 52. Effect of DPP4-inhibition in senescence-escape. (A-B) The cell viability of MCF-10A, MCF-7 cells **(A)** and BrdU-, GEM- and PALBO-induced senescent MCF-7 cells **(B)** was measured by SRB assay after 72 hours treatment of sitagliptin. Experiments were repeated three times with six technical replicates, values were normalised to vehicle-treated controls, error bars represent \pm SEM. After senescence induction by BrdU- and GEM-treatment cells were incubated for 10 days with sitagliptin treatment. **(C)** The senescence-escaping ability of the cells are assessed by the combination of Ki-67 expression and cell concentration represented as the number of Ki-67 positive cells. Values were normalised to the vehicle-treated cells. Graphs representing the Ki-67 expression and cell concentrations separately are included in supplementary (Supplementary Figure 7). **(D)** Representative images of the colony formation of BrdU- and GEM-treated senescence-escaped cells after sitagliptin treatment. Cells were seeded with 3×10^5 cells/well, incubated for 10 days with sitagliptin treatment and stained with crystal violet. **(E)** The senescence-escaping ability of the cells were assessed by colony formation assay, represented as the number of colonies normalised respectively to the vehicle-treated BrdU- and GEM-escaped cells. Experiments were repeated with three technical replicates. Bar graphs represent the mean of three independent experiments \pm SEM. Statistical significance (in relation to control): ns $p > 0.05$; * $p \leq 0.05$; ** $p \leq 0.01$; *** $p \leq 0.001$; ****

4.4.5 Investigating the effect of the combination treatment with azithromycin and sitagliptin in MCF-7 cells

As demonstrated before, MCF-7 cells were able to escape from senescence after azithromycin treatment **(Figure 14)**, therefore, to increase the effect of azithromycin, the combination of azithromycin (AZI) and sitagliptin (SITA) was tested on BrdU- and GEM-induced senescent cells. After senescence induction using BrdU or GEM, senescent cells were treated with 100 μ M AZI for 72 hours. Then, the cells were incubated with or without 250 μ M SITA treatment for 10 days, and the senescence-escaping ability of the cells was assessed by Ki-67 staining **(Figure 19.A)**. Based on our results, using sitagliptin subsequent to the treatment with azithromycin improved the effect of azithromycin in BrdU- and GEM-induced senescence-models, by further decreasing the number of Ki-67 expressing cells to \sim 5-10% **(Figure 19.B, Supplementary Figure 9.A-B)**. However, the combination treatment was not effective to decrease senescence-escape in PALBO-induced senescent cells **(Supplementary Figure 9.C)**. These results indicate a synergistic effect of the combination treatment of azithromycin and sitagliptin in MCF-7 cells, resulting in a reduced number of senescence-escaped cells, compared to using azithromycin alone.

A



B

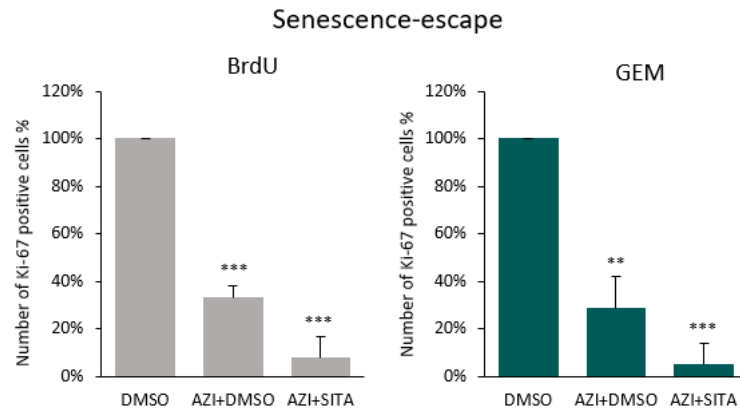


Figure 55. Analysis of senescence-escape after the combination of azithromycin and sitagliptin treatment. (A) Schematic figure representing the workflow of combination treatment using azithromycin and sitagliptin (B) The senescence-escaping ability of the cells were assessed by the combination of Ki-67 expression and cell concentration represented as the number of Ki-67 positive cells. Values were normalised to the vehicle-treated cells. Graphs representing the Ki-67 expression and cell concentrations separately are included in supplementary (S. Figure 8.A-B). Bar graphs represent the mean of three independent experiments \pm SEM. Statistical significance (in relation to control): ns $p > 0.05$; * $p \leq 0.05$; ** $p \leq 0.01$; *** $p \leq 0.001$; **** $p \leq 0.0001$.

4.5 Senescence induction in MDA-MB-231 cells

4.5.1 Establishing and analysing TIS models using bromodeoxyuridine (BrdU), gemcitabine (GEM) and Palbociclib (PALBO) in MDA-MB-231 cells

Although MCF-7 is a widely used cell-line in studies of therapy-induced senescence (Elmore et al., 2002, Karimi-Busheri et al., 2010, Tonnessen-Murray et al., 2019, Bojko et al., 2020, Mosieniak et al., 2015), it is a cellular model for hormone receptor-positive, HER2 negative (human epidermal growth factor receptor 2) luminal A subtype of breast cancer, that is generally treated with endocrine therapy instead of chemotherapy (Waks and Winer, 2019, Dai et al., 2017). To extend our investigation of therapy-induced senescence and to include a cellular model of triple-negative breast cancer, that is treated with chemotherapy in clinical settings, we induced senescence in MDA-MB-231 cells (Dai et al., 2017). Initially, the effect of BrdU, GEM and PALBO was tested on the cell viability of MDA-MB-231 cells to determine the drug concentration to use for senescence-induction (**Figure 20.A**). The aim was to arrest the proliferation of the cells without inducing significant amount of cell death. The IC_{50} of BrdU was more than the highest tested concentration (2 mM), the IC_{50} of GEM was more than the highest tested concentration 1 μ M and the IC_{50} of PALBO was 25 μ M, however, apoptosis and proliferation arrest are not distinguishable with cell viability test (**Figure 20.A**). Based on these results and the relevant literature, the optimal drug concentrations and incubation times were empirically determined and described in the Methods section. Briefly, to induce senescence in MDA-MB-231 cells, the cells were treated for 7 days with 50 μ M BrdU and 200 nM GEM, and 14 days with 1 μ M PALBO. To confirm the induction of senescence, different markers of cellular senescence were examined. First, the morphology of the cells was examined by flow cytometry by measuring the forward scatter values (FSC), indicating cell size, and side scatter values (SSC), indicating granularity (**Figure 20.B**). Compared to control cells FSC/SSC values were both significantly increased in all the senescent models; however, the SSC values were increased more than the FSC (**Figure 20.B**). Measured by flow-cytometry, the number of Ki-67 expressing cells was significantly decreased after senescence induction, however, ~5% of BrdU-induced, ~15% of GEM-induced and ~10% of PALBO-induced senescent cells still expressed Ki-67 (**Figure 20.D**). Despite these small populations of cells that remained positive for Ki-67 staining after senescence-inducing treatment, according to a cell proliferation assay (measured by SRB) after BrdU-, GEM and PALBO-treatment MCF-7 cells stopped proliferating (**Figure 20.E**). Investigating whether these drugs induced DNA-damage

in MDA-MB-231 cells, the expression of γ H2AX was analysed after senescence-induction. According to the results, GEM-induced senescent cells had a significant increase in the number of γ H2AX expressing cells (~60%), while after senescence induction with BrdU and PALBO there was no significant increase of γ H2AX-expression compared to the control cells (Figure 20.C).

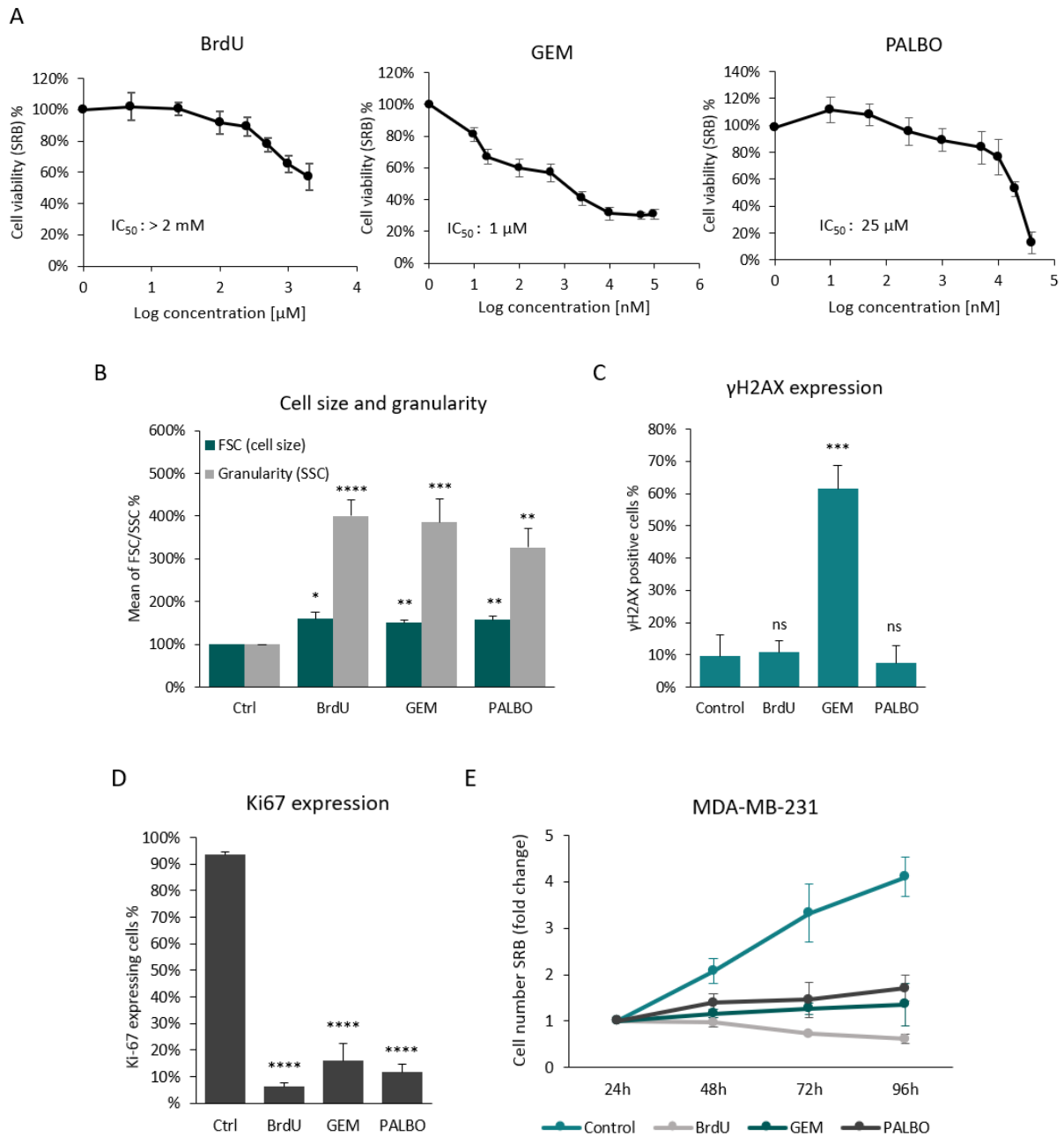


Figure 58. Senescence induction in MDA-MB-231 cells. (A) The cell viability of MDA-MB-231 cells was measured by SRB assay after 72 hours treatment of BrdU, GEM and PALBO using different drug concentrations. Experiments were repeated three times with six technical replicates, values were normalised to vehicle-treated controls, error bars represent \pm SEM. **(B)** The cell size and granularity of MDA-MB-231 cells were measured by the mean signal intensity of FSC and SSC by flow cytometry, values were normalised to non-senescent MDA-MB-231 cells. **(C)** The expression of Ki-67 is represented as the percentage of positively stained cells compared to the total population. The gates for Ki-67-positive cells were adjusted by using unstained cells. **(D)** The expression of γ H2AX is represented as the percentage of positively stained cells compared to the total population. The gates for γ H2AX-positive cells were adjusted by using unstained cells. Bar graphs represent the mean of three independent experiments \pm SEM. Statistical significance (in relation to control): ns $p > 0.05$; * $p \leq 0.05$; ** $p \leq 0.01$; *** $p \leq 0.001$; **** $p \leq 0.0001$. **(E)** Cell proliferation of control and senescent MDA-MB-231 cells was measured by SRB assay at different time-points, values were normalised to the baseline values measured 24 hours after cell seeding and represented as fold change. Graph represents the mean of two independent experiments \pm SEM.

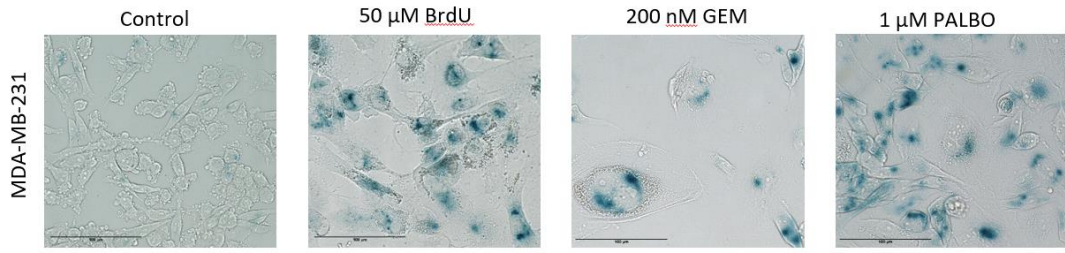
Measured by both chromogenic and fluorogenic SA- β -Gal assay, SA- β -Gal expression was significantly increased in each senescent models compared to the control MDA-MB-231 cells; however, it was less increased in the GEM-induced senescent cells (**Figure 21.A, Figure 21.B, Figure 21.C**). The images of SA- β -Gal staining also showed that the senescent cells had a flattened shape and larger size, however, the shape of the PALBO-induced senescent cells were more similar to the control cells and the size and shape of GEM-induced senescent cells were highly heterogeneous (**Figure 21.A**). To further investigate the increased expression of DPP4/CD26 as a marker of senescence in cancer, it was tested in BrdU-, GEM- and PALBO-induced senescent MDA-MB-231 cells as well (**Figure 21.D**). Senescent MDA-MB-231 cells showed a significantly increased expression of DPP4/CD26 compared to non-senescent (control) cells, demonstrated in a \sim 45-fold increase in BrdU-induced, a \sim 30-fold increase in GEM-induced, and a \sim 20-fold increase in PALBO-induced senescent cells (**Figure 21.D**). Similar increase of DPP4/CD26 expression in senescent MDA-MB-231 cells was detected by western blot as well (**Supplementary Figure 2.B**).

The analysis of SASP secretion (IL-6, IL-8, CXCL12) of MDA-MB-231 cells showed that compared to MCF-7 cells (**Figure 7.F**), MDA-MB-231 cells had a substantially higher basal expression of IL-6 and IL-8 (falling into ng/ml/100000 cells range), however, their expression of CXCL12 was below the detection threshold of the assay (**Figure 21.E**). According to our results, IL-6 and IL-8 levels, but not CXCL12 levels, were significantly increased in senescent

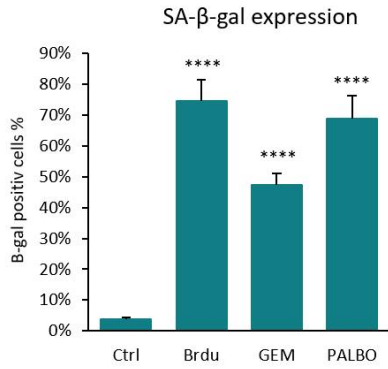
MDA-MB-231 cells, although at different levels depending on the senescence-inducing drug (**Figure 21.E**). In contrast with PALBO-induced MCF-7 cells (**Figure 7.F**), PALBO-induced senescent MDA-MB-231 cells showed a significantly increased expression of both IL-6 and IL-8 compared to non-senescent (control) cells (**Figure 21.E**). In more details, PALBO- and GEM-induced senescent cells had a higher expression of IL-6 than BrdU-induced senescent cells, while the highest level of IL-8 was secreted by the GEM-induced senescent cells (**Figure 21.E**).

Based on the assessment of senescence-markers, such as the altered cell morphology (increased cell size, flattened shape, increased granularity), the increased SA- β -Gal expression decreased Ki-67 expression and SASP secretion (IL-6, IL-8), we confirmed the establishment of senescence models in MDA-MB-231 cells. Moreover, the increased expression of DPP4/CD26 was confirmed in MDA-MB-231 cells as well. The results of γ H2AX-expression indicates that in MDA-MB-231 cells GEM induced senescence via DNA-damage induction, whereas BrdU and PALBO induced senescence through different mechanisms, independently from DNA-damage induction. However, compared to the MCF-7 cells (**Figure 6.D, Figure 7.A**) GEM treatment induced a more heterogeneous DNA-damage in MDA-MB-231 cells (**Figure 20.C, Figure 21.A**) leading to a more heterogeneous population of GEM-induced senescent cells.

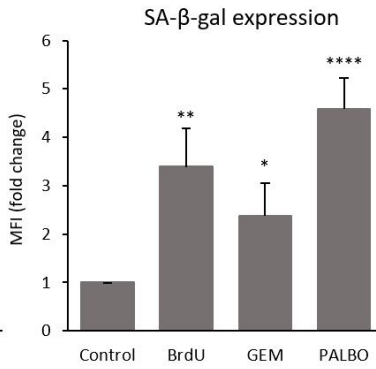
A



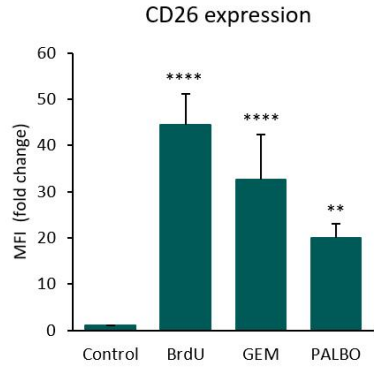
B



C



D



E

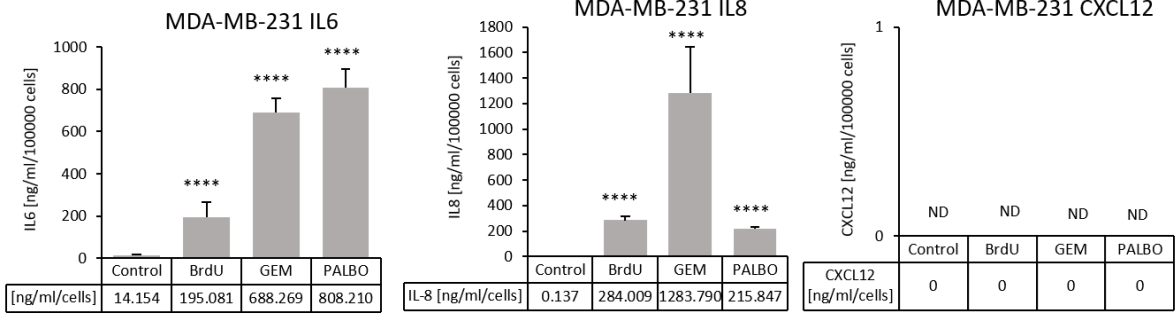


Figure 61. Analysis of senescence-markers in MDA-MB-231 cells. (A) Representative images of control and BrdU-, GEM- and PALBO-induced senescent MDA-MB-231 cells. Cells were fixed and stained with X-gal, imaged by EVOS with 20x magnification, scale bars indicate 100 μ m. The blue colour indicates SA- β -galactosidase activity. **(B)** Quantification of chromogenic (X-gal) SA- β -gal assay. The expression of SA- β -gal is represented as the percentage of positively stained cells compared to the total population. For the quantification of total cell number cells were co-stained with DAPI nuclear stain. The number of positively stained cells and total cell numbers were quantified by ImageJ software, counting masks were adjusted manually based on unstained cells. **(C)** The SA- β -gal expression of MCF-7 cells is represented as mean fluorescence intensity (MFI) of FDG staining measured by flow cytometry, values were normalised to the MFI of non-senescent MDA-MB-231 cells represented as fold change. **(D)** The expression of CD26 (DPP4) is represented as fold change of mean fluorescence intensity (MFI) compared to the control MDA-MB-231 cells, measured by flow cytometry. **(E)** The secretion of IL-6, IL-8 and CXCL12 was measured by ELISA assay. The graphs represent the amount of IL-6, IL-8 and CXCL12 as ng/ml/cells, quantified by known-concentrations of standards and normalised by cell numbers. ND: not detected. Experiments were repeated with two (ELISA) or three technical replicates, bar graphs represent the mean of three independent experiments \pm SEM. Statistical significance (in relation to control): ns $p > 0.05$; * $p \leq 0.05$; ** $p \leq 0.01$; *** $p \leq 0.001$; **** $p \leq 0.0001$.

4.5.2 Analysing the cell cycle of senescent MDA-MB-231 cells by the double staining of Ki-67 expression and DNA-content (PI)

To further characterise the senescence-induction in MDA-MB-231 cells, control and senescent cells were co-stained with Ki-67 and propidium-iodide (PI). The cell cycle categories were generated as presented and described before using MCF-7 cells (**Figure 8.A**). Based on the results of cell cycle analysis, the number of cells in G1-arrest and G2-arrest was significantly increased after senescence-induction, with \sim 70% of the BrdU- and PALBO-induced senescent cells being arrested at the G1 phase and \sim 20% (BrdU) and \sim 10% (PALBO) in G2 phase; while the number of cells associated with active proliferation (G1-S-G2-M) was significantly decreased (**Figure 22.A-B**). As demonstrated before, GEM treatment induced a more heterogenous population of senescence cells, consisting of \sim 50% G1-arrested cells, \sim 30% of cells in G1-S-G2-M phase and \sim 20% of G2-arrested cells (**Figure 22.A-B**). Besides, GEM-induced senescence cells showed a significantly increased population of cells in sub-G1 phase and polyploid cells compared to control MDA-MB-231 cells (**Supplementary Figure 6.D-E**). Consistent with the increased γ -H2AX expression induced by GEM-treatment (**Figure 21.C**), the increased sub-G1 population can indicate apoptotic cells in GEM-induced senescent cells. The detection of cell cycle arrest further confirmed the senescence phenotype of BrdU-, GEM- and PALBO-treated MDA-MB-231 cells.

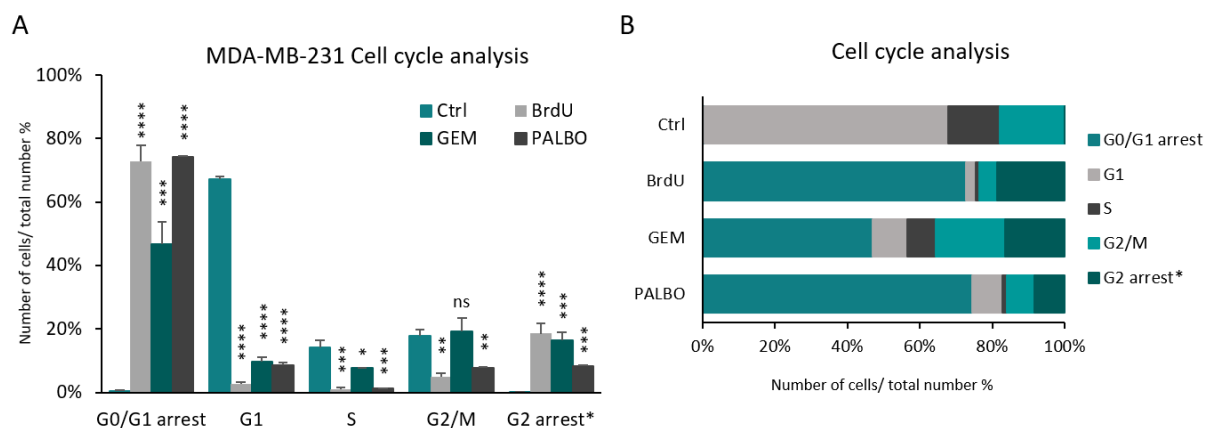


Figure 64. Cell cycle analysis of senescent MDA-MB-231 cells. (A) Representative figure of the cell cycle analysis of control, BrdU-, GEM- and PALBO-induced senescent MDA-MB-231 cells using Ki-67 and PI staining. Cells were manually categorised to cell-cycle stages based on their DNA content stained by PI, the gates for Ki-67-positive cells were adjusted by using unstained cells. **(B)** The graph represents the percentage of cells in each category of cell cycle compared to the total cell population. * The category of G2 arrested cells were based on the research of Miller et al. (2018). Bar graphs represent the mean of three independent experiments \pm SEM. Statistical significance (in relation to control): ns $p > 0.05$; * $p \leq 0.05$; ** $p \leq 0.01$; *** $p \leq 0.001$; **** $p \leq 0.0001$.

4.5.3 Comparing senescence-escape in BrdU-, GEM- and PALBO-induced senescent MD-MB-231 cells

As demonstrated before with MCF-7 cells (**Figure 10.A, Figure 11**), incubating the senescent MDA-MB-231 cells without the senescence-inducing drug allowed the cells to restart their proliferation, thus allowing escape from senescence (**Figure 23.A-B**). Figure 18.A also demonstrates the difference in the morphology of senescent and senescence-escaped MDA-MB-231 cells, and it also reveals the appearance of “giant” GEM-induced senescent cells (with $\sim 500 \mu\text{m}$ in diameter), that appeared after GEM-treatment (**Figure 23.A**). To compare the senescence-escaping ability of BrdU-, GEM- and PALBO-induced senescent MD-MB-231 cells, the escaping cells were monitored for a prolonged period of time (10-12 days). The senescence-escaping ability of the cells was assessed by Ki-67 expression, and it demonstrated that senescence-escaped cells (with increased Ki-67 expression) started to appear ~ 5 days after the removal of BrdU/GEM. However, as presented before (**Figure 20.D**), the initial expression of Ki-67 was different depending on the senescence-inducing drug, with GEM-induced senescent MDA-MB-231 cells exhibiting the highest basal Ki-67 expression level (**Figure 23.B**). Similarly to what was demonstrated in MCF-7 cells (**Figure 11**), PALBO-induced senescent cells started to escape from senescence shortly (~ 3 days) after the removal of

PALBO, indicating that PALBO-treatment induced a transient, less stable growth-arrest in MDA-MB-231 cells compared to the BrdU and GEM treatment (**Figure 23.B**). Due to this transient growth-arrest induced by PALBO-treatment, PALBO-induced senescent cells might not be a suitable model to study senescence-escape, therefore in subsequent experiments senescence-escape was assessed only in BrdU- and GEM-induced senescent cells.

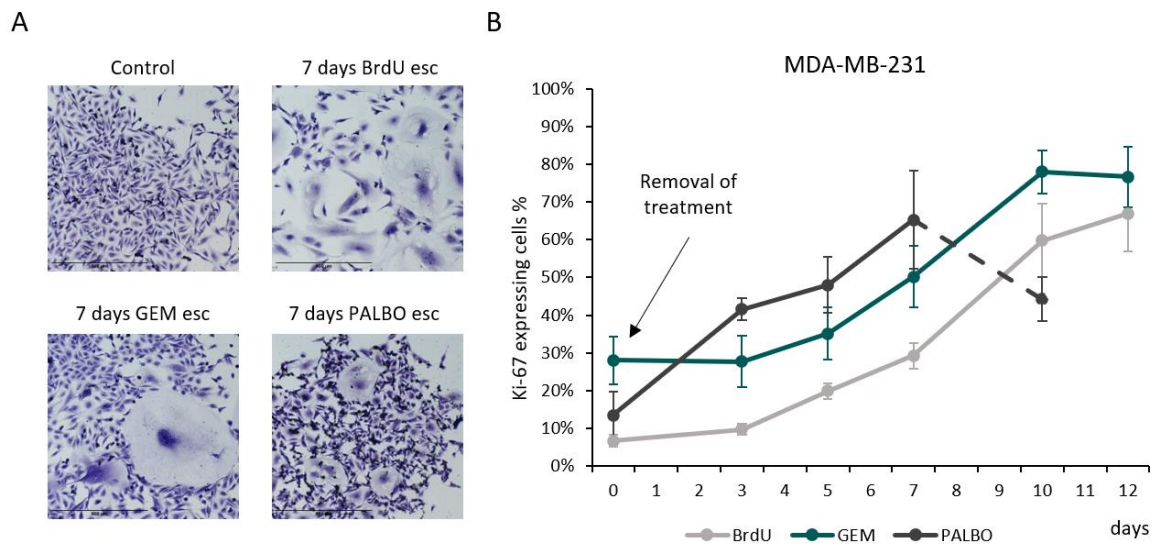
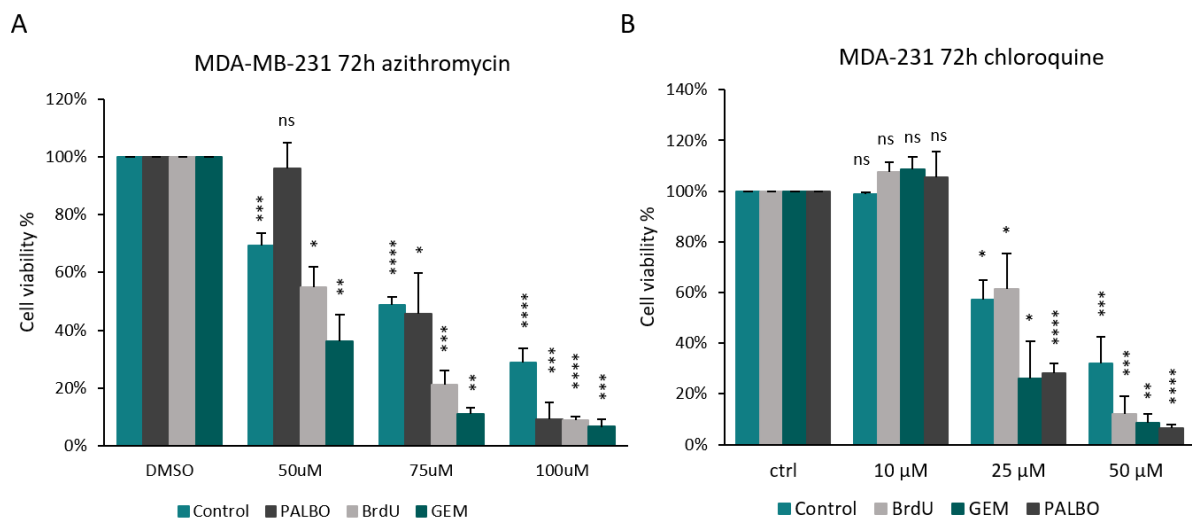


Figure 67. Senescence-escape in BrdU-, GEM- and PALBO-induced senescent MDA-MB-231 cells. (A) Representative images of control and senescence-escaped BrdU-, GEM- and PALBO-treated MDA-MB-231 cells. Cells were stained with crystal violet, imaged by EVOS using 10x magnification, scale bars indicate 500 μ m. **(B)** Analysis of senescence-escape based on the percentage of Ki-67-expressing cells compared to the total cell number measured by flow cytometry at different time points. Arrow indicates the removal of treatment representing day 0. Dashed line represents the decrease of Ki-67 expression due to reaching confluency. The graph represents the mean of three independent experiments \pm SEM.

4.5.4 Validating the senolytic effect of azithromycin in senescent MDA-MB-231 cells compared with the effect of chloroquine

To further investigate the senolytic effect of azithromycin (AZI), AZI treatment was tested in senescent MDA-MB-231 cells and compared to the effect of chloroquine (CQ) treatment as well (**Figure 24.A-B**). Based on the cell viability assays (SRB), AZI treatment concentration-dependently decreased the viability of both non-senescent (control) and senescent MDA-MB-231 cells, however, AZI was more selective towards senescent MDA-MB-231 cells at a concentration of 75 μ M and 100 μ M (**Figure 24.A**). The senolytic effect of AZI treatment on senescent MDA-MB-231 cells was dependent on the senescence-inducing drug. Similarly to

the PALBO induced senescent MCF-7 cells, PALBO-induced senescent MDA-MB-231 cells were more resistant to AZI treatment (**Figure 12.B, Figure 24.A**). 100 μ M AZI treatment decreased the viability of control MDA-MB-231 cells to \sim 30%, and it almost eliminated the BrdU-, GEM- and PALBO-induced senescent cells by decreasing their viability to \sim 10% (**Figure 24.A**). Moreover, 5 days treatment with 100 μ M AZI further decreased the viability of senescent MDA-MB-231 cells to \sim 1-3% (**Supplementary Figure 5**). Because senescent MDA-MB-231 cells were almost completely eliminated after 100 μ M AZI treatment, the senescence-escaping ability of AZI-treated MDA-MB-231 cells were not further investigated. The effect of chloroquine was similar to azithromycin, by decreasing the viability of both control and senescent MDA-MB-231 cells (**Figure 24.B**). These results indicate that azithromycin treatment was more effective in MDA-MB-231 cells compared to MCF-7 cells. Although AZI and CQ had similar effect in MDA-MB-231 cells, as described before, AZI was less toxic to fibroblast (MRC-5) cells compared to CQ, which indicates that AZI could be more suitable to use in cancer treatment (**Figure 12.C, Figure 13.E**).



4.6 Investigating the expression and function of dipeptidyl peptidase-4 (DPP4/CD26) in senescent MDA-MB-231 cells

4.6.1 Silencing the expression of DPP4 in MDA-MB-231 cells

To investigate the potential function of DPP4/CD26 in senescent MDA-MB-231 cells as well, the expression of DPP4 (DPP4 siRNA) was silenced in MDA-MB-231 cells by lentiviral vector-mediated gene silencing. The silencing was confirmed by both western blot and flow cytometry (**Figure 25.A-B**). Similarly to the results in MCF-7 cells (**Figure 16.C-E**), the silencing of DPP4 expression had no effect on cell proliferation, and it did not affect the expression of SA- β -Gal and lysosomal mass in senescent cells (**Figure 25. C-E**). Due to the GFP-expression of the transduced cells, the fluorogenic SA- β -Gal staining (FDG) could not be detected, therefore the assessment of lysosomal mass was used as an additional marker, that could be quantified easier than chromogenic SA- β -Gal staining (X-gal) (**Figure 25.E**). Consistent with the results in MCF-7 cells (**Figure 16**), although the expression of DPP4/CD26 was increased in senescent MDA-MB-231 cells, its expression was not essential for senescence-induction.

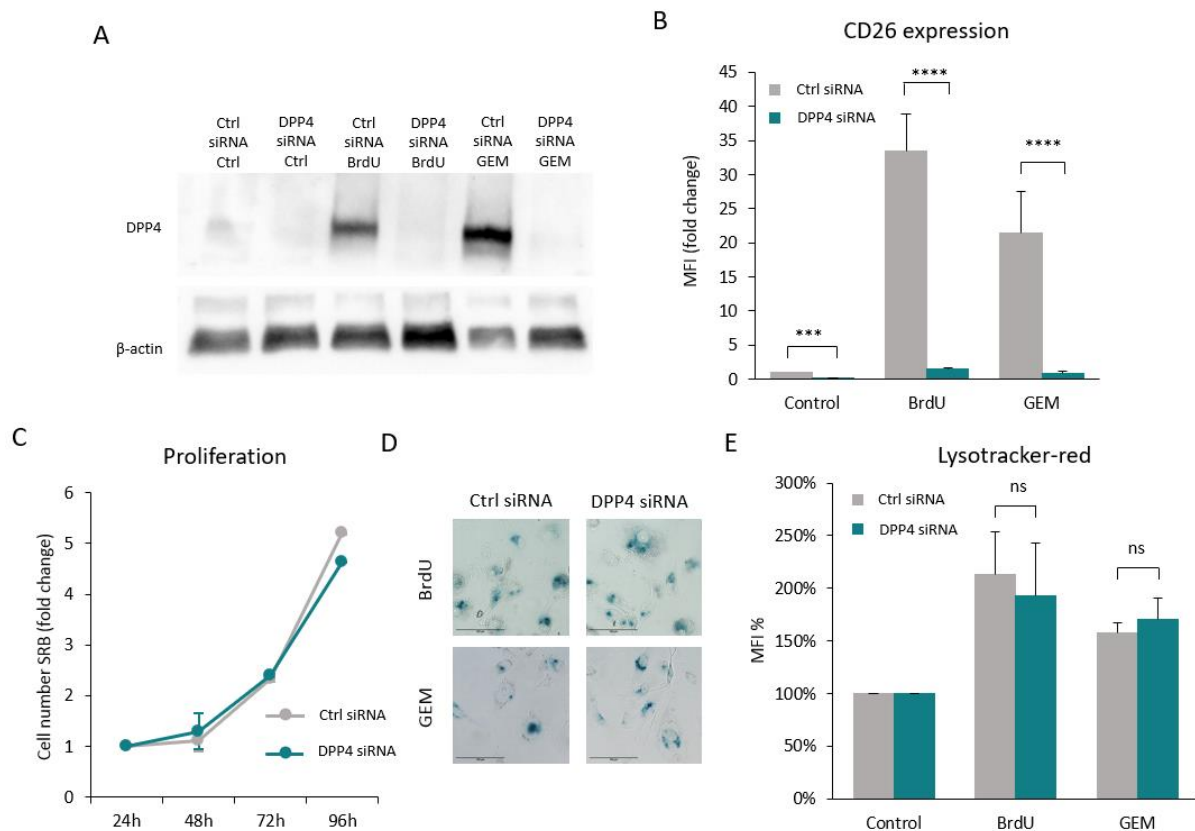


Figure 73. Effect of DPP4-silencing on the senescence-induction in MDA-MB-231 cells. The expression of DPP4 was silenced in MDA-MB-231 cells by lentiviral vector-mediated gene silencing, cells were labelled as DPP4 siRNA. Cells transduced with scrambled vector were used as experimental controls, labelled as ctrl siRNA. **(A)** Representative images of western blot analysis of control and senescent MDA-MB-231 cells, demonstrating the silencing of DPP4 expression. **(B)** CD26 expression is represented as mean fluorescence intensity (MFI) of CD26-PE staining measured by flow cytometry, values were normalised to the MFI of non-senescent ctrl siRNA cells and represented as fold change. **(C)** Cell proliferation was measured by SRB assay at different time-points, values were normalised to the baseline values measured 24 hours after cell seeding and represented as fold change. Graph represents the mean of three independent experiments \pm SEM. **(D)** Representative images of BrdU- and GEM-induced senescent ctrl siRNA and DPP4 siRNA cells. Cells were fixed and stained with X-gal, imaged by EVOS with 20x magnification, scale bars indicate 100 μ m. The blue colour indicates SA- β -galactosidase activity. **(E)** Lysosomal content is represented as mean fluorescence intensity (MFI) of LysoTracker deep red staining measured by flow cytometry, values were normalised to the MFI of non-senescent ctrl siRNA cells. Bar graphs represent the mean of three independent experiments \pm SEM. Statistical significance: ns $p > 0.05$; * $p \leq 0.05$; ** $p \leq 0.01$; *** $p \leq 0.001$; **** $p \leq 0.0001$.

4.6.2 Investigating the effect of DPP4/CD26 in senescence-escape (MDA-MB-231)

To investigate whether the expression of DPP4/CD26 has a role in senescence-escape, the senescence-escaping ability of DPP4-silenced (DPP4 siRNA) senescent cells was analysed by Ki-67 staining and compared with control senescent cells (ctrl siRNA). As described before, due to the transient growth-arrest induced by PALBO-treatment (**Figure 23.B**), PALBO-induced senescent cells might not be a suitable model to study senescence-escape, therefore senescence-escape was assessed only in BrdU- and GEM-induced senescent cells. The adjustment of gates for the measurement of Ki-67 expression by flow cytometry is presented in Supplementary Figure 7.B. Consistent with the previous observation that DPP4 is not required for senescence-induction in MDA-MB-231 cells (**Figure 25**), DPP4 silencing did not change the Ki-67 expression in control and senescent (BrdU/GEM) cells (**Figure 26.A, Supplementary Figure 7.B**). In contrast with the results in MCF-7 cells (**Figure 17**), the proportion of Ki-67 expressing cells was increased in the senescence-escaped DPP4 siRNA cells compared to ctrl siRNA senescence-escaped cells, even though this increase was only significant in the GEM-induced senescent cells (**Figure 26.A, Supplementary Figure 7.B**). To better demonstrate the difference between the DPP4 siRNA and ctrl siRNA senescence-escaped cells, the analysis of Ki-67 expression was combined with the measurement of cell numbers (**Figure 26.B**), representing the number of senescence-escaped cells (**Figure 26.C**).

The number of senescence-escaped cells was increased by ~50% in BrdU-induced and by ~2 folds in GEM-induced senescent DPP4 siRNA cells compared to ctrl siRNA cells, indicating that silencing of DPP4 promotes senescence escape in MDA-MB-231 cells (**Figure 26.C**). Unfortunately, these results could not be confirmed by crystal violet staining, since the senescence-escaped MDA-MB-231 cells did not form colonies (as in the case of MCF-7 cells) that could be used to evaluate senescence-escape (**Supplementary Figure 10.B**). Based on the results of DPP4 silencing, we tested whether the inhibition of DPP4 by sitagliptin treatment would have similar effect on the senescence escape of MDA-MB-231 cells. According to results of senescence-escape analysis by Ki-67 staining, 250 μ M sitagliptin treatment did not affect senescence-escape after BrdU-induced senescence, however, it seemed to increase senescence-escape in GEM-induced senescent MDA-MB-231 cells (**Figure 26.D**). Sitagliptin treatment at 500 μ M concentration resulted in decreased senescence-escape in both BrdU- and GEM-induced senescent cells, which might indicate a cytostatic or cytotoxic side-effect of long-term high concentration sitagliptin treatment (**Figure 26.D**). These results indicate that DPP4/CD26 could have a cell-type dependent role in the regulation of senescence-escape, either preventing (MCF-7 cells) or promoting (MDA-MB-231 cells) it.

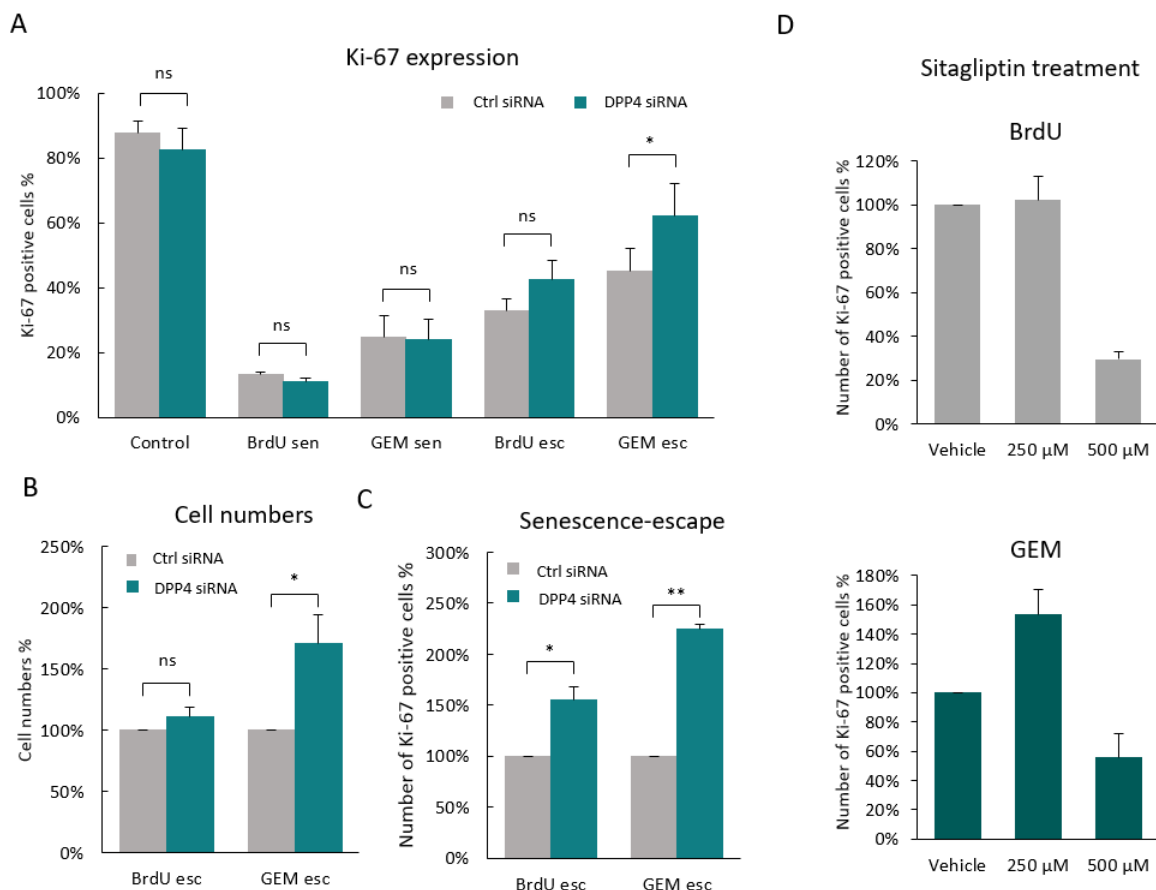


Figure 76. Effect of DPP4 silencing and DPP4 inhibition on the senescence-escape of MDA-MB-231 cells. (A) The expression of Ki-67 is represented as the percentage of positively stained cells compared to the total population. The gates for Ki-67-positive cells were adjusted by using unstained cells. **(B)** The cell concentrations were measured by flow cytometry using the samples from the measurement of Ki-67 expression represented as count/ μl (cell number/ μl). The samples were collected with the same volume, therefore the cell concentration is proportional to the cell numbers of each sample. Values were respectively normalised to the BrdU- and GEM-escaped ctrl siRNA cells. **(C)** The senescence-escaping ability of the cells were assessed by the combination of Ki-67 expression and cell concentration represented as the number of Ki-67 positive cells. Values were respectively normalised to the BrdU- and GEM-escaped ctrl siRNA cells. Bar graphs represent the mean of three independent experiments \pm SEM. Statistical significance: ns $p > 0.05$; * $p \leq 0.05$; ** $p \leq 0.01$; *** $p \leq 0.001$; **** $p \leq 0.0001$. **(D)** After senescence induction by BrdU- and GEM-treatment cells were incubated for 10 days with sitagliptin treatment. The senescence-escaping ability of the cells were assessed by the combination of Ki-67 expression and cell concentration represented as the number of Ki-67 positive cells. Values were to the vehicle-treated cells, bar graphs represent the mean of two independent experiments \pm SEM.

4.7 Isolating and analysing senescence-escaped cells

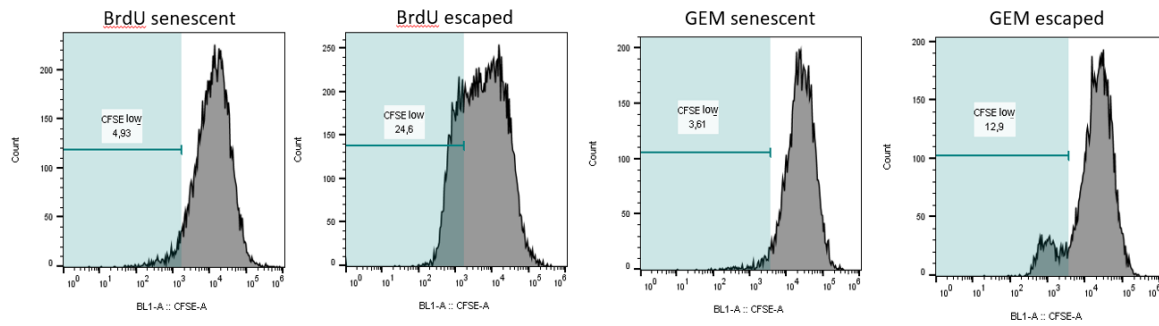
4.7.1 Establishing a method to isolate senescence-escaped MCF-7 and MDA-MB-231 cells

Although analysing the expression of Ki-67 can be used to quantify senescence-escape, due to the staining method the cells are fixed and cannot be used in functional assays that require live cells. Therefore, we established a different method for the isolation/purification of senescence-escaped cells by fluorescence-activated cell sorting (FACS), using a fluorescent dye known as CFSE (carboxyfluorescein succinimidyl ester). CFSE is a cell permeable fluorescent dye that covalently binds to intracellular proteins, providing a homogeneous and stable green fluorescent signal, which progressively decreases after each cell division (Lyons and Parish, 1994). Our hypothesis was that by staining the cells with CFSE after senescence induction by BrdU or GEM treatment, the decreased intensity of CFSE staining could identify the actively proliferating senescence-escaped cells. Thus, the differences in CFSE signal intensity could be used to isolate senescence-escaped cells from a mixed population of senescent and escaped cells. Our results demonstrated that 10 days after the removal of BrdU or GEM treatment (which allowed the senescent cells to escape), MCF-7 and MDA-MB-231 cells had a decreased signal intensity of CFSE compared to the cells without the 10-days incubation (senescent cells) (**Figure 27. A-B**). The gates were adjusted manually to the basis

of the histogram generated by the CFSE signal of BrdU- and GEM-induced senescent cells, and the percentage of cells with low expression of CFSE (CFSE low) was considered as proliferating (senescence-escaped) cells (**Figure 27. A-B**). To further validate the CFSE staining-based isolation of senescence-escaped cells, BrdU- and GEM-induced senescent cells were stained with CFSE, incubated for 10 days without the senescence-inducing drug (to allow senescence escape) and co-stained with Ki-67. This would allow to assess the overlap of the population of cells with low CFSE staining (CFSE low) and the population of Ki-67 expressing cells (Ki-67 pos) (**Figure 27.C**). Based on this population comparison, ~73% of CFSE low BrdU- or GEM-treated MCF-7 cells were positively stained for Ki-67, and ~65% of CFSE low BrdU-treated and ~77% of CFSE low GEM-treated MDA-MB-231 cells showed a correlation with Ki-67-positive cells (**Figure 27.C**). Altogether these results suggest that CFSE low cells are largely Ki67 positive and that CFSE staining could be used to isolate senescence-escaped cells.

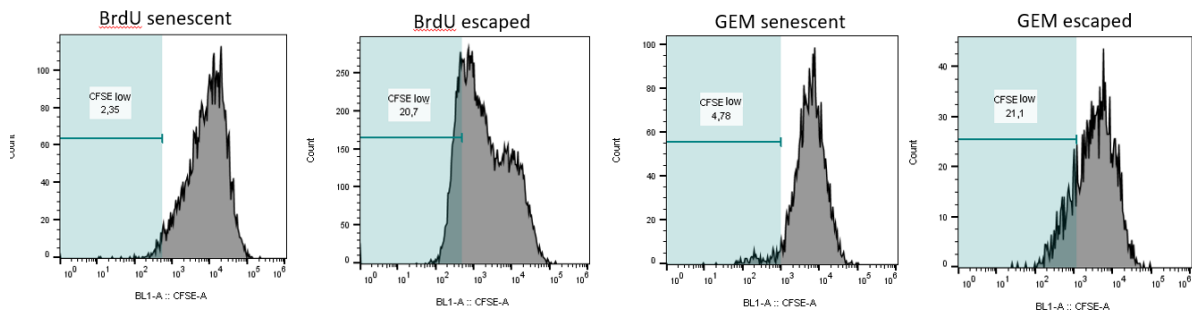
A

CellTrace CFSE staining of MCF-7 cells



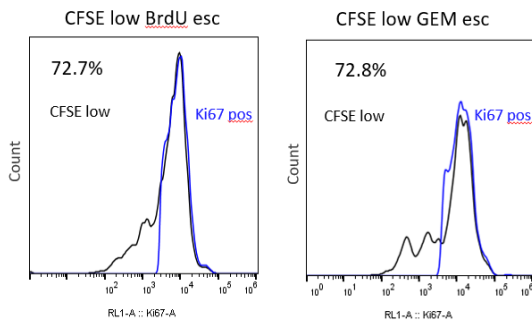
B

CellTrace CFSE staining of MDA-MB-231 cells



C

MCF-7 population comparison



D

MDA-MB-231 population comparison

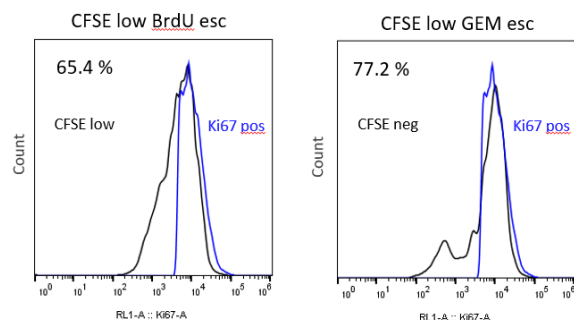


Figure 27. Isolation of senescence-escaped MCF-7 and MDA-MB-231 cells by CFSE-staining. (A-B) Representative figures of the gating strategies for the isolation of senescence-escaped cells by flow cytometry using CFSE staining. The gates were adjusted manually to the basis of the histogram generated by the CFSE signal of BrdU- and GEM-induced senescent cells, and cells with low expression of CFSE (CFSE low) was considered as senescence-escaped cells. Figures were generated by FlowJo software. **(C-D)** Representative figures of the results of population comparisons by FlowJo. The senescent cells were co-stained with CFSE and Ki-67, and the population of cells with low CFSE staining (CFSE low) were compared with the population of Ki-67 expressing cells (Ki-67 pos). The percentages represented next to the graphs indicate the correlation of the two populations.

Based on the previously established method for isolating/purifying senescence-escaped cells (**Figure 27**), we optimised a protocol for subsequent investigations by live-cell based functional assays (**Figure 28**). After senescence-induction in MCF-7 and MDA-MB-231 cells with either BrdU or GEM treatment, cells were stained with CFSE and incubated in drug-free medium for 10 days, and the population of senescent and senescence-escaped cells were isolated by FACS (**Figure 28**). The gates for sorting were adjusted as demonstrated before (**Figure 27**); however, for a more accurate isolation of senescence-escaped and senescent cells, the cells represented in the middle part of the histogram of CFSE-signal were not included in the sorting (**Supplementary Figure 11**). The control (non-senescent) MCF-7 and MDA-MB-231 cells were stained with CFSE 1 day after seeding, and they were incubated for 4 days (allowing them to grow without reaching confluency) before sorting by FACS (**Figure 28**). Although control (non-senescent) cells were not sorted to different categories (CFSE-low or CFSE-high), applying the CFSE staining and passing the cells through the FACS machine generated a more accurate control for the functional assays (**Figure 28, Supplementary Figure 11**). The stem cell activity, metastatic potential and proliferative capacity of the isolated senescence-escaped, senescent and control cells were investigated by mammosphere formation, cell migration and colony formation assays.

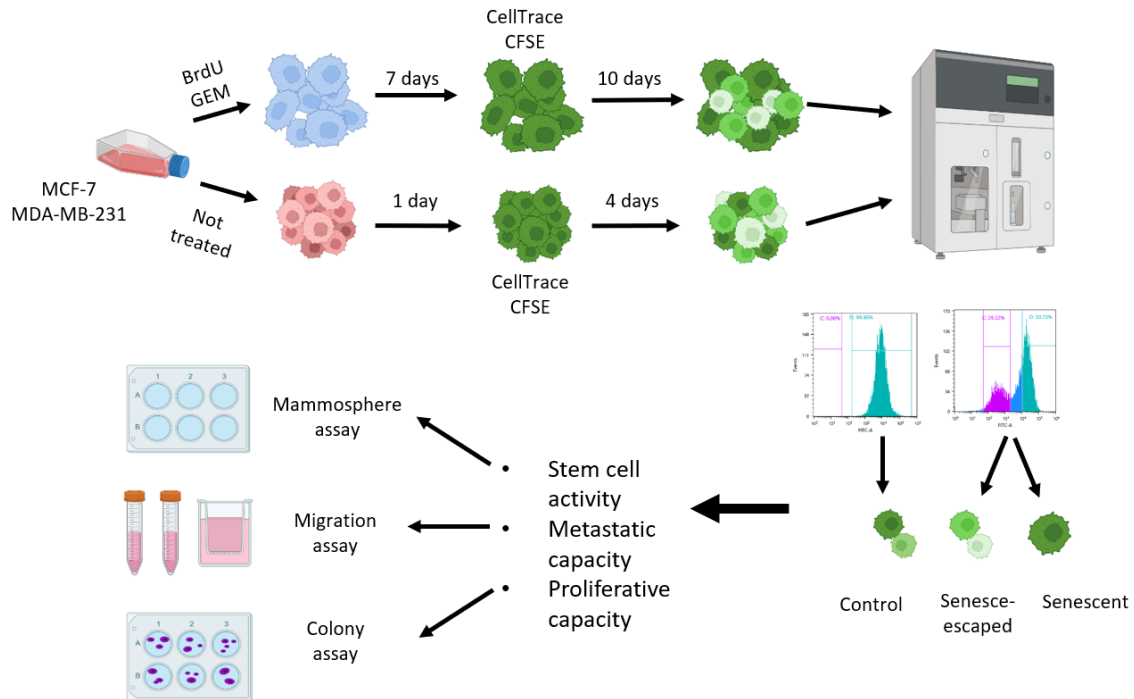


Figure 79. Schematic figure of the isolation of senescence-escaped MCF-7 and MDA-MB-231 cells and the experimental strategy. The figure represents the workflow for the isolation of senescence-escaped cells by FACS. The figure was generated with BioRender. Detailed gating strategy for the isolation is represented in supplementary (Supplementary Figure 11).

4.7.2 Investigating the effect of senescence-escape in cancer progression

4.7.2.1 Analysis stem cell activity in senescence-escaped cells by mammosphere formation assay

Mammosphere formation assay is a regularly used assay to evaluate stem cell activity and self-renewal capacity in breast cancer cells (Shaw et al., 2012). According to the results of mammosphere formation assays in MCF-7 cells, BrdU- and GEM-induced senescent cells had a significantly decreased mammosphere formation efficacy (MFE), decreasing by ~60% (BrdU) and ~80% (GEM) compared to the control cells (**Figure 29.A**). Although, senescence-escaped MCF-7 cells restored the mammosphere formation capacity to similar levels the control (non-senescent) cells (**Figure 29.A**). Similarly in MDA-MB-231 cells, the mammosphere formation efficacy of BrdU- and GEM-induced senescent cells were decreased by ~40%; and the senescence-escaped cells reacquired the ability of mammosphere formation, however, they formed less mammospheres (~80%) compared to the control (non-senescent) cells (**Figure 29.B**). These results indicate that stem-cell activity was increased in senescence-escaped cells

compared to senescent cells and it was restored to similar levels as in parental non-senescent cells.

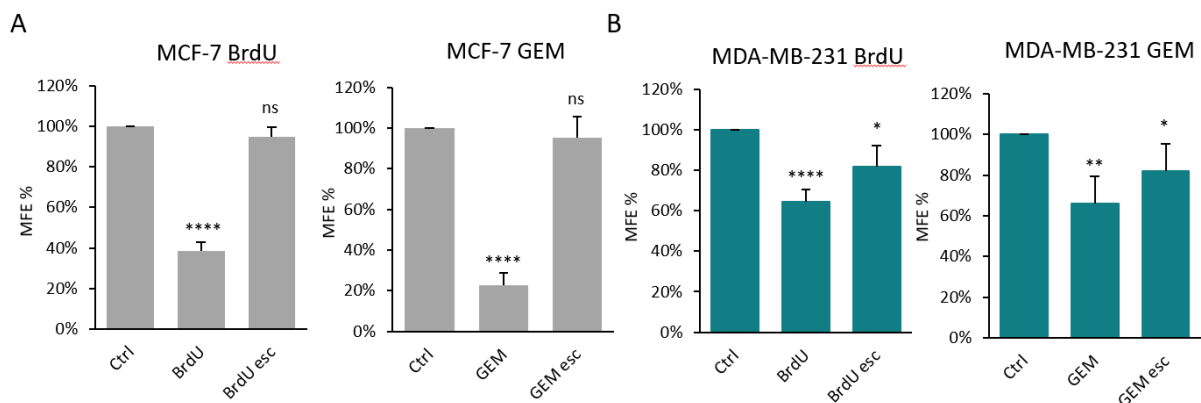


Figure 82. Analysis of stem cell activity in senescence-escaped MCF-7 and MDA-MB-231 cells by mammosphere formation assay. (A-B) The graphs represent the mammosphere formation efficiency (MFE) of control, senescent and senescence-escaped cells after cell sorting, normalised to the MFE of the control MCF-7 and MDA-MB-231 cells. Experiments were repeated with three technical replicates, bar graphs represent the mean of three independent experiments \pm SEM. Statistical significance (in relation to control): ns $p > 0.05$; * $p \leq 0.05$; ** $p \leq 0.01$; *** $p \leq 0.001$; **** $p \leq 0.0001$.

4.7.2.2 Analysis of migration capacity in senescence-escaped cells

In vitro cell migration assays are used to investigate the migratory abilities of cancer cells, which is an essential step in the process of invasion and metastasis (Pijuan et al., 2019). The migration ability of senescence and senescence-escaped MCF-7 and MDA-MB-231 cells were examined by transwell cell migration assay. According to the results, the migration of BrdU- and GEM-induced senescent MCF-7 cells was significantly decreased, however, after senescence-escape the cells had a significantly increased migration ability compared to the control (non-senescent) cells (**Figure 30.A-B**). Similarly in MDA-MB-231 cells, BrdU- and GEM-induced senescent cells had a decreased migration ability; and senescence-escaped cells reacquired their migration capacity to a similar level than control (non-senescent) cells (**Figure 30.A, Figure 30.C**). However, the migration capacity of GEM-induced senescence-escaped was decreased compared to control (non-senescent) cells (**Figure 30.A, Figure 30.C**). These results indicate that senescence-escaped MCF-7 cells had a significantly increased migration capacity compared to the parental cells, while in MDA-MB-231 cells senescence-escape did not increase the migration capacity of the cells.

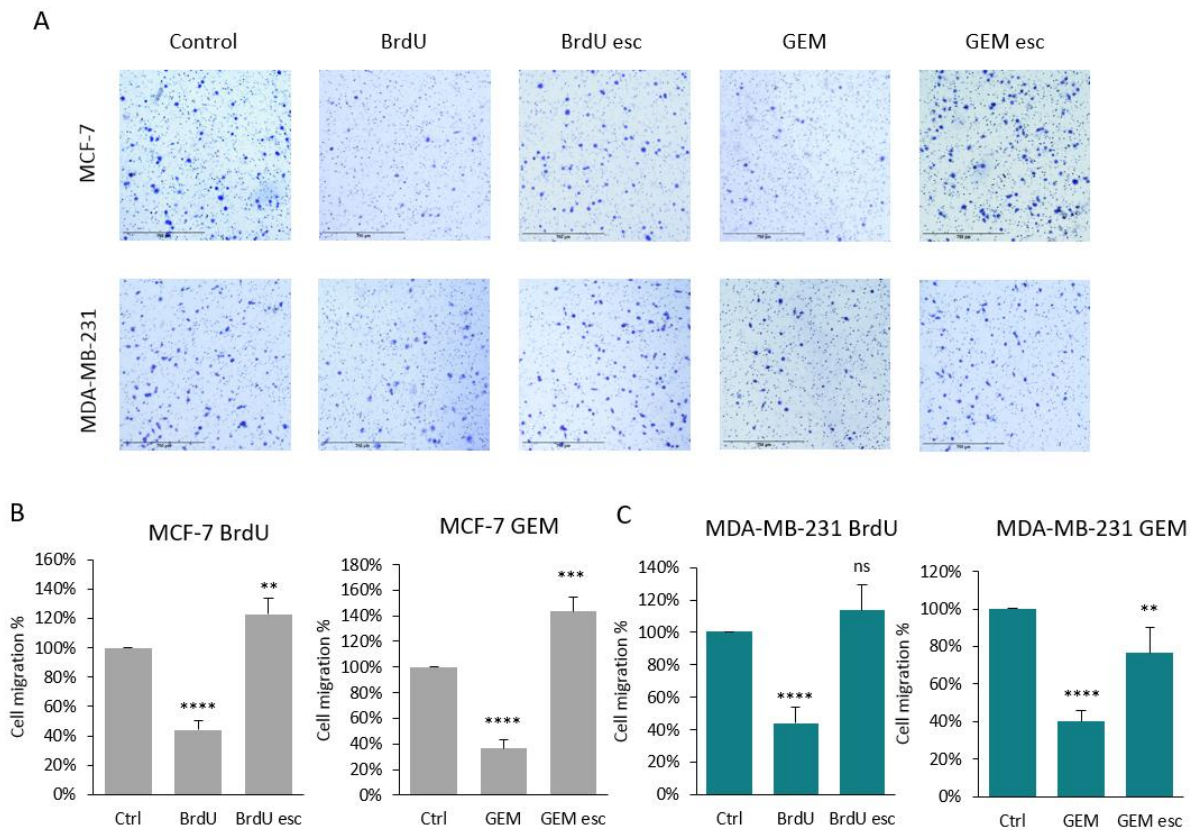


Figure 85. Analysis of metastatic-capacity in senescence-escaped MCF-7 and MDA-MB-231 cells by migration-assay. (A) Representative images of the migration of control, senescent and senescence-escaped MCF-7 and MDA-MB-231 cells. Cells were stained with crystal violet and imaged by EVOS using 10x magnification, scale bars indicate 750 μ m. **(B-C)** For evaluating cell migration, the number of cells were counted by ImageJ, using 4 pictures from each sample. Experiments were repeated with two technical replicates, bar graphs represent the mean of three independent experiments \pm SEM. Statistical significance (in relation to control): ns $p > 0.05$; * $p \leq 0.05$; ** $p \leq 0.01$; *** $p \leq 0.001$; **** $p \leq 0.0001$.

4.7.2.3 Analysis of proliferative capacity in senescence-escaped cells by colony formation assay

Colony forming (or clonogenic) assay is a widely used *in vitro* technique to determine the self-renewal capacity of a single cell by forming a colony of 50 or more cells, and it is also used to assess the ability of cancer stem-like cells to potentially develop a new tumour (Franken et al., 2006, Rajendran and Jain, 2018). According to the results, BrdU- and GEM-induced senescent MCF-7 cells had a significantly lower colony formation capacity compared to the control (non-senescent) cells, decreased to \sim 10% after BrdU-treatment and \sim 1% after GEM-treatment (**Figure 31.A-B**). Compared to the senescent MCF-7 cells, the colony formation capacity of senescence-escaped BrdU- and GEM-treated cells greatly increased, although, they formed less colonies (\sim 70-80%) compared to control (non-senescent) cells (**Figure 31.A-**

B). Similarly to the results of MCF-7 cells, the colony formation efficacy were significantly decreased (~20%) in BrdU- and GEM-induced senescent MDA-MB-231 cells, and the senescence-escaped BrdU- and GEM-treated cells reacquired their colony formation ability, however, not at the same level as control cells (~70-80%) (**Figure 31.A, Figure 31.C**). These results indicate that the senescence-escaped MCF-7 and MDA-231 cells are able to form new populations of cancer cells, although with decreased proliferation capacity.

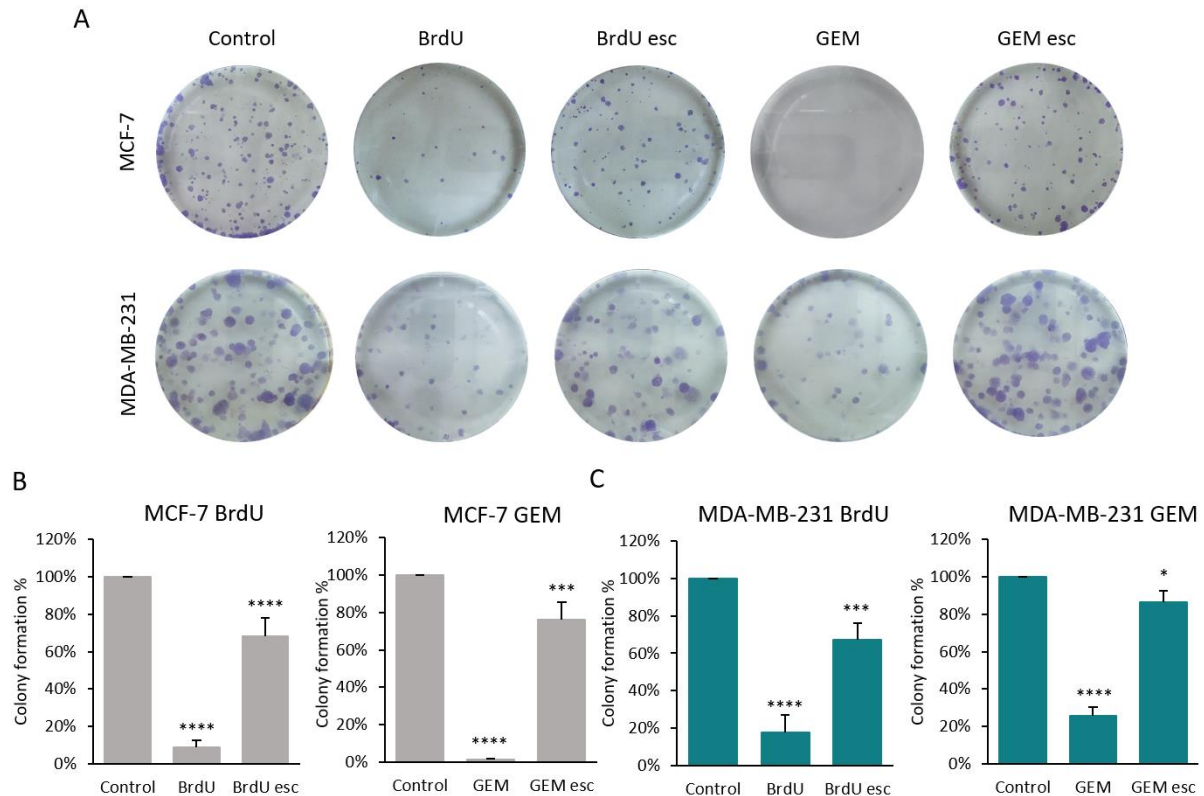


Figure 88. Analysis of proliferative capacity in senescence-escaped MCF-7 and MDA-MB-231 cells by colony formation assay. (A) Representative images of the colony formation of control, senescent and senescence-escaped MCF-7 and MDA-MB-231 cells. Cells were stained with crystal violet, images represent the entire surface of a well of a 6 well plate. (B-C) For evaluating the colony formation ability of the cells, the number of colonies with more than 50 cells were counted by ImageJ. Experiments were repeated with three technical replicates, bar graphs represent the mean of three independent experiments \pm SEM. Statistical significance (in relation to control): ns $p > 0.05$; * $p \leq 0.05$; ** $p \leq 0.01$; *** $p \leq 0.001$; **** $p \leq 0.0001$.

4.8 Summary of results

- Bromodeoxyuridine (BrdU), gemcitabine (GEM) and Palbociclib (PALBO) induced senescence in MCF-7 and MDA-MB-231 breast cancer cells through different mechanism of action
- The simultaneous measurement of Ki-67 expression and DAN content (PI) could be used to identify cell cycle arrested/senescent cell populations by using flow cytometry
- The levels of expression of different senescence-markers in MCF-7 and MDA-MB-231 cells were dependent on the drug used for senescence-induction
- IL-6, IL-8 and CXCL12 secretion was highly increased in BrdU- and GEM-induced senescent MCF-7 cells, but it was not increased in PALBO-induced senescent cells
- IL-6 and IL-8 secretion was significantly increased in senescent MDA-MB-231 cells
- The senescence-escaping ability of cancer cells could be evaluated by the measurement of Ki-67 expression and cell numbers by flow cytometry; and by the assessment of senescence-escaped colonies stained by crystal-violet staining
- PALBO-induced senescent MCF-7 and MDA-MB-231 cells were able to escape from senescence shortly after the removal of PALBO treatment, resulting an unstable/transient senescence phenotype
- BrdU- and GEM-treatment resulted in a more stable growth arrest/senescence, however, cells were able to escape from senescence and restart proliferation
- The senolytic effect of azithromycin was confirmed in senescent MCF-7 and MDA-MB-231 cells, and its inhibitory effect on autophagy was confirmed in MCF-7 cells
- The cell surface expression of DPP4/CD26 was highly increased in senescent MCF-7 and MDA-MB-231 cells, however, its expression was not essential for senescence-induction
- The silencing or inhibition of DPP4 resulted in decreased senescence-escaping ability of MCF-7 cells and increased/unchanged senescence-escaping ability of senescent MDA-MB-231 cells
- Senescent MCF-7 cells were able to escape after azithromycin (AZI) treatment, however, the senescence-escaping ability of AZI-treated the cells was decreased by DPP4 inhibition (sitagliptin treatment)

- Senescence-escaped cells could be isolated by FACS, using CellTrace CFSE staining for the identification of proliferating cells
- After senescence-escape, MCF-7 and MDA-MB-231 cells resembled to the parental (non-senescent) cells in terms of stemness activity and proliferation capacity
- Senescence-escape increased the migration capacity of MCF-7 cells, but not MDA-MB-231 cells

5. Discussion

The role of therapy-induced senescence (TIS) in tumour progression and therapy resistance is highly complex, which resulted in contradictory findings about the effect of TIS on the clinical outcomes of cancer therapies. Based on the relevant literature along with our recent findings, our standpoint is that the presence of senescent tumour cells and the ability of cancer cells to escape from senescence should be considered as a detrimental side-effect of cancer therapy, that could potentially contribute to therapy resistance and tumour recurrence (Pare et al., 2016, Demaria et al., 2017, Wyld et al., 2020, Wagner and Gil, 2020). The investigation of the characteristics of senescent cancer cells and the underlying mechanism of senescence-escape is essential to better understand the consequences of TIS, and to identify potential targets to eliminate senescent cancer cells.

To optimise an *in vitro* cellular model for the investigation of TIS and senescence-escape we used MCF-7 and MDA-MB-231 breast cancer cells (Figure 6-8, Figure 23-25). MCF-7 is a cellular model for hormone receptor-positive and HER2 negative breast cancer, and it is a widely used cell line in studies of TIS (Elmore et al., 2002, Karimi-Busheri et al., 2010, Tonnessen-Murray et al., 2019, Bojko et al., 2020, Mosieniak et al., 2015). In most of the studies with MCF-7 cells a DNA-damaging chemotherapeutic drug is used for senescence-induction, however, endocrine therapy (tamoxifen) has also been described to induce senescence in MCF-7 cells (Lee et al., 2014, Wyld et al., 2020). Although tamoxifen is a clinically relevant drug for the treatment of hormone receptor-positive breast cancer cells, in *in vitro* experiments tamoxifen treatment created a more heterogeneous population consisting of both senescent and non-senescent compared to the effect of DNA-damaging drugs (Taylor et al., 2011). MDA-MB-231 cell line is a cellular model for triple-negative breast cancer, that is generally treated with chemotherapy, although, it is not commonly used for studying TIS (Dai et al., 2017). One of the reasons why MDA-MB-231 cells are rarely used in senescence studies might be that they carry a mutation in the gene encoding p53, which has an important role in senescence-induction. However, senescence can be induced even in cancer cells lacking active p53/p21^{Waf1/Cip1} and/or p16^{Ink4a}/Rb signalling pathways (Elmore et al., 2002, Roberson et al., 2005, Jackson et al., 2012). In fact, a wide range of

chemotherapeutic drugs were demonstrated to induce senescence in MDA-MB-231 cells (Bojko et al., 2019).

A wide range of compounds were described to induce senescence in cancer cells through various molecular pathways, creating different phenotypes of senescent cells, which ultimately leads to a substantial variability of experimental results (Petrova et al., 2016, Hernandez-Segura et al., 2017). To carry out a thorough investigation of senescence in cancer, and to potentially generate different senescent phenotypes, we used three different drugs, namely bromodeoxyuridine (BrdU), gemcitabine (GEM) and Palbociclib (PALBO), to induce senescence in MCF-7 and MDA-MB-231 cells.

BrdU is a synthetic analogue of the nucleoside thymidine, that has been described to induce senescence in various cell types, including cancer cells (Michishita et al., 1999, Masterson and O'Dea, 2007, Ross et al., 2008). Previous studies investigating the effect of BrdU suggested that BrdU activates a common senescence pathway in both mortal and immortal cells, by being incorporated into specific AT-rich sequences and regulating the expression of senescence-associated genes (Michishita et al., 1999). Moreover, it was found that BrdU was able to induce senescence in cell lines lacking functional p53, p21^{Waf1/Cip1} or p16^{Ink4a}, and suggested that DNA-damage did not contribute to the senescence-induction mechanism of BrdU (Suzuki et al., 2001). Supporting this concept, several studies have demonstrated that BrdU can be used to radiosensitise cells by being incorporated into the DNA and inducing DNA-damage only when the cells are exposed to ionizing radiation (Cecchini et al., 2005, Levkoff et al., 2008). In contrast, other studies have proposed that BrdU induces DNA damage, and induced cellular senescence through the activation of DNA-damage response (Masterson and O'Dea, 2007, Lee et al., 2011).

According to our results, BrdU treatment did not induce DNA-damage in MCF-7 and MDA-MB-231 cells (Figure 6.D, Figure 20.D, Supplementary Fig 1.A, Supplementary Fig 6.B, D), indicating that it is more likely that it induced senescence by the upregulation of senescence-associated genes. This type of senescence induction might be similar to epigenetically induced senescence, in which the senescence state is maintained by directly activated molecular pathways without the induction of cellular stress, resembling aging-associated or oncogene-induced senescence (Petrova et al., 2016). BrdU-treated MCF-7 and MDA-MB-231 cells expressed all the senescence markers that were investigated, including altered cell

morphology, increased SA- β -gal expression, proliferation arrest and increased expression of senescence-associated cytokines (Figure 6-8, 20-22, 27). Besides, it induced a stable but reversible growth-arrest (Figure 11, 23), which makes it a suitable model to investigate senescence-escape.

Based on the conclusion that BrdU did not induce DNA damage in MCF-7 and MDA-MB-231 cells, another pyrimidine analogue compound, gemcitabine, which is well-known for its DNA-damage inducing activity, was included in our experiments. Gemcitabine is chemotherapeutic drug that belongs to the group of antimetabolites, and it is widely used in the treatment of different kinds of solid tumours (Xie et al., 2018). Although it is not the most commonly used chemotherapeutic drug in breast cancer treatment, gemcitabine has been used in advanced breast cancer patients as a single agent or in combination with taxanes (class of diterpenoid compounds used in chemotherapy), resulting in improved therapy outcomes (Xie et al., 2018). As an analogue of deoxycytidine, it incorporates into the newly synthesized DNA, which causes DNA-damage, and it also inhibits DNA polymerase, ribonucleotide reductase and thymidylate synthase, that are further enhancing its DNA-damaging activity (Honeywell et al., 2015). Although its activity has been extensively characterised, the senescence-inducing ability of gemcitabine was only tested in pancreatic cancer cell lines (Modrak et al., 2009, Song et al., 2016). According to our results, gemcitabine treatment induced DNA-damage in both MCF-7 and MDA-MB-231 cells (Figure 6.D, Figure 20.D). Gemcitabine-treated MCF-7 and MDA-MB-231 cells expressed all the senescence markers that were investigated, including altered cell morphology, increased SA- β -gal expression, proliferation arrest and increased expression of senescence-associated cytokines (Figure 6-8, 20-22, 27).

Although by using the empirically determined concentration of gemcitabine mostly induced senescence in MCF-7 cells, MDA-MB-231 cells had a more heterogeneous response to gemcitabine-treatment, resulting in a more heterogeneous senescence population and the appearance of cells in sub-G1 phase indicating increased apoptosis (Figure 20.D, Figure 21.A, Supplementary Figure 6.D). It has been described, that most of the DNA-damaging chemotherapeutic drugs induce apoptosis rather than senescence when used at higher concentrations, and the induction of DNA damage-induced cellular senescence requires a sustained but mild DNA damage and it mostly depend on the p53-p21^{WAF1/Cip1} or the p16^{INK4a}-Rb pathway (Petrova et al., 2016). In agreement with other studies, we found that MCF-7 cells

did not express p16^{INK4a}, thus we hypothesised that gemcitabine induces senescence through the p53-p21^{WAF1/Cip1} pathway (Supplementary Figure 1.B) (Craig et al., 1998, Karimi-Busheri et al., 2010, Todd et al., 2017). Moreover, low p16^{INK4a} expression can contribute to the reversibility of senescence, promoting senescence-escape (Beausejour et al., 2003, Roberson et al., 2005). Cells with wild type p53 gene, such as MCF-7 cells, are more resistant to DNA damage-induced apoptosis and they mostly respond to DNA-damage with the activation of cellular senescence (Alkhalaf and El-Mowafy, 2003, Jackson et al., 2012). In contrast, p53 mutant cells, such as MDA-MB-231 cells, are more sensitive to DNA-damaging agents, which mostly induce apoptosis via a p53-independent pathway (Hui et al., 2006, Bertheau et al., 2002, Varna et al., 2011). Therefore, the cytotoxicity of gemcitabine treatment limited the efficacy of senescence-induction in MDA-MB-231 cells, leading to a more heterogeneous senescence-population compared to MCF-7 cells. Interestingly, in MDA-MB-231 cells gemcitabine treatment induced the appearance of giant cells (with ~500 µm in diameter) and polyploid cells (Figure 23.A, Supplementary Figure 6.E). The appearance of these giant, polyploid cells have already been described in doxorubicin-induced senescent MDA-MB-231 cells, that started to divide asymmetrically during senescence-escape, generating escaped cells resembling the parental MDA-MB-231 cells (Bojko et al., 2020). Similarly to the effect of BrdU-treatment, gemcitabine induced a stable but reversible growth-arrest in both cell lines (Figure 6, 18), which makes it a suitable model to investigate senescence-escape.

The third compound that has been used in our experiments for senescence-induction was Palbociclib. Palbociclib (PD0332991, Ibrance) is a selective cyclin-dependent kinase 4/6 (CDK4/6) inhibitor that has been approved for advanced hormone receptor-positive and HER2 negative breast cancer treatment, after demonstrating efficacy in clinical trials by improving the progression-free survival of breast cancer patients, in combination with letrozole or fluvestrant (Turner et al., 2015, Finn et al., 2015, Bollard et al., 2017). CDK4/6 is responsible for the phosphorylation of retinoblastoma (Rb) protein, which leads to the activation of a transcriptional program for inducing the progression from G1 phase to S phase of the cell cycle. By inhibiting of CDK4/6, palbociclib induces cell cycle exit in Rb-positive cancer cells, which ultimately leads to quiescent or senescent state (Blagosklonny, 2014, Klein et al., 2018).

In fact, it has been proved in a variety of different cell types that Palbociclib treatment induced a reversible quiescence or a more stable senescence state, depending on which signalling

pathways were activated after cell cycle arrest (Leontieva and Blagosklonny, 2013, Kovatcheva et al., 2015, Morris-Hanon et al., 2019, Goel et al., 2017). It has been demonstrated in different cancer cells, that the conversion from cell cycle arrest to senescence (geroconversion) requires a sustained mTORC1 activity, indicating that mTORC1 could be the main regulator of palbociclib-induced senescence (Kovatcheva et al., 2015, Leontieva and Blagosklonny, 2013, Klein et al., 2018, Leontieva et al., 2012, Morris-Hanon et al., 2019, Maskey et al., 2020). Other molecular mechanisms that has been described to induce geroconversion in Palbociclib-treated cells are the downregulation of MDM2 (E3 ubiquitin-protein ligase Mdm2), the repression of *HRAS* (gene encoding the HRas small G protein) transcription, the redistribution of the chromatin-remodelling enzyme ATRX (ATP-dependent helicase ATRX) and the inhibition of MAPK (mitogen-activated protein kinase) signalling pathway (Kovatcheva et al., 2015, Ruscetti et al., 2018).

Since both MCF-7 and MDA-MB-231 cells are Rb-positive, they respond to Palbociclib treatment with cell-cycle arrest in G1 phase (Robinson et al., 2013). According to our results, Palbociclib-treatment induced senescence in MCF-7 and MDA-MB-231 cells, demonstrated in altered cell morphology, increased SA- β -gal expression, and proliferation arrest (Figure 6-8, 20-22). However, the senescent MCF-7 and MDA-MB-231 cells re-entered the cell cycle and resumed normal proliferation shortly after the removal of PALBO, indicating that it induced a less stable growth-arrest (senescent phenotype) compared to the BrdU- and GEM-induced senescence models (Figure 11, 23). Interestingly, this phenomenon was observed in patient-derived glioma stem cells, in human liver cancer cell lines and in other breast cancer cell lines as well, and it was described as senescent-like quiescence or incomplete senescence (Morris-Hanon et al., 2019, Bollard et al., 2017, Maskey et al., 2020). The investigation of cytokine expression of senescent cells revealed that PALBO-induced senescent MCF-7 cells did not have an increase in the expression of IL-6, IL-8 and CXCL12 compared to the control cells, however, in MDA-MB-231 cells PALBO-treatment significantly increased the expression of both IL-6 and IL-8 (Figure 7.F, Figure 21.E). These differences of IL-6 and IL-8 expression in PALBO-induced senescent cells were reported by others as well, indicating that the increased expression of IL-6 and IL-8 induced by PALBO treatment is cell line specific (Goel et al., 2017, Morris-Hanon et al., 2019).

Based on the expression of senescence markers and the immediate regain of proliferative capacity, we suggest that Palbociclib-treatment induced a transient or reversible senescent phenotype in MCF-7 and MDA-MB-231 cells, which is different from the BrdU- or GEM-induced senescent phenotype. Due to the induction of this transient senescent phenotype, PALBO-induced senescence is not ideal model for investigating senescence-escape, however, the results could be important in terms of the clinical use of Palbociclib. In clinical settings Palbociclib is administered on a 3-weeks-on/1-week-off schedule, that could provide the cancer cells sufficient time to resume proliferation between the treatment cycles (Finn et al., 2015). Moreover, there is an increasing number of breast cancer patients that are resistant to CDK4/6 inhibition, and according to a recent analysis of an ongoing clinical trial, the addition of Palbociclib to adjuvant endocrine therapy did not improve progression-free survival in breast cancer patients compared with endocrine therapy alone, which might be caused by the induction of this transient/reversible senescence phenotype (Portman et al., 2019, Mayer et al., 2021).

Besides the development of *in vitro* senescence-models, the reliable identification and assessment of cellular senescence is essential for investigating the effects of therapy-induced senescence in cancer. There are several cell surface markers of cellular senescence that has been identified for the detection of senescent cells, however, further validation of their specificity is required to exploit their diagnostic and therapeutic potential (Althubiti et al., 2014, Kim et al., 2017a). Although dipeptidyl-peptidase IV (DPP4/CD26) was identified as a cell surface marker for senescent fibroblast cells, it has not been validated in other cell types, such as in cancer cells (Kim et al., 2017a). However, the role of DPP4 activity in senescence-induction was described in endothelial senescence and in senescence-associated bone loss as well (Chen et al., 2020, Wang et al., 2021). According to our results, the expression of DPP4/CD26 was significantly increased in BrdU-, GEM- and PALBO-induced senescent MCF-7 and MDA-MB-231 cells as well (Figure 10, Figure 16.D). In both cell lines BrdU-treatment induced the highest increase in DPP4/CD26 expression compared to GEM- and PALBO-treatment, however, we could not determine the reason for this variation in the levels of DPP4/CD26 expression (Figure 10, Figure 16.D). As measured by flow cytometry in MCF-7 cells, in parallel with SA- β -galactosidase expression, the expression of DPP4/CD26 time-dependently increased during senescence-induction, indicating a strong connection between

DPP4/CD26 expression and the development senescent phenotype (Figure 10.B). Moreover, three other breast cancer cells lines, CAMA-1, MDA-MB-468 and T47D demonstrated an increased expression of both SA- β -galactosidase and DPP4/CD26 after BrdU-treatment (Supplementary Figure 12). Based on these results, DPP4/CD26 could be a promising new marker to detect senescent cancer cells, however, similarly to other senescence-markers its increased expression has to be compared to a basal level of expression, which can be increased in different tumour types independently from senescence (Enz et al., 2019).

The advantage of using specific surface markers is that it allows the isolation and investigation of senescent cells or certain subpopulations of senescent cells by flow cytometry, without disrupting membrane integrity and cell viability (Rossi and Abdelmohsen, 2021). For example, by using magnetic-activated cell sorting (MACS) we isolated a subpopulation of senescent MCF-7 cells with the highest expression of DPP4/CD26 (Supplementary Figure 13). According to our results the sorted cells (CD26 high) exhibited similar senescence-associated characteristics compared to the non-sorted population of senescent cells (Supplementary Figure 14). Moreover, cell surface molecules can be used as potential therapeutic targets for antibody-directed immunotherapies and for the administration of senolytic drugs by using antibody-drug conjugates (Rossi and Abdelmohsen, 2021). For example, DPP4/CD26 and another cell surface marker of senescence uPAR (urokinase plasminogen activator receptor) has been already described as potential therapeutic targets for the activation of antibody-dependent cell-mediated cytotoxicity and for CAR T cell (chimeric antigen receptor T cell) therapy, resulting in the selective elimination of senescent cells *in vitro* and *in vivo* as well (Kim et al., 2017a, Amor et al., 2020).

Although there are numerous studies about the effects of SASP (senescence-associated secretory phenotype) in cancer, the secretion of SASP factors directly from senescent cancer cells has been rarely analysed (Faget et al., 2019). Therefore, we assessed and compared the secretion of three SASP factors (IL-6, IL-8 and CXCL12) in BrdU-, GEM- and PALBO-induced senescent MCF-7 and MDA-MB-231 cells (Figure 7.F, Figure 21.E). As described before, these three cytokines are well-known SASP factors with a potential a role in cancer progression, moreover, the activity of CXCL12 is regulated (inhibited) by DPP4 (Lambeir et al., 2001, Wronkowitz et al., 2014, Faget et al., 2019). IL-6 is a pro-inflammatory cytokine involved in the regulation of immune reactions, and it is a major activator of the JAK/STAT signalling

pathway (Ma et al., 2017). IL-8 and CXCL12 are pro-inflammatory chemokines promoting the migration of granulocytes and lymphocytes, and they are involved in the activation of multiple intracellular signalling pathways via G-protein coupled chemokine receptors such as CXCR1, CXCR2 (IL-8) and CXCR4, CXCR7 (CXCL12) (Iliopoulos et al., 2011). The increased expression of IL-6, IL-8 and CXCL12 has been associated with tumour progression, survival, angiogenesis, cell proliferation and migration *in vitro* and *in vivo* as well (Canino et al., 2012, Tato-Costa et al., 2016, Angelini et al., 2013, Kim et al., 2017b, Ortiz-Montero et al., 2017, Yang et al., 2019a). Moreover, clinical studies have demonstrated that elevated IL-6, IL-8 and CXCL12 serum concentration is correlated to increased clinical stage of disease, lymph node metastasis and poor survival of breast cancer patients (Kang et al., 2005, Kozłowski et al., 2003, Ma et al., 2017).

According to our results, the secretion of IL-6 and IL-8 was significantly increased in senescent MCF-7 and MDA-MB-231 cells, however, in PALBO-induced senescent MCF-7 cells this increase was not detected (Figure 7.F, Figure 21.E). As described in other studies as well, MDA-MB-231 cells showed a significantly higher basal secretion of IL-6 and IL-8 compared to MCF-7 cells (Figure 7.F, Figure 21.E). Moreover, these studies also demonstrated that IL-6 and IL-8 are able to increase the invasiveness of non-aggressive ER-positive breast cancer cells, such as MCF-7 cells, increasing their tumorigenic potential (Freund et al., 2003, Freund et al., 2004, Ortiz-Montero et al., 2017). These results could explain the increased migration capacity of senescence-escaped MCF-7 cells, due to their prolonged exposure to increased levels of IL-6 and IL-8 secreted by the senescent cancer cells (Figure 30.B). Regarding the secretion of CXCL12 we found that BrdU- and GEM-induced senescent MCF-7 cells had an increased CXCL12 secretion, however, it was not secreted by control and senescent MDA-MB-231 cells (Figure 7.F, Figure 21.E). This observation has been reported in other studies as well, and interestingly, the lack of CXCL12 expression in MDA-MB-231 cells was associated with its increased metastatic capacity (Sun et al., 2014, Wendt et al., 2008). Although breast cancer cells have a relatively low expression of CXCL12, CXCR4 receptors are highly expressed in breast cancer cells and in malignant breast tumours, and their activation by CXCL12 is associated with increased tumour growth, EMT (epithelial-mesenchymal transition) and metastasis *in vitro* and *in vivo* as well (Müller et al., 2001, Wendt et al., 2008, Hattermann et al., 2014, Yang et al., 2019a). Moreover, the increased expression of CXCL12 by senescent

tumour cells has been described to function as a chemoattractant during the collective invasion and metastasis of tumour cells (Kim et al., 2017b). Based on our results, the analysis of cytokine secretion further demonstrated the complexity of senescence phenotypes induced by different drugs in different cell lines. Furthermore, it supported the concept that the presence of senescent cancer cells is potentially detrimental, and by the secretion of pro-inflammatory cytokines, senescent cancer cells could promote the development of metastasis.

Although cellular senescence has been defined as an irreversible form of cell cycle arrest, in therapy-induced senescent models the emergence of senescence-escaped cells was reported by several research groups, challenging the definition of senescence. Besides these reports, there are other studies demonstrating the emergence of senescent cells that were able to resume proliferation termed as senescent-like cells, premature, reversible, or incomplete senescence, leading to a confusion regarding the terminology of senescence-escape (Chitikova et al., 2014, Maskey et al., 2020, Petrova et al., 2016). As already described, the limitation of studies about senescence-escape is the lack of confirmation that the population of escaped cells originated from senescent cells, excluding the possibility that the examined cell population bypassed the senescent state. To resolve this issue, the senescence models should be optimised by either generating a relatively homogeneous population of senescent cells, or by sorting the senescence-induced cells based on a senescence-marker such as increased granularity or β -galactosidase expression (Alotaibi et al., 2016, Saleh et al., 2019a, Saleh et al., 2019b).

To investigate senescence-escape in MCF-7 and MDA-MB-231 cells we optimised a treatment strategy to establish different senescence models, in which the expression of several senescence markers was detected together, and their expression was relatively homogenous within the senescent cell populations. As described in other studies as well, the senescence-escaped cells lost their characteristics of senescence, such as cell cycle arrest, altered cell morphology and SA- β -galactosidase expression (Figure 6.C, Figure 18.A) (Elmore et al., 2005, Bojko et al., 2020). We demonstrated that during senescence-induction the Ki-67 expression of BrdU-treated cells gradually decreased, while in senescence-escaped cells the expression of Ki-67 was increased again, which made the senescence-escaped cells clearly distinguishable (Figure 4, Figure 5.A-B). For better understanding the cellular processes that

regulates senescence-escape, the assessment of the ability of cells to escape from senescence is essential. Generally, the increasing number of cells and the colony formation ability of the cells are used to indicate and evaluate senescence-escape (Roberson et al., 2005, Yang et al., 2017a, Alotaibi et al., 2016, Was et al., 2018). To establish a more accurate and quantitative method for the evaluation of senescence-escape, we measured the proportion of Ki-67 expressing cells along with the cell numbers and the number of escaped cell colonies (Figure 5). However, the quantification of escaped cell colonies is only suitable for cell types that are forming colonies during senescence-escape, such as MCF-7 cells (Figure 5.C, Figure 6.C, Supplementary Figure 10.B). Using flow cytometry to detect Ki-67 expression facilitates the quantification of senescence-escape and allows accurate detection even when the number of senescence-escaped cells are relatively low.

To further investigate the senescence-escaped cell with live-cell based assays, we established a method to isolate senescence-escaped cells by FACS based on their restored proliferative capacity using CFSE live-cell staining (Figure 23-24). Although a similar staining method (using a membrane dye known as Dil) has been used to detect senescence-escape (Was et al., 2017), in most of the experiments a prolonged incubation time (2-3 weeks) was used to ensure that the number of senescence-escaped cells greatly outweigh the number of senescent cells (Elmore et al., 2005, Roberson et al., 2005, Yang et al., 2017a, Was et al., 2018).

The isolation of senescence-escaped cells was tested on the different assays to measure the stem-cell activity, the proliferative and metastatic capacity of MCF-7 and MDA-MB-231 cells after senescence-escape (Figure 28). The analysis of mammosphere-formation assay demonstrated that senescent MCF-7 and MDA-MB-231 cells had a decreased mammosphere-formation ability compared to the non-senescent cells (Figure 29). These results indicate that in senescent cells there are either less cancer stem cells, or the cancer stem cells had a decreased stem cell activity, however, these could only be differentiated by the secondary generation of mammospheres (Shaw et al., 2012). In senescent MDA-MB-231 cells the stem-cell activity/quantity and proliferative capacity was decreased less than in senescent MCF-7 cells, indicating that MDA-MB-231 cells are more likely to escape-from senescence (Figure 29, Figure 31). This is also supported by the assessment of senescence-escape, which demonstrated that in MDA-MB-231 cells the number of senescence-escaping (Ki-67 expressing) cells started to increase earlier compared to MCF-7 cells (Figure 11.B, Figure 23.B).

Although further investigation of stemness markers would be required to assess the effect of senescence-escape in cancer stem cell activity.

Although different studies described that senescence-escaped cells became more aggressive and exhibited stem-like features (Achuthan et al., 2011, Milanovic et al., 2018), other studies found that senescence-escaped cells had a hybrid phenotype, demonstrating an increased expression of only certain markers of stemness (Was et al., 2018), or did not have an increase of stemness markers at all (Yang et al., 2017a). According to our results, cell proliferation, stem cell activity and migration capability were all increased in senescence-escaped cells compared to senescent cells and restored to similar levels as in parental non-senescent cells (Figure 29, 30, 31). Interestingly, Iliopoulos et al. (2011) demonstrated that in different cancer cell lines there is a dynamic equilibrium between normal/bulk cancer cells and cancer stem cells, resulting in a relatively constant proportion of both cell type within the total population (Iliopoulos et al., 2011). Altogether, our results indicate that the senescence-escaped cells are able to form a new population of cells with decreased proliferation, but with a restored proportion of stem cells, resembling to the parental cell population.

It has been described that senescence-escaped cells had a more invasive phenotype, reflecting in increased migration and invasion capacity compared to the cells they were originated from (Jonchere et al., 2015, Yang et al., 2017a). Although MCF-7 cells have a low metastatic capacity, according to our results the senescence-escaped MCF-7 cells had a significantly increased migration capacity compared to the parental cells, indicating that senescence-escape could promote the emergence of a more invasive type of MCF-7 cells (Figure 30.B). In contrast, the migration ability of senescence-escaped MDA-MB-231 was not increased (Figure 30.C). Regarding the migration-ability of senescent cells, it was proposed that senescent cancer cells might invade into the lymphovascular system together with non-senescent tumour cells, however, the migration and invasion capability of senescent cancer cells has not been investigated (Kim et al., 2017b). Our results demonstrated that despite their increased cell size, senescent MCF-7 and MDA-MB-231 cells are able to migrate, although their migration ability was significantly decreased in comparison with non-senescent cells (Figure 30).

After identifying therapy-induced senescent cells inside a tumour, it is important to consider adjuvant therapies for eliminating the tumour derived senescent cells, and thus potentially

improve the outcome of cancer treatment (Campisi, 2013). Azithromycin was described as a novel senolytic drug, selectively targeting senescent fibroblast cells, however its effect has not been tested in senescent cancer cells (Ozsvari et al., 2018). It is a type of macrolide antibiotic, that is used for the treatment of a wide range of bacterial infections (Southern et al., 2012). Autophagy inhibition by azithromycin was first reported by Renna et al. (2011), demonstrating that azithromycin treatment impaired autophagosome degradation by the inhibition of lysosomal acidification (Renna et al., 2011). Besides azithromycin, other macrolide antibiotics has been reported to impair autophagic flux, however, azithromycin appeared to be a more effective autophagy inhibitor compared to the other macrolides (Moriya et al., 2013, Mukai et al., 2016). Moreover, azithromycin enhanced the cytotoxic effect of different DNA-damaging drugs and tyrosine kinase inhibitors in cancer cells by inhibiting lysosomal function and autophagy, that were increased due to the treatment with DNA-damaging drugs or tyrosine kinase inhibitors (Tanaka et al., 2020, Toriyama et al., 2021). Although in these studies azithromycin was not considered as a senolytic compound, its enhancing effect was dependent on wild-type p53 status, indicating that its effect might be connected to its senolytic activity (Toriyama et al., 2021).

We found that azithromycin treatment selectively decreased the viability of BrdU-, GEM- and PALBO-induced senescent cells in both MCF-7 and MDA-MB-231 senescence models, however, it showed a selective effect of PALBO-induced senescent cells only at the concentration of 100 μ M (Figure 12.B, 24.A). This reduced effect of azithromycin treatment might be connected to the different (reversible) senescence phenotype induced by Palbociclib treatment. Although azithromycin decreased the viability of non-senescent MCF-7 and MDA-MB-231 cells as well, it showed no toxicity in normal epithelial and fibroblast cells (Figure 12.C, Supplementary Figure 4.B) (Ozsvari et al., 2018). Comparing the two cell lines, normal and senescent MCF-7 cells were less sensitive to azithromycin treatment than MDA-MB-231 cells, in which the senescent cells were eliminated after 5 days azithromycin treatment (Figure 12.B, Figure 24.A, Supplementary Figure 5). The increased sensitivity of MDA-MB-231 cells to azithromycin treatment can be explained by their increased dependence of autophagy compared to MCF-7 cells, that has been categorised as autophagy-independent cells (Maycotte et al., 2014). Moreover, MCF-7 cells do not express caspase-3 protein, which has

an important role in mediating autophagy induced apoptosis, thus they are more resistant to apoptosis induced by the disruption of autophagy (Devarajan et al., 2002, Wu et al., 2014).

After azithromycin treatment, a population of senescent MCF-7 cells remained alive, indicating resistance to azithromycin treatment, and in addition, they were able to escape senescence and continue to proliferate, similarly to the senescent cells that did not receive azithromycin (Figure 14). The ability of senescent cells to escape after senolytic treatment was also described in doxorubicin-induced senescent colon cancer cells, where the adjuvant bafilomycin (autophagy inhibitor) treatment resulted in the appearance of a surviving cell population, that were able to restore their autophagic activity, and exhibited increased cell proliferation and increased ability of tumour formation in mice (Was et al., 2017). Furthermore, senescent lung tumour cells treated by Bcl2 inhibitor ABT-737 formed more colonies than the senescent cells without any additional treatment, indicating that ABT-737 treatment promotes the proliferation of the surviving cells (Yang et al., 2017a).

The mechanism of autophagy inhibition by azithromycin is almost identical to the antimalarial drug chloroquine, which is well known for its effect to alter the pH of lysosomes, thus interrupting the fusion of autophagosomes with lysosomes (Ferreira et al., 2021). Chloroquine has been described to act as a senolytic drug in several *in vitro* and *in vivo* studies, moreover, it was recently reported that hydroxychloroquine treatment decreased the number of senescence-escaped lung cancer cells after cisplatin treatment (Tsubone TM, 2020, L'Hôte et al., 2021, Li et al., 2022, Olszewska et al., 2022). It became a widely used drug to sensitize cancer cells to therapy, and there are several clinical trials that demonstrated promising results by examining the effect of autophagy inhibition combined with radio- or chemotherapies in cancer patients by using either chloroquine or hydroxychloroquine (Xu et al., 2018, Zeh et al., 2020, Ferreira et al., 2021).

Comparing the effect of azithromycin and chloroquine in senescent MCF-7 and MDA-MB-231 cells, we found that chloroquine treatment was more toxic to both normal and senescent cells, and it was the most effective in the PALBO-induced senescent cells (Figure 13.E, Figure 24.A). This increased effect of chloroquine in PALBO-induced senescent cells might be connected to the observation, that due to its weakly basic and lipophilic nature Palbociclib accumulates in lysosomes through a mechanism known as lysosomal-trapping, and therefore it could contribute to the inhibition of lysosomal acidification caused by the chloroquine

treatment (Llanos et al., 2019). In MCF-7 cells chloroquine treatment showed a lower selectivity than azithromycin towards senescent cells (Figure 12.B, Figure 13.D). We also demonstrated that chloroquine treatment increased more the expression of LC3B compared to the effect of azithromycin, however, the expression of p62/SQSTM1 was more increased after azithromycin treatment (Figure 13. A-C). The increased LC3B expression, which represents the increased number of autophagosomes indicates that chloroquine is a more potent autophagy inhibitor compared to azithromycin, however, azithromycin was more selective towards senescent MCF-7 cells and less toxic to non-malignant epithelial and fibroblast cells (Figure 13.B, Supplementary Figure 4.B).

Senescent cells contains impaired mitochondria, which leads to decreased mitochondrial membrane potential and increased mitochondrial ROS generation, making the senescent cells more vulnerable to mitochondria-targeted therapies (Chapman et al., 2019). For example, mitochondria-targeted tamoxifen (MitoTam) eliminated senescent cells *in vitro* and *in vivo* (Hubackova et al., 2019). Because the antibiotic activity of azithromycin is based on its ability to interfere with bacterial protein synthesis by the inhibition of the 50S subunit of bacterial ribosome, it can also inhibit the large subunit of mitochondrial ribosome, thus disrupting mitochondrial activity in cancer cells (Southern et al., 2012, Lamb et al., 2015). Therefore, the effect of azithromycin on mitochondrial metabolism might contribute to its senolytic activity (Ozsvari et al., 2018). In fact, the accumulation of p62/SQSTM1 after azithromycin treatment (Figure 8.A) could be an indicator of increased metabolic stress, based on the observation that in autophagy-defective tumour cells high expression of p62/SQSTM1 was related to elevated oxidative stress (Mathew et al., 2009, Lee et al., 2021). Moreover, targeting metabolism in senescent cells increases their susceptibility to autophagy inhibition, which for example has been demonstrated by using a mitochondrial inhibitor (oleanolic acid) combined with an autophagy inhibitor (chloroquine), resulting in increased apoptosis in senescent cancer cells compared to using chloroquine alone (Dörr et al., 2013, Tsubone TM, 2020). Based on these observations, azithromycin could be more suitable to use as an adjuvant senolytic treatment in cancer therapy compared to chloroquine.

Although it has been demonstrated that the expression of DPP4/CD26 increased in senescent cells, its potential function in cellular senescence is still undetermined. However, several studies reported that DPP4 inhibition or silencing hinders the induction of senescence in

epithelial cells, fibroblasts, chondrocytes and in mice, indicating that DPP4/CD26 contributes to the development of senescence phenotype (Li et al., 2018, Chen et al., 2020, Wang et al., 2021, Bi et al., 2019). To investigate the function of DPP4/CD26 in MCF-7 and MDA-MB-231 cells, we silenced the expression of DPP4 in both cell lines and treated them with BrdU, GEM and PALBO to determine the connection of DPP4/CD26 expression to senescence-induction (Figure 16.A-B, Figure 25.A-B). In contrast with the previously described role of DPP4 expression in senescence induction, DPP4 silencing did not have an effect on senescence-induction in MCF-7 and MDA-MB-231 cells (Figure 16.D-E, Figure 25.D-E). These results indicate that although the increased expression of DPP4/CD26 could be a potential marker of senescence in cancer, it is not essential for the induction of senescence.

To investigate whether the silencing or inhibition of DPP4 has an effect on the process of senescence-escape we used the methods established before for assessing the senescence-escaping ability of the cells. Our results demonstrated that DPP4 inhibition and silencing decreased the appearance of senescence-escaped MCF-7 cells, however, in MDA-MB-231 cells DPP4 inhibition and silencing did not affect (BrdU-induced) or increased (GEM-induced) senescence-escape (Figure 16-19, Figure 26). These results indicate that DPP4/CD26 could have a cell-type dependent role in the regulation of senescence-escape, either preventing or promoting it. This contradictory effect of DPP4 inhibition in cancer has been described in other studies as well. For example, the inhibition or silencing of DPP4 decreased tumour development, tumour growth and neoplastic cellular transformation *in vitro* and *in vivo*, moreover, and according to different meta-analysis studies DPP4 inhibition (by alogliptin, linagliptin, saxagliptin, sitagliptin, and vildagliptin) improved overall survival in colorectal, prostate and lung cancer patients (Angevin et al., 2017, Bishnoi et al., 2019, Shah et al., 2020, Inamoto et al., 2006). In contrast, other studies demonstrated that the inhibition of DPP4 increased the metastatic potential and chemotherapy resistance of breast cancer cells *in vitro* and *in vivo* (Yang et al., 2019b, Li et al., 2020).

According to the previously described results, a small number of MCF-7 cells were able to survive after azithromycin treatment and resumed proliferation by escaping senescence (Figure 14). Therefore, we targeted these senescence-escaping cells by using sitagliptin, an inhibitor of DPP4, to potentiate the senolytic effect of azithromycin in MCF-7 cells. Our results demonstrated a synergistic effect of the combination treatment with azithromycin and

sitagliptin, resulting in a significant reduction of senescence-escaped cells (Figure 19). Altogether these results indicate that DPP4 inhibition could improve the effect of senolytics, by decreasing the senescence-escaping ability of the surviving cells, however, the distinct role of DPP4 in different types of cancer cells and its role in the inactivation of several chemokines could limit the application of DPP4 inhibitors in cancer therapy (Yang et al., 2019a).

6. Conclusion

The general aim of the research project was to investigate the characteristics of senescent cancer cells using *in vitro* TIS and senescence-escape models, and to investigate potential markers and treatment strategies, that could be exploited to improve the outcome of cancer therapies. Based on the research objectives, the project led to the following results:

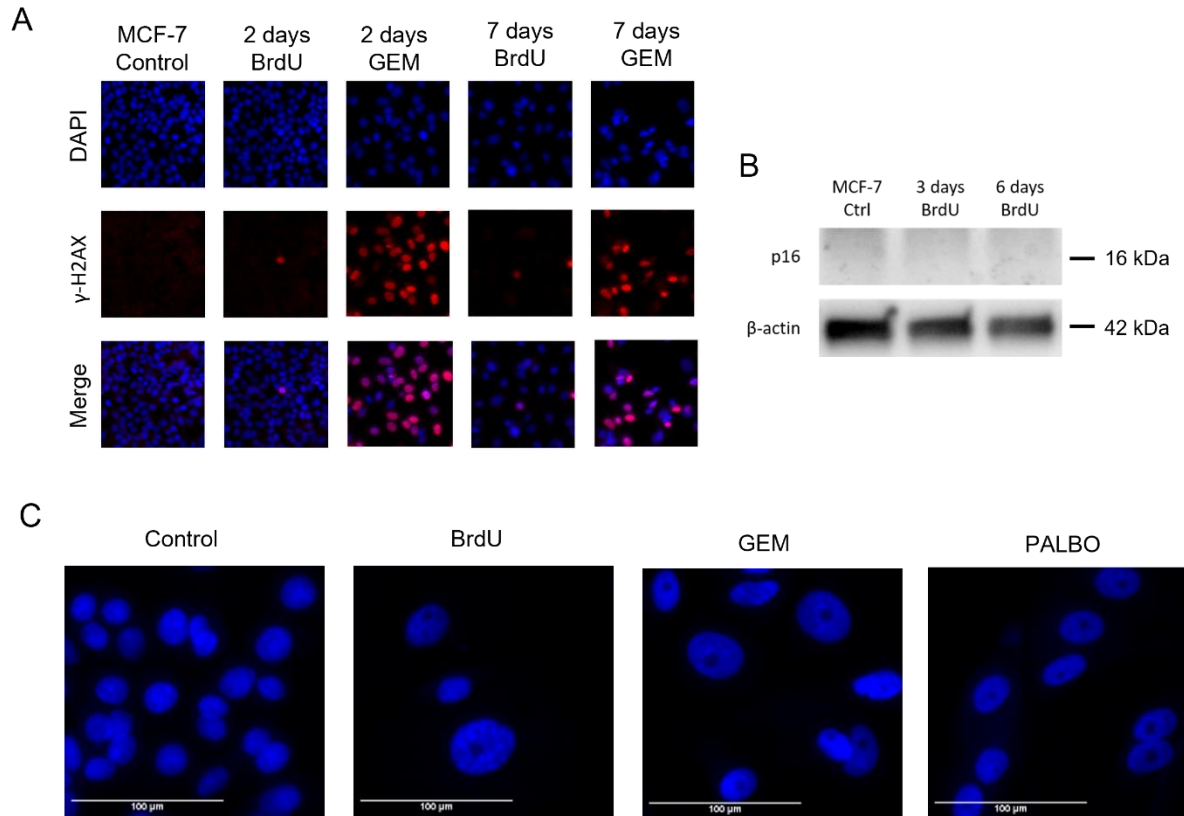
- I. Optimising, analysing and comparing different *in vitro* models for therapy-induced senescence using breast cancer cells
 - Bromodeoxyuridine (BrdU), gemcitabine (GEM) and palbociclib (PALBO) induced senescence in MCF-7 and MDA-MB-231 breast cancer cells through different mechanism of action
 - The simultaneous measurement of Ki-67 expression and DAN content (PI) could be used to identify cell cycle arrested/senescent cell populations by using flow cytometry
 - The levels of expression of different senescence-markers in MCF-7 and MDA-MB-231 cells were dependent on the drug used for senescence-induction
 - IL-6, IL-8 and CXCL12 secretion was highly increased in BrdU- and GEM-induced senescent MCF-7 cells, but it was not increased in PALBO-induced senescent cells; IL-6 and IL-8 secretion was significantly increased in senescent MDA-MB-231 cells
 - The senescence-escaping ability of cancer cells could be evaluated by the measurement of Ki-67 expression and cell numbers by flow cytometry; and by the assessment of senescence-escaped colonies stained by crystal-violet staining
 - PALBO-induced senescent MCF-7 and MDA-MB-231 cells were able to escape from senescence shortly after the removal of PALBO treatment, resulting an unstable/transient senescence phenotype
 - BrdU- and GEM-treatment resulted in a more stable growth arrest/senescence, however, cells were able to escape from senescence and restart proliferation
- II. Developing a two-hit treatment strategy using azithromycin as a senolytic drug
 - The senolytic effect of azithromycin was confirmed in senescent MCF-7 and MDA-MB-231 cells, and its inhibitory effect on autophagy was confirmed in MCF-7 cells

- Senescent MCF-7 cells were able to escape after azithromycin (AZI) treatment, however, the senescence-escaping ability of AZI-treated the cells was decreased by DPP4 inhibition (sitagliptin treatment)
- III. Investigating the cell surface protein DPP4 (Dipeptidyl peptidase-4; CD26) as a marker of cellular senescence in cancer and identifying its potential function
- The cell surface expression of DPP4/CD26 was highly increased in senescent MCF-7 and MDA-MB-231 cells, however, its expression was not essential for senescence-induction
 - The silencing or inhibition of DPP4 resulted in decreased senescence-escaping ability of MCF-7 cells and increased/unchanged senescence-escaping ability of senescent MDA-MB-231 cells
- IV. Establishing a method to quantify and isolate senescence-escaped cells for further investigations
- Senescence-escaped cells could be isolated by FACS, using CellTrace CFSE staining for the identification of proliferating cells
 - After senescence-escape, MCF-7 and MDA-MB-231 cells resembled to the parental (non-senescent) cells in terms of stemness activity and proliferation capacity
 - Senescence-escape increased the migration capacity of MCF-7 cells, but not MDA-MB-231 cells

Altogether, the research project highlighted the importance of detailed characterisation of senescent cancer cells for the investigation of therapy induced senescence. Our results suggested that therapy induced senescence in cancer could potentially contribute to cancer progression and tumour relapse, via the secretion of different cytokines (IL-6, IL-8, CXCL12) and senescence-escape. Furthermore, the results of the project indicated that senolytic treatments, such as azithromycin treatment, could improve the outcome of senescence-inducing cancer therapies, and that DPP4/CD26 could be a promising marker and a novel target to be exploited in cancer diagnosis and treatment. The established methods for the evaluation of senescence-escape could contribute to the comprehensive investigation of the mechanisms of senescence-escape, and to the identification of potential therapeutic targets for decreasing senescence-escape.

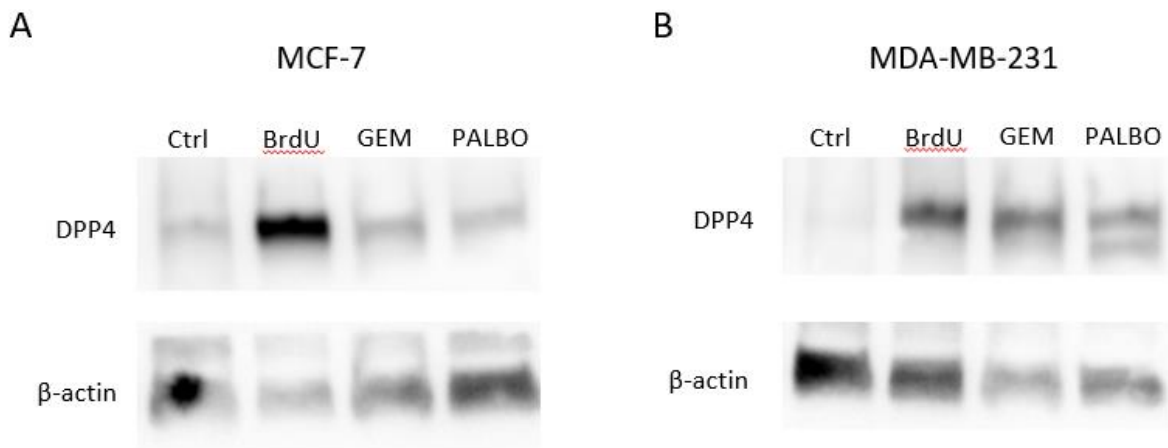
7. Supplementary figures

Supplementary Figure 1. γ -H2AX immunostaining, p16 expression of MCF-7 cells, DAPI staining of nucleus (increased image size)



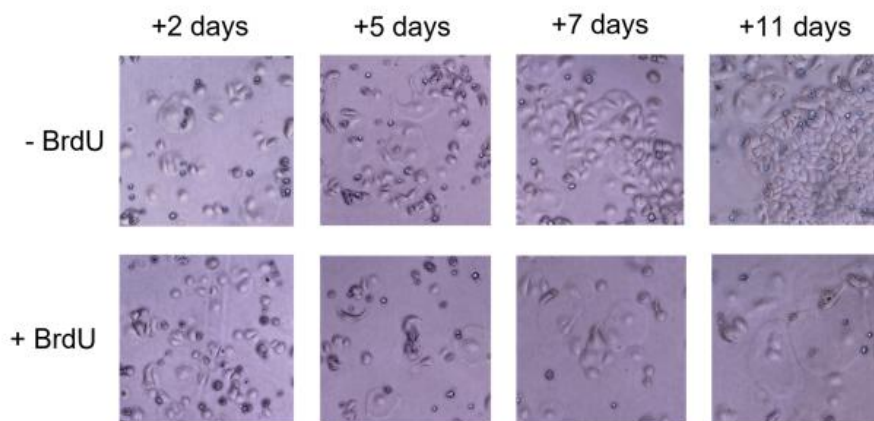
Supplementary Figure 1. (A) Representative images of DNA-damage induction represented by nuclei staining with DAPI and γ H2AX expression. Cells were fixed at different time points during senescence induction by BrdU- and GEM-treatment, stained by immunostaining and imaged by EVOS using 20x magnification. Control represents untreated MCF-7 cells, scale bars indicate 100 μ m. **(B)** Representative image of western blot assay representing the lack of p16 expression in control and BrdU-treated MCF-7 cells. **(C)** Representative images of nuclei staining of control and senescent MCF-7 cells. Cells were fixed and stained with DAPI nuclei stain, imaged by EVOS using 20x magnification, scale bars indicate 100 μ m.

Supplementary Figure 2. Western blot images of DPP4 expression in MCF-7 and MDA-MB-231 cells



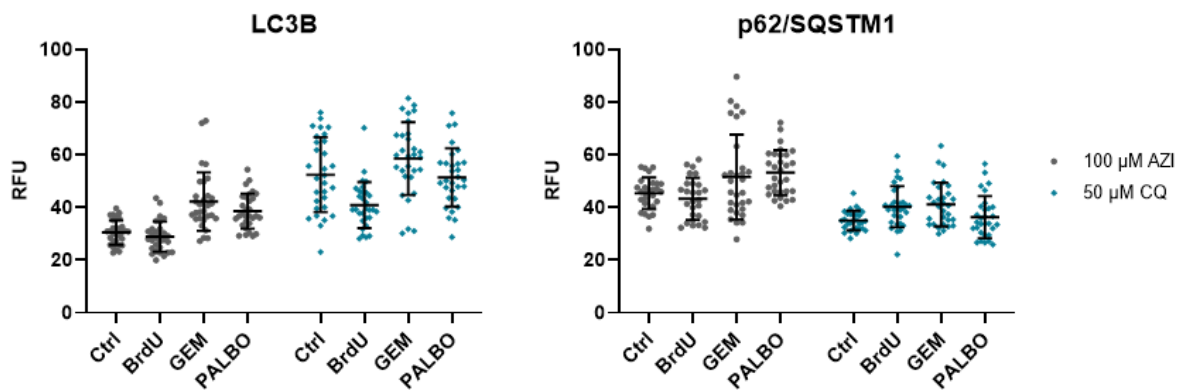
Supplementary Figure 2. Representative images of western blot analysis of DPP4/CD26 expression in control and senescent MCF-7 (A) and MDA-MB-231 (B) cells.

Supplementary Figure 3. Senescence-escape in BrdU-induced senescent MCF-7 cells



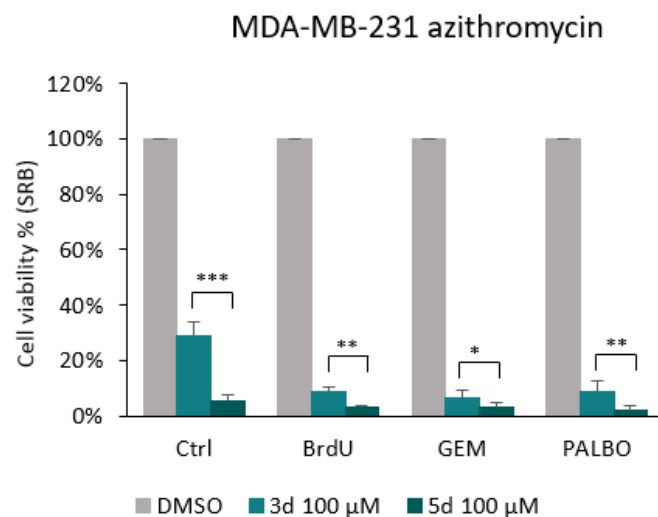
Supplementary Figure 3. Representative images of the senescence escape of BrdU-induced senescent cells, imaged at different time points after senescence-induction. Cells represented by the upper panel were incubated without BrdU, allowing them to escape from senescence, cells represented by the bottom panel were incubated in the presence of BrdU treatment, remaining senescent.

Supplementary Figure 4. Analysis of LC3B and p62/SQSTM1 expression without signal area correction



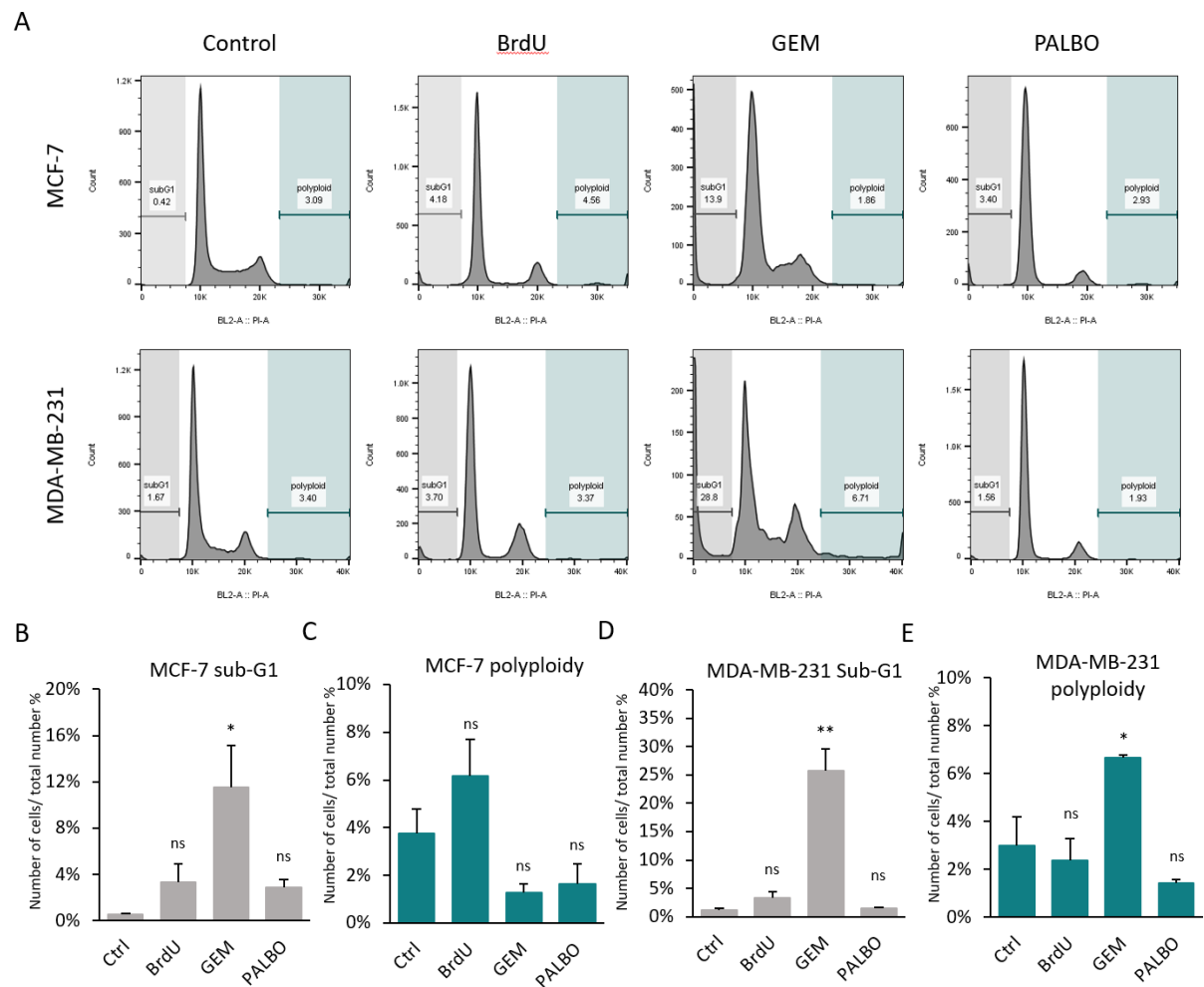
Supplementary Figure 4. (A) Analysis of LC3B and p62/SQSTM1 expression in control, BrdU-, GEM- and PALBO-induced senescent cells after azithromycin or chloroquine treatment. Experiments were repeated three times with two technical replicates. The graphs represent the relative fluorescent unit (RFU) based on the analysis of fluorescent signal intensity of 30 cells for each condition (10 cells from each experimental replicates) measured by ImageJ software. Error bars represent mean \pm SD.

Supplementary Figure 5. Effect of 3 days and 5 days of azithromycin treatment in MDA-MB-231 cells



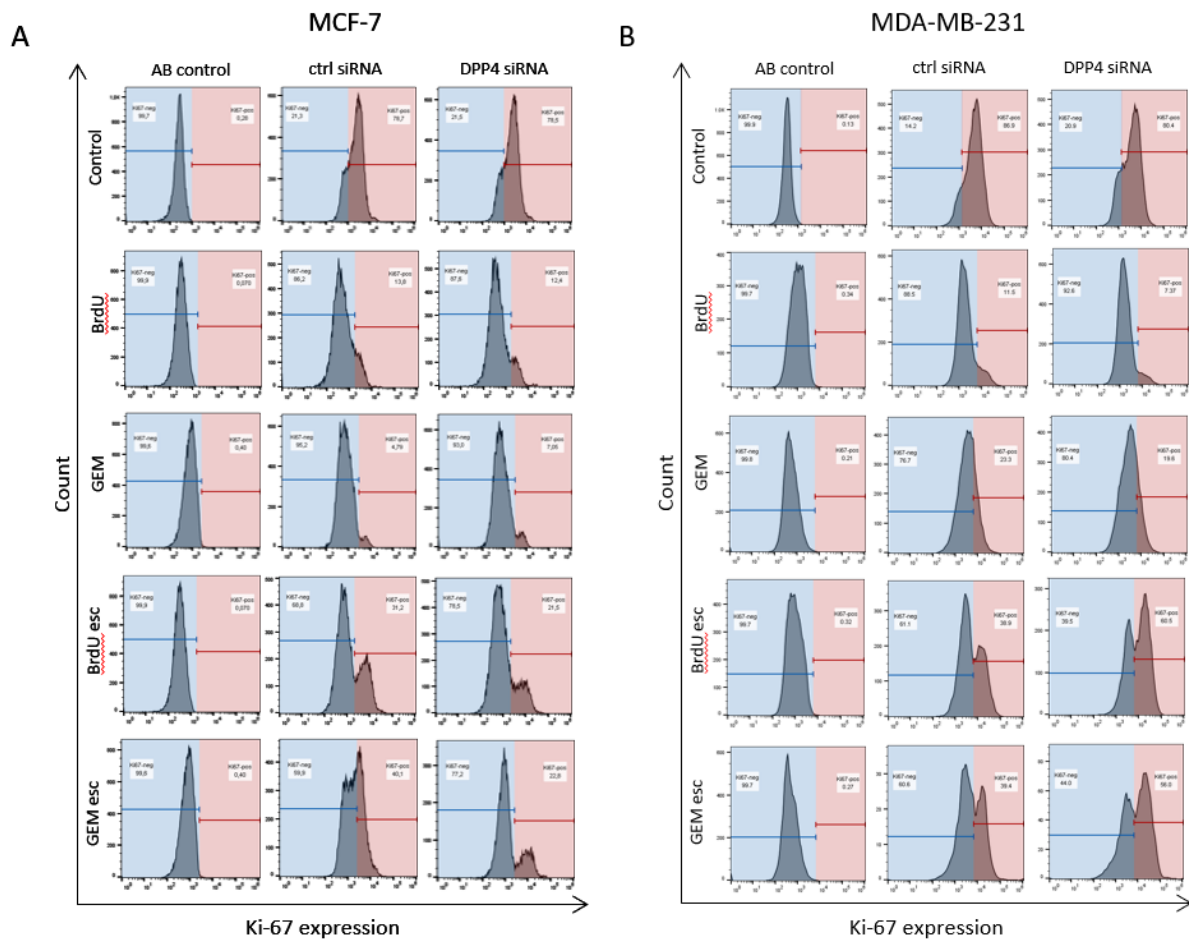
Supplementary Figure 5. The cell viability of control, BrdU-, GEM- and PALBO-induced senescent MDA-MB-231 cells was measured by SRB assay after 3 days and 5 days of treatment with azithromycin. Experiments were repeated three times with six technical replicates, values were normalised respectively to vehicle-treated (DMSO) control BrdU-, GEM- and PALBO-induced senescent cells, error bars represent \pm SEM. Statistical significance: ns $p > 0.05$; * $p \leq 0.05$; ** $p \leq 0.01$; *** $p \leq 0.001$; **** $p \leq 0.0001$.

Supplementary Figure 6. Cell cycle analysis of MCF-7 and MDA-MB-231 cells - sub-G1 and polyploid cell populations



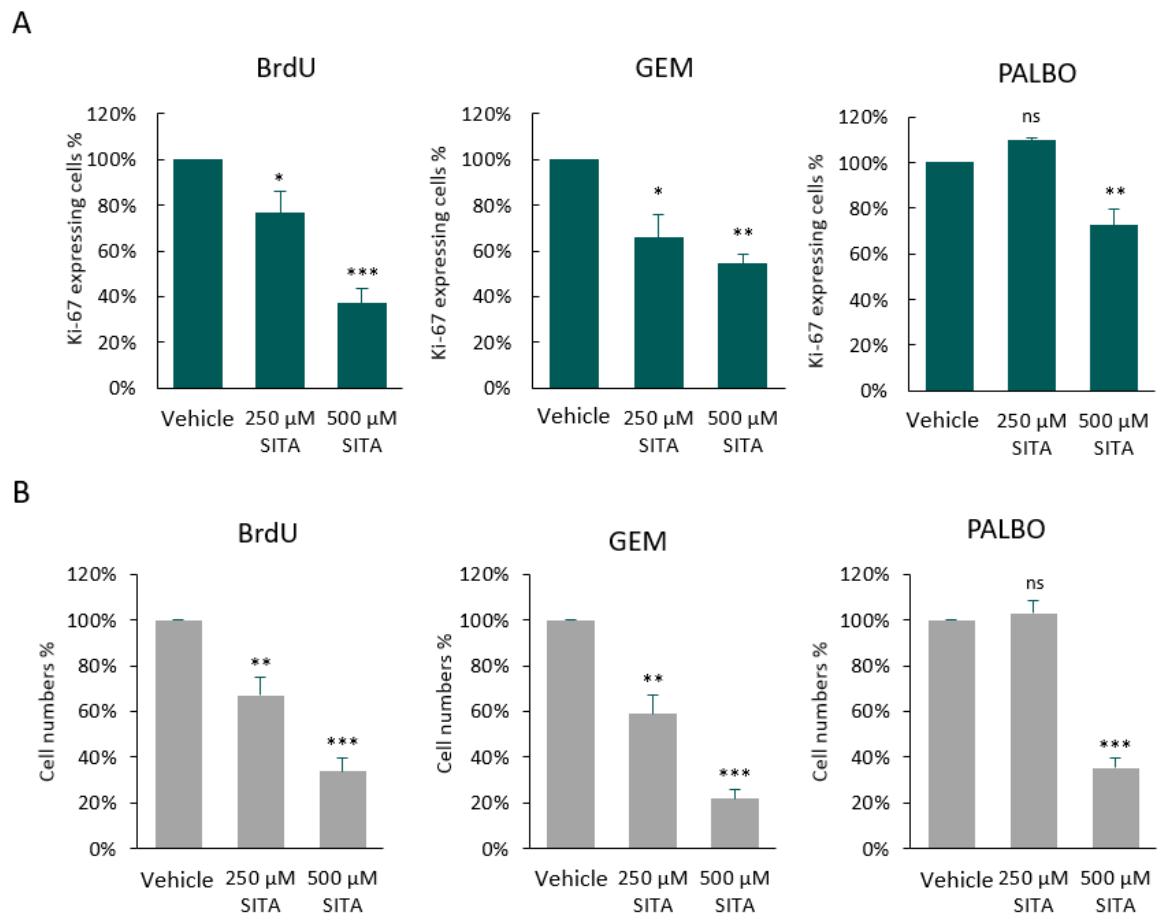
Supplementary Figure 6. (A) Representative figures of cell cycle analysis using PI staining. The gates were adjusted manually to the sub-G1 and polyploid populations. The bar graphs represent the sub-G1 and polyploid populations in MCF-7 (**B-C**) and MDA-MB-231 (**D-E**) cells. Bar graphs represent the mean of three independent experiments \pm SEM. Statistical significance (in relation to control): ns $p > 0.05$; * $p \leq 0.05$; ** $p \leq 0.01$; *** $p \leq 0.001$; **** $p \leq 0.0001$.

Supplementary Figure 7. Evaluation of senescence-escape in ctrl siRNA and DPP4 siRNA MCF-7 and MDA-MB-231 cells (representative figures)



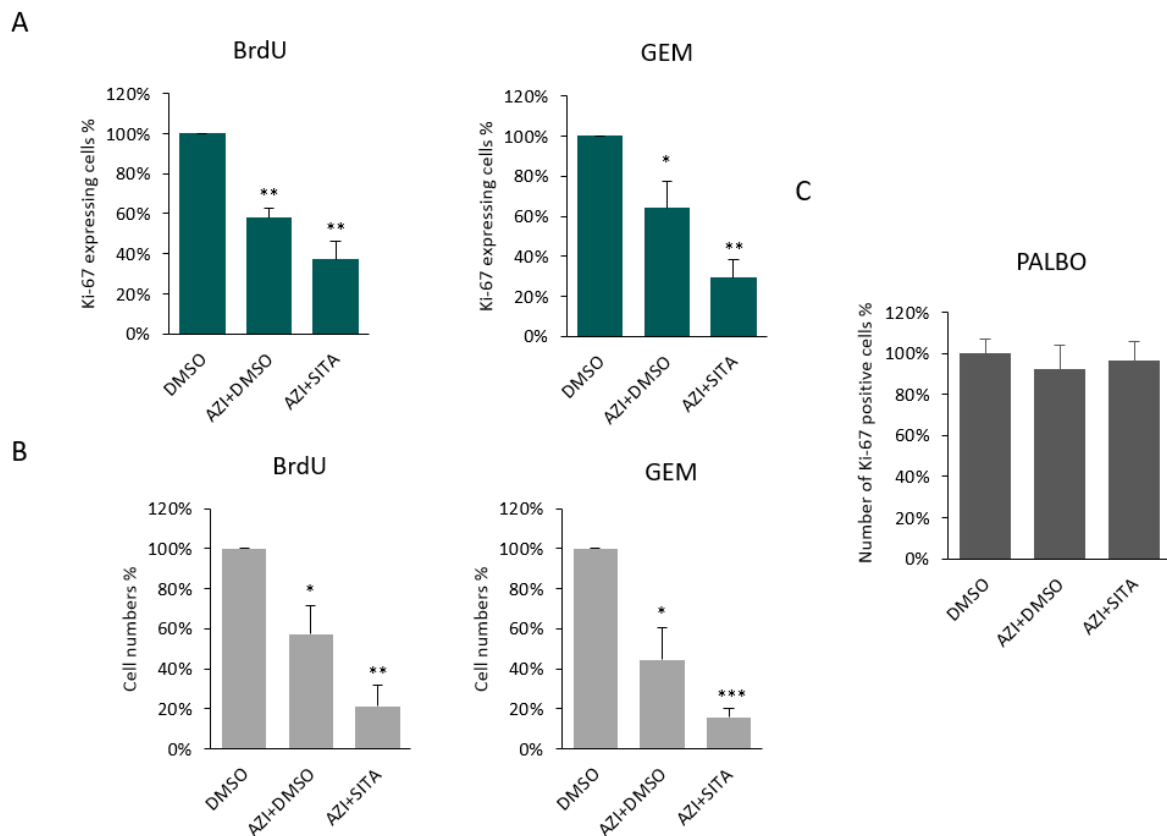
Supplementary Figure 7. Representative figures of evaluating senescence-escape in ctrl siRNA and DPP4 siRNA MCF-7 (A) and MDA-MB-231 (B) cells, based on Ki-67 expression measured by flow cytometry. The figures demonstrate the adjustment of gates based on AB control cells (antibody control, stained only with the secondary antibody), that represent the background staining. The cells were categorised to Ki-67 negative (blue) and Ki-67 positive (red) populations. The bar graphs in Figure 12.A and Figure 21.A represents the Ki-67 positive populations.

Supplementary Figure 8. Effect of sitagliptin treatment on senescence-escape in MCF-7 cells – Ki-67 expression and cell numbers



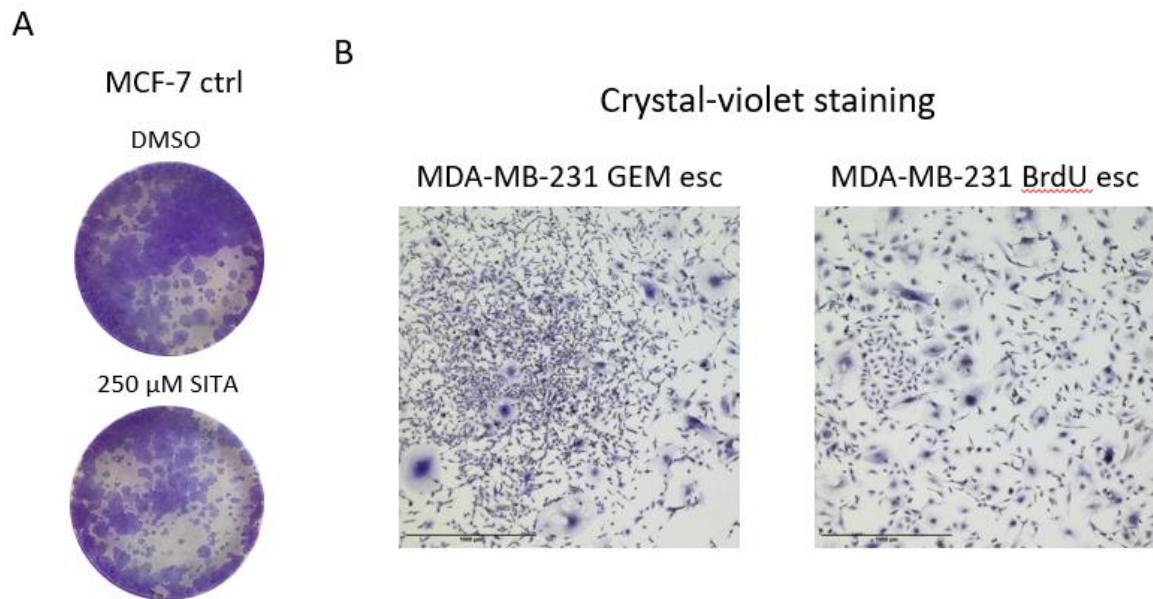
Supplementary Figure 8. (A) The expression of Ki-67 in MCF-7 cells is represented as the percentage of positively stained cells compared to the total population. The gates for Ki-67-positive cells were adjusted by using unstained cells. **(B)** The cell concentrations were measured by flow cytometry using the samples from the measurement of Ki-67 expression represented as count/ μl (cell number/ μl). The samples were collected with the same volume, therefore the cell concentration is proportional to the cell numbers of each sample. Values were normalised to the vehicle-treated cells. Bar graphs represent the mean of three independent experiments \pm SEM. Statistical significance (in relation to control): ns $p > 0.05$; * $p \leq 0.05$; ** $p \leq 0.01$; *** $p \leq 0.001$; **** $p \leq 0.0001$.

Supplementary Figure 9. Effect of AZI+SITA on senescence-escape in MCF-7 cells – Ki-67 expression and cell numbers



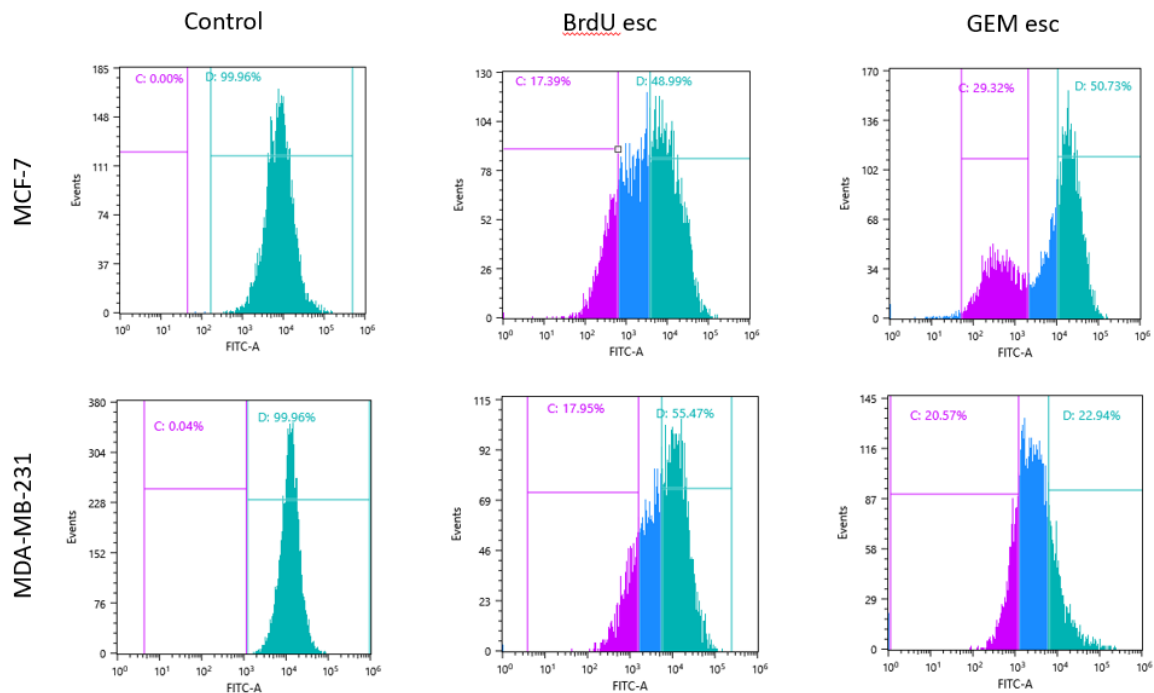
Supplementary Figure 9. (A) The expression of Ki-67 in MCF-7 cells is represented as the percentage of positively stained cells compared to the total population. The gates for Ki-67-positive cells were adjusted by using unstained cells. (B) The cell concentrations were measured by flow cytometry using the samples from the measurement of Ki-67 expression represented as count/ μl (cell number/ μl). The samples were collected with the same volume, therefore the cell concentration is proportional to the cell numbers of each sample. Values were normalised to the vehicle-treated cells. (C) The senescence-escaping ability of the cells are assessed by the combination of Ki-67 expression and cell concentration represented as the number of Ki-67 positive cells. Values were normalised to the vehicle treated (DMSO) cells. Bar graphs represent the mean of three independent experiments \pm SEM. Statistical significance (in relation to control): ns $p > 0.05$; * $p \leq 0.05$; ** $p \leq 0.01$; *** $p \leq 0.001$; **** $p \leq 0.0001$.

Supplementary Figure 10. Effect of SITA on control MCF-7 cells, and senescence-escape of MDA-MB-231 cells – crystal violet staining



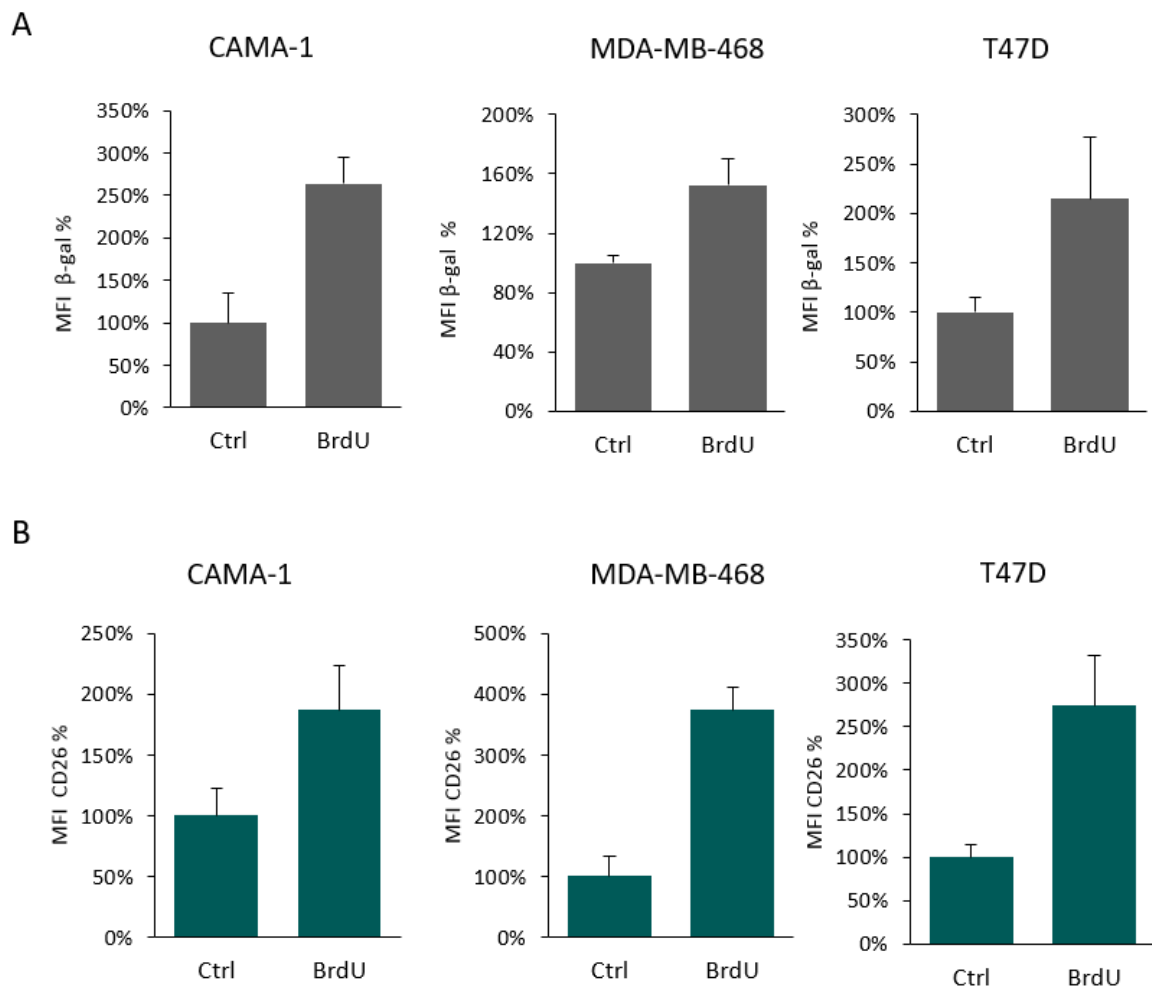
Supplementary Figure 10. (A) Representative images of the colony formation of non-senescent MCF-7 cells after sitagliptin treatment. Cells were seeded with 1×10^3 cells/well (in 24-well plate), incubated for 10 days with sitagliptin treatment and stained with crystal violet. **(B)** Representative images of senescence-escaped BrdU- and GEM-treated MDA-MB-231 cells. Cells were stained with crystal violet, imaged by EVOS using 4x magnification, scale bars indicate 1000 μ m.

Supplementary Figure 11. Gating strategies for the isolation of senescence-escaped cells by FACS



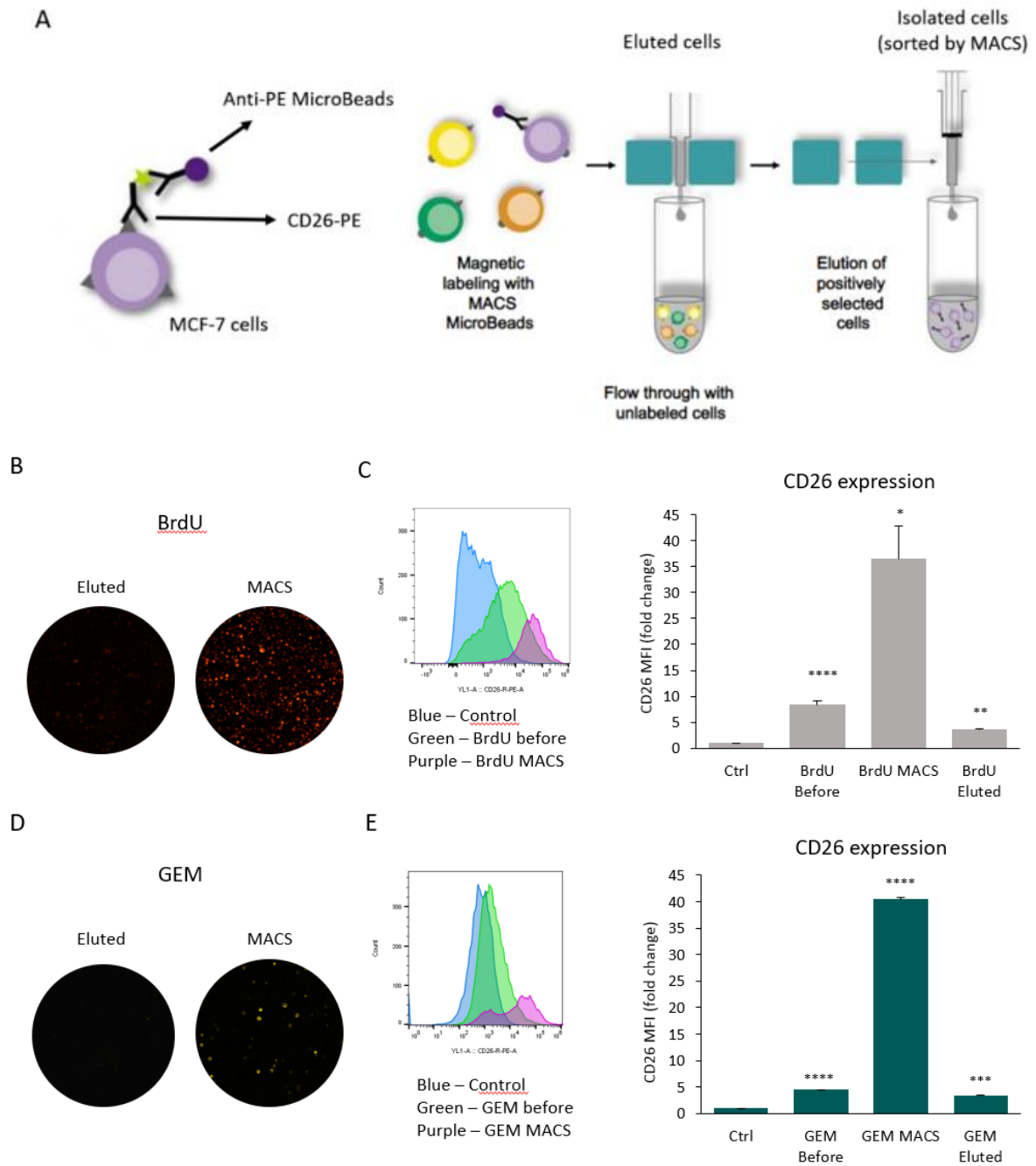
Supplementary Figure 11. Representative figures of the gating strategies for the isolation of senescence-escaped cells by FACS using CFSE staining. The gates were adjusted manually based on the CFSE signal of BrdU- and GEM-induced senescent cells. Control (non-senescent) MCF-7 and MDA-MB-231 cells were not sorted to different categories, thus the total cell population was gated. Cells with low expression of CFSE (magenta) was considered as senescence-escaped cells and cells with high expression of CFSE (green) was considered as senescent cells. The cells represented in the middle part of the histogram (blue) of CFSE-signal were not included in the sorting. Figures were generated by the software of Sony cell sorter.

Supplementary Figure 12. SA- β -gal and CD26 expression in BrdU-treated CAMA-1, MDA-MB-468 and T47D cells



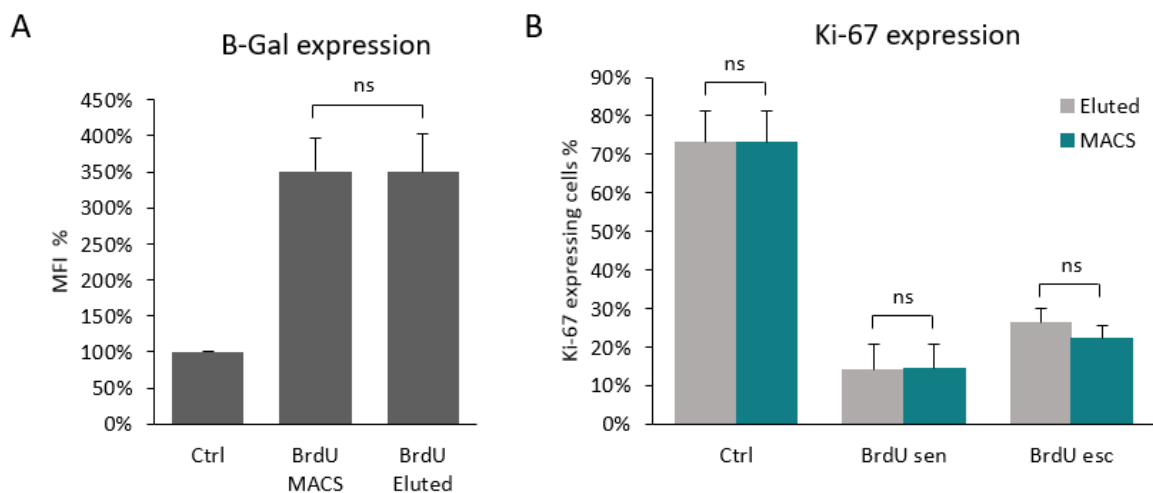
Supplementary Figure 12. (A-B) CAMA-1, MDA-MB-468 and T47D breast cancer cells were treated with 5 μ M BrdU for 7 days. The expression of SA- β -galactosidase **(A)** and CD26 **(B)** in control and BrdU-treated cells was measured by flow cytometry. The SA- β -galactosidase and CD26 expression is represented as mean fluorescence intensity (MFI) of FDG and CD26-PE staining measured separately by flow cytometry, values were normalised to the MFI of non-senescent cells. Bar graphs represent the mean of three independent experiments \pm SEM.

Supplementary Figure 13. MACS sorting of MCF-7 cells



Supplementary Figure 13. (A) Schematic figure representing the workflow of magnetic-activated cell sorting (MACS) using MCF-7 cells stained by CD26-PE staining. **(B, D)** Representative images of the eluted and sorted (MACS) BrdU-induced **(B)** and GEM-induced **(D)** senescent MCF-7 cells, cells were stained with CD26-PE, imaged by EVOS using 10x magnification. **(C, E)** Analysis of sorting efficiency by flow cytometry. Figure represents the shift in CD26-PE signal intensity of BrdU-induced **(C)** and GEM-induced **(E)** senescent cells before and after sorting (MACS) compared with the non-senescent cells. The graph represents mean fluorescence intensity (MFI) of CD26-PE staining measured by flow cytometry, values were normalised to the MFI of non-senescent cells (ctrl) represented as fold change. Bar graphs represent the mean of three independent experiments \pm SEM. Statistical significance (in relation to control): ns $p > 0.05$; * $p \leq 0.05$; ** $p \leq 0.01$; *** $p \leq 0.001$; **** $p \leq 0.0001$.

Supplementary Figure 14. SA- β -gal and Ki-67 expression of MACS sorted MCF-7 cells



Supplementary Figure 14. (A) Graph represents the expression of SA- β -galactosidase in control and BrdU-induced senescent sorted (MACS) and eluted cells measured by flow cytometry. The SA- β -galactosidase expression is represented as mean fluorescence intensity (MFI) of FDG, values were normalised to the MFI of non-senescent (ctrl) cells. **(B)** The expression of Ki-67 is represented as the percentage of positively stained cells compared to the total population. The gates for Ki-67-positive cells were adjusted by using unstained cells. BrdU sen: BrdU-induced senescent cells, BrdU esc: BrdU-treated senescence escaped cells. Bar graphs represent the mean of three independent experiments \pm SEM. Statistical significance (in relation to control): ns $p > 0.05$; * $p \leq 0.05$; ** $p \leq 0.01$; *** $p \leq 0.001$; **** $p \leq 0.0001$.

8. Supplementary methods

8.1. Cell lines and cell culturing

CAMA-1, MDA-MB-468 and T47D human breast cancer cell lines were obtained commercially from the ATCC, and maintained in Dulbecco's Modified Eagle Medium, High glucose (DMEM, Sigma) supplemented with 10% Heat Inactivated (HI) FBS (Gibco), 1% Glutamax (100X, Gibco), and 1% Penicillin-Streptomycin (Gibco) in a humidified incubator at 37°C and 5% CO₂. To seed the cells for experiments, culture medium was removed, cells were washed with sterile phosphate buffered saline (1X PBS, Gibco) and detached with Trypsin-EDTA solution (Sigma). Cells were collected by centrifugation (1200 RPM, 5 minutes) and resuspended in culture medium. Cell numbers were counted by BioRad TC20 Automated Cell Counter using 0.4%(v/v) Trypan Blue staining (Gibco) to exclude dead cells from cell counting.

8.2. Magnetic-activated cell sorting (MACS)

For separating cells based on DPP4/CD26 expression, the MACS[®] Cell Separation technology was used (Miltenyi Biotec). MCF-7 cells were labelled with CD26-PE antibody diluted 1:50 in sterile 1% BSA solution following the protocol described in the materials and methods section (CD26 staining). After, cells were washed with 1 ml PBS, centrifuged (5 minutes, 1200 RPM, at 6 °C) and resuspended in 80 µl of sterile 1% BSA solution. Then, 20 µl of Anti-PE MicroBeads (Miltenyi Biotec) was added to the cells, mixed and incubated for 15 minutes on ice in dark. Cells were washed and resuspended in 500 µl of sterile 1% BSA solution. The magnetically labelled cells were loaded into the LS MACS Column (Miltenyi Biotec) and the cells with low/no expression of DPP4/CD26 were collected by washing the column three times with 3 ml sterile 1% BSA solution. Cells with high expression of DPP4/CD26 remained in the column and were eluted using 5 ml sterile 1% BSA solution. After separation, cells were analysed with Attune NxT Flow Cytometer or centrifuged, resuspended in cell culture medium and seeded in T25 flasks or 6-well plates for further experiments.

9. List of publications

Fiorillo M, **Tóth F**, Sotgia F, Lisanti MP. Doxycycline, Azithromycin and Vitamin C (DAV): A potent combination therapy for targeting mitochondria and eradicating cancer stem cells (CSCs). *Aging (Albany NY)*. 2019 Apr 19;11(8):2202-2216. doi: 10.18632/aging.101905. PMID: 31002656; PMCID: PMC6520007.

Fiorillo M, **Tóth F**, Brindisi M, Sotgia F, Lisanti MP. Deferiprone (DFP) Targets Cancer Stem Cell (CSC) Propagation by Inhibiting Mitochondrial Metabolism and Inducing ROS Production. *Cells*. 2020 Jun 23;9(6):1529. doi: 10.3390/cells9061529. PMID: 32585919; PMCID: PMC7349387.

10. Appendix

thesis

ORIGINALITY REPORT

21 %
SIMILARITY INDEX

17 %
INTERNET SOURCES

12 %
PUBLICATIONS

5 %
STUDENT PAPERS

PRIMARY SOURCES

1	www.oncotarget.com Internet Source	2 %
2	www.mdpi.com Internet Source	1 %
3	www.science.gov Internet Source	1 %
4	www.frontiersin.org Internet Source	1 %
5	www.nature.com Internet Source	1 %
6	hdl.handle.net Internet Source	<1 %
7	www.ncbi.nlm.nih.gov Internet Source	<1 %
8	scholarbank.nus.edu.sg Internet Source	<1 %
9	d-nb.info Internet Source	<1 %

11. References

- ACHUTHAN, S., SANTHOSHKUMAR, T. R., PRABHAKAR, J., NAIR, S. A. & PILLAI, M. R. 2011. Drug-induced senescence generates chemoresistant stemlike cells with low reactive oxygen species. *J Biol Chem*, 286, 37813-29.
- AIRD, K. M. & ZHANG, R. 2013. Detection of senescence-associated heterochromatin foci (SAHF). *Methods in molecular biology (Clifton, N.J.)*, 965, 185-196.
- ALIMBETOV, D., DAVIS, T., BROOK, A. J., COX, L. S., FARAGHER, R. G., NURGOZHIN, T., ZHUMADILOV, Z. & KIPLING, D. 2016. Suppression of the senescence-associated secretory phenotype (SASP) in human fibroblasts using small molecule inhibitors of p38 MAP kinase and MK2. *Biogerontology*, 17, 305-15.
- ALKHALAF, M. & EL-MOWAFY, A. M. 2003. Overexpression of wild-type p53 gene renders MCF-7 breast cancer cells more sensitive to the antiproliferative effect of progesterone. *J Endocrinol*, 179, 55-62.
- ALOTAIBI, M., SHARMA, K., SALEH, T., POVIRK, L. F., HENDRICKSON, E. A. & GEWIRTZ, D. A. 2016. Radiosensitization by PARP Inhibition in DNA Repair Proficient and Deficient Tumor Cells: Proliferative Recovery in Senescent Cells. *Radiat Res*, 185, 229-45.
- ALTHUBITI, M., LEZINA, L., CARRERA, S., JUKES-JONES, R., GIBLETT, S. M., ANTONOV, A., BARLEV, N., SALDANHA, G. S., PRITCHARD, C. A., CAIN, K. & MACIP, S. 2014. Characterization of novel markers of senescence and their prognostic potential in cancer. *Cell Death & Disease*, 5, e1528-e1528.
- AMJAD, M. T., CHIDHARLA, A. & KASI, A. 2022. Cancer Chemotherapy. *StatPearls*. Treasure Island (FL): StatPearls Publishing
- Copyright © 2022, StatPearls Publishing LLC.
- AMOR, C., FEUCHT, J., LEIBOLD, J., HO, Y.-J., ZHU, C., ALONSO-CURBELO, D., MANSILLA-SOTO, J., BOYER, J. A., LI, X., GIAVRIDIS, T., KULICK, A., HOULIHAN, S., PEERSCHKE, E., FRIEDMAN, S. L., PONOMAREV, V., PIERSIGILLI, A., SADELAIN, M. & LOWE, S. W. 2020. Senolytic CAR T cells reverse senescence-associated pathologies. *Nature*, 583, 127-132.
- AMORI, R. E., LAU, J. & PITTAS, A. G. 2007. Efficacy and safety of incretin therapy in type 2 diabetes: systematic review and meta-analysis. *Jama*, 298, 194-206.
- ANGELINI, P. D., ZACARIAS FLUCK, M. F., PEDERSEN, K., PARRA-PALAU, J. L., GUIU, M., BERNADO MORALES, C., VICARIO, R., LUQUE-GARCIA, A., NAVALPOTRO, N. P., GIRALT, J., CANALS, F., GOMIS, R. R., TABERNERO, J., BASELGA, J., VILLANUEVA, J. & ARRIBAS, J. 2013. Constitutive HER2 signaling promotes breast cancer metastasis through cellular senescence. *Cancer Res*, 73, 450-8.
- ANGEVIN, E., ISAMBERT, N., TRILLET-LENOIR, V., YOU, B., ALEXANDRE, J., ZALCMAN, G., VIELH, P., FARACE, F., VALLEIX, F., PODOLL, T., KURAMOCHI, Y., MIYASHITA, I., HOSONO, O., DANG, N. H., OHNUMA, K., YAMADA, T., KANEKO, Y. & MORIMOTO, C. 2017. First-in-human phase 1 of YS110, a monoclonal antibody directed against CD26 in advanced CD26-expressing cancers. *Br J Cancer*, 116, 1126-1134.
- ANSELMO, A. C. & MITRAGOTRI, S. 2019. Nanoparticles in the clinic: An update. *Bioeng Transl Med*, 4, e10143.

- BAISANTRY, A., BHAYANA, S., WREDE, C., HEGERMANN, J., HALLER, H., MELK, A. & SCHMITT, R. 2016. The impact of autophagy on the development of senescence in primary tubular epithelial cells. *Cell Cycle*, 15, 2973-2979.
- BASKAR, R., LEE, K. A., YEO, R. & YEOH, K. W. 2012. Cancer and radiation therapy: current advances and future directions. *Int J Med Sci*, 9, 193-9.
- BAVIK, C., COLEMAN, I., DEAN, J. P., KNUDSEN, B., PLYMATE, S. & NELSON, P. S. 2006. The gene expression program of prostate fibroblast senescence modulates neoplastic epithelial cell proliferation through paracrine mechanisms. *Cancer Res*, 66, 794-802.
- BEAUSEJOUR, C. M., KRTOLICA, A., GALIMI, F., NARITA, M., LOWE, S. W., YASWEN, P. & CAMPISI, J. 2003. Reversal of human cellular senescence: roles of the p53 and p16 pathways. *Embo j*, 22, 4212-22.
- BERNIER, J., HALL, E. J. & GIACCIA, A. 2004. Radiation oncology: a century of achievements. *Nat Rev Cancer*, 4, 737-47.
- BERTHEAU, P., PLASSA, F., ESPIÉ, M., TURPIN, E., DE ROQUANCOURT, A., MARTY, M., LERBOURS, F., BEUZARD, Y., JANIN, A. & DE THÉ, H. 2002. Effect of mutated TP53 on response of advanced breast cancers to high-dose chemotherapy. *Lancet*, 360, 852-4.
- BERTOLO, A., BAUR, M., GUERRERO, J., PÖTZEL, T. & STOYANOV, J. 2019. Autofluorescence is a Reliable in vitro Marker of Cellular Senescence in Human Mesenchymal Stromal Cells. *Scientific Reports*, 9, 2074.
- BERTRAM, J. S. 2000. The molecular biology of cancer. *Mol Aspects Med*, 21, 167-223.
- BI, J., CAI, W., MA, T., DENG, A., MA, P., HAN, Y., LOU, C. & WU, L. 2019. Protective effect of vildagliptin on TNF- α -induced chondrocyte senescence. *IUBMB Life*, 71, 978-985.
- BISHNOI, R., HONG, Y. R., SHAH, C., ALI, A., SKELTON, W. P. T., HUO, J., DANG, N. H. & DANG, L. H. 2019. Dipeptidyl peptidase 4 inhibitors as novel agents in improving survival in diabetic patients with colorectal cancer and lung cancer: A Surveillance Epidemiology and Endpoint Research Medicare study. *Cancer Med*, 8, 3918-3927.
- BLAGOSKLONNY, M. V. 2014. Geroconversion: irreversible step to cellular senescence. *Cell Cycle*, 13, 3628-35.
- BOJKO, A., CZARNECKA-HEROK, J., CHARZYNSKA, A., DABROWSKI, M. & SIKORA, E. 2019. Diversity of the Senescence Phenotype of Cancer Cells Treated with Chemotherapeutic Agents. *Cells*, 8.
- BOJKO, A., STANIAK, K., CZARNECKA-HEROK, J., SUNDERLAND, P., DUDKOWSKA, M., ŚLIWIŃSKA, M. A., SALMINA, K. & SIKORA, E. 2020. Improved Autophagic Flux in Escapers from Doxorubicin-Induced Senescence/Polyploidy of Breast Cancer Cells. *International Journal of Molecular Sciences*, 21.
- BOLLARD, J., MIGUELA, V., RUIZ DE GALARRETA, M., VENKATESH, A., BIAN, C. B., ROBERTO, M. P., TOVAR, V., SIA, D., MOLINA-SANCHEZ, P., NGUYEN, C. B., NAKAGAWA, S., LLOVET, J. M., HOSHIDA, Y. & LUJAMBIO, A. 2017. Palbociclib (PD-0332991), a selective CDK4/6 inhibitor, restricts tumour growth in preclinical models of hepatocellular carcinoma. *Gut*, 66, 1286-1296.
- BOONACKER, E. & VAN NOORDEN, C. J. F. 2003. The multifunctional or moonlighting protein CD26/DPPIV. *European Journal of Cell Biology*, 82, 53-73.
- BRITO, A. F., RIBEIRO, M., ABRANTES, A. M., PIRES, A. S., TEIXO, R. J., TRALHAO, J. G. & BOTELHO, M. F. 2015. Quercetin in Cancer Treatment, Alone or in Combination with Conventional Therapeutics? *Curr Med Chem*, 22, 3025-39.
- BURD, C. E., SORRENTINO, J. A., CLARK, K. S., DARR, D. B., KRISHNAMURTHY, J., DEAL, A. M., BARDEESY, N., CASTRILLON, D. H., BEACH, D. H. & SHARPLESS, N. E. 2013. Monitoring

- tumorigenesis and senescence in vivo with a p16(INK4a)-luciferase model. *Cell*, 152, 340-51.
- CAHU, J., BUSTANY, S. & SOLA, B. 2012. Senescence-associated secretory phenotype favors the emergence of cancer stem-like cells. *Cell Death Dis*, 3, e446.
- CAI, Y., ZHOU, H., ZHU, Y., SUN, Q., JI, Y., XUE, A., WANG, Y., CHEN, W., YU, X., WANG, L., CHEN, H., LI, C., LUO, T. & DENG, H. 2020. Elimination of senescent cells by β -galactosidase-targeted prodrug attenuates inflammation and restores physical function in aged mice. *Cell Research*, 30, 574-589.
- CALCINOTTO, A., KOHLI, J., ZAGATO, E., PELLEGRINI, L., DEMARIA, M. & ALIMONTI, A. 2019. Cellular Senescence: Aging, Cancer, and Injury. *Physiol Rev*, 99, 1047-1078.
- CAMPISI, J. 2013. Aging, cellular senescence, and cancer. *Annu Rev Physiol*, 75, 685-705.
- CAMPISI, J. & D'ADDA DI FAGAGNA, F. 2007. Cellular senescence: when bad things happen to good cells. *Nat Rev Mol Cell Biol*, 8, 729-40.
- CANINO, C., MORI, F., CAMBRIA, A., DIAMANTINI, A., GERMONI, S., ALESSANDRINI, G., BORSELLINO, G., GALATI, R., BATTISTINI, L., BLANDINO, R., FACCILOLO, F., CITRO, G., STRANO, S., MUTI, P., BLANDINO, G. & CIOCE, M. 2012. SASP mediates chemoresistance and tumor-initiating-activity of mesothelioma cells. *Oncogene*, 31, 3148-63.
- CASTRO-VEGA, L. J., JOURAVLEVA, K., ORTIZ-MONTERO, P., LIU, W. Y., GALEANO, J. L., ROMERO, M., POPOVA, T., BACCHETTI, S., VERNOT, J. P. & LONDONO-VALLEJO, A. 2015. The senescent microenvironment promotes the emergence of heterogeneous cancer stem-like cells. *Carcinogenesis*, 36, 1180-92.
- CECCHINI, S., MASSON, C., LA MADELEINE, C., HUELS, M. A., SANCHE, L., WAGNER, J. R. & HUNTING, D. J. 2005. Interstrand cross-link induction by UV radiation in bromodeoxyuridine-substituted DNA: dependence on DNA conformation. *Biochemistry*, 44, 16957-66.
- CHAFFER, C. L. & WEINBERG, R. A. 2011. A perspective on cancer cell metastasis. *Science*, 331, 1559-64.
- CHAKRABARTY, A., CHAKRABORTY, S., BHATTACHARYA, R. & CHOWDHURY, G. 2021. Senescence-Induced Chemoresistance in Triple Negative Breast Cancer and Evolution-Based Treatment Strategies. *Frontiers in Oncology*, 11.
- CHAPMAN, J., FIELDER, E. & PASSOS, J. F. 2019. Mitochondrial dysfunction and cell senescence: deciphering a complex relationship. *FEBS Lett*, 593, 1566-1579.
- CHEN, Z., TROTMAN, L. C., SHAFFER, D., LIN, H. K., DOTAN, Z. A., NIKI, M., KOUTCHER, J. A., SCHER, H. I., LUDWIG, T., GERALD, W., CORDON-CARDO, C. & PANDOLFI, P. P. 2005. Crucial role of p53-dependent cellular senescence in suppression of Pten-deficient tumorigenesis. *Nature*, 436, 725-30.
- CHEN, Z., YU, J., FU, M., DONG, R., YANG, Y., LUO, J., HU, S., LI, W., XU, X. & TU, L. 2020. Dipeptidyl peptidase-4 inhibition improves endothelial senescence by activating AMPK/SIRT1/Nrf2 signaling pathway. *Biochemical Pharmacology*, 177, 113951.
- CHEUNG, A. H., IYER, D. N., LAM, C. S., NG, L., WONG, S. K. M., LEE, H. S., WAN, T., MAN, J., CHOW, A. K. M., POON, R. T., PANG, R. & LAW, W. L. 2017. Emergence of CD26+ Cancer Stem Cells with Metastatic Properties in Colorectal Carcinogenesis. *Int J Mol Sci*, 18.
- CHITADZE, G., WEHKAMP, U., JANSSEN, O., BRÜGGEMANN, M. & LETTAU, M. 2021. The Serine Protease CD26/DPP4 in Non-Transformed and Malignant T Cells. *Cancers (Basel)*, 13.
- CHITIKOVA, Z. V., GORDEEV, S. A., BYKOVA, T. V., ZUBOVA, S. G., POSPELOV, V. A. & POSPELOVA, T. V. 2014. Sustained activation of DNA damage response in irradiated

- apoptosis-resistant cells induces reversible senescence associated with mTOR downregulation and expression of stem cell markers. *Cell Cycle*, 13, 1424-39.
- CHOI, H. J., KIM, J. Y., LIM, S. C., KIM, G., YUN, H. J. & CHOI, H. S. 2015. Dipeptidyl peptidase 4 promotes epithelial cell transformation and breast tumorigenesis via induction of PIN1 gene expression. *Br J Pharmacol*, 172, 5096-109.
- COLLADO, M. & SERRANO, M. 2006. The power and the promise of oncogene-induced senescence markers. *Nat Rev Cancer*, 6, 472-6.
- COLLADO, M. & SERRANO, M. 2010. Senescence in tumours: evidence from mice and humans. *Nat Rev Cancer*, 10, 51-7.
- COPPE, J. P., DESPREZ, P. Y., KRTOLICA, A. & CAMPISI, J. 2010. The senescence-associated secretory phenotype: the dark side of tumor suppression. *Annu Rev Pathol*, 5, 99-118.
- COURTOIS-COX, S., JONES, S. L. & CICHOWSKI, K. 2008. Many roads lead to oncogene-induced senescence. *Oncogene*, 27, 2801-9.
- COWARD, J. & HARDING, A. 2014. Size Does Matter: Why Polyploid Tumor Cells are Critical Drug Targets in the War on Cancer. *Frontiers in Oncology*, 4.
- CRAIG, C., KIM, M., OHRI, E., WERSTO, R., KATAYOSE, D., LI, Z., CHOI, Y. H., MUDAHAR, B., SRIVASTAVA, S., SETH, P. & COWAN, K. 1998. Effects of adenovirus-mediated p16INK4A expression on cell cycle arrest are determined by endogenous p16 and Rb status in human cancer cells. *Oncogene*, 16, 265-72.
- CRO, L., MORABITO, F., ZUCAL, N., FABRIS, S., LIONETTI, M., CUTRONA, G., ROSSI, F., GENTILE, M., FERRARIO, A., FERRARINI, M., MOLICA, S., NERI, A. & BALDINI, L. 2009. CD26 expression in mature B-cell neoplasia: its possible role as a new prognostic marker in B-CLL. *Hematol Oncol*, 27, 140-7.
- CRUICKSHANKS, H. A., MCBRYAN, T., NELSON, D. M., VANDERKRAATS, N. D., SHAH, P. P., VAN TUYN, J., SINGH RAI, T., BROCK, C., DONAHUE, G., DUNICAN, D. S., DROTAR, M. E., MEEHAN, R. R., EDWARDS, J. R., BERGER, S. L. & ADAMS, P. D. 2013. Senescent cells harbour features of the cancer epigenome. *Nat Cell Biol*, 15, 1495-506.
- DAI, X., CHENG, H., BAI, Z. & LI, J. 2017. Breast Cancer Cell Line Classification and Its Relevance with Breast Tumor Subtyping. *J Cancer*, 8, 3131-3141.
- DAS, A. T., TENENBAUM, L. & BERKHOUT, B. 2016. Tet-On Systems For Doxycycline-inducible Gene Expression. *Curr Gene Ther*, 16, 156-67.
- DAVIES, S., BECKENKAMP, A. & BUFFON, A. 2015. CD26 a cancer stem cell marker and therapeutic target. *Biomedicine & Pharmacotherapy*, 71, 135-138.
- DEMARIA, M., O'LEARY, M. N., CHANG, J., SHAO, L., LIU, S., ALIMIRAH, F., KOENIG, K., LE, C., MITIN, N., DEAL, A. M., ALSTON, S., ACADEMIA, E. C., KILMARX, S., VALDOVINOS, A., WANG, B., DE BRUIN, A., KENNEDY, B. K., MELOV, S., ZHOU, D., SHARPLESS, N. E., MUSS, H. & CAMPISI, J. 2017. Cellular Senescence Promotes Adverse Effects of Chemotherapy and Cancer Relapse. *Cancer Discov*, 7, 165-176.
- DEVARAJAN, E., SAHIN, A. A., CHEN, J. S., KRISHNAMURTHY, R. R., AGGARWAL, N., BRUN, A.-M., SAPINO, A., ZHANG, F., SHARMA, D., YANG, X.-H., TORA, A. D. & MEHTA, K. 2002. Down-regulation of caspase 3 in breast cancer: a possible mechanism for chemoresistance. *Oncogene*, 21, 8843-8851.
- DOMÍNGUEZ-VIGIL, I. G., MORENO-MARTÍNEZ, A. K., WANG, J. Y., ROEHL, M. H. A. & BARRERA-SALDAÑA, H. A. 2018. The dawn of the liquid biopsy in the fight against cancer. *Oncotarget*, 9, 2912-2922.

- DONNENBERG, V. S., ZHANG, J. J., MORAVCIKOVA, E., MEYER, E. M., LU, H., CARSON, C. T. & DONNENBERG, A. D. 2018. Antibody-based cell-surface proteome profiling of metastatic breast cancer primary explants and cell lines. *Cytometry A*, 93, 448-457.
- DÖRR, J. R., YU, Y., MILANOVIC, M., BEUSTER, G., ZASADA, C., DÄBRITZ, J. H. M., LISEC, J., LENZE, D., GERHARDT, A., SCHLEICHER, K., KRATZAT, S., PURFÜRST, B., WALENTA, S., MUELLER-KLIESER, W., GRÄLER, M., HUMMEL, M., KELLER, U., BUCK, A. K., DÖRKEN, B., WILLMITZER, L., REIMANN, M., KEMPA, S., LEE, S. & SCHMITT, C. A. 2013. Synthetic lethal metabolic targeting of cellular senescence in cancer therapy. *Nature*, 501, 421.
- DOU, Z. & BERGER, S. L. 2018. Senescence Elicits Stemness: A Surprising Mechanism for Cancer Relapse. *Cell Metab*, 27, 710-711.
- DRAGO, J. Z., MODI, S. & CHANDARLAPATY, S. 2021. Unlocking the potential of antibody–drug conjugates for cancer therapy. *Nature Reviews Clinical Oncology*, 18, 327-344.
- EGGERT, T., WOLTER, K., JI, J., MA, C., YEVSAN, T., KLOTZ, S., MEDINA-ECHEVERZ, J., LONGERICH, T., FORGUES, M., REISINGER, F., HEIKENWALDER, M., WANG, X. W., ZENDER, L. & GRETEN, T. F. 2016. Distinct Functions of Senescence-Associated Immune Responses in Liver Tumor Surveillance and Tumor Progression. *Cancer Cell*, 30, 533-547.
- ELMORE, L. W., DI, X., DUMUR, C., HOLT, S. E. & GEWIRTZ, D. A. 2005. Evasion of a single-step, chemotherapy-induced senescence in breast cancer cells: implications for treatment response. *Clin Cancer Res*, 11, 2637-43.
- ELMORE, L. W., REHDER, C. W., DI, X., MCCHESENEY, P. A., JACKSON-COOK, C. K., GEWIRTZ, D. A. & HOLT, S. E. 2002. Adriamycin-induced senescence in breast tumor cells involves functional p53 and telomere dysfunction. *J Biol Chem*, 277, 35509-15.
- ENZ, N., VliegEN, G., DE MEESTER, I. & JUNGRAITHMAYR, W. 2019. CD26/DPP4 - a potential biomarker and target for cancer therapy. *Pharmacology & Therapeutics*, 198, 135-159.
- ERENPREISA, J. & CRAGG, M. S. 2013. Three steps to the immortality of cancer cells: senescence, polyploidy and self-renewal. *Cancer Cell Int*, 13, 92.
- EWALD, J. A., DESOTELLE, J. A., WILDING, G. & JARRARD, D. F. 2010. Therapy-induced senescence in cancer. *J Natl Cancer Inst*, 102, 1536-46.
- FAGET, D. V., REN, Q. & STEWART, S. A. 2019. Unmasking senescence: context-dependent effects of SASP in cancer. *Nat Rev Cancer*, 19, 439-453.
- FAN, T., DU, Y., ZHANG, M., ZHU, A. R. & ZHANG, J. 2022. Senolytics Cocktail Dasatinib and Quercetin Alleviate Human Umbilical Vein Endothelial Cell Senescence via the TRAF6-MAPK-NF-κB Axis in a YTHDF2-Dependent Manner. *Gerontology*.
- FANELLI, G. N., NACCARATO, A. G. & SCATENA, C. 2020. Recent Advances in Cancer Plasticity: Cellular Mechanisms, Surveillance Strategies, and Therapeutic Optimization. *Frontiers in Oncology*, 10.
- FERNANDO, R. I., CASTILLO, M. D., LITZINGER, M., HAMILTON, D. H. & PALENA, C. 2011. IL-8 signaling plays a critical role in the epithelial-mesenchymal transition of human carcinoma cells. *Cancer Res*, 71, 5296-306.
- FERREIRA, P. M. P., SOUSA, R. W. R., FERREIRA, J. R. O., MILITÃO, G. C. G. & BEZERRA, D. P. 2021. Chloroquine and hydroxychloroquine in antitumor therapies based on autophagy-related mechanisms. *Pharmacol Res*, 168, 105582.
- FINN, R. S., CROWN, J. P., LANG, I., BOER, K., BONDARENKO, I. M., KULYK, S. O., ETTL, J., PATEL, R., PINTER, T., SCHMIDT, M., SHPARYK, Y., THUMMALA, A. R., VOYTKO, N. L., FOWST, C., HUANG, X., KIM, S. T., RANDOLPH, S. & SLAMON, D. J. 2015. The cyclin-dependent kinase 4/6 inhibitor palbociclib in combination with letrozole versus letrozole alone as

- first-line treatment of oestrogen receptor-positive, HER2-negative, advanced breast cancer (PALOMA-1/TRIO-18): a randomised phase 2 study. *Lancet Oncol*, 16, 25-35.
- FLEURY, H., MALAQUIN, N., TU, V., GILBERT, S., MARTINEZ, A., OLIVIER, M. A., SAURIOL, A., COMMUNAL, L., LECLERC-DESAULNIERS, K., CARMONA, E., PROVENCHER, D., MESMASSON, A. M. & RODIER, F. 2019. Exploiting interconnected synthetic lethal interactions between PARP inhibition and cancer cell reversible senescence. *Nat Commun*, 10, 2556.
- FRANKEN, N. A., RODERMOND, H. M., STAP, J., HAVEMAN, J. & VAN BREE, C. 2006. Clonogenic assay of cells in vitro. *Nat Protoc*, 1, 2315-9.
- FREUND, A., CHAUVEAU, C., BROUILLET, J. P., LUCAS, A., LACROIX, M., LICZNAR, A., VIGNON, F. & LAZENNEC, G. 2003. IL-8 expression and its possible relationship with estrogen-receptor-negative status of breast cancer cells. *Oncogene*, 22, 256-65.
- FREUND, A., JOLIVEL, V., DURAND, S., KERSUAL, N., CHALBOS, D., CHAVEY, C., VIGNON, F. & LAZENNEC, G. 2004. Mechanisms underlying differential expression of interleukin-8 in breast cancer cells. *Oncogene*, 23, 6105-6114.
- GALANOS, P., VOUGAS, K., WALTER, D., POLYZOS, A., MAYA-MENDOZA, A., HAAGENSEN, E. J., KOKKALIS, A., ROUMELIOTI, F. M., GAGOS, S., TZETIS, M., CANOVAS, B., IGEA, A., AHUJA, A. K., ZELLWEGER, R., HAVAKI, S., KANAVAKIS, E., KLETSAS, D., RONINSON, I. B., GARBIS, S. D., LOPES, M., NEBRED, A., THANOS, D., BLOW, J. J., TOWNSEND, P., SORENSEN, C. S., BARTEK, J. & GORGOULIS, V. G. 2016. Chronic p53-independent p21 expression causes genomic instability by deregulating replication licensing. *Nat Cell Biol*, 18, 777-89.
- GEORGAKILAS, A. G., MARTIN, O. A. & BONNER, W. M. 2017. p21: A Two-Faced Genome Guardian. *Trends Mol Med*, 23, 310-319.
- GEORGAKOPOULOU, E. A., TSIMARATOU, K., EVANGELOU, K., FERNANDEZ MARCOS, P. J., ZOUMPOURLIS, V., TROUGAKOS, I. P., KLETSAS, D., BARTEK, J., SERRANO, M. & GORGOULIS, V. G. 2013. Specific lipofuscin staining as a novel biomarker to detect replicative and stress-induced senescence. A method applicable in cryo-preserved and archival tissues. *Aging (Albany NY)*, 5, 37-50.
- GHANI, F. I., YAMAZAKI, H., IWATA, S., OKAMOTO, T., AOE, K., OKABE, K., MIMURA, Y., FUJIMOTO, N., KISHIMOTO, T., YAMADA, T., XU, C. W. & MORIMOTO, C. 2011. Identification of cancer stem cell markers in human malignant mesothelioma cells. *Biochem Biophys Res Commun*, 404, 735-42.
- GILBERT, L. A. & HEMANN, M. T. 2010. DNA damage-mediated induction of a chemoresistant niche. *Cell*, 143, 355-66.
- GOEHE, R. W., DI, X., SHARMA, K., BRISTOL, M. L., HENDERSON, S. C., VALERIE, K., RODIER, F., DAVALOS, A. R. & GEWIRTZ, D. A. 2012. The autophagy-senescence connection in chemotherapy: must tumor cells (self) eat before they sleep? *J Pharmacol Exp Ther*, 343, 763-78.
- GOEL, S., DECRISTO, M. J., WATT, A. C., BRINJONES, H., SCENEAY, J., LI, B. B., KHAN, N., UBELLACKER, J. M., XIE, S., METZGER-FILHO, O., HOOG, J., ELLIS, M. J., MA, C. X., RAMM, S., KROP, I. E., WINER, E. P., ROBERTS, T. M., KIM, H.-J., MCALLISTER, S. S. & ZHAO, J. J. 2017. CDK4/6 inhibition triggers anti-tumour immunity. *Nature*, 548, 471-475.
- GONZÁLEZ-GUALDA, E., BAKER, A. G., FRUK, L. & MUÑOZ-ESPÍN, D. 2021. A guide to assessing cellular senescence in vitro and in vivo. *Febs j*, 288, 56-80.

- GUILLON, J., PETIT, C., MOREAU, M., TOUTAIN, B., HENRY, C., ROCHE, H., BONICHON-LAMICHHANE, N., SALMON, J. P., LEMONNIER, J., CAMPONE, M., VERRIELE, V., LELIEVRE, E., GUETTE, C. & COQUERET, O. 2019. Regulation of senescence escape by TSP1 and CD47 following chemotherapy treatment. *Cell Death Dis*, 10, 199.
- HANAHAHAN, D. 2022. Hallmarks of Cancer: New Dimensions. *Cancer Discov*, 12, 31-46.
- HANAHAHAN, D. & WEINBERG, R. A. 2000. The hallmarks of cancer. *Cell*, 100, 57-70.
- HANAHAHAN, D. & WEINBERG, R. A. 2011. Hallmarks of cancer: the next generation. *Cell*, 144, 646-74.
- HATANO, R., OHNUMA, K., YAMAMOTO, J., DANG, N. H. & MORIMOTO, C. 2013. CD26-mediated co-stimulation in human CD8(+) T cells provokes effector function via pro-inflammatory cytokine production. *Immunology*, 138, 165-72.
- HATTERMANN, K., HOLZENBURG, E., HANS, F., LUCIUS, R., HELD-FEINDT, J. & MENTLEIN, R. 2014. Effects of the chemokine CXCL12 and combined internalization of its receptors CXCR4 and CXCR7 in human MCF-7 breast cancer cells. *Cell Tissue Res*, 357, 253-66.
- HAVRE, P. A., ABE, M., URASAKI, Y., OHNUMA, K., MORIMOTO, C. & DANG, N. H. 2008. The role of CD26/dipeptidyl peptidase IV in cancer. *Front Biosci*, 13, 1634-45.
- HEGDE, P. S. & CHEN, D. S. 2020. Top 10 Challenges in Cancer Immunotherapy. *Immunity*, 52, 17-35.
- HERMAN, G. A., STEIN, P. P., THORNBERRY, N. A. & WAGNER, J. A. 2007. Dipeptidyl peptidase-4 inhibitors for the treatment of type 2 diabetes: focus on sitagliptin. *Clin Pharmacol Ther*, 81, 761-7.
- HERNANDEZ-SEGURA, A., DE JONG, T. V., MELOV, S., GURYEV, V., CAMPISI, J. & DEMARIA, M. 2017. Unmasking Transcriptional Heterogeneity in Senescent Cells. *Curr Biol*, 27, 2652-2660.e4.
- HERNANDEZ-SEGURA, A., NEHME, J. & DEMARIA, M. 2018. Hallmarks of Cellular Senescence. *Trends Cell Biol*, 28, 436-453.
- HERRANZ, N., GALLAGE, S., MELLONE, M., WUESTEFELD, T., KLOTZ, S., HANLEY, C. J., RAGUZ, S., ACOSTA, J. C., INNES, A. J., BANITO, A., GEORGILIS, A., MONTOYA, A., WOLTER, K., DHARMALINGAM, G., FAULL, P., CARROLL, T., MARTINEZ-BARBERA, J. P., CUTILLAS, P., REISINGER, F., HEIKENWALDER, M., MILLER, R. A., WITHERS, D., ZENDER, L., THOMAS, G. J. & GIL, J. 2015. mTOR regulates MAPKAPK2 translation to control the senescence-associated secretory phenotype. *Nat Cell Biol*, 17, 1205-17.
- HERRMANN, H., SADOVNIK, I., CERNY-REITERER, S., RÜLICHE, T., STEFANZL, G., WILLMANN, M., HOERMANN, G., BILBAN, M., BLATT, K., HERNDLHOFER, S., MAYERHOFER, M., STREUBEL, B., SPERR, W. R., HOLYOAKE, T. L., MANNHALTER, C. & VALENT, P. 2014. Dipeptidylpeptidase IV (CD26) defines leukemic stem cells (LSC) in chronic myeloid leukemia. *Blood*, 123, 3951-62.
- HICKSON, L. J., LANGHI PRATA, L. G. P., BOBART, S. A., EVANS, T. K., GIORGADZE, N., HASHMI, S. K., HERRMANN, S. M., JENSEN, M. D., JIA, Q., JORDAN, K. L., KELLOGG, T. A., KHOSLA, S., KOERBER, D. M., LAGNADO, A. B., LAWSON, D. K., LEBRASSEUR, N. K., LERMAN, L. O., MCDONALD, K. M., MCKENZIE, T. J., PASSOS, J. F., PIGNOLO, R. J., PIRTSKHALAVA, T., SAADIQ, I. M., SCHAEFER, K. K., TEXTOR, S. C., VICTORELLI, S. G., VOLKMAN, T. L., XUE, A., WENTWORTH, M. A., WISSLER GERDES, E. O., ZHU, Y., TCHKONIA, T. & KIRKLAND, J. L. 2019. Senolytics decrease senescent cells in humans: Preliminary report from a clinical trial of Dasatinib plus Quercetin in individuals with diabetic kidney disease. *EBioMedicine*, 47, 446-456.

- HINGE, N., PANDEY, M. M., SINGHVI, G., GUPTA, G., MEHTA, M., SATIJA, S., GULATI, M., DUREJA, H. & DUA, K. 2020. 8 - Nanomedicine advances in cancer therapy. *In: TOIT, L. C. D., KUMAR, P., CHOONARA, Y. E. & PILLAY, V. (eds.) Advanced 3D-Printed Systems and Nanosystems for Drug Delivery and Tissue Engineering.* Elsevier.
- HONEYWELL, R. J., RUIZ VAN HAPEREN, V. W., VEERMAN, G., SMID, K. & PETERS, G. J. 2015. Inhibition of thymidylate synthase by 2',2'-difluoro-2'-deoxycytidine (Gemcitabine) and its metabolite 2',2'-difluoro-2'-deoxyuridine. *Int J Biochem Cell Biol*, 60, 73-81.
- HOUSMAN, G., BYLER, S., HEERBOTH, S., LAPINSKA, K., LONGACRE, M., SNYDER, N. & SARKAR, S. 2014. Drug resistance in cancer: an overview. *Cancers (Basel)*, 6, 1769-92.
- HUBACKOVA, S., DAVIDOVA, E., ROHLENOVA, K., STURSA, J., WERNER, L., ANDERA, L., DONG, L., TERP, M. G., HODNY, Z., DITZEL, H. J., ROHLENA, J. & NEUZIL, J. 2019. Selective elimination of senescent cells by mitochondrial targeting is regulated by ANT2. *Cell Death Differ*, 26, 276-290.
- HUI, L., ZHENG, Y., YAN, Y., BARGONETTI, J. & FOSTER, D. A. 2006. Mutant p53 in MDA-MB-231 breast cancer cells is stabilized by elevated phospholipase D activity and contributes to survival signals generated by phospholipase D. *Oncogene*, 25, 7305-10.
- ILIOPOULOS, D., HIRSCH, H. A., WANG, G. & STRUHL, K. 2011. Inducible formation of breast cancer stem cells and their dynamic equilibrium with non-stem cancer cells via IL6 secretion. *Proc Natl Acad Sci U S A*, 108, 1397-402.
- INAMOTO, T., YAMADA, T., OHNUMA, K., KINA, S., TAKAHASHI, N., YAMOCHI, T., INAMOTO, S., KATSUOKA, Y., HOSONO, O., TANAKA, H., DANG, N. H. & MORIMOTO, C. 2007. Humanized anti-CD26 monoclonal antibody as a treatment for malignant mesothelioma tumors. *Clin Cancer Res*, 13, 4191-200.
- INAMOTO, T., YAMOCHI, T., OHNUMA, K., IWATA, S., KINA, S., INAMOTO, S., TACHIBANA, M., KATSUOKA, Y., DANG, N. H. & MORIMOTO, C. 2006. Anti-CD26 monoclonal antibody-mediated G1-S arrest of human renal clear cell carcinoma Caki-2 is associated with retinoblastoma substrate dephosphorylation, cyclin-dependent kinase 2 reduction, p27(kip1) enhancement, and disruption of binding to the extracellular matrix. *Clin Cancer Res*, 12, 3470-7.
- JACKSON, J. G., PANT, V., LI, Q., CHANG, L. L., QUINTÁS-CARDAMA, A., GARZA, D., TAVANA, O., YANG, P., MANSHOORI, T., LI, Y., EL-NAGGAR, A. K. & LOZANO, G. 2012. p53-mediated senescence impairs the apoptotic response to chemotherapy and clinical outcome in breast cancer. *Cancer Cell*, 21, 793-806.
- JANG, J. H., JANKER, F., DE MEESTER, I., ARNI, S., BORGEAUD, N., YAMADA, Y., GIL BAZO, I., WEDER, W. & JUNGRAITHMAYR, W. 2019. The CD26/DPP4-inhibitor vildagliptin suppresses lung cancer growth via macrophage-mediated NK cell activity. *Carcinogenesis*, 40, 324-334.
- JIANG, P. & MIZUSHIMA, N. 2015. LC3- and p62-based biochemical methods for the analysis of autophagy progression in mammalian cells. *Methods*, 75, 13-8.
- JONCHERE, B., VETILLARD, A., TOUTAIN, B., LAM, D., BERNARD, A. C., HENRY, C., DE CARNE TRECESSON, S., GAMELIN, E., JUIN, P., GUETTE, C. & COQUERET, O. 2015. Irinotecan treatment and senescence failure promote the emergence of more transformed and invasive cells that depend on anti-apoptotic Mcl-1. *Oncotarget*, 6, 409-26.
- KAHLEM, P., DORKEN, B. & SCHMITT, C. A. 2004. Cellular senescence in cancer treatment: friend or foe? *J Clin Invest*, 113, 169-74.
- KAMADA, S., NAMEKAWA, T., IKEDA, K., SUZUKI, T., KAGAWA, M., TAKESHITA, H., YANO, A., OKAMOTO, K., ICHIKAWA, T., HORIE-INOUE, K., KAWAKAMI, S. & INOUE, S. 2021.

- Functional inhibition of cancer stemness-related protein DPP4 rescues tyrosine kinase inhibitor resistance in renal cell carcinoma. *Oncogene*, 40, 3899-3913.
- KANG, H., WATKINS, G., PARR, C., DOUGLAS-JONES, A., MANSEL, R. E. & JIANG, W. G. 2005. Stromal cell derived factor-1: its influence on invasiveness and migration of breast cancer cells in vitro, and its association with prognosis and survival in human breast cancer. *Breast Cancer Res*, 7, R402-10.
- KANG, T. W., YEVSAN, T., WOLLER, N., HOENICKE, L., WUESTEFELD, T., DAUCH, D., HOHMEYER, A., GEREKE, M., RUDALSKA, R., POTAPOVA, A., IKEN, M., VUCUR, M., WEISS, S., HEIKENWALDER, M., KHAN, S., GIL, J., BRUDER, D., MANNS, M., SCHIRMACHER, P., TACKE, F., OTT, M., LUEDDE, T., LONGERICH, T., KUBICKA, S. & ZENDER, L. 2011. Senescence surveillance of pre-malignant hepatocytes limits liver cancer development. *Nature*, 479, 547-51.
- KARIMI-BUSHERI, F., RASOULI-NIA, A., MACKEY, J. R. & WEINFELD, M. 2010. Senescence evasion by MCF-7 human breast tumor-initiating cells. *Breast Cancer Res*, 12, R31.
- KEATING, G. M. 2017. Dasatinib: A Review in Chronic Myeloid Leukaemia and Ph+ Acute Lymphoblastic Leukaemia. *Drugs*, 77, 85-96.
- KHIN, E. E., KIKKAWA, F., INO, K., KAJIYAMA, H., SUZUKI, T., SHIBATA, K., TAMAKOSHI, K., NAGASAKA, T. & MIZUTANI, S. 2003. Dipeptidyl peptidase IV expression in endometrial endometrioid adenocarcinoma and its inverse correlation with tumor grade. *Am J Obstet Gynecol*, 188, 670-6.
- KIM, K. H. & SEDERSTROM, J. M. 2015. Assaying Cell Cycle Status Using Flow Cytometry. *Curr Protoc Mol Biol*, 111, 28.6.1-28.6.11.
- KIM, K. M., NOH, J. H., BODOGAI, M., MARTINDALE, J. L., YANG, X., INDIG, F. E., BASU, S. K., OHNUMA, K., MORIMOTO, C., JOHNSON, P. F., BIRAGYN, A., ABDELMOHSEN, K. & GOROSPE, M. 2017a. Identification of senescent cell surface targetable protein DPP4. *Genes Dev*, 31, 1529-1534.
- KIM, Y. H., CHOI, Y. W., LEE, J., SOH, E. Y., KIM, J. H. & PARK, T. J. 2017b. Senescent tumor cells lead the collective invasion in thyroid cancer. *Nat Commun*, 8, 15208.
- KIRKLAND, J. L. & TCHKONIA, T. 2020. Senolytic drugs: from discovery to translation. *J Intern Med*, 288, 518-536.
- KLEIN, M. E., KOVATCHEVA, M., DAVIS, L. E., TAP, W. D. & KOFF, A. 2018. CDK4/6 Inhibitors: The Mechanism of Action May Not Be as Simple as Once Thought. *Cancer Cell*, 34, 9-20.
- KLEMANN, C., WAGNER, L., STEPHAN, M. & VON HÖRSTEN, S. 2016. Cut to the chase: a review of CD26/dipeptidyl peptidase-4's (DPP4) entanglement in the immune system. *Clin Exp Immunol*, 185, 1-21.
- KOROLCHUK, V. I., MIWA, S., CARROLL, B. & VON ZGLINICKI, T. 2017. Mitochondria in Cell Senescence: Is Mitophagy the Weakest Link? *EBioMedicine*, 21, 7-13.
- KOVATCHEVA, M., LIU, D. D., DICKSON, M. A., KLEIN, M. E., O'CONNOR, R., WILDER, F. O., SOCCI, N. D., TAP, W. D., SCHWARTZ, G. K., SINGER, S., CRAGO, A. M. & KOFF, A. 2015. MDM2 turnover and expression of ATRX determine the choice between quiescence and senescence in response to CDK4 inhibition. *Oncotarget*, 6, 8226-43.
- KOZŁOWSKI, L., ZAKRZEWSKA, I., TOKAJUK, P. & WOJTUKIEWICZ, M. Z. 2003. Concentration of interleukin-6 (IL-6), interleukin-8 (IL-8) and interleukin-10 (IL-10) in blood serum of breast cancer patients. *Rocz Akad Med Bialymst*, 48, 82-4.

- KRTOLICA, A., PARRINELLO, S., LOCKETT, S., DESPREZ, P. Y. & CAMPISI, J. 2001. Senescent fibroblasts promote epithelial cell growth and tumorigenesis: a link between cancer and aging. *Proc Natl Acad Sci U S A*, 98, 12072-7.
- KRUGER, S., ILMER, M., KOBOLD, S., CADILHA, B. L., ENDRES, S., ORMANN, S., SCHUEBBE, G., RENZ, B. W., D'HAESE, J. G., SCHLOESSER, H., HEINEMANN, V., SUBKLEWE, M., BOECK, S., WERNER, J. & VON BERGWELT-BAILDON, M. 2019. Advances in cancer immunotherapy 2019 – latest trends. *Journal of Experimental & Clinical Cancer Research*, 38, 268.
- KRZYSZCZYK, P., ACEVEDO, A., DAVIDOFF, E. J., TIMMINS, L. M., MARRERO-BERRIOS, I., PATEL, M., WHITE, C., LOWE, C., SHERBA, J. J., HARTMANSHENN, C., O'NEILL, K. M., BALTER, M. L., FRITZ, Z. R., ANDROULAKIS, I. P., SCHLOSS, R. S. & YARMUSH, M. L. 2018. The growing role of precision and personalized medicine for cancer treatment. *Technology (Singap World Sci)*, 6, 79-100.
- L'HÔTE, V., COURBEYRETTE, R., PINNA, G., CINTRAT, J. C., LE PAVEC, G., DELAUNAY-MOISAN, A., MANN, C. & THURET, J. Y. 2021. Ouabain and chloroquine trigger senolysis of BRAF-V600E-induced senescent cells by targeting autophagy. *Aging Cell*, 20, e13447.
- LABERGE, R. M., ZHOU, L., SARANTOS, M. R., RODIER, F., FREUND, A., DE KEIZER, P. L., LIU, S., DEMARIA, M., CONG, Y. S., KAPAHI, P., DESPREZ, P. Y., HUGHES, R. E. & CAMPISI, J. 2012. Glucocorticoids suppress selected components of the senescence-associated secretory phenotype. *Aging Cell*, 11, 569-78.
- LAM, C. S., CHEUNG, A. H., WONG, S. K., WAN, T. M., NG, L., CHOW, A. K., CHENG, N. S., PAK, R. C., LI, H. S., MAN, J. H., YAU, T. C., LO, O. S., POON, J. T., PANG, R. W. & LAW, W. L. 2014. Prognostic significance of CD26 in patients with colorectal cancer. *PLoS One*, 9, e98582.
- LAMB, R., OZSVARI, B., LISANTI, C. L., TANOWITZ, H. B., HOWELL, A., MARTINEZ-OUTSCHOORN, U. E., SOTGIA, F. & LISANTI, M. P. 2015. Antibiotics that target mitochondria effectively eradicate cancer stem cells, across multiple tumor types: treating cancer like an infectious disease. *Oncotarget*, 6, 4569-84.
- LAMBEIR, A.-M., PROOST, P., DURINX, C., BAL, G., SENTEN, K., AUGUSTYNS, K., SCHARPÉ, S., VAN DAMME, J. & DE MEESTER, I. 2001. Kinetic Investigation of Chemokine Truncation by CD26/Dipeptidyl Peptidase IV Reveals a Striking Selectivity within the Chemokine Family*. *Journal of Biological Chemistry*, 276, 29839-29845.
- LAWRENSON, K., GRUN, B., BENJAMIN, E., JACOBS, I. J., DAFOU, D. & GAYTHER, S. A. 2010. Senescent fibroblasts promote neoplastic transformation of partially transformed ovarian epithelial cells in a three-dimensional model of early stage ovarian cancer. *Neoplasia*, 12, 317-25.
- LE DUFF, M., GOUJU, J., JONCHERE, B., GUILLON, J., TOUTAIN, B., BOISSARD, A., HENRY, C., GUETTE, C., LELIEVRE, E. & COQUERET, O. 2018. Regulation of senescence escape by the cdk4-EZH2-AP2M1 pathway in response to chemotherapy. *Cell Death Dis*, 9, 199.
- LECCIA, F., NARDONE, A., CORVIGNO, S., VECCHIO, L. D., DE PLACIDO, S., SALVATORE, F. & VENEZIANI, B. M. 2012. Cytometric and biochemical characterization of human breast cancer cells reveals heterogeneous myoepithelial phenotypes. *Cytometry A*, 81, 960-72.
- LEE, B. Y., HAN, J. A., IM, J. S., MORRONE, A., JOHUNG, K., GOODWIN, E. C., KLEIJER, W. J., DIMAIO, D. & HWANG, E. S. 2006. Senescence-associated beta-galactosidase is lysosomal beta-galactosidase. *Aging Cell*, 5, 187-95.

- LEE, M., NAM, H. Y., KANG, H.-B., LEE, W. H., LEE, G.-H., SUNG, G.-J., HAN, M. W., CHO, K.-J., CHANG, E.-J., CHOI, K.-C., KIM, S. W. & KIM, S. Y. 2021. Epigenetic regulation of p62/SQSTM1 overcomes the radioresistance of head and neck cancer cells via autophagy-dependent senescence induction. *Cell Death & Disease*, 12, 250.
- LEE, S. & SCHMITT, C. A. 2019. The dynamic nature of senescence in cancer. *Nature Cell Biology*, 21, 94-101.
- LEE, S. H., HAO, E., LEVINE, F. & ITKIN-ANSARI, P. 2011. Id3 upregulates BrdU incorporation associated with a DNA damage response, not replication, in human pancreatic β -cells. *Islets*, 3, 358-66.
- LEE, Y.-H., KANG, B. S. & BAE, Y.-S. 2014. Premature senescence in human breast cancer and colon cancer cells by tamoxifen-mediated reactive oxygen species generation. *Life Sciences*, 97, 116-122.
- LEONTIEVA, O. V. & BLAGOSKLONNY, M. V. 2013. CDK4/6-inhibiting drug substitutes for p21 and p16 in senescence: duration of cell cycle arrest and MTOR activity determine geroconversion. *Cell Cycle*, 12, 3063-9.
- LEONTIEVA, O. V., NATARAJAN, V., DEMIDENKO, Z. N., BURDELYA, L. G., GUDKOV, A. V. & BLAGOSKLONNY, M. V. 2012. Hypoxia suppresses conversion from proliferative arrest to cellular senescence. *Proc Natl Acad Sci U S A*, 109, 13314-8.
- LEVKOFF, L. H., MARSHALL, G. P., 2ND, ROSS, H. H., CALDEIRA, M., REYNOLDS, B. A., CAKIROGLU, M., MARIANI, C. L., STREIT, W. J. & LAYWELL, E. D. 2008. Bromodeoxyuridine inhibits cancer cell proliferation in vitro and in vivo. *Neoplasia*, 10, 804-16.
- LI, L., VAN BREUGEL, PIETER C., LOAYZA-PUCH, F., UGALDE, A. P., KORKMAZ, G., MESSIKAGOLD, N., HAN, R., LOPES, R., BARBERA, E. P., TEUNISSEN, H., DE WIT, E., SOARES, R. J., NIELSEN, B. S., HOLMSTRØM, K., MARTÍNEZ-HERRERA, D. J., HUARTE, M., LOULOUP, A., DROST, J., ELKON, R. & AGAMI, R. 2018. LncRNA-OIS1 regulates DPP4 activation to modulate senescence induced by RAS. *Nucleic Acids Research*, 46, 4213-4227.
- LI, S., FAN, Y., KUMAGAI, A., KAWAKITA, E., KITADA, M., KANASAKI, K. & KOYA, D. 2020. Deficiency in Dipeptidyl Peptidase-4 Promotes Chemoresistance Through the CXCL12/CXCR4/mTOR/TGF β Signaling Pathway in Breast Cancer Cells. *International Journal of Molecular Sciences*, 21, 805.
- LI, W., ZOU, Z., CAI, Y., YANG, K., WANG, S., LIU, Z., GENG, L., CHU, Q., JI, Z., CHAN, P., LIU, G.-H., SONG, M., QU, J. & ZHANG, W. 2022. Low-dose chloroquine treatment extends the lifespan of aged rats. *Protein & Cell*.
- LI, Y., WANG, Z., AJANI, J. A. & SONG, S. 2021. Drug resistance and Cancer stem cells. *Cell Communication and Signaling*, 19, 19.
- LIEBER, J., KIRCHNER, B., EICHER, C., WARMANN, S. W., SEITZ, G., FUCHS, J. & ARMEANU-EBINGER, S. 2010. Inhibition of Bcl-2 and Bcl-X enhances chemotherapy sensitivity in hepatoblastoma cells. *Pediatr Blood Cancer*, 55, 1089-95.
- LIU, S., UPPAL, H., DEMARIA, M., DESPREZ, P. Y., CAMPISI, J. & KAPAHI, P. 2015. Simvastatin suppresses breast cancer cell proliferation induced by senescent cells. *Sci Rep*, 5, 17895.
- LIU, X.-L., DING, J. & MENG, L.-H. 2018. Oncogene-induced senescence: a double edged sword in cancer. *Acta Pharmacologica Sinica*, 39, 1553-1558.

- LLANOS, S., MEGIAS, D., BLANCO-APARICIO, C., HERNANDEZ-ENCINAS, E., ROVIRA, M., PIETROCOLA, F. & SERRANO, M. 2019. Lysosomal trapping of palbociclib and its functional implications. *Oncogene*, 38, 3886-3902.
- LYONS, A. B. & PARISH, C. R. 1994. Determination of lymphocyte division by flow cytometry. *Journal of Immunological Methods*, 171, 131-137.
- MA, Y., REN, Y., DAI, Z. J., WU, C. J., JI, Y. H. & XU, J. 2017. IL-6, IL-8 and TNF- α levels correlate with disease stage in breast cancer patients. *Adv Clin Exp Med*, 26, 421-426.
- MAH, L. J., EL-OSTA, A. & KARAGIANNIS, T. C. 2010. gammaH2AX: a sensitive molecular marker of DNA damage and repair. *Leukemia*, 24, 679-86.
- MALANCHI, I., SANTAMARIA-MARTÍNEZ, A., SUSANTO, E., PENG, H., LEHR, H. A., DELALOYE, J. F. & HUELSKEN, J. 2011. Interactions between cancer stem cells and their niche govern metastatic colonization. *Nature*, 481, 85-9.
- MANI, S. A., GUO, W., LIAO, M. J., EATON, E. N., AYYANAN, A., ZHOU, A. Y., BROOKS, M., REINHARD, F., ZHANG, C. C., SHIPITSIN, M., CAMPBELL, L. L., POLYAK, K., BRISKEN, C., YANG, J. & WEINBERG, R. A. 2008. The epithelial-mesenchymal transition generates cells with properties of stem cells. *Cell*, 133, 704-15.
- MANSOORI, B., MOHAMMADI, A., DAVUDIAN, S., SHIRJANG, S. & BARADARAN, B. 2017. The Different Mechanisms of Cancer Drug Resistance: A Brief Review. *Adv Pharm Bull*, 7, 339-348.
- MARGUET, D., BAGGIO, L., KOBAYASHI, T., BERNARD, A. M., PIERRES, M., NIELSEN, P. F., RIBEL, U., WATANABE, T., DRUCKER, D. J. & WAGTMANN, N. 2000. Enhanced insulin secretion and improved glucose tolerance in mice lacking CD26. *Proc Natl Acad Sci U S A*, 97, 6874-9.
- MASKEY, R. S., WANG, F., LEHMAN, E., WANG, Y., EMMANUEL, N., ZHONG, W., JIN, G., ABRAHAM, R. T., ARNDT, K. T., MYERS, J. S. & MAZUREK, A. 2020. Sustained mTORC1 activity during palbociclib-induced growth arrest triggers senescence in ER+ breast cancer cells. *Cell Cycle*, 1-16.
- MASTERSON, J. C. & O'DEA, S. 2007. 5-Bromo-2-deoxyuridine activates DNA damage signalling responses and induces a senescence-like phenotype in p16-null lung cancer cells. *Anticancer Drugs*, 18, 1053-68.
- MATHEW, R., KARP, C. M., BEAUDOIN, B., VUONG, N., CHEN, G., CHEN, H. Y., BRAY, K., REDDY, A., BHANOT, G., GELINAS, C., DIPOLA, R. S., KARANTZA-WADSWORTH, V. & WHITE, E. 2009. Autophagy suppresses tumorigenesis through elimination of p62. *Cell*, 137, 1062-75.
- MATJUSAITIS, M., CHIN, G., SARNOSKI, E. A. & STOLZING, A. 2016. Biomarkers to identify and isolate senescent cells. *Ageing Res Rev*, 29, 1-12.
- MATTIUZZI, C. & LIPPI, G. 2019. Current Cancer Epidemiology. *J Epidemiol Glob Health*, 9, 217-222.
- MATUSZAK, M., LEWANDOWSKI, K., CZYŻ, A., KIERNICKA-PARULSKA, J., PRZYBYŁOWICZ-CHALECKA, A., JARMUŻ-SZYMCZAK, M., LEWANDOWSKA, M. & KOMARNICKI, M. 2016. The prognostic significance of surface dipeptidylpeptidase IV (CD26) expression in B-cell chronic lymphocytic leukemia. *Leukemia Research*, 47, 166-171.
- MAUTHE, M., ORHON, I., ROCCHI, C., ZHOU, X., LUHR, M., HIJLKEMA, K.-J., COPPES, R. P., ENGEDAL, N., MARI, M. & REGGIORI, F. 2018. Chloroquine inhibits autophagic flux by decreasing autophagosome-lysosome fusion. *Autophagy*, 14, 1435-1455.

- MAY, C. D., SPHYRIS, N., EVANS, K. W., WERDEN, S. J., GUO, W. & MANI, S. A. 2011. Epithelial-mesenchymal transition and cancer stem cells: a dangerously dynamic duo in breast cancer progression. *Breast Cancer Res*, 13, 202.
- MAYCOTTE, P., GEARHEART, C. M., BARNARD, R., ARYAL, S., MULCAHY LEVY, J. M., FOSMIRE, S. P., HANSEN, R. J., MORGAN, M. J., PORTER, C. C., GUSTAFSON, D. L. & THORBURN, A. 2014. STAT3-mediated autophagy dependence identifies subtypes of breast cancer where autophagy inhibition can be efficacious. *Cancer Res*, 74, 2579-90.
- MAYER, E. L., DUECK, A. C., MARTIN, M., RUBOVSKY, G., BURSTEIN, H. J., BELLET-EZQUERRA, M., MILLER, K. D., ZDENKOWSKI, N., WINER, E. P., PFEILER, G., GOETZ, M., RUIZ-BORREGO, M., ANDERSON, D., NOWECKI, Z., LOIBL, S., MOULDER, S., RING, A., FITZAL, F., TRAINA, T., CHAN, A., RUGO, H. S., LEMIEUX, J., HENAO, F., LYSS, A., ANTOLIN NOVOA, S., WOLFF, A. C., VETTER, M., EGLE, D., MORRIS, P. G., MAMOUNAS, E. P., GILGIL, M. J., PRAT, A., FOHLER, H., METZGER FILHO, O., SCHWARZ, M., DUFRANE, C., FUMAGALLI, D., THEALL, K. P., LU, D. R., BARTLETT, C. H., KOEHLER, M., FESL, C., DEMICHELE, A. & GNANT, M. 2021. Palbociclib with adjuvant endocrine therapy in early breast cancer (PALLAS): interim analysis of a multicentre, open-label, randomised, phase 3 study. *Lancet Oncol*, 22, 212-222.
- MENG, Y., EFIMOVA, E. V., HAMZEH, K. W., DARGA, T. E., MAUCERI, H. J., FU, Y. X., KRON, S. J. & WEICHSELBAUM, R. R. 2012. Radiation-inducible immunotherapy for cancer: senescent tumor cells as a cancer vaccine. *Mol Ther*, 20, 1046-55.
- MENTLEIN, R. 1999. Dipeptidyl-peptidase IV (CD26)--role in the inactivation of regulatory peptides. *Regul Pept*, 85, 9-24.
- METZEMAEKERS, M., VAN DAMME, J., MORTIER, A. & PROOST, P. 2016. Regulation of Chemokine Activity – A Focus on the Role of Dipeptidyl Peptidase IV/CD26. *Frontiers in Immunology*, 7.
- MICHISHITA, E., NAKABAYASHI, K., SUZUKI, T., KAUL, S. C., OGINO, H., FUJII, M., MITSUI, Y. & AYUSAWA, D. 1999. 5-Bromodeoxyuridine induces senescence-like phenomena in mammalian cells regardless of cell type or species. *J Biochem*, 126, 1052-9.
- MILANOVIC, M., FAN, D. N. Y., BELENKI, D., DABRITZ, J. H. M., ZHAO, Z., YU, Y., DORR, J. R., DIMITROVA, L., LENZE, D., MONTEIRO BARBOSA, I. A., MENDOZA-PARRA, M. A., KANASHOVA, T., METZNER, M., PARDON, K., REIMANN, M., TRUMPP, A., DORKEN, B., ZUBER, J., GRONEMEYER, H., HUMMEL, M., DITTMAR, G., LEE, S. & SCHMITT, C. A. 2018. Senescence-associated reprogramming promotes cancer stemness. *Nature*, 553, 96-100.
- MILLER, I., MIN, M., YANG, C., TIAN, C., GOOKIN, S., CARTER, D. & SPENCER, S. L. 2018. Ki67 is a Graded Rather than a Binary Marker of Proliferation versus Quiescence. *Cell Rep*, 24, 1105-1112.e5.
- MODRAK, D. E., LEON, E., GOLDENBERG, D. M. & GOLD, D. V. 2009. Ceramide regulates gemcitabine-induced senescence and apoptosis in human pancreatic cancer cell lines. *Mol Cancer Res*, 7, 890-6.
- MOISEEVA, O., DESCHENES-SIMARD, X., ST-GERMAIN, E., IGELMANN, S., HUOT, G., CADAR, A. E., BOURDEAU, V., POLLAK, M. N. & FERBEYRE, G. 2013. Metformin inhibits the senescence-associated secretory phenotype by interfering with IKK/NF-kappaB activation. *Aging Cell*, 12, 489-98.
- MONGIARDI, M. P., PELLEGRINI, M., PALLINI, R., LEVI, A. & FALCHETTI, M. L. 2021. Cancer Response to Therapy-Induced Senescence: A Matter of Dose and Timing. *Cancers (Basel)*, 13.

- MOOI, W. J. & PEEPER, D. S. 2006. Oncogene-induced cell senescence--halting on the road to cancer. *N Engl J Med*, 355, 1037-46.
- MOORE, N. & LYLE, S. 2011. Quiescent, slow-cycling stem cell populations in cancer: a review of the evidence and discussion of significance. *J Oncol*, 2011.
- MORGUNOVA, G. V., KOLESNIKOV, A. V., KLEBANOV, A. A. & KHOKHLOV, A. N. 2015. Senescence-associated β -galactosidase—A biomarker of aging, DNA damage, or cell proliferation restriction? *Moscow University Biological Sciences Bulletin*, 70, 165-167.
- MORIYA, S., CHE, X. F., KOMATSU, S., ABE, A., KAWAGUCHI, T., GOTOH, A., INAZU, M., TOMODA, A. & MIYAZAWA, K. 2013. Macrolide antibiotics block autophagy flux and sensitize to bortezomib via endoplasmic reticulum stress-mediated CHOP induction in myeloma cells. *Int J Oncol*, 42, 1541-50.
- MORRIS-HANON, O., MARAZITA, M. C., ROMORINI, L., ISAJA, L., FERNANDEZ-ESPINOSA, D. D., SEVLEVER, G. E., SCASSA, M. E. & VIDELA-RICHARDSON, G. A. 2019. Palbociclib Effectively Halts Proliferation but Fails to Induce Senescence in Patient-Derived Glioma Stem Cells. *Mol Neurobiol*, 56, 7810-7821.
- MORRISON, M. E., VIJAYASARADHI, S., ENGELSTEIN, D., ALBINO, A. P. & HOUGHTON, A. N. 1993. A marker for neoplastic progression of human melanocytes is a cell surface ectopeptidase. *J Exp Med*, 177, 1135-43.
- MORTIER, A., GOUWY, M., VAN DAMME, J., PROOST, P. & STRUYF, S. 2016. CD26/dipeptidylpeptidase IV-chemokine interactions: double-edged regulation of inflammation and tumor biology. *J Leukoc Biol*, 99, 955-69.
- MOSIENIAK, G., SLIWINSKA, M. A., ALSTER, O., STRZESZEWSKA, A., SUNDERLAND, P., PIECHOTA, M., WAS, H. & SIKORA, E. 2015. Polyploidy Formation in Doxorubicin-Treated Cancer Cells Can Favor Escape from Senescence. *Neoplasia*, 17, 882-893.
- MUKAI, S., MORIYA, S., HIRAMOTO, M., KAZAMA, H., KOKUBA, H., CHE, X. F., YOKOYAMA, T., SAKAMOTO, S., SUGAWARA, A., SUNAZUKA, T., ŌMURA, S., HANDA, H., ITOI, T. & MIYAZAWA, K. 2016. Macrolides sensitize EGFR-TKI-induced non-apoptotic cell death via blocking autophagy flux in pancreatic cancer cell lines. *Int J Oncol*, 48, 45-54.
- MÜLLER, A., HOMEY, B., SOTO, H., GE, N., CATRON, D., BUCHANAN, M. E., MCCLANAHAN, T., MURPHY, E., YUAN, W., WAGNER, S. N., BARRERA, J. L., MOHAR, A., VERÁSTEGUI, E. & ZLOTNIK, A. 2001. Involvement of chemokine receptors in breast cancer metastasis. *Nature*, 410, 50-6.
- MYRIANTHOPOULOS, V., EVANGELOU, K., VASILEIOU, P. V. S., COOKS, T., VASSILAKOPOULOS, T. P., PANGALIS, G. A., KOULOUKOUSSA, M., KITTAS, C., GEORGAKILAS, A. G. & GORGOULIS, V. G. 2019. Senescence and senotherapeutics: a new field in cancer therapy. *Pharmacol Ther*, 193, 31-49.
- NASRI, H. & RAFIEIAN-KOPAEI, M. 2014. Metformin: Current knowledge. *J Res Med Sci*, 19, 658-64.
- NOH, Y., JEON, S. M. & SHIN, S. 2019. Association between glucose-lowering treatment and cancer metastasis among patients with preexisting type 2 diabetes and incident malignancy. *Int J Cancer*, 144, 1530-1539.
- NOVAIS, E. J., TRAN, V. A., JOHNSTON, S. N., DARRIS, K. R., ROUPAS, A. J., SESSIONS, G. A., SHAPIRO, I. M., DIEKMAN, B. O. & RISBUD, M. V. 2021. Long-term treatment with senolytic drugs Dasatinib and Quercetin ameliorates age-dependent intervertebral disc degeneration in mice. *Nature Communications*, 12, 5213.
- OAKES, S. R., VAILLANT, F., LIM, E., LEE, L., BRESLIN, K., FELEPPA, F., DEB, S., RITCHIE, M. E., TAKANO, E., WARD, T., FOX, S. B., GENERALI, D., SMYTH, G. K., STRASSER, A., HUANG,

- D. C., VISVADER, J. E. & LINDEMAN, G. J. 2012. Sensitization of BCL-2-expressing breast tumors to chemotherapy by the BH3 mimetic ABT-737. *Proc Natl Acad Sci U S A*, 109, 2766-71.
- OHNUMA, K., DANG, N. H. & MORIMOTO, C. 2008. Revisiting an old acquaintance: CD26 and its molecular mechanisms in T cell function. *Trends Immunol*, 29, 295-301.
- OLSZEWSKA, A., BORKOWSKA, A., GRANICA, M., KAROLCZAK, J., ZGLINICKI, B., KIEDA, C. & WAS, H. 2022. Escape From Cisplatin-Induced Senescence of Hypoxic Lung Cancer Cells Can Be Overcome by Hydroxychloroquine. *Frontiers in Oncology*, 11.
- ORTIZ-MONTERO, P., LONDONO-VALLEJO, A. & VERNOT, J. P. 2017. Senescence-associated IL-6 and IL-8 cytokines induce a self- and cross-reinforced senescence/inflammatory milieu strengthening tumorigenic capabilities in the MCF-7 breast cancer cell line. *Cell Commun Signal*, 15, 17.
- OUBAHA, M., MILOUDI, K., DEJDA, A., GUBER, V., MAWAMBO, G., GERMAIN, M. A., BOURDEL, G., POPOVIC, N., REZENDE, F. A., KAUFMAN, R. J., MALLETT, F. A. & SAPIEHA, P. 2016. Senescence-associated secretory phenotype contributes to pathological angiogenesis in retinopathy. *Sci Transl Med*, 8, 362ra144.
- OVADYA, Y. & KRIZHANOVSKY, V. 2018. Strategies targeting cellular senescence. *The Journal of Clinical Investigation*, 128, 1247-1254.
- OZSVARI, B., NUTTALL, J. R., SOTGIA, F. & LISANTI, M. P. 2018. Azithromycin and Roxithromycin define a new family of "senolytic" drugs that target senescent human fibroblasts. *Aging (Albany NY)*, 10, 3294-3307.
- PANG, R., LAW, W. L., CHU, A. C. Y., POON, J. T., LAM, C. S. C., CHOW, A. K. M., NG, L., CHEUNG, L. W. H., LAN, X. R., LAN, H. Y., TAN, V. P. Y., YAU, T. C., POON, R. T. & WONG, B. C. Y. 2010. A Subpopulation of CD26+ Cancer Stem Cells with Metastatic Capacity in Human Colorectal Cancer. *Cell Stem Cell*, 6, 603-615.
- PARE, R., SHIN, J. S. & LEE, C. S. 2016. Increased expression of senescence markers p14(ARF) and p16(INK4a) in breast cancer is associated with an increased risk of disease recurrence and poor survival outcome. *Histopathology*, 69, 479-91.
- PARK, J. T., LEE, Y.-S., CHO, K. A. & PARK, S. C. 2018. Adjustment of the lysosomal-mitochondrial axis for control of cellular senescence. *Ageing Research Reviews*, 47, 176-182.
- PARK, Y. Y., AN, C. H., OH, S. T., CHANG, E. D. & LEE, J. 2019. Expression of CD133 is associated with poor prognosis in stage II colorectal carcinoma. *Medicine (Baltimore)*, 98, e16709.
- PATEL, P. L., SURAM, A., MIRANI, N., BISCHOF, O. & HERBIG, U. 2016. Derepression of hTERT gene expression promotes escape from oncogene-induced cellular senescence. *Proc Natl Acad Sci U S A*, 113, E5024-33.
- PENG, Q., ZHAO, L., HOU, Y., SUN, Y., WANG, L., LUO, H., PENG, H. & LIU, M. 2013. Biological characteristics and genetic heterogeneity between carcinoma-associated fibroblasts and their paired normal fibroblasts in human breast cancer. *PLoS One*, 8, e60321.
- PETROVA, N. V., VELICHKO, A. K., RAZIN, S. V. & KANTIDZE, O. L. 2016. Small molecule compounds that induce cellular senescence. *Aging Cell*, 15, 999-1017.
- PIJUAN, J., BARCELÓ, C., MORENO, D. F., MAIQUES, O., SISÓ, P., MARTI, R. M., MACIÀ, A. & PANOSA, A. 2019. In vitro Cell Migration, Invasion, and Adhesion Assays: From Cell Imaging to Data Analysis. *Frontiers in Cell and Developmental Biology*, 7.
- PLESCA, D., MAZUMDER, S. & ALMASAN, A. 2008. DNA damage response and apoptosis. *Methods Enzymol*, 446, 107-22.

- PORTMAN, N., ALEXANDROU, S., CARSON, E., WANG, S., LIM, E. & CALDON, C. E. 2019. Overcoming CDK4/6 inhibitor resistance in ER-positive breast cancer. *Endocr Relat Cancer*, 26, R15-r30.
- RAJENDRAN, V. & JAIN, M. V. 2018. In Vitro Tumorigenic Assay: Colony Forming Assay for Cancer Stem Cells. *Methods Mol Biol*, 1692, 89-95.
- RATHMANN, W. & KOSTEV, K. 2017. Association of dipeptidyl peptidase 4 inhibitors with risk of metastases in patients with type 2 diabetes and breast, prostate or digestive system cancer. *Journal of Diabetes and its Complications*, 31, 687-692.
- RENNA, M., SCHAFFNER, C., BROWN, K., SHANG, S., TAMAYO, M. H., HEGYI, K., GRIMSEY, N. J., CUSENS, D., COULTER, S., COOPER, J., BOWDEN, A. R., NEWTON, S. M., KAMPMANN, B., HELM, J., JONES, A., HAWORTH, C. S., BASARABA, R. J., DEGROOTE, M. A., ORDWAY, D. J., RUBINSZTEIN, D. C. & FLOTO, R. A. 2011. Azithromycin blocks autophagy and may predispose cystic fibrosis patients to mycobacterial infection. *The Journal of Clinical Investigation*, 121, 3554-3563.
- ROBERSON, R. S., KUSSICK, S. J., VALLIERES, E., CHEN, S. Y. & WU, D. Y. 2005. Escape from therapy-induced accelerated cellular senescence in p53-null lung cancer cells and in human lung cancers. *Cancer Res*, 65, 2795-803.
- ROBINSON, T. J., LIU, J. C., VIZEACOMAR, F., SUN, T., MACLEAN, N., EGAN, S. E., SCHIMMER, A. D., DATTI, A. & ZACKSENHAUS, E. 2013. RB1 status in triple negative breast cancer cells dictates response to radiation treatment and selective therapeutic drugs. *PLoS One*, 8, e78641.
- ROMANOV, S. R., KOZAKIEWICZ, B. K., HOLST, C. R., STAMPFER, M. R., HAUPT, L. M. & TLSTY, T. D. 2001. Normal human mammary epithelial cells spontaneously escape senescence and acquire genomic changes. *Nature*, 409, 633-7.
- ROSS, H. H., LEVKOFF, L. H., MARSHALL, G. P., 2ND, CALDEIRA, M., STEINDLER, D. A., REYNOLDS, B. A. & LAYWELL, E. D. 2008. Bromodeoxyuridine induces senescence in neural stem and progenitor cells. *Stem Cells*, 26, 3218-27.
- ROSSI, M. & ABDELMOHSEN, K. 2021. The Emergence of Senescent Surface Biomarkers as Senotherapeutic Targets. *Cells*, 10.
- RUNWAL, G., STAMATAKOU, E., SIDDIQI, F. H., PURI, C., ZHU, Y. & RUBINSZTEIN, D. C. 2019. LC3-positive structures are prominent in autophagy-deficient cells. *Scientific Reports*, 9, 10147.
- RUSCETTI, M., LEIBOLD, J., BOTT, M. J., FENNEL, M., KULICK, A., SALGADO, N. R., CHEN, C. C., HO, Y. J., SANCHEZ-RIVERA, F. J., FEUCHT, J., BASLAN, T., TIAN, S., CHEN, H. A., ROMESSER, P. B., POIRIER, J. T., RUDIN, C. M., DE STANCHINA, E., MANCHADO, E., SHERR, C. J. & LOWE, S. W. 2018. NK cell-mediated cytotoxicity contributes to tumor control by a cytostatic drug combination. *Science*, 362, 1416-1422.
- SACCON, T. D., NAGPAL, R., YADAV, H., CAVALCANTE, M. B., NUNES, A. D. C., SCHNEIDER, A., GESING, A., HUGHES, B., YOUSEFZADEH, M., TCHKONIA, T., KIRKLAND, J. L., NIEDERNHOFER, L. J., ROBBINS, P. D. & MASTERNAK, M. M. 2021. Senolytic Combination of Dasatinib and Quercetin Alleviates Intestinal Senescence and Inflammation and Modulates the Gut Microbiome in Aged Mice. *J Gerontol A Biol Sci Med Sci*, 76, 1895-1905.
- SADAIE, M., SALAMA, R., CARROLL, T., TOMIMATSU, K., CHANDRA, T., YOUNG, A. R., NARITA, M., PÉREZ-MANCERA, P. A., BENNETT, D. C., CHONG, H., KIMURA, H. & NARITA, M. 2013. Redistribution of the Lamin B1 genomic binding profile affects rearrangement

- of heterochromatic domains and SAHF formation during senescence. *Genes Dev*, 27, 1800-8.
- SAGE, J., MILLER, A. L., PEREZ-MANCERA, P. A., WYSOCKI, J. M. & JACKS, T. 2003. Acute mutation of retinoblastoma gene function is sufficient for cell cycle re-entry. *Nature*, 424, 223-8.
- SALEH, T., TYUTYNUK-MASSEY, L., CUDJOE, E. K., JR., IDOWU, M. O., LANDRY, J. W. & GEWIRTZ, D. A. 2018. Non-Cell Autonomous Effects of the Senescence-Associated Secretory Phenotype in Cancer Therapy. *Front Oncol*, 8, 164.
- SALEH, T., TYUTYUNYK-MASSEY, L. & GEWIRTZ, D. A. 2019a. Tumor Cell Escape from Therapy-Induced Senescence as a Model of Disease Recurrence after Dormancy. *Cancer Res*, 79, 1044-1046.
- SALEH, T., TYUTYUNYK-MASSEY, L., MURRAY, G. F., ALOTAIBI, M. R., KAWALE, A. S., ELSAYED, Z., HENDERSON, S. C., YAKOVLEV, V., ELMORE, L. W., TOOR, A., HARADA, H., REED, J., LANDRY, J. W. & GEWIRTZ, D. A. 2019b. Tumor cell escape from therapy-induced senescence. *Biochem Pharmacol*, 162, 202-212.
- SANOFF, H. K., DEAL, A. M., KRISHNAMURTHY, J., TORRICE, C., DILLON, P., SORRENTINO, J., IBRAHIM, J. G., JOLLY, T. A., WILLIAMS, G., CAREY, L. A., DROBISH, A., GORDON, B. B., ALSTON, S., HURRIA, A., KLEINHANS, K., RUDOLPH, K. L., SHARPLESS, N. E. & MUSS, H. B. 2014. Effect of cytotoxic chemotherapy on markers of molecular age in patients with breast cancer. *J Natl Cancer Inst*, 106, dju057.
- SARKISIAN, C. J., KEISTER, B. A., STAIRS, D. B., BOXER, R. B., MOODY, S. E. & CHODOSH, L. A. 2007. Dose-dependent oncogene-induced senescence in vivo and its evasion during mammary tumorigenesis. *Nat Cell Biol*, 9, 493-505.
- SCHEEN, A. J. 2012. DPP-4 inhibitors in the management of type 2 diabetes: a critical review of head-to-head trials. *Diabetes Metab*, 38, 89-101.
- SCHMITT, C. A., FRIDMAN, J. S., YANG, M., LEE, S., BARANOV, E., HOFFMAN, R. M. & LOWE, S. W. 2002. A senescence program controlled by p53 and p16INK4a contributes to the outcome of cancer therapy. *Cell*, 109, 335-46.
- SCHOLZEN, T. & GERDES, J. 2000. The Ki-67 protein: from the known and the unknown. *J Cell Physiol*, 182, 311-22.
- SCHOSSERER, M., GRILLARI, J. & BREITENBACH, M. 2017. The Dual Role of Cellular Senescence in Developing Tumors and Their Response to Cancer Therapy. *Front Oncol*, 7, 278.
- SHAH, C., HONG, Y. R., BISHNOI, R., ALI, A., SKELTON, W. P. T., DANG, L. H., HUO, J. & DANG, N. H. 2020. Impact of DPP4 Inhibitors in Survival of Patients With Prostate, Pancreas, and Breast Cancer. *Front Oncol*, 10, 405.
- SHAW, F. L., HARRISON, H., SPENCE, K., ABLETT, M. P., SIMOES, B. M., FARNIE, G. & CLARKE, R. B. 2012. A detailed mammosphere assay protocol for the quantification of breast stem cell activity. *J Mammary Gland Biol Neoplasia*, 17, 111-7.
- SHERMAN, M. Y., MENG, L., STAMPFER, M., GABAI, V. L. & YAGLOM, J. A. 2011. Oncogenes induce senescence with incomplete growth arrest and suppress the DNA damage response in immortalized cells. *Aging Cell*, 10, 949-61.
- SHORT, S., FIELDER, E., MIWA, S. & VON ZGLINICKI, T. 2019. Senolytics and senostatics as adjuvant tumour therapy. *EBioMedicine*, 41, 683-692.
- SIDI, R., PASELLO, G., OPITZ, I., SOLTERMANN, A., TUTIC, M., REHRAUER, H., WEDER, W., STAHEL, R. A. & FELLE-BOSCO, E. 2011. Induction of senescence markers after neo-adjuvant chemotherapy of malignant pleural mesothelioma and association with clinical outcome: an exploratory analysis. *Eur J Cancer*, 47, 326-32.

- SIEBEN, C. J., STURMLECHNER, I., VAN DE SLUIS, B. & VAN DEURSEN, J. M. 2018. Two-Step Senescence-Focused Cancer Therapies. *Trends Cell Biol*, 28, 723-737.
- SONG, Y., BABA, T. & MUKAIDA, N. 2016. Gemcitabine induces cell senescence in human pancreatic cancer cell lines. *Biochem Biophys Res Commun*, 477, 515-9.
- SOTGIA, F., FIORILLO, M. & LISANTI, M. P. 2019. Hallmarks of the cancer cell of origin: Comparisons with "energetic" cancer stem cells (e-CSCs). *Aging (Albany NY)*, 11, 1065-1068.
- SOUTHERN, K. W., BARKER, P. M., SOLIS-MOYA, A. & PATEL, L. 2012. Macrolide antibiotics for cystic fibrosis. *Cochrane Database Syst Rev*, 11, Cd002203.
- SUN, Y., MAO, X., FAN, C., LIU, C., GUO, A., GUAN, S., JIN, Q., LI, B., YAO, F. & JIN, F. 2014. CXCL12-CXCR4 axis promotes the natural selection of breast cancer cell metastasis. *Tumour Biol*, 35, 7765-73.
- SUN, Y. X., PEDERSEN, E. A., SHIOZAWA, Y., HAVENS, A. M., JUNG, Y., WANG, J., PIENTA, K. J. & TAICHMAN, R. S. 2008. CD26/dipeptidyl peptidase IV regulates prostate cancer metastasis by degrading SDF-1/CXCL12. *Clin Exp Metastasis*, 25, 765-76.
- SUZUKI, T., MINAGAWA, S., MICHISHITA, E., OGINO, H., FUJII, M., MITSUI, Y. & AYUSAWA, D. 2001. Induction of senescence-associated genes by 5-bromodeoxyuridine in HeLa cells. *Exp Gerontol*, 36, 465-74.
- SWANSON, E., RAPKIN, L., BAZETT-JONES, D. & LAWRENCE, J. 2015. Unfolding the Story of Chromatin Organization in Senescent Cells. *Nucleus (Austin, Tex.)*, 6.
- TAKEBAYASHI, S., TANAKA, H., HINO, S., NAKATSU, Y., IGATA, T., SAKAMOTO, A., NARITA, M. & NAKAO, M. 2015. Retinoblastoma protein promotes oxidative phosphorylation through upregulation of glycolytic genes in oncogene-induced senescent cells. *Aging Cell*, 14, 689-97.
- TANAKA, H., HINO, H., MORIYA, S., KAZAMA, H., MIYAZAKI, M., TAKANO, N., HIRAMOTO, M., TSUKAHARA, K. & MIYAZAWA, K. 2020. Comparison of autophagy inducibility in various tyrosine kinase inhibitors and their enhanced cytotoxicity via inhibition of autophagy in cancer cells in combined treatment with azithromycin. *Biochem Biophys Rep*, 22, 100750.
- TASCHNER-MANDL, S., SCHWARZ, M., BLAHA, J., KAUER, M., KROMP, F., FRANK, N., RIFATBEGOVIC, F., WEISS, T., LADENSTEIN, R., HOHENEGGER, M., AMBROS, I. M. & AMBROS, P. F. 2016. Metronomic topotecan impedes tumor growth of MYCN-amplified neuroblastoma cells in vitro and in vivo by therapy induced senescence. *Oncotarget*, 7, 3571-86.
- TATO-COSTA, J., CASIMIRO, S., PACHECO, T., PIRES, R., FERNANDES, A., ALHO, I., PEREIRA, P., COSTA, P., CASTELO, H. B., FERREIRA, J. & COSTA, L. 2016. Therapy-Induced Cellular Senescence Induces Epithelial-to-Mesenchymal Transition and Increases Invasiveness in Rectal Cancer. *Clin Colorectal Cancer*, 15, 170-178.e3.
- TAYLOR, J., LEHMANN, B., CHAPPELL, W., ABRAMS, S., STEELMAN, L. & MCCUBREY, J. 2011. Cooperative Effects of Akt-1 and Raf-1 on the Induction of Cellular Senescence in Doxorubicin or Tamoxifen Treated Breast Cancer Cells. *Oncotarget*, 2, 610-26.
- TE POELE, R. H., OKOROKOV, A. L., JARDINE, L., CUMMINGS, J. & JOEL, S. P. 2002. DNA damage is able to induce senescence in tumor cells in vitro and in vivo. *Cancer Res*, 62, 1876-83.
- TODD, M. C., LANGAN, T. A. & SCLAFANI, R. A. 2017. Doxycycline-Regulated p16(MTS1) Expression Suppresses the Anchorage-Independence and Tumorigenicity of Breast Cancer Cell Lines that Lack Endogenous p16. *J Cancer*, 8, 190-198.

- TONNESSEN-MURRAY, C. A., FREY, W. D., RAO, S. G., SHAHBANDI, A., UNGERLEIDER, N. A., OLAYIWOLA, J. O., MURRAY, L. B., VINSON, B. T., CHRISEY, D. B., LORD, C. J. & JACKSON, J. G. 2019. Chemotherapy-induced senescent cancer cells engulf other cells to enhance their survival. *The Journal of Cell Biology*, jcb.201904051.
- TORIYAMA, K., TAKANO, N., KOKUBA, H., KAZAMA, H., MORIYA, S., HIRAMOTO, M., ABE, S. & MIYAZAWA, K. 2021. Azithromycin enhances the cytotoxicity of DNA-damaging drugs via lysosomal membrane permeabilization in lung cancer cells. *Cancer Sci*, 112, 3324-3337.
- TOSO, A., REVANDKAR, A., DI MITRI, D., GUCCINI, I., PROIETTI, M., SARTI, M., PINTON, S., ZHANG, J., KALATHUR, M., CIVENNI, G., JARROSSAY, D., MONTANI, E., MARINI, C., GARCIA-ESCUADERO, R., SCANZIANI, E., GRASSI, F., PANDOLFI, P. P., CATAPANO, C. V. & ALIMONTI, A. 2014. Enhancing chemotherapy efficacy in Pten-deficient prostate tumors by activating the senescence-associated antitumor immunity. *Cell Rep*, 9, 75-89.
- TRIANA-MARTINEZ, F., LOZA, M. I. & DOMINGUEZ, E. 2020. Beyond Tumor Suppression: Senescence in Cancer Stemness and Tumor Dormancy. *Cells*, 9.
- TSUBONE TM, R. C., TONOLLI PN, II-SEI W, STOLF BS 2020. In vitro Autophagy Modulation with Chloroquine: Some Lessons to Learn. *Adv Biochem Biotechnol*.
- TURNER, N. C., RO, J., ANDRÉ, F., LOI, S., VERMA, S., IWATA, H., HARBECK, N., LOIBL, S., HUANG BARTLETT, C., ZHANG, K., GIORGETTI, C., RANDOLPH, S., KOEHLER, M. & CRISTOFANILLI, M. 2015. Palbociclib in Hormone-Receptor-Positive Advanced Breast Cancer. *N Engl J Med*, 373, 209-19.
- VAN DEN OORD, J. J. 1998. Expression of CD26/dipeptidyl-peptidase IV in benign and malignant pigment-cell lesions of the skin. *Br J Dermatol*, 138, 615-21.
- VARNA, M., BOUSQUET, G., PLASSA, L. F., BERTHEAU, P. & JANIN, A. 2011. TP53 status and response to treatment in breast cancers. *J Biomed Biotechnol*, 2011, 284584.
- VERA-RAMIREZ, L., VODNALA, S. K., NINI, R., HUNTER, K. W. & GREEN, J. E. 2018. Autophagy promotes the survival of dormant breast cancer cells and metastatic tumour recurrence. *Nat Commun*, 9, 1944.
- VOLONTE, D. & GALBIATI, F. 2020. Caveolin-1, a master regulator of cellular senescence. *Cancer Metastasis Rev*.
- WAGNER, V. & GIL, J. 2020. Senescence as a therapeutically relevant response to CDK4/6 inhibitors. *Oncogene*, 39, 5165-5176.
- WAKS, A. G. & WINER, E. P. 2019. Breast Cancer Treatment: A Review. *Jama*, 321, 288-300.
- WANG, C., VEGNA, S., JIN, H., BENEDICT, B., LIEFTINK, C., RAMIREZ, C., DE OLIVEIRA, R. L., MORRIS, B., GADIOT, J., WANG, W., DU CHATINIER, A., WANG, L., GAO, D., EVERS, B., JIN, G., XUE, Z., SCHEPERS, A., JOCHEMS, F., SANCHEZ, A. M., MAINARDI, S., TE RIELE, H., BEIJERSBERGEN, R. L., QIN, W., AKKARI, L. & BERNARDS, R. 2019. Inducing and exploiting vulnerabilities for the treatment of liver cancer. *Nature*, 574, 268-272.
- WANG, H., LIU, X., LONG, M., HUANG, Y., ZHANG, L., ZHANG, R., ZHENG, Y., LIAO, X., WANG, Y., LIAO, Q., LI, W., TANG, Z., TONG, Q., WANG, X., FANG, F., ROJO DE LA VEGA, M., OUYANG, Q., ZHANG, D. D., YU, S. & ZHENG, H. 2016a. NRF2 activation by antioxidant antidiabetic agents accelerates tumor metastasis. *Sci Transl Med*, 8, 334ra51.
- WANG, L. & BERNARDS, R. 2018. Taking advantage of drug resistance, a new approach in the war on cancer. *Front Med*, 12, 490-495.
- WANG, L., LEITE DE OLIVEIRA, R., WANG, C., FERNANDES NETO, J. M., MAINARDI, S., EVERS, B., LIEFTINK, C., MORRIS, B., JOCHEMS, F., WILLEMSSEN, L., BEIJERSBERGEN, R. L. &

- BERNARDS, R. 2017. High-Throughput Functional Genetic and Compound Screens Identify Targets for Senescence Induction in Cancer. *Cell Rep*, 21, 773-783.
- WANG, Q., WU, P. C., DONG, D. Z., IVANOVA, I., CHU, E., ZELIADT, S., VESSELLE, H. & WU, D. Y. 2013. Polyploidy road to therapy-induced cellular senescence and escape. *Int J Cancer*, 132, 1505-15.
- WANG, T., YANG, L., LIANG, Z., WANG, L., SU, F., WANG, X., YOU, X. & HE, C. 2021. Targeting cellular senescence prevents glucocorticoid-induced bone loss through modulation of the DPP4-GLP-1 axis. *Signal Transduction and Targeted Therapy*, 6, 143.
- WANG, Y., CHEN, C. L., PAN, Q. Z., WU, Y. Y., ZHAO, J. J., JIANG, S. S., CHAO, J., ZHANG, X. F., ZHANG, H. X., ZHOU, Z. Q., TANG, Y., HUANG, X. Q., ZHANG, J. H. & XIA, J. C. 2016b. Decreased TPD52 expression is associated with poor prognosis in primary hepatocellular carcinoma. *Oncotarget*, 7, 6323-34.
- WAS, H., BARSZCZ, K., CZARNECKA, J., KOWALCZYK, A., BERNAS, T., UZAROWSKA, E., KOZA, P., KLEJMAN, A., PIWOCKA, K., KAMINSKA, B. & SIKORA, E. 2017. Bafilomycin A1 triggers proliferative potential of senescent cancer cells in vitro and in NOD/SCID mice. *Oncotarget*, 8, 9303-9322.
- WAS, H., CZARNECKA, J., KOMINEK, A., BARSZCZ, K., BERNAS, T., PIWOCKA, K. & KAMINSKA, B. 2018. Some chemotherapeutics-treated colon cancer cells display a specific phenotype being a combination of stem-like and senescent cell features. *Cancer Biology & Therapy*, 19, 63-75.
- WEIDENFELD, K. & BARKAN, D. 2018. EMT and Stemness in Tumor Dormancy and Outgrowth: Are They Intertwined Processes? *Front Oncol*, 8, 381.
- WENDT, M. K., COOPER, A. N. & DWINELL, M. B. 2008. Epigenetic silencing of CXCL12 increases the metastatic potential of mammary carcinoma cells. *Oncogene*, 27, 1461-71.
- WILEY, C. D., FLYNN, J. M., MORRISSEY, C., LEBOSKY, R., SHUGA, J., DONG, X., UNGER, M. A., VIJG, J., MELOV, S. & CAMPISI, J. 2017. Analysis of individual cells identifies cell-to-cell variability following induction of cellular senescence. *Aging Cell*, 16, 1043-1050.
- WOOD, W. A., KRISHNAMURTHY, J., MITIN, N., TORRICE, C., PARKER, J. S., SNAVELY, A. C., SHEA, T. C., SERODY, J. S. & SHARPLESS, N. E. 2016. Chemotherapy and Stem Cell Transplantation Increase p16(INK4a) Expression, a Biomarker of T-cell Aging. *EBioMedicine*, 11, 227-238.
- WRONKOWITZ, N., GÖRGENS, S. W., ROMACHO, T., VILLALOBOS, L. A., SÁNCHEZ-FERRER, C. F., PEIRÓ, C., SELL, H. & ECKEL, J. 2014. Soluble DPP4 induces inflammation and proliferation of human smooth muscle cells via protease-activated receptor 2. *Biochim Biophys Acta*, 1842, 1613-21.
- WU, H., CHE, X., ZHENG, Q., WU, A., PAN, K., SHAO, A., WU, Q., ZHANG, J. & HONG, Y. 2014. Caspases: a molecular switch node in the crosstalk between autophagy and apoptosis. *Int J Biol Sci*, 10, 1072-83.
- WYLD, L., BELLANTUONO, I., TCHKONIA, T., MORGAN, J., TURNER, O., FOSS, F., GEORGE, J., DANSON, S. & KIRKLAND, J. L. 2020. Senescence and Cancer: A Review of Clinical Implications of Senescence and Senotherapies. *Cancers (Basel)*, 12.
- XIE, Z., ZHANG, Y., JIN, C. & FU, D. 2018. Gemcitabine-based chemotherapy as a viable option for treatment of advanced breast cancer patients: a meta-analysis and literature review. *Oncotarget*, 9, 7148-7161.

- XU, R., JI, Z., XU, C. & ZHU, J. 2018. The clinical value of using chloroquine or hydroxychloroquine as autophagy inhibitors in the treatment of cancers: A systematic review and meta-analysis. *Medicine*, 97.
- YAN, L., ROSEN, N. & ARTEAGA, C. 2011. Targeted cancer therapies. *Chin J Cancer*, 30, 1-4.
- YANG, F., TAKAGAKI, Y., YOSHITOMI, Y., IKEDA, T., LI, J., KITADA, M., KUMAGAI, A., KAWAKITA, E., SHI, S., KANASAKI, K. & KOYA, D. 2019a. Inhibition of Dipeptidyl Peptidase-4 Accelerates Epithelial-Mesenchymal Transition and Breast Cancer Metastasis via the CXCL12/CXCR4/mTOR Axis. *Cancer Res*, 79, 735-746.
- YANG, F., TAKAGAKI, Y., YOSHITOMI, Y., IKEDA, T., LI, J., KITADA, M., KUMAGAI, A., KAWAKITA, E., SHI, S., KANASAKI, K. & KOYA, D. 2019b. Inhibition of Dipeptidyl Peptidase-4 Accelerates Epithelial-Mesenchymal Transition and Breast Cancer Metastasis via the CXCL12/CXCR4/mTOR Axis. *Cancer Research*, 79, 735-746.
- YANG, L., FANG, J. & CHEN, J. 2017a. Tumor cell senescence response produces aggressive variants. *Cell Death Discov*, 3, 17049.
- YANG, L., SHI, P., ZHAO, G., XU, J., PENG, W., ZHANG, J., ZHANG, G., WANG, X., DONG, Z., CHEN, F. & CUI, H. 2020. Targeting cancer stem cell pathways for cancer therapy. *Signal Transduction and Targeted Therapy*, 5, 8.
- YANG, X., ZHANG, X., WU, R., HUANG, Q., JIANG, Y., QIN, J., YAO, F., JIN, G. & ZHANG, Y. 2017b. DPPIV promotes endometrial carcinoma cell proliferation, invasion and tumorigenesis. *Oncotarget*, 8, 8679-8692.
- YANG, X., ZHU, Y., SHI, Q., ZHAO, X., HUANG, Y., YAO, F., ZHANG, Y. & WANG, Z. 2021. Dipeptidyl peptidase IV is required for endometrial carcinoma cell proliferation and tumorigenesis via the IL-6/STAT3 pathway. *J Obstet Gynaecol Res*, 47, 2449-2459.
- YOSEF, R., PILPEL, N., PAPISMADOV, N., GAL, H., OVADYA, Y., VADAI, E., MILLER, S., PORAT, Z., BEN-DOR, S. & KRIZHANOVSKY, V. 2017. p21 maintains senescent cell viability under persistent DNA damage response by restraining JNK and caspase signaling. *Embo j*, 36, 2280-2295.
- YOSEF, R., PILPEL, N., TOKARSKY-AMIEL, R., BIRAN, A., OVADYA, Y., COHEN, S., VADAI, E., DASSA, L., SHAHAR, E., CONDIOTTI, R., BEN-PORATH, I. & KRIZHANOVSKY, V. 2016. Directed elimination of senescent cells by inhibition of BCL-W and BCL-XL. *Nat Commun*, 7, 11190.
- YUN, M. H. 2018. Cellular senescence in tissue repair: every cloud has a silver lining. *Int J Dev Biol*, 62, 591-604.
- ZEH, H. J., BAHARY, N., BOONE, B. A., SINGHI, A. D., MILLER-OCUIN, J. L., NORMOLLE, D. P., ZUREIKAT, A. H., HOGG, M. E., BARTLETT, D. L., LEE, K. K., TSUNG, A., MARSH, J. W., MURTHY, P., TANG, D., SEISER, N., AMARAVADI, R. K., ESPINA, V., LIOTTA, L. & LOTZE, M. T. 2020. A Randomized Phase II Preoperative Study of Autophagy Inhibition with High-Dose Hydroxychloroquine and Gemcitabine/Nab-Paclitaxel in Pancreatic Cancer Patients. *Clin Cancer Res*, 26, 3126-3134.
- ZHANG, H. & CHEN, J. 2018. Current status and future directions of cancer immunotherapy. *J Cancer*, 9, 1773-1781.
- ZHANG, T., TONG, X., ZHANG, S., WANG, D., WANG, L., WANG, Q. & FAN, H. 2021. The Roles of Dipeptidyl Peptidase 4 (DPP4) and DPP4 Inhibitors in Different Lung Diseases: New Evidence. *Frontiers in Pharmacology*, 12.
- ZHANG, Y. & ZHANG, Z. 2020. The history and advances in cancer immunotherapy: understanding the characteristics of tumor-infiltrating immune cells and their therapeutic implications. *Cellular & Molecular Immunology*, 17, 807-821.

ZHONG, L., LI, Y., XIONG, L., WANG, W., WU, M., YUAN, T., YANG, W., TIAN, C., MIAO, Z., WANG, T. & YANG, S. 2021. Small molecules in targeted cancer therapy: advances, challenges, and future perspectives. *Signal Transduction and Targeted Therapy*, 6, 201.